

# Tuning of Optical and Charge Transport Properties in Linear and Star-shaped Thiophene Based Organic Materials: A DFT Insight

A thesis  
Submitted to NIT Kurukshetra for the Degree of

**Doctor of Philosophy**  
**In**  
**Chemistry**

**Submitted by**

**Anuj Tripathi**  
**(2K17/NITK/Ph.D/6170083)**

**Under the supervision of**  
**Dr. ChettiPrabhakar**



**Department of Chemistry**  
**National Institute of Technology**  
**Kurukshetra-136119, Haryana, India**  
**September 2020**

## Declaration

---

This is certifying that the thesis entitled “**Tuning of Optical and Charge Transport Properties in Linear and Star-shaped Thiophene Based Organic Materials: A DFT Insight**” submitted by me to the Department of Chemistry, National Institute of Technology, Kurukshetra, in partial fulfilment for award of the Degree of Doctor of Philosophy in Chemistry, is a bonafide record of research work carried out by me under the **supervision** of **Dr.ChettiPrabhakar, Assistant Professor, Department of Chemistry**. The content of this thesis, and parts, have not been submitted to any other institute or university for award of same or any other degree.

**Date:**

**Anuj Tripathi**  
**2K17/NITK/Ph.D/6170083**  
Department of Chemistry  
National Institute of Technology (NIT)  
Kurukshetra, Haryana, India

**NATIONAL INSTITUTE OF TECHNOLOGY**  
**(Institution of National Importance)**  
**KURUKSHETRA**

**Dr. Chetti Prabhakar**  
**Assistant Professor**  
**Department of Chemistry**

**Dated:**

**CERTIFICATE**

This is to certify that the work incorporated in this thesis titled “**Tuning of Optical and Charge Transport Properties in Linear and Star-shaped Thiophene Based Organic Materials: A DFT Insight**” submitted by **Mr. Anuj Tripathi** has been carried out by the candidate under my supervision. This work is original and has not been submitted in part or full for any other degree or diploma of this or any other university.

**(Chetti Prabhakar)**

**Research Supervisor**

*Dedicated to my beloved  
Parents*



# Acknowledgements

*It is hard to acknowledge all the people that contributed, in different ways, to help me enjoying this five-year long trip. Thanks to these people I have been able to grow up from a human point of view, other than intellectual.*

*First and foremost, I would like to express my endless appreciation to my supervisor **Dr. Chetti Prabhakar**, Assistant Professor, Department of Chemistry, NIT Kurukshetra for the continuous support and guidance throughout my PhD journey. His patience, motivation, and immense knowledge helped me to make my research truly wonderful experience. He has been a supportive and understanding mentor for the last five year helping me with research, writing, presentations, and professional development. His guidance helped me all the time by giving me precious advises. I could not have imagined having a better boss and mentor for my PhD study. The enthusiasm and commitment that I kept during my work are justified by his skilful direction.*

*I owe my sincere thanks to Dr. Minati Baral, Head of Department of Chemistry, NIT Kurukshetra for providing laboratory facilities. I am also grateful to Prof. D.P. Singh, Prof. J. K. Kapoor, Prof. Dinesh Kumar and other faculty member of Department of Chemistry, NIT, Kurukshetra for their valuable suggestions and motivation.*

*I take the opportunity to sincerely thank the Director of National Institute of Technology Kurukshetra, **Dr. Satish Kumar**, whose urge for raising the pinnacle research level at the institute, has persuaded me to work hard with a thought to excel.*

*With genuine perception of moral obligations, I acknowledge my sincere thanks and appreciation to my research group Promila, Vidya V.M., and Ritu Mittal for standing by my side and sharing great bond as compassionate friends. Also, I would like to thanks to all the master's students, Arpita Prasantini Joshi, Ananta Ganjoo, Satyajit Beura and Shubhangi Srivastava for the warmth shown by them.*

*I would like to special thanks to two of my best friend Vijay Dangi and Vikas Sangwan for their constant support and appreciation. I will remember all the arguing and laughter we had together. I will remember those days when we went to lots of conference and workshop together. I would also like to thank all my friends Rahul Kaushik, Rahul Sakla, Pawan Kumar, Nikhil Rajput, Aman Garg, Ramesh Redhu,*

*Tanmay Rom, Rajendiran Kanagraj, Muthukumar, Anita Bhatia, Naveen Kumari, Nidhi Nehra, Nancy Sharma, Srushti Gadiyaram from department of chemistry and other departments that have helped me not only with research, but also shared their spare time with me.*

*A number of other people who helped to make this dream possible. I owe many thanks to my childhood friends Utkarsh Srivastava, Aditya Kumar Sahu, Raghwendra Shukla, Ankur Shukla, Ashish Kumar Kesarwani, Satyendra Tripathi and Sandeep Chaudhary for supporting and listening to me during my good and bad times, though many of them are not from the research background.*

*I would like to give my deepest gratitude to my parent's mother (Mrs. Meenakshi Tripathi) and father (Mr. Shiva Kant Tripathi), giving life to me, for nursing me, inspiring the support for pursuing higher education. I am grateful to my sibling, sister (Garima Tripathi) and brothers (Gaurav Tripathi and Arpit Tripathi) for their moral and emotional support throughout my PhD journey. I probably would not have made it without your support.*

*Lastly, my thanks to all those well-wishers who directly and indirectly helped me in completing the research work and to God, who made all things possible. My apologies to all those who have helped me but are not acknowledged.*

*Finally, I would like to thank all the people who won't stop at the Acknowledgements page but will read this work till the end: thanks both!*

**ANUJ TRIPATHI**

**THESIS CONTENTS**

	<b>Page no.</b>
Thesis Content	i
List of Tables	iv
List of Figures	viii
List of Schemes	xii
Abstract of thesis	xiii

**Chapter 1: Introduction**

<b>1.1</b>	Introduction	2
<b>1.2</b>	Optical Properties in Organic Materials	3
<b>1.3</b>	Electronic Properties in Organic Materials	4
<b>1.4</b>	Charge transport properties in Organic Materials	6
	<b>1.4.1</b> Band transport Model	7
	<b>1.4.2</b> Hopping Model	8
	<b>1.4.2.1</b> Marcus Theory	7
	<b>1.4.2.2</b> Reorganization Energy ( $\lambda$ )	10
	<b>1.4.2.3</b> Examples of hole and electron transport organic materials	12
	<b>1.4.2.4</b> Charge injection Parameters: Ionization Potential (IP) and Electron Affinity (EA)	13
<b>1.5</b>	Thiophene-based organic materials	14
<b>1.6</b>	Literature survey	
	<b>1.6.1</b> Simple and fused thiophene system for organic materials	16
	<b>1.6.2</b> Thiophene based fused heteroacene system for organic materials	18
	<b>1.6.3</b> Star-Shaped thiophene based organic materials	23
<b>1.7</b>	Theoretical Methods	26
<b>1.8</b>	Density Functional Theory (DFT)	27
<b>1.9</b>	Outline of Thesis	29

**Chapter 2: Lowest electronic excitations and charge transport properties of Chalcogen (O, S and Se) based linear acenes**

<b>2.1</b>	Introduction	38
<b>2.2</b>	Computational Methodology	40
<b>2.3</b>	Results and Discussions	
	<b>2.3.1</b> Geometry and structure	42
	<b>2.3.2</b> Absorption properties	48
	<b>2.3.3</b> Molecular orbital energies	56
	<b>2.3.4</b> Ionization potential and electron affinities	64
	<b>2.3.5</b> Hole extraction potential and electron extraction potential	64
	<b>2.3.6</b> Reorganization energy	
<b>2.4</b>	Conclusion	71

**Chapter 3A: Optoelectronic and charge transport properties of benzotrithiophene (BTT) isomers**

<b>3A.1</b>	Introduction	76
<b>3A.2</b>	Computational methodology	78
<b>3A.3</b>	Results and Discussions	
<b>3A.3.1</b>	Geometry and structural parameter	79
<b>3A.3.2</b>	Linear optical properties	86
<b>3A.3.3</b>	Ionization potential (IP), electron affinity (EA)	93
<b>3A.3.4</b>	Reorganization energies ( $\lambda$ )	94
<b>3A.4</b>	Conclusion	95

**Chapter 3B: Tuning of optoelectronic and charge transport properties in symmetrical benzotrithiophene and its oligomers**

<b>3B.1</b>	Introduction	100
<b>3B.2</b>	Computational methodology	103
<b>3B.3</b>	Results and Discussions	
<b>3B.3.1</b>	Geometry and structure	104
<b>3B.3.2</b>	Electronic excitations	107
<b>3B.3.3</b>	Ionization potential (IP), electron affinity (EA) and	119
<b>3B.3.3</b>	Hole extraction potentials (HEP) and electron extraction	121
	potentials (EEP)	
<b>3B.3.3</b>	Reorganization energies ( $\lambda$ )	122
<b>3B.4</b>	Conclusion	124

**Chapter 4A: Electronic excitations, charge transport properties and nucleus independent chemical shift (NICS) studies of benzotrithiophene (BTT) isomers and its heteroatomic (NH, O and Se) analogs**

<b>4A.1</b>	Introduction	128
<b>4A.2</b>	Material and methods	130
<b>4A.3</b>	Result and discussions	
<b>4A.3.1</b>	Geometry and structure	130
<b>4A.3.2</b>	NICS calculations	134
<b>4A.3.3</b>	Electronic excitations	138
<b>4A.3.4</b>	Frontier molecular orbitals (FMOs)	144
<b>4A.3.5</b>	Ionization potential (IP), electron affinity (EA)	148
<b>4A.3.6</b>	Reorganization energies ( $\lambda$ )	149
<b>4A.4</b>	Conclusion	153

**Chapter 4B: Linear optical and charge transport properties of truxene(isotruxene) and thiatruxene (isothiatruxene) and its heteroatomic (N, O, and Si) analogs**

<b>4B.1</b>	Introduction	158
<b>4B.2</b>	Computational methodology	161
<b>4B.3</b>	Result and discussions	
<b>4B.3.1</b>	Molecular structure and Geometry	162
<b>4B.3.2</b>	Linear optical properties	165

	<b>4B.3.3</b> Ionization potential (IP), electron affinity (EA) HEP and EEP	175
	<b>4B.3.4</b> Reorganization energy ( $\lambda$ )	177
<b>4B.4</b>	Conclusion	179

**Chapter 5A: Impact of replacement of central benzene ring in anthracene by heterocyclic ring on electronic excitations and reorganization energies in Anthtratetrathiophene (ATT)**

<b>5A.1</b>	Introduction	184
<b>5A.2</b>	Computational methods	185
<b>5A.3</b>	Results and Discussions	
	<b>5A.3.1</b> Optical properties	187
	<b>5A.3.2</b> Frontier Molecular Orbitals (FMOs)	194
	<b>5A.3.3</b> Ionization Potential (IP), Electron Affinity (EA), HEP and EEP	196
	<b>5A.3.4</b> Reorganization energy ( $\lambda$ )	197
<b>5A.4</b>	Conclusion	200

**Chapter 5B: Impact of replacement of central benzene ring in anthracene by heterocyclic ring on electronic excitations and reorganization energies in Anthtratetrathiazole (ATTz)**

<b>5B.1</b>	Introduction	204
<b>5B.2</b>	Methodology	207
<b>5B.3</b>	Results and discussions	
	<b>5B.3.1</b> Electronic Excitations	207
	<b>5B.3.2</b> Frontier Molecular Orbitals (FMOs)	217
	<b>5B.3.3</b> Ionization Potentials (IP), Electron Affinities (EA), HEP and EEP	219
	<b>5B.3.4</b> Reorganization energy ( $\lambda$ )	222
<b>5B.4</b>	Conclusion	227

<b>List of Publications</b>	230
-----------------------------	-----

<b>Conferences and Workshops attended</b>	233
---	-----

---

**List of Tables**

<b>Table No.</b>		<b>Page No.</b>
<b>Chapter 1</b>		
<b>1.1</b>	Charge transport properties of oligoacenes	12
<b>Chapter 2</b>		
<b>2.1</b>	Optimized Structures and relative energy (RE in Kcal) of benzene and naphthalene based hetero acenes	42
<b>2.2</b>	Optimized Structures and relative energy (RE in Kcal) of anthracene based hetero acenes	43
<b>2.3</b>	Optimized Structures and relative energy (RE in Kcal) of tetracene based hetero acenes	45
<b>2.4</b>	Optimized Structures and relative energy (RE in Kcal) of pentacene based hetero acenes	47
<b>2.5</b>	Computed lowest electronic excitations ( $\lambda_{CAL}$ in nm) of anti-isomers with different functionals calculated at B3LYP/6-311+G (d, p) optimized geometries	49
<b>2.6</b>	Computed lowest electronic excitations ( $\lambda_{CAL}$ in nm) of syn-isomers with different functionals calculated at B3LYP/6-311+G (d, p) optimized geometries	50
<b>2.7</b>	Computed lowest electronic excitations ( $\lambda_{CAL}$ in nm) Oscillator strength ( $f$ ) major transitions (MT) and % weight (%C <sub>i</sub> ) of anti-isomers at TD-B3LYP/6-311+G (d, p) method	52
<b>2.8</b>	Computed lowest electronic excitations ( $\lambda_{CAL}$ in nm) Oscillator strength ( $f$ ) major transitions (MT) and % weight (%C <sub>i</sub> ) of syn-isomers at TD-B3LYP/6-311+G (d, p) method	53
<b>2.9</b>	Calculated HOMO, LUMO energies (in eV) and HOMO-LUMO gap (HLG) of syn-isomers and anti-isomers	57
<b>2.10</b>	Molecular orbital pictures of anti-isomers	58
<b>2.11</b>	Molecular orbital pictures of syn-isomers	61
<b>2.12</b>	Calculated hole and electron ( $\lambda_h$ and $\lambda_e$ ) reorganization energy (in meV), Ionization Potential (IP), Electron Affinity (EA), HEP and EEP(in eV) of anti-isomers at B3LYP/6-311+ G (d,p) level of theory	66
<b>2.13</b>	Calculated hole and electron ( $\lambda_h$ and $\lambda_e$ ) reorganization energy (in meV), Ionization Potential (IP), Electron Affinity (EA), HEP and EEP(in eV) of syn-isomers at B3LYP/6-311+ G (d,p) level of theory	67
<b>2.14</b>	Calculated hole and electron ( $\lambda_h$ and $\lambda_e$ ) reorganization energy (in meV) using functionals for anti and syn-isomers	70
<b>Chapter 3A</b>		
<b>3A.1</b>	Optimized structure, Symmetry and Relative energy (RE, in Kcal) of isomers calculated at B3LYP/6-311+G (d, p) level	80
<b>3A.2</b>	Calculated bond length (in Å) and bond angles (in degree (°)) for the symmetrical BTTs (BTT1, BTT2, BTT3, and BTT4) isomers obtained at B3LYP/6-311+G (d, p) level of theory	82

---

<b>3A.3</b>	Calculated bond length (in Å) and bond angles (in degree (°)) for the unsymmetrical BTTs (BTT5, BTT6, and BTT7) isomers obtained at B3LYP/6-311+G (d, p) level of theory	83
<b>3A.4</b>	Bond lengths (BL <sup>cal</sup> and BL <sup>exp</sup> in Å) and Bond angles (BA <sup>cal</sup> and BA <sup>exp</sup> in degree (°)) of optimized structure of BTT1 calculated at B3LYP/6-311+ G (d, p) level	84
<b>3A.5</b>	Bond lengths (BL <sup>cal</sup> and BL <sup>exp</sup> in Å) and Bond angles (BA <sup>cal</sup> and BA <sup>exp</sup> in degree (°)) of optimized structure of BTT2 calculated at B3LYP/6-311+G (d, p) level	85
<b>3A.6</b>	Absorption energies ( $\lambda_{\max}$ in nm) calculated at TDDFT method 6-311+G (d, p) basis set with different functional	87
<b>3A.7</b>	Calculated absorption maxima $\lambda_{\max}$ (nm), Oscillator strength ( $f$ ), Major Transitions (MT), and %weight (%C <sub>i</sub> >10) at TD-B3LYP method using 6-311+G (d, p) basis sets	87
<b>3A.8</b>	Absorption( $\lambda_{\max}$ in nm) of isomers in different solvents	91
<b>3A.9</b>	Computed HOMO and LUMO energies and Energy Gap (in eV)	92
<b>3A.10</b>	Calculated Ionization Potential (IP), Electron Affinity (EA) and reorganization energy ( $\lambda_h$ and $\lambda_e$ ) in gas phase at B3LYP/6-311+G (d, p) level of theory	94

### Chapter 3B

<b>3B.1.</b>	Comparative study of Bond lengths (BL) and Bond angles (BA) of Crystal structure and Optimized geometry at B3LYP/6-31G (d, p) level for the molecule Di-BTT	105
<b>3B.2</b>	Comparison of Bond lengths(BL) and Bond angles (BA) of Di-BTT optimized by using B3LYP functionals with 6-311+G (d, p) and 6-31G (d, p) basis set	106
<b>3B.3</b>	Calculated Absorption ( $\lambda$ ) and Oscillator strength ( $f$ ) with different functionals using 6-311++G(d, p) at B3LYP/6-31G(d, p) optimized geometry	108
<b>3B.4</b>	Experimental ( $\lambda^{\text{Exp}}$ in nm) and Calculated absorption maxima ( $\lambda^{\text{Cal}}$ in nm), Oscillator strength ( $f$ ), Major Transitions (MT), %weight (%C <sub>i</sub> , contributions >10% are shown) at PBE0 method using 6-311++G (d, p) basis sets	111
<b>3B.5</b>	Optimized geometries with dihedral angles	114
<b>3B.6</b>	HOMO, LUMO energies and corresponding HOMO-LUMO gap (in eV)	115
<b>3B.7</b>	Calculated reorganization energy ( $\lambda_h$ and $\lambda_e$ ) (in meV), Ionization Potential (IP), Electron Affinity (EA), HEP and EEP (in eV) at B3LYP/6-31G (d, p) level of theory	119

### Chapter 4A

<b>4A.1</b>	Relative energy (in kcal) of the isomers of BTP, BTF, BTT and BTSe	131
<b>4A.2</b>	Bond lengths and Dihedral angles of the isomers of BTP, BTF, BTT and BTSe	132
<b>4A.3</b>	Calculated Nucleus Independent chemical shift NICS(0) at center (in ppm) for all the isomers obtained at B3LYP/6-311+G (d, p) level	135
<b>4A.4</b>	Calculated Nucleus Independent Chemical Shift at 1 Å above the ring center (in ppm) (i.e. NICS(1)) for all the isomers obtained at B3LYP/6-311+ G (d, p) level	137
<b>4A.5</b>	Absorption maxima $\lambda_{\max}$ (nm), Oscillator strength ( $f$ ), Major Transitions (MT) and %weight (%C <sub>i</sub> ) obtained at TD-B3LYP method using 6-311+G (d, p) basis set	139
<b>4A.6</b>	Calculated absorption energies ( $\lambda_{\max}$ in nm) with different functional at B3LYP optimized geometries	141
<b>4A.7</b>	Molecular orbital pictures of BTP, BTF and BTSe isomers	144

<b>4A.8</b>	Calculated HOMO and LUMO energies (in eV) and HOMO-LUMO gap (HLG in eV) for all the isomers	148
<b>4A.9</b>	Hole and electron ( $\lambda_h$ and $\lambda_e$ ) reorganization energy (in meV), Ionization Potential (IP), Electron Affinity (EA), HEP and EEP(in eV) calculated at B3LYP/6-311+ G (d, p) level of theory	150

### Chapter 4B

<b>4B.1</b>	Structures, Relative Energy (RE) and Symmetry of studied molecules	162
<b>4B.2</b>	Absorption maxima with different functionals calculated at B3LYP optimized geometries with 6-311+G (d, p) basis set	167
<b>4B.3</b>	Computed lowest electronic excitations ( $\lambda_{max}$ in nm), Oscillator strength ( $f$ ), Major Transitions (MT) and % weight (% $C_i > 10\%$ ) at TD-B3LYP/6-311+G (d, p) method	168
<b>4B.4</b>	HOMO, LUMO Energies and HOMO-LUMO Gap (HLG) (in eV)	175
<b>4B.5</b>	Calculated ionization potentials (IP), electron affinities (EA), hole and electron extraction potentials (HEP& EEP) and hole and electron reorganization energies ( $\lambda_h$ and $\lambda_e$ ) at B3LYP/6-311+ G (d, p) level of theory	176

### Chapter 5A

<b>5A.1</b>	Computed lowest three electronic excitations ( $\lambda_{max}$ in nm), experimental absorption ( $\lambda_{max}^{Exp}$ in nm), Oscillator strength ( $f$ ), Major Transitions (MT) and % weight (% $C_i$ ) at TD-B3LYP/6-311+G (d, p) method	189
<b>5A.2</b>	Absorption maxima ( $\lambda_{max}$ in nm) in different solvents calculated at TD-B3LYP-PCM/6-311+ G (d, p) method	190
<b>5A.3</b>	Calculated energies of HOMO, LUMO and HOMO-LUMO gap (in eV) for all the molecules	195
<b>5A.4</b>	Calculated Ionization Potentials (IP in eV), Electron Affinities (EA in eV), Hole Extraction potentials (HEP in eV), Electron Extraction potentials (EEP in eV) and reorganization energies ( $\lambda_h$ and $\lambda_e$ in meV) at B3LYP/6-311+G (d, p) level of theory	197

### Chapter 5B

<b>5B.1</b>	Calculated absorption energies ( $\lambda_{max}$ in nm) and oscillator strength ( $f$ ) with different functional for molecules A, B and C	208
<b>5B.2</b>	Calculated absorption energies ( $\lambda_{max}$ in nm) in gas phase and different solvents at TD-B3LYP/6311 + G (d, p) method in gas phase	208
<b>5B.3</b>	Calculated Absorption energies ( $\lambda_{max}$ in nm), Oscillator strength ( $f$ ), Configurations and % weight (% $C_i$ ) at TD-B3LYP/6-311+G (d, p) method for molecules A, B and C	209
<b>5B.4</b>	Calculated Absorption energies ( $\lambda_{max}$ in nm), Oscillator strength ( $f$ ), Configurations and % weight (% $C_i$ ) at TD-B3LYP/6-311+G (d, p) method for molecules <b>1a'</b> to <b>5a'</b>	214
<b>5B.5</b>	Calculated Absorption energies ( $\lambda_{max}$ in nm), Oscillator strength ( $f$ ), Configurations and % weight (% $C_i$ ) at TD-B3LYP/6-311+G (d, p) method for molecules <b>1b'</b> to <b>5b'</b>	214
<b>5B.6</b>	Computed absorption ( $\lambda_{max}$ in nm) and Oscillator strength ( $f$ ), with different functionals at TD-B3LYP/6-311+G (d, p) optimized geometries	215



<b>5B.7</b>	HOMO, LUMO energy and H-L gap (in eV)	218
<b>5B.8</b>	Calculated Ionization Potentials ( $IP_v$ and $IP_a$ in eV), Electron Affinities ( $EA_v$ and $EA_a$ in eV), Extraction potentials (HEP and EEP in eV) and reorganization energies ( $\lambda_h$ and $\lambda_e$ in meV) at B3LYP/6-311+ G (d, p) level of theory for all the molecules	220
<b>5B.9</b>	Calculated hole ( $\lambda_h$ ) and electron ( $\lambda_e$ ) reorganization energies of all the molecules with different functionals	225

---

## List of Figures

Figure No.		Page No.
<b>Chapter 1</b>		
1.1	Jablonski diagram: $S_0$ , $S_1$ and $S_2$ are ground, first and second excited states respectively. $T_1$ is triplet state. Energy levels and transitions in an isolated organic molecule	3
1.2.a	Representation of $sp_2$ hybridization of carbon atom	5
1.2.b	$\sigma$ -bond and $\pi$ -bond formation for two $sp_2$ hybridized carbon atom	5
1.3	Molecular structure of benzene and its energy diagram	6
1.4	Calculation of Internal reorganization energy	11
1.5	Examples of well-known Hole and electron transport materials for OLEDs	13
1.6	Oligothiophene structures ( $Th_n$ )	17
1.7	Structure of fused thiophenes system thienothiophene (1 to 4) dithienothiophene (5) and bis(dithienothiophene) (6)	18
1.8	Structures of linear acenes as organic materials: anthracene (6), tetracene (7), rubrene (8) and pentacene (9)	19
1.9	Thiophene based fused acene molecules reported by Takimiya group	21
1.10	Thiophene based pentacene and heptacene molecules reported by Neckers group	22
1.11	Thiophene based linear molecule showing high mobility	23
1.12	Star-shaped oligothiophene synthesized by Ponomarenko et al.	24
1.13	Reported star-shaped thiophene based molecules by (a) Pie; (b) Roncali; and (c) Kim	25
1.14	Designed star-shaped thiophene based molecules by R. Jin for organic solar cells and OLEDs	26
1.15	Flowchart for different Computational approaches	27
<b>Chapter 2</b>		
2.1	Normalized Absorption spectra of anti-isomers of thiophene based acenes	54
2.2	Normalized Absorption spectra of anti-isomers of furan based acenes	54
2.3	Normalized Absorption spectra of anti-isomers of selenophene based acenes	55
2.4	Normalized Absorption spectra of anti-isomer of anthracene and pentacene based hetero acenes	55
2.5	HOMO and LUMO gap with their molecular orbital pictures of anti-isomer of ADF, ADT and ADSe	56
2.6	HOMO and LUMO energies with their molecular orbital pictures Anti isomers of thiophenes based acenes	58
2.7	Hole reorganization energies of syn and anti-isomers	68
2.8	Electron reorganization energies of syn and anti-isomers	68
2.9	Calculated hole reorganization energies of anti-isomers with different functionals	69

---

<b>2.10</b>	Calculated electron reorganization energies of anti-isomers with different functionals	69
-------------	--	----

### Chapter 3A

<b>3A.1</b>	Electronic excitations with their molecular orbitals of BTT1 and BTT2	88
<b>3A.2</b>	Electronic excitations with their molecular orbitals of BTT3 and BTT4	89
<b>3A.3</b>	Electronic excitations with their molecular orbitals of BTT5	89
<b>3A.4</b>	Electronic excitations with their molecular orbitals of BTT6 and BTT7	90
<b>3A.5</b>	Normalized spectra of all the isomers of BTT calculated at B3LYP/6-311+G (d, p) level	90
<b>3A.6</b>	HOMO, LUMO energy levels and HOMO-LUMO gap of all the isomers of BTT	93

### Chapter 3B

<b>3B.1</b>	Seven possible isomers of Benzotrithiophene (BTT); Symmetrical (BTT1-BTT4) and Asymmetrical (BTT5-BTT7) isomers (with dihedral angle between two thiophene ring)	103
<b>3B.2</b>	Calculated absorption energies with different functionals	109
<b>3B.3</b>	Normalized absorption spectra of BTT and its oligomers	113
<b>3B.4</b>	HOMO-LUMO levels and energy gap (in eV) of BTT and its oligomers	113
<b>3B.5</b>	Major electronic excitations and molecular orbital pictures of M-BTT	116
<b>3B.6</b>	Major electronic excitations and molecular orbital pictures of Di-BTT	116
<b>3B.7</b>	Major electronic excitations and molecular orbital pictures of Tri-BTT	117
<b>3B.8</b>	Major electronic excitations and molecular orbital pictures of Tetra-BTT	117
<b>3B.9</b>	Major electronic excitations and molecular orbital pictures of Hexa-BTT	118
<b>3B.10</b>	Major electronic excitations and molecular orbital pictures of Deca-BTT	118
<b>3B.11</b>	Graphical representation of Adiabatic Ionization Potentials ( $IP_a$ ) and Electron Affinities ( $EA_a$ ) of all the oligomers	120
<b>3B.12</b>	Graphical representation of Vertical Ionization Potentials ( $IP_v$ ) and Electron Affinities ( $EA_v$ ) of all the oligomers	120
<b>3B.13</b>	Graphical representation of Hole Extraction Potentials (HEP) and Electron Extraction Potentials (EEP) of all the oligomers	121
<b>3B.14</b>	Hole and Electron reorganization energies of BTT and its oligomers	123

### Chapter 4A

<b>4A.1</b>	Structures with their Relative energies	131
<b>4A.2</b>	Normalized Absorption spectra of BTP isomers	142
<b>4A.3</b>	Normalized Absorption spectra of BTF isomers	143

<b>4A.4</b>	Normalized Absorption spectra of BTSe isomers	143
<b>4A.5</b>	HOMO, LUMO energy levels and energy gap of all the isomers of BTP	146
<b>4A.6</b>	HOMO, LUMO energy levels and energy gap of all the isomers of BTF	146
<b>4A.7</b>	HOMO, LUMO energy levels and energy gap of all the isomers of BTSe	147
<b>4A.8</b>	HOMO, LUMO energy levels and energy gap of all the isomers of BTT	147
<b>4A.9</b>	Hole reorganization energies for BTP, BTF, BTSe and BTT isomers	151
<b>4A.10</b>	Electron reorganization energies for BTP, BTF, BTSe and BTT isomers	152

### Chapter 4B

<b>4B.1</b>	Calculated absorption energies of the molecules using functionals B3LYP, BLYP, BHandHLYP, M06, PBE, LCWPBE, CAM-B3LYP and WB97XD at 6-311+G (d,p) level	166
<b>4B.2</b>	Calculated Absorption spectra of symmetrical molecules, <b>T-TS</b>	170
<b>4B.3</b>	Calculated Absorption spectra of asymmetrical molecules, <b>IT-ITS</b>	170
<b>4B.4</b>	Major Electronic transitions with their molecular orbitals for the molecules <b>TN</b> and <b>ITN</b>	171
<b>4B.5</b>	Major Electronic transitions with their molecular orbitals for the molecules <b>TO</b> and <b>ITO</b>	171
<b>4B.6</b>	Major Electronic transitions with their molecular orbitals for the molecules <b>TSi</b> and <b>ITSi</b>	172
<b>4B.7</b>	Major Electronic transitions with their molecular orbitals for molecule <b>T</b> and <b>TS</b>	172
<b>4B.8</b>	Major Electronic transitions with their molecular orbitals for the molecules <b>IT</b> and <b>ITS</b>	173
<b>4B.9</b>	Energy levels of HOMO, LUMO and HOMO-LUMO gap for all the molecules	174
<b>4B.10</b>	Hole reorganization energies for all the molecules with B3LYP, BHandHLYP, PBE0 and CAM-B3LYP functionals	178
<b>4B.11</b>	Electron reorganization energies for all the molecules with B3LYP, BHandHLYP, PBE0 and CAM-B3LYP functionals	178

### Chapter 5A

<b>5A.1</b>	Electronic transitions with their molecular orbitals for molecule <b>1a</b> and <b>2a</b>	190
<b>5A.2</b>	Electronic transitions with their molecular orbitals for molecule <b>1b</b> and <b>2b</b>	191
<b>5A.3</b>	Electronic transitions with their molecular orbitals for molecule <b>3a</b> and <b>3b</b>	191
<b>5A.4</b>	Electronic transitions with their molecular orbitals for molecule <b>4a</b> and <b>4b</b>	192
<b>5A.5</b>	Electronic transitions with their molecular orbitals for molecule <b>5a</b> and <b>5b</b>	192
<b>5A.6</b>	Normalized Absorption spectra of isomer 'a' ( <b>1a-5a</b> ).	193
<b>5A.7</b>	Normalized Absorption spectra of isomer 'b' ( <b>1b-5b</b> ).	193
<b>5A.8</b>	HOMO, LUMO energy levels and HOMO-LUMO energy gap for 'a' isomers	194

---

<b>5A.9</b>	HOMO, LUMO energy levels and HOMO-LUMO energy gap for ‘b’ isomers	195
<b>5A.10</b>	Graphical representations of hole and electron reorganization energies of ‘a’ isomers	198
<b>5A.11</b>	Graphical representations of hole and electron reorganization energies of ‘b’ isomers	199

### Chapter 5B

<b>5B.1</b>	Major electronic excitations with molecular orbital pictures of <b>1a’</b> and <b>2a’</b>	210
<b>5B.2</b>	Major electronic excitations with molecular orbital pictures of <b>1b’</b> and <b>2b’</b>	211
<b>5B.3</b>	Major electronic excitations with molecular orbital pictures of <b>3a’</b> and <b>3b’</b>	212
<b>5B.4</b>	Major electronic excitations with molecular orbital pictures of <b>4a’</b> and <b>4b’</b>	213
<b>5B.5</b>	Major electronic excitations with molecular orbital pictures of <b>5a’</b> and <b>5b’</b>	213
<b>5B.6</b>	Normalized absorption spectra of ‘a’ series isomers	216
<b>5B.7</b>	Normalized absorption spectra of ‘b’ series isomers	216
<b>5B.8</b>	Energy levels of Frontier molecular orbitals and their energy gap for ‘a’ series isomers	219
<b>5B.9</b>	Energy levels of Frontier molecular orbitals and their energy gap for ‘b’ series isomers	219
<b>5B.10</b>	Adiabatic Ionization Potential ( $IP_a$ ) and Electron Affinity ( $EA_a$ ) for <b>a’</b> and <b>b’</b> series molecules obtained at B3LYP/6-311 + G (d, p) level	221
<b>5B.11</b>	Vertical Ionization Potential ( $IP_v$ ) and Electron Affinity ( $EA_v$ ) for <b>a’</b> and <b>b’</b> series molecules obtained at B3LYP/6-311 + G (d, p) level	221
<b>5B.12</b>	Hole extraction potential (HEP) and Electron extraction potentials (EEP) for <b>a’</b> and <b>b’</b> series molecules obtained at B3LYP/6-311 + G (d, p) level.	222
<b>5B.13</b>	Variation of Hole Reorganization Energy ( $\lambda_h$ in meV) with B3LYP functional	223
<b>5B.14</b>	Calculated Electron Reorganization Energy ( $\lambda_e$ in meV) with B3LYP functional	224
<b>5B.15</b>	Variation of Hole Reorganization Energy ( $\lambda_h$ in meV) with B3LYP, PBE0 and M06 functionals	226
<b>5B.16</b>	Variation of Electron Reorganization Energy ( $\lambda_e$ in meV) with B3LYP, PBE0 and M06 functionals	226

**List of Schemes**

<b>Scheme</b>		<b>Page</b>
<b>No.</b>		<b>No.</b>
<b>2.1</b>	Molecular structures of chalcogen (O, S and Se) based acene molecules	41
<b>3A.1</b>	The Possible symmetric (BTT1-BTT4) and asymmetric (BTT5-BTT7) isomers of Benzotrithiophene (BTT)	78
<b>3B.1</b>	Structure of BTT and its oligomers	102
<b>4A.1</b>	Structures of seven possible isomers of BTP, BTF, BTT and BTSe	129
<b>4B.1</b>	Structures of Truxene ( <b>T</b> , meta-meta connectivity) and Isotruxene ( <b>IT</b> , ortho-para connectivity)	159
<b>4B.2</b>	Structures of <b>T</b> , <b>IT</b> and its hetero-atomic ( <b>N</b> , <b>O</b> , <b>Si</b> and <b>S</b> ) analogs	161
<b>5A.1</b>	Structure of ATT- based molecules consider for this study	186
<b>5B.1</b>	Structures of Anthratetrarthiophene (ATT) molecules (A & B) and dibenzothienotetrathiophene (C)	205
<b>5B.2</b>	Structure of ATTz- based molecules consider for study	206

## **Abstract**

Organic materials are fascinating class of materials for large-area and flexible devices for organic semiconductors. Among them thiophene based organic semiconductors with new molecular and macromolecular structures were explored for the possible applications in optoelectronic devices. The present thesis is divided into five chapters. Chapter 1 includes introduction of organic materials, and their optical, electronic and charge transport properties in these materials are studied in this chapter. Literature survey on thiophene based organic materials and methodology used in achieving the goal are also discussed in this chapter. In Chapter 2, the study starts with simple thiophene based linear acene molecules and calculation of their charge transport parameters using DFT methodology. Further to make study broader and comparative, furan and selenophene based acene molecules are also included. Chapter 3 divided into two subchapters, first part of the chapter deals with optical and charge transport properties of benzotrithiophene (BTT) and their possible isomers. It is shown that the studied isomers are better for hole and electron transport materials. The second part of the chapter 3 deals with the study of optical and transport properties of oligomers of BTT (most stable isomer). It is shown that the addition of BTT-units to the core BTT, results in enhanced charge transport properties. Chapter 4 also discussed in two parts, first part of chapter 4 deals with the study of linear optical and charge transport properties of heteroatomic (O, NH and Se) analogues of BTT isomers. In the second part of chapter 4 is on the study of truxene & isotruxene, thiatruxene & isothiatruxene and their heteroatomic (N, O and Si) analogue and shown that thiatruxene are better for hole transporting material while azatruxene are better for electron transporting materials. Last chapter (i.e. chapter 5) deals with impact of replacement of central benzene ring in anthracene with different heterocyclic ring on optical and charge transport properties in anthratetrathiophene (ATT) and anthratetrathiazole (ATTz) molecules. It is also studied the effect of heteroatom (S and N) on charge transport parameters at the periphery on ATTz molecule. Overall, aim of the thesis is to design those organic materials which are having high hole and electron transport properties and may find applications in organic semiconductor materials.

# *Chapter 1*



*Introduction*







## 1.1. Introduction

Organic semiconductors (OSCs) are organic materials which exhibit semiconductor properties. These are class of carbon-based materials that shows optical and electronic properties. They have been mainly focusing to advancement of potential low-cost, light-weight and flexible optoelectronic devices, such as organic field effect transistors (OFETs), organic photovoltaic cells (OPVs), solar cells, organic lasers, organic light emitting diodes(OLEDs) [1-6]. One of the major advantages of organic optoelectronic devices are they are economically cheap, efficient, and their environmentally friendly nature makes them promising area for research and its continuous development help the society [7-9].

Literature reports says that organic optoelectronic materials are known for almost a century and their optical and electronic properties are first reported in the year 1910s [10]. But, with discovery of electroluminescence property in molecular crystal and polymer, much interest has been focused in 1960s and 1970s. During last 20 years, a real flood in field of organic optoelectronic materials arisen due to progress in material design and refinement techniques lead to momentous boost to material performance [10].

OSCs are differing from the inorganic semiconductor in their interactions; former creates solids due to van der Waals interactions while later solids, bonds are covalent in nature. Generally inorganic materials are pure rigid crystalline solids and require very accurate processing under difficult conditions. However organic materials are showing novel semiconducting electronic properties with easy processing and manufacturing. Today there are infinite numbers of variety of organic materials and their properties can be tuned by altering their chemical structures making them multipurpose. In addition to these organic semiconductors deliver us flat and flexible materials, and light emission from these materials mostly when electricity is applied to thin film of material to give out light. Also soluble organic materials enable ink jet printing, a low cost designing method compatible with high output roll to roll processing [11]. In addition to above all the organic materials offers limitless design of materials with unique structures tailored for specific optoelectronic applications.

Though there is continuous advancement in the fields of OSCs but currently, these semiconductors are suffering from several drawbacks. Organic materials show weak vander

waals interaction between molecules which results in minimal orbital overlay between molecules. The characteristic properties of organic devices such as stability, solubility, charge carrier mobility, reproducibility, etc. are inferior to those of inorganic semiconductors. Also, the power conversion efficiencies (PCE) of OSCs devices are less than that of analogous of inorganic devices. For some applications the low cost of organic devices is more important than device performance, and therefore organic semiconductors have become competitive within niche technologies. Hence there is need to understand the factor that influences the characteristics properties and efficiency as well as lifetime of OSCs for designing better organic devices.

## 1.2. Optical Properties in Organic Materials

The optical properties in OSCs are in some way different from inorganic semiconductors. In OSCs materials, molecular energy levels are conventionally defined in terms of highest occupied molecular orbital (HOMO) and lowest unoccupied molecular orbital (LUMO). In inorganic semiconductors HOMO and LUMO levels have the same meanings, valance and conduction bands, respectively [12]. In organic semiconductors, HOMO and LUMO levels do not map nicely on the single particle electronic levels and are usually written as  $S_n$  and  $T_n$  for singlet and triplet states respectively. However, HOMO-LUMO energy gap (HLG) is approximately equal to sum of  $S_0$ - $S_1$  gap and exciton binding energy. In figure 1.1, various transitions and energy levels for an isolated organic molecule are pictured.

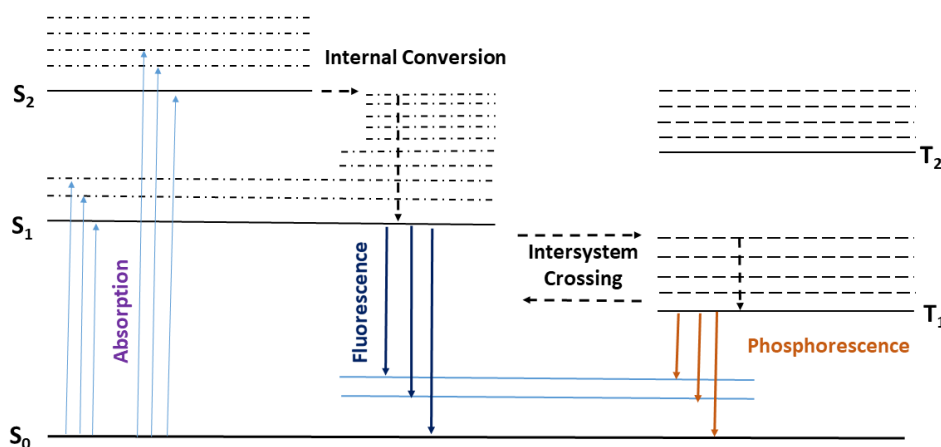


Figure 1.1: Jablonski diagram:  $S_0$ ,  $S_1$  and  $S_2$  are ground, first and second excited states respectively.  $T_1$  is triplet state. Energy levels and transitions involved in an isolated organic molecule

---

When light is absorbed by OSC, vertical excitation of electron take place from  $S_0$  to  $S_n$  (i.e. *absorption* take place from HOMO or lower occupied levels to an excited state) or one of the vibrational sublevels of  $S_n$  and it occurs in about  $10^{-15}$  s. As  $S_1$  and  $S_2$  are singlet excited state and electron is paired by opposite spin with ground state electron. In majority of materials transitions from  $S_n$  to  $S_1$  (LUMO) state occur more quickly than transition from  $S_1$  to  $S_0$  [13]. According to Kasha's rule, fluorescence takes place when electron is returned to ground state ( $S_0$ ) from lowest excited state, i.e.  $S_1$  [14]. This return of electron may occur to higher vibrational level of  $S_0$  and then electron will relax to lowest vibrational level of  $S_0$  within  $10^{-12}$  s by internal conversion. The emission of light in the form of radiative decay for nanoscale time from excited singlet state is known as *fluorescence*. There is possibility for  $S_1$ , conversion to triplet state ( $T_1$ ) by *intersystem crossing*, where electron has same spin as ground state spin and therefore return to ground state is spin-forbidden. OSCs are normally characterized by weak spin-orbit coupling and hence emission form triplet state is doubtful. However, emission from triplet state occurs over milliseconds to second and in known as *phosphorescence*. These emissions i.e. fluorescence and phosphorescence are originated by photoexcitation and are generally called photo-luminescence.

### 1.3. Electronic Properties in Organic Materials

In OSCs materials, electrical conductivity is due to properties of carbon atom in conjugated system [6]. In ground state electronic configuration of carbon atom is  $1s^2 2s^2 2p^2$ . To explain the geometry of carbon based compounds concept of hybridisation is introduced. Hybridisation is mixing of orbitals (s or p) which results in new hybrid orbitals with different shape, size, energy and orientation than its unhybridized counterpart. For conjugated system carbon is  $sp^2$  hybridized, results from mixing of 2s orbital with two 2p orbital (out of three 2p orbital presented in figure 1.2.a) forming three  $sp^2$  hybrid orbital having one electron each. These hybrid orbitals are in same plane with an angle of  $120^\circ$  among them, and form 3  $\sigma$ -bond with nearby atom. The unhybridized 2p orbital ( $2p_z$ ) which does not take part in hybridisation is also having one electron and is perpendicular to  $sp^2$  plane. When this unhybridized  $2p_z$  orbital overlap with another  $2p_z$  orbital of carbon atom then a double bond (or  $\pi$ -bond) is formed by sideways overlapping of the orbitals as shown in figure 1.2.b for ethene molecule. The electron cloud due to formation of  $\pi$ -bond lies above and below the  $\sigma$ -bond plane. Also molecular bond

forms due to overlap of two  $2p_z$  orbital splitting into  $\pi$ -bonding molecular orbital and  $\pi^*$ -antibonding molecular orbital. The resultant  $\pi$ -orbital is lower energy while  $\pi^*$ -orbital is at higher energy than original  $p_z$  orbital as shown in figure 1.2.b. Due to lower energy of  $\pi$ -orbital, in ground state two electrons upcoming from  $p_z$  orbital occupy  $\pi$ -orbital. Likewise, overlapping of two  $sp^2$  orbital give rise to formation of  $\sigma$ -bonding and  $\sigma^*$ -antibonding molecular orbitals and are in lower and higher energy than respective  $\pi$ -orbitals (shown in figure 1.2.b).

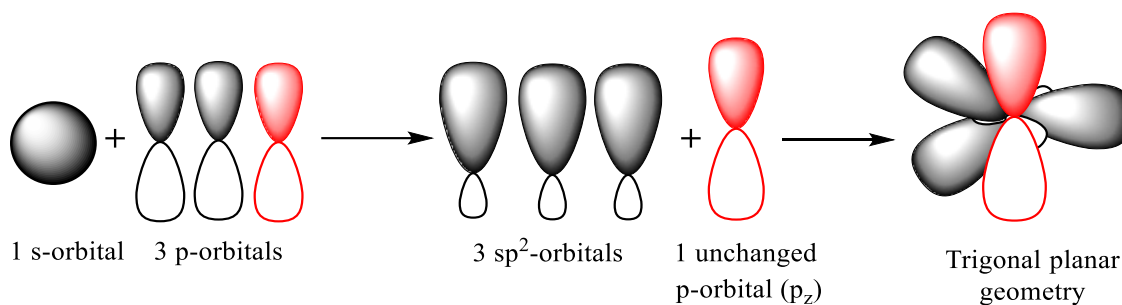


Figure 1.2.a: Representation of  $sp^2$  hybridization of carbon atom

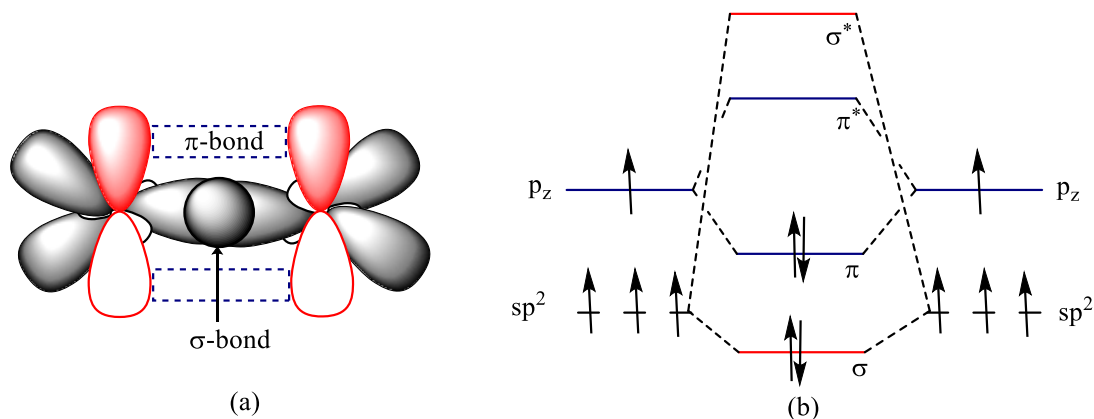


Figure 1.2.b:  $\sigma$ -bond and  $\pi$ -bond formation for two  $sp^2$  hybridized carbon atom

With increase in number of  $sp^2$  hybridized carbon atom results in continuous bands of occupied and unoccupied state. The highest  $\pi$ -bonding molecular orbital is known as highest occupied molecular orbital (HOMO) and lowest  $\pi^*$ -antibonding molecular orbital is known as lowest unoccupied molecular orbital (LUMO). For benzene molecule the HOMO and LUMO are shown in figure 1.3, and energy difference between them is termed as energy gap (HLG). This

energy gap defines some of the semiconductor properties, like for organic conjugated molecule HLG is mainly in between 1.5 eV to 3.0 eV lead to optical transition in visible and NIR region of electromagnetic spectrum [15].

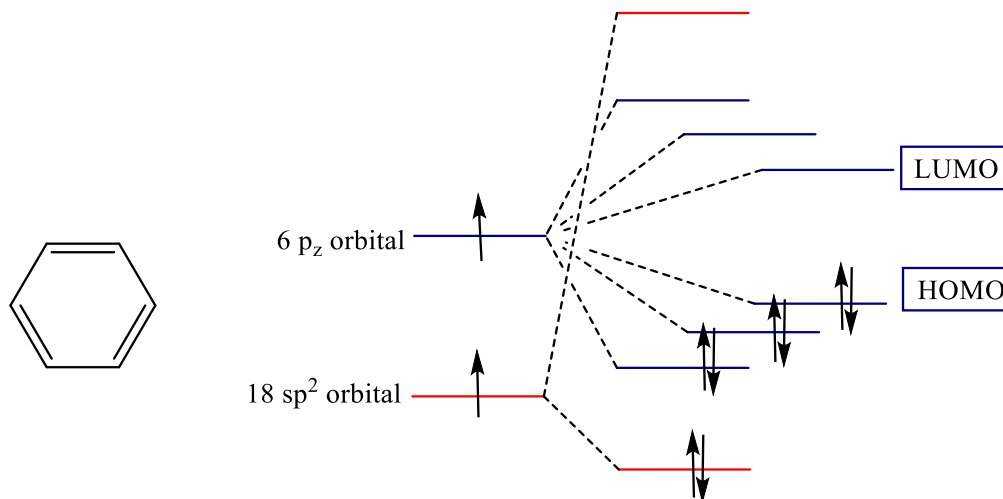


Figure 1.3: Molecular structure of benzene and its energy diagram

#### 1.4. Charge transport properties in Organic Materials

Charge transport properties are directly associated with performance of optoelectronic devices based on OSCs and it is function of chemical structure, their physical and chemical properties and dynamics of materials. Charge mobility ( $\mu$ ) is one of the important characteristics property of a material and it can be measured through time-of-flight (TOF), Field effect transistors (FET), space charge limiting current (SCLC) or time-resolved microwave conductivity (TRMC) [16-20]. One can define mobility by using Einstein relation, and is comes from kinetic theory based on random walk model [21]

$$\mu = \frac{eD}{k_b T} \dots \dots \dots 1.1$$

Here  $e$  is electronic charge,  $D$ ,  $k_b$  and  $T$  are diffusion constant, Boltzmann constant and temperature respectively. To define charge carrier mobility for OSCs from equation 1.1, need to understand charge transport mechanism in OSCs. The two models proposed in literature for charge transport in OSCs which depend on localization of charge carriers are:

##### 1) Band Transport Model

## 2) Hopping Model

In band transport model charge carriers are fully delocalized at edges of valence and conduction band. Here motions of charge carrier are well-correlated and their momentum is well defined. However, in hopping model charge carrier are localized to individual sites due to scattering and movement of charge carrier via thermally activated hops.

### 1.4.1. Band transport Model

As already stated in band model charge carrier are delocalized in bands, i.e. holes are delocalized in valence band while electrons are delocalized in conduction band. In general band model applicable in periodic solids and hence valid for inorganic materials. Though for organic pure crystal showing strong coupling between molecules are also appropriate to this model. Pentacene and other oligoacenes crystals are the examples of organic molecules where band like transport model have been applied [22,24].

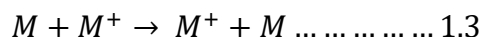
According to band transport model mobility is given by

$$\mu = \frac{e\tau}{m^*} \dots \dots \dots 1.2$$

Here  $e$  is electronic charge,  $\tau$  is relaxation time and  $m^*$  is effective mass of an electron.

### 1.4.2. Hopping Model

The OSCs are classically too disordered to be consider with a band transport model. Therefore, in hopping model it is assumed that charge carrier is localized and moved by thermally activated hops. The sites in hopping models can be defined as individual molecules, a group of molecules, or molecular segments (such as monomer units in a polymer), but they must have weak coupling between them. The charge transport is then described by hopping rates between these sites. Based on the Hopping model for charge transfer, the electron or hole transport process at the molecular level is a transfer reaction between the neighbouring molecule. Taking this model into account, a hole intermolecular transfer can portray in the form of equation-1.3[25]





### 1.4.2.1. Marcus Theory

One of the most popular methods describing charge transport in OSCs is given by Marcus and he provided an equation to calculate rate constant for charge transport in OSCs known as Marcus equation [26, 28]. It is semi-classical theory for determining rate of charge hopping between weakly coupled sites. Though, Marcus made some approximations before describing charge transfer event from site  $i$  to site  $j$ , following are four postulates made by Marcus for describing charge transfer

1. Born-Oppenheimer approximation: The nuclear and electronic motion of molecules can be divided, where the electronic wave function depends parametrically on the nuclear positions.
2. Franck Condon principle: during charge carrier transfer, nuclear coordinates are considered to be invariant.
3. The transition is semi classical so that vibronic energy scale is smaller than the other energy scales, such as the barrier height and the energy difference of the two states.
4. There is weak electronic coupling between sites and a non-adiabatic intersection between potential energy curves, so the interaction between the initial and final states is small enough to be treated as a perturbation.

An outline of derivation as proposed by Jortner et al. is shown below and derivation is started with last approximation (Fermi Golden Rule) [29, 30]

$$k_{ij} = \frac{2\pi}{\hbar} |\langle \psi_i | \hat{H} | \psi_j \rangle|^2 \delta(E_i - E_j) \dots \dots \dots 1.4$$

Where  $k_{ij}$  is rate of hopping between site  $i$  and  $j$ ,  $\hat{H}$  is Hamiltonian and  $\delta(E_i - E_j)$  is infinite small energy difference. Using Born Oppenheimer approximation to split wave function into electronic and nuclear part and assuming perturbation act on electronic part only

$$\langle \psi_i | \hat{H} | \psi_j \rangle = \langle \psi_i | H | \psi_j \rangle \langle \Omega_i | \Omega_j \rangle \dots \dots \dots 1.5$$

Transfer integral ( $J_{ij}$ ) is defined as

$$J_{ij} = \langle \psi_i | \hat{H} | \psi_j \rangle \dots \dots \dots 1.6$$

from eq. 1.5 and 1.6, eq. 1.4 become

$$k_{ij} = \frac{2\pi}{\hbar} |J_{ij} \langle \Omega_i | \Omega_j \rangle|^2 \delta(E_i - E_j) \dots \dots \dots 1.7$$

Further assuming system is in thermal average of vibronic state, and taking sum over initial vibronic state allowing each term by Boltzmann probability in that state gives

$$k_{ij} = \frac{2\pi}{\hbar} |J_{ij}|^2 \sum_{ij} |\langle \Omega_i | \Omega_j \rangle|^2 \delta(E_i - E_j) \exp(-E/k_b T) Z^{-1} \dots \dots \dots 1.8$$

Where  $Z = \sum_i \exp(-E/k_b T)$  is partition function.

In order to simplify above equation  $\delta$  function is treated with Fourier transform and analytical form of vibrational coupling is obtained by assuming that vibrational modes are quadratic and have same angular frequency. Also at high temperature  $\hbar\omega \ll kT$ , and that there is weak coupling  $|J_{ij}| \ll \lambda$ , then equation is reduced to

$$k_{ij} = \frac{|J_{ij}|^2}{\hbar} \sqrt{\frac{\pi}{\lambda k_b T}} \exp\left(-\frac{(\Delta E_{ij} + \lambda)^2}{4\lambda k_b T}\right) \dots \dots \dots 1.9$$

The rate constant ( $k$ ) is for self-exchange reactions in which the standard free energy of the reaction is equal to zero, i.e.  $\Delta E_{ij}=0$ . In reduced form Marcus equation become (removing sites notation  $k_{ij}=K$  and  $|J_{ij}|=\Delta H$ ) and its simpler form is shown in equation 1.10 [28]

$$K = \left(\frac{4\pi^2}{\hbar}\right) \Delta H^2 (4\pi\lambda k_b T)^{-1/2} \exp\left(-\lambda/4k_b T\right) \dots \dots \dots 1.10$$

Here  $K$  is hopping rate,  $\Delta H$  (or  $J_{ij}$ ) is transfer integral between sites,  $\lambda$  is reorganization energy. It is clear from equation 1.10, hopping rate is directly proportional to transfer integral ( $J_{ij}$  or  $\Delta H$ ) and is inversely proportional to reorganization energy ( $\lambda$ ). Literature reports say that calculation of transfer integral is possible only if we have crystal structure of the molecule [31-32]. However, theoretically it is possible to calculate  $\lambda$  and is the leading factor for charge transport in organic molecule.

The Marcus theory has been already applied to organic molecule to calculate charge transport in polymer, p-type (linear acene and oligothiophene) and n-type organic crystal [33-38]. The

disordered OSCs like Alq3, fullerene and DNA segments are also successfully treated with Marcus theory [39-41].

#### 1.4.2.2. Reorganization Energy ( $\lambda$ )

Reorganization energy is the energy related with readjustment in the molecule and their surrounding during charge transport phenomenon and an important factor that governs the charge transport properties. As clear from equation 1.10, lesser the value of  $\lambda$  higher will be the charge transfer rate. Further,  $\lambda$  is comprises of the outer shell (external reorganization energy,  $\lambda_{\text{ext}}$ ) and inner shell (internal reorganization energy,  $\lambda_{\text{int}}$ ) contribution where former arises from a change in the surrounding media and later arises due to change in the geometry of molecules. In total reorganization energy, inner shell contribution is more dominant as compared to outer shell contribution, so here focused only on reorganization energies due to inner shell contribution [42].

Inner shell contribution is a gauge of geometrical distortion from neutral to corresponding cationic/anionic form. Internal reorganization energy ( $\lambda_{\text{int}}$ ) is formulated by four-point method i.e. single point calculations are executed on charged and neutral molecule in charged and neutral geometry [43]. This method accepts that after charge transfer process there is no change in geometry of molecule which means molecule orientation relative to each other does not matter. Let us consider for relaxation of charged and neutral molecule be  $\lambda^*$  and  $\lambda^g$ . According to above mentioned method relaxation of neutral, ( $\lambda^g$ ) and charged ( $\lambda^*$ ) molecule are given by following equation

$$\lambda^g = E^g(M_*) - E^g(M_g) \dots \dots \dots 1.11$$

$$\lambda^* = E^*(M_g) - E^*(M_*) \dots \dots \dots 1.12$$

And total internal reorganization energy is sum of above two equations

$$\lambda_{\text{int}} = \lambda^g + \lambda^* = E^g(M_*) - E^g(M_g) + E^*(M_g) - E^*(M_*) \dots \dots \dots 1.13$$

In the above equations  $E^g$  and  $E^*$  is energy of neutral and charged molecule,  $M_g$  and  $M_*$  is energies are calculated in ground state geometries of neutral and charge molecule.

Further depending on type of charge carriers, reorganization energies are classified as hole reorganization energy ( $\lambda_h$ ) and electron reorganization energy ( $\lambda_e$ ) and if  $\lambda_h < \lambda_e$  then molecule is used for hole transporting materials while  $\lambda_e < \lambda_h$  lead to electron transport materials. For the calculation of hole and electron transport properties in molecule, calculation of hole ( $\lambda_h$ ) and electron ( $\lambda_e$ ) reorganization energies using equation 1.10 and 1.11, respectively

$$\lambda_h = \lambda_1 + \lambda_2 = [E^+(M_0) - E^+(M_+)] + [E^0(M_+) - E^0(M_0)] \dots \dots \dots 1.14$$

$$\lambda_e = \lambda_3 + \lambda_4 = [E^-(M_0) - E^-(M_-)] + [E^0(M_-) - E^0(M_0)] \dots \dots \dots 1.15$$

Here,  $\lambda_1$  is the energy difference between the energy of cation (obtained at ground state neutral molecule,  $E^+(M_0)$ ) and energy of cation molecule in its lowest energy geometry ( $E^+(M_+)$ ),  $\lambda_2$  is the energy difference between the energy of neutral molecule (obtained at optimized cationic state  $E^0(M_+)$ ) and energy of a neutral molecule in its lowest energy geometry ( $E^0(M_0)$ ). Similarly,  $\lambda_3$  is energy difference between the energy of anion (obtained at ground state neutral molecule,  $E^-(M_0)$ ) and energy of anion molecule in its lowest energy geometry ( $E^-(M_-)$ ),  $\lambda_4$  is energy difference between the energy of neutral molecule (obtained at optimized anionic state,  $E^0(M_-)$ ) and energy of neutral molecule in its lowest energy geometry ( $E^0(M_0)$ ). In figure 1.4, a model is shown for calculation of internal reorganization energies.

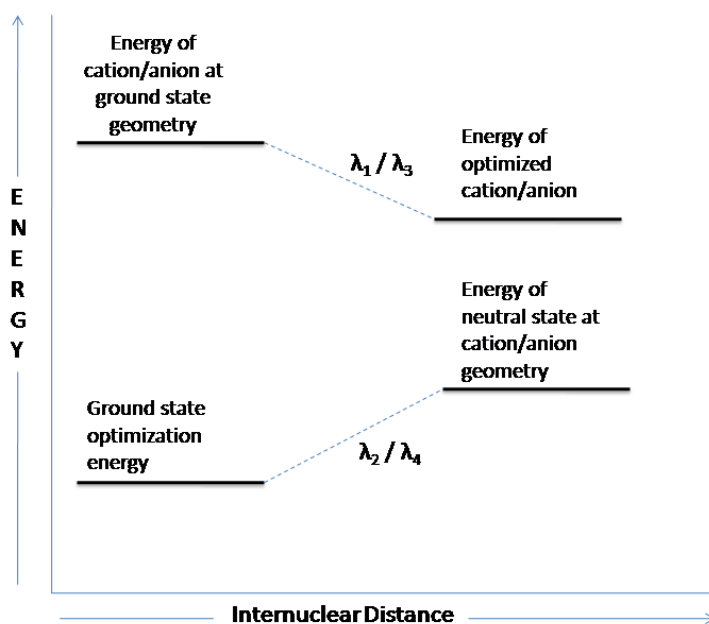


Figure 1.4: Calculation of Internal reorganization energy

Takimiya et al. in one of their reports shows that relation between mobility and reorganization energy is inversely proportional to each other [44]. They considered linear oligoacenes from naphthalene to hexacene, and theoretically computed their hole reorganization energies ( $\lambda_h$ ) for these acenes molecules. In table 1.1, calculated hole mobility and reorganization energies of oligoacenes are shown (results of Takimiya et al.) and it is observed from table on increasing the size of acene  $\lambda_h$  decreases while  $\mu$  increases giving there is inverse relation between  $\lambda_h$  and  $\mu$  i.e.

$$\mu \propto \frac{1}{\lambda} \dots \dots \dots 1.16$$

Table 1.1: Charge transport properties of oligoacenes

————— Decreasing Hole Reorganization Energy —————→

Molecule	Naphthalene	Anthracene	Tetracene	Pentacene	Hexacene
$\lambda_h$ (in meV)	183	138	113	95	79
$\mu$ ( $\text{cm}^2\text{V}^{-1}\text{s}^{-1}$ )	0.05	0.16	0.47	0.83	1.46

←————— Increasing Hole Mobility —————→

#### 1.4.2.3. Examples of hole and electron transport organic materials

As stated above smaller value of  $\lambda_{\text{int}}$  (now referred as  $\lambda$ ) higher will be charge transfer rate which in turns increases the charge transport in molecule. The smaller value  $\lambda$  is appropriate for high performance of OSCs as it helps in both charge separation and charge transport and can be calculated theoretically before actual synthesis of the designed molecule. There are many reports available in literature for hole and electron transport materials which finds applications in OLEDs. Among them renowned materials for hole transport layer (HTL) and electron transport layer (ETL) are diamine derivatives (N,N'-diphenyl-N,N'-bis(3-methylphenyl)-(1,1'-biphenyl)-4,4'-diamine (TPD)) and tris(8-hydroxyquinolino)aluminum(III) (Alq3) respectively. In figure 1.5, examples of few well-known hole and electron transport materials are shown. According to literature reports the hole mobility of TPD, N,N'-bis-(1-naphthyl)-N,N'-diphenylbenzidine (NPD), N,N'-bis(1-naphthyl)-

N,N'-diphenyl-1,1-biphenyl-4,4-diamine (NPB), N,N'-di-1-naphthalenyl-[1,1':4',1'':4'',1'''-quaterphenyl]-4,4'''-diamine(4P-NPD) (shown in figure 1.5) are showing two to three order higher magnitude than typical electron transport materials [45]. In figure 1.5, addition to hole transporting material some well-known electron transport materials for OLEDs are also shown viz. 2,9-dimethyl-4,7-diphenyl-1,10-phenanthroline (BCP), Bphen, tris(8-quinolinolato) aluminum (Alq3), 4-biphenyloxolaluminum(III) bis(2-methyl-8-quinolinato)-4-phenylphenolate (BAIq). The calculated hole ( $\lambda_h$ ) and electron ( $\lambda_e$ ) reorganization energies for TPD and Alq3 are 290 meV and 276meV respectively and are characteristics materials for OLEDs [46-48].

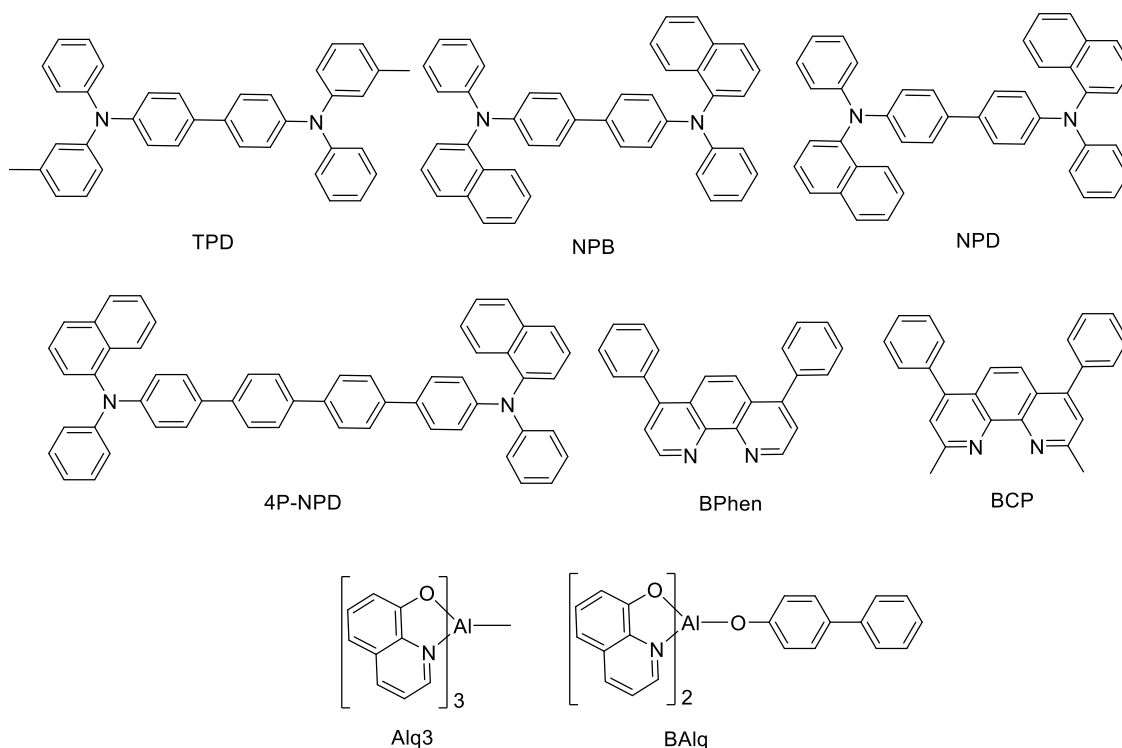


Figure 1.5: Examples of well-known Hole and electron transport materials for OLEDs

#### 1.4.2.4. Charge injection Parameters: Ionization Potential (IP) and Electron Affinity (EA)

In addition to reorganization energy the other properties which affects the efficiency of materials are ionization potential (IP) and electron affinity (EA). For the better performance of the optoelectronic device, there should be an efficient injection of hole and electron into an

organic molecule. The energy barrier for the injection of the holes and electrons were evaluated by IP and EA. IP defined as the energy required by the system when an electron is removed, and it must be sufficiently low for efficient hole injection into the HOMO of the molecule. EA defined as the energy released when an electron is added to the system. EA must be high enough to allow an efficient electron injection into LUMO of the molecule. The lower the IP of the hole-transport layer (HTL), the easier will be the injection of holes from ITO (Indium tin oxide) to HTL, higher the EA of the electron-transport layer (ETL), and easier the injection of electrons from the cathode to ETL. The lower IP and higher EA revealed that material would be a better hole and electron transporter, respectively. The calculated values of adiabatic ( $a$ , optimized structure of both charged and neutral molecule) and vertical ( $v$ , geometry of neutral molecule). In addition to this, calculation of adiabatic and vertical ionization potentials ( $IP_a$  and  $IP_v$ ), and electron affinities ( $EA_a$  and  $EA_v$ ) are formulated by using equation 1.17 and 1.18.

$$IP_a = E^+(M_+) - E^0(M_0) \dots \dots \dots 1.17a$$

$$IP_v = E^+(M_0) - E^0(M_0) \dots \dots \dots 1.17b$$

$$EA_a = E^0(M_0) - E^-(M_-) \dots \dots \dots 1.18a$$

$$EA_v = E^0(M_0) - E^-(M_0) \dots \dots \dots 1.18b$$

Further Hole extraction potential (HEP) and Electron extraction potential (EEP) are also one of the important factor regarding charge injection phenomenon in materials. HEP and EEP are formulated by using equations 1.19 and 1.20 respectively.

$$HEP = E^+(M_+) - E^0(M_+) \dots \dots \dots 1.19$$

$$EEP = E^0(M_-) - E^-(M_-) \dots \dots \dots 1.20$$

### 1.5. Thiophene-based organic materials

The word thiophene has emerged from the fusion of Greek word **theion** (sulfur in Greek) and **phaino** (shining in Greek). The thiophene was first discovered by Victor Meyer in 1883, by isolating it from blue dyes consisting of 1H-indole-2,3-dione (isatin) and sulfuric acid in crude benzene [49]. Thiophene is a colourless stable liquid compound which smells benzene but is more reactive than benzene toward electrophiles due to its high  $\pi$ -electron density, has a five membered planar structure with sulfur as a heteroatom having molecular formula  $C_4H_4S$  [49].

Thiophenes and their derivatives are most basic class of heterocyclic compounds in field of material chemistry. As it is already stated that thiophene is planar, five-member aromatic ring, comprising of sulfur atom heterocyclic compound symbolize important heterocyclic compounds showing interesting electronic properties. Sulfur present in thiophene has formal oxidation state with two lone pair of electron out which one contribute towards ring aromatization. Due to large 3s and 3p orbitals, S-atom has high polarizability which facilitates thiophene electron donating properties and is readily available for non-boding interactions. Also S-atom can expand it octet upon contribution of 3d orbitals and this hypervalency property facilitates functionalization of thiophene sulfur with oxygen to form polythiophene-S,S-dioxides which display strange optical and electrical properties [50].

In the last few years, thousands of research papers on thiophene based compounds are published, and many of them are in the field of material chemistry. Thiophene-based materials are known for their semiconducting nature, nonlinear optical response, luminescence, sensing properties and active charge transport properties. Based on donor ability in the field of semiconducting materials, thiophene and its derivatives are one of the most popular and most studied since 1980s. Due to its ready availability and low cost, a number of small molecules, oligomers and polymers based on thiophene has been reported. Among them, oligothiophenes and polythiophenes have been widely implemented for the generation of organic solar cell building blocks. Oligomers and polymers based on thiophene have attracted considerable attention in both experimental and theoretical aspects. The well-defined physicochemical relationships provide an outstanding synthetic control in their molecular electronic structures through control of the thiophene chain length, and substituent variety (to tune the molecular orbital energies), charge-carrier mobilities, and spectral properties of the individual molecular species. Thiophene based conjugated molecules are an essential area of research as they possess numerous possibilities, such as ring functionalization and chain elongation. The adaptability of thiophene chemistry helps to obtain useful thiophene based chemical structures for organic semiconductors OSCs. Thiophene is selectively modified at  $\alpha$ - and  $\beta$ - position to sulfur atom and even at a sulfur atom itself. This unique property of functionalization in thiophene leads to designing and synthesis of oligomer and polymer that allow fine-tuning of desirable properties for OSCs [51-52]. There is enough literature available for linear, branched



and star-shaped oligomer of thiophene. For example, a combination of  $\alpha$ -linked thiophene unit with oligomer render an effective conjugation, on the other hand, attachment of long alkyl chain at  $\alpha$ - and  $\beta$ -positions increases the solubility.

The semiconducting properties of thiophene-based compounds significantly depend on the degree of  $\pi$ -conjugation in a molecule, which affects frontier molecular orbital (FMO) energies, energy gaps, optical and electronic properties. Thiophene-based compounds are showing exceptionally well optical and conductivity properties than other known OSCs used for electronic applications [53-55]. Among various strategies of synthesizing thiophene-based materials, synthetic chemists are mainly focusing on the tuning of HOMO-LUMO energy levels and energy gap. As energy gap between HOMO-LUMO, i.e. band gap play leading role in defining the physical properties of conducting molecule and hence most of the researcher and scientists have focused on designing and synthesis of those materials by considering structure-property relation of these materials.

## **1.6. Literature survey**

### **1.6.1. Simple and fused thiophene system for organic materials**

It is well reported in literature that  $\alpha$ -linked oligothiophene are among the most well-known p-type  $\pi$ -conjugated materials (shown in figure 1.6 where 'N' can vary from 0-5). They have been used as the core constituents in various optoelectronic and electronic devices such as OPVs, OLEDs, and OFETs, owing to their light-emitting and absorbing, hole transporting, and charge carrier properties. In addition to this due to presence of electropositive sulphur atom, oligothiophene possess multiple intermolecular interactions. The single crystal X-ray diffraction and structure analysis of oligothiophenes proved that there is presence of van der Waals interactions,  $\pi$ - $\pi$  stacking, and a variety of anisotropic oriented donor (D)- acceptor(A) intra- and intermolecular C-H...S, C-H...O, C-H... $\pi$ , and S...S interactions [56-59].

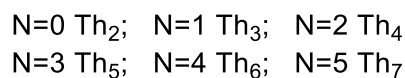
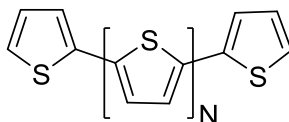


Figure 1.6: Oligothiophene structures (Th<sub>n</sub>)

In order to improve the device performance of OPVs, thiophene-based conjugated oligomers with low band gap, broad absorption and suitable energy levels are necessary. In past few years, numerous donor-acceptor (D-A) oligomers having electron rich thiophenes/oligothiophenes have been developed as donor materials for high performance OPVs [60]. In addition to D-A systems, small acceptor-donor-acceptor (A-D-A) systems are also attracted great interest in recent years due to their excellent photovoltaic performance.

One of the advantageous methods for fine-tuning of bandgap is utilization of fused thiophene which incites a greater conjugation in ground state. It is evident from the literature that fused thiophenes are the most extensively studied heteroatomic compounds due to their stability, electron-donating capability and the possibility to form intermolecular interactions such as S...S bonds [61-65]. Differing from thiophene, fused thiophenes possess rigid structure with extended  $\pi$ -conjugation which helps in altering the bandgap of the organic materials and increasing intermolecular interaction in solid state. The first member of the fused thiophene is thienothiophene (TTs) having two annulated thiophene units. TTs are electron-rich molecule which helps them to construct conjugated and low band gap organic semiconductors materials. Based on the connectivity of two thiophene moiety there are four geometrical isomers of thieno thiophene (molecule **1-4** in figure1.7) are known. The IUPAC nomenclature of the isomers are thieno[3,2-b]thiophene (**1**), thieno[2,3-b]thiophene (**2**), thieno[3,4-b]thiophene (**3**) and thieno[3,4-c]thiophene (**4**). The synthesis and polymerization of all the TTs are known except TT-4 which is unstable. TTs i.e. **1-3** are having stable and electron rich structures and are finds applications as building block in OSCs [49]. Among various isomer of TTs, **3** is having four different functionalization positions which provide unique property of quinoid-resonance effect to this isomer which enable to modulate electronic structure [66].

With the addition of one more thiophene unit to TTs give rise to three thiophene fused system recognized as dithienothiophenes (DTTs, **5** in figure 1.7), and due to flat and rigid structure of DTTs widely used as building block in organic materials. Further addition of thiophene results in thienoacenes which also finds application in various optoelectronic devices. Bis(dithienothiophene) (B-DTT, **6** in figure 1.7) is dimerized version of DTTs and in great example of OSCs. The hole mobility of B-DTTs was measured as high as  $0.05\text{cm}^2\text{V}^{-1}\text{s}^{-1}$  [67-68].

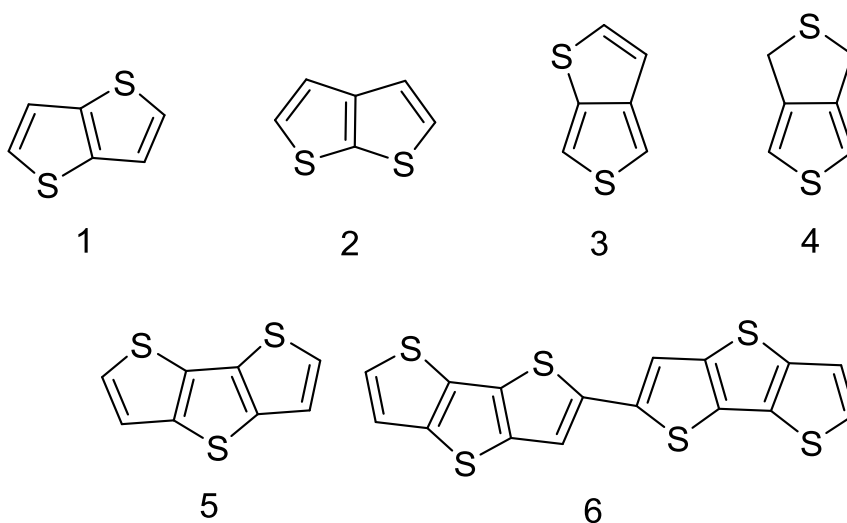


Figure 1.7: Structure of fused thiophenes system thienothiophene (1 to 4) dithienothiophene (5) and bis(dithienothiophene) (6)

Zhang et al. performed computational studies to TT-1 and shown that it as p-type semiconductor by considering it high electron injection carrier [69]. They also shown that on replacing the hydrogen with electron withdrawing group the nature of the semiconductor is reversed i.e. it is showing n-type semiconductor property rather than p-type semiconductor [69]. It is well known that thiophene shows weaker aromaticity than benzene, lower steric hindrance and extra S...S interaction in solid state.

### 1.6.2. Thiophene based fused heteoacene system for organic materials

It is well-reported in literature that applications of linear acenes are classified into two classes of electronic device: (1) field effect transistors (FETs, also known as thin-film transistors, TFTs) and (2) organic light-emitting diodes (OLEDs). Within acenes anthracene (**6** in figure 1.8) due to high oxidation potentials, small surface and high fluorescence quantum yield find

application in light emitting systems. Though recent reports suggest functionalized anthracene and their derivative used for organic field effect transistors. One of the examples is anthracene functionalized with electron withdrawing (4-trifluoromethylphenyl) group behave as an n-type semiconductor, showing electron mobility of  $0.003\text{cm}^2\text{V}^{-1}\text{s}^{-1}$  [70]. However, this mobility is not high but use of anthracene core of semiconductor imparts higher stability and advantages of larger acenes which is the deciding factor in applications of semiconductor where durability is preferred over performance. Also, anthracene derivatives due to their fluorescence features find applications in LEDs (light-emitting diodes) [71-72]. Similarly, higher members of acene, i.e. tetracene (**7** in figure 1.8) and pentacene (**9** in figure 1.8) are also showing good optical and efficient charge transport properties, and are suitable for optoelectronic applications. Rubrene (**8** figure 1.8) is one of the tetracene derivatives, and mixture of it with polystyrene and diphenyl anthracene when deposited on bottom-contact of FET substrate yielded device hole mobility of  $0.7\text{cm}^2\text{V}^{-1}\text{s}^{-1}$  [73]. Among different acenes, pentacene (structure **9** in figure 1.8) is the largest unsubstituted acene which is isolated in its pure form and characterized. It is well-known p-type material in organic solar cells and its thin-film transistor mobility are similar to that of silicon and reported mobilities are in the range of  $1.5\text{cm}^2\text{V}^{-1}\text{s}^{-1}$  to  $5\text{cm}^2\text{V}^{-1}\text{s}^{-1}$  [74-75]. Moreover, pentacene can behave as ambipolar charge transport materials though electron mobility is very low (n-type behavior only observed in vacuum) [76-77]. Although higher member of acene molecules i.e. hexacene, heptacene even octacene and nonacene and their photophysical properties are reported. But electronic and materials properties of these higher acenes are members are not yet explored [78-79].

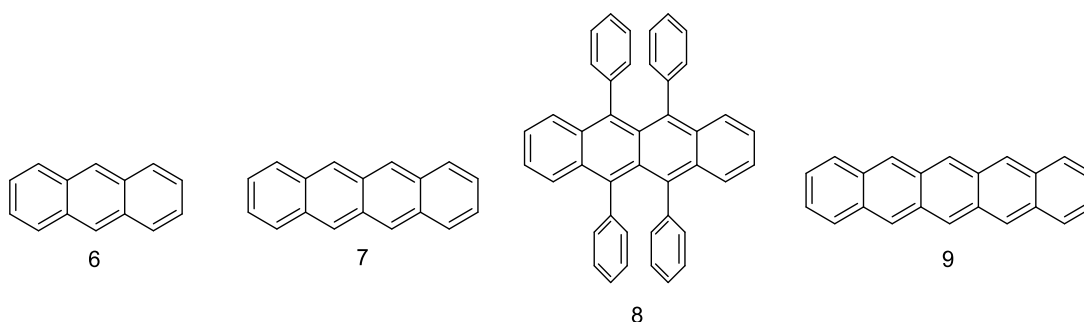


Figure 1.8: Structures of linear acenes as organic materials: anthracene (6), tetracene (7), rubrene (8) and pentacene (9)

Though acenes molecules finds various application in field of material chemistry but these molecules are suffering from several drawbacks like low solubility and poor air stability [80-81]. To overcome these limitations different schemes have been applied by substrate variation and functionalization of the molecular structure [82-84]. Within these techniques alterations higher thienoacenes having five to seven fused system have been synthesized. Recently thienothiophene fascinated more attention due to high mobility and stability in the air. It is evident from the literature that fused thiophenes are the most extensively studied heteroatomic compounds due to their stability, electron-donating capability and the possibility to form intermolecular interactions such as S...S bonds [85-88]. The restricted number of sulfur atom in these compounds results in smaller reorganization energies and hence higher mobilities. This modification process i.e. substitution of different molecular fragment with thiophene and acene inspired scientists and researchers to develop organic semiconductors with high mobility and stability. Among vast number of material developed thienoacenes due to their rigid and planar structures are showing better properties for OSCs devices. Bao and coworkers with the help of computational and experimental characterization shows that proper substitution of thiophene and acenes lead to new high performance organic semiconductor for various electronic applications [89].

K. Takimiya and coworkers introduced a heteroaromatic-benzene system and synthesized number of thiophene fused acene molecules and shown that these molecules are relatively improved air stability with high mobilities ( $\mu=3.0 \text{ cm}^2\text{V}^{-1}\text{s}^{-1}$ ) [90]. They started their study with simple benzodithiophene (BDT, **10**) having three ring fused system and extended up to nine ring fused system i.e. BNTBDT (**17**) [90-94]. Particularly heteroacenes benzodithiophene (BDT, **10**), naphthodithiophene (NDT, **11**) and anthradithiophene (ADT, **12**) are isostructural analogues of anthracene (**6**), tetracene (**7**) and pentacene (**9**) respectively and are building block for polymer and synthetic intermediate for extended heteroacene. Takimiya et al synthesized series of chalcogen based molecules while working on BDT for high performance semiconductor for OFETs [95-96]. They also gave direct synthetic route for linear and angular shaped (NDT, **11**) and showed their applicability in OFETs. It is also found that the linear-shaped NDTs are showing lower oxidation potentials and show red-shifted absorption compared to their angular shaped NDTs and hence promising candidates for organic semiconductors [97]. Among all studied fused acenes, anthradithiophene (ADT, **12**) is the most

studied fused acene by different groups due to structural similarity to pentacene. Katz et al. shown molecule **12** (ADT) and its alkyl derivatives are more soluble and stable than pentacene and exhibit hole mobility like pentacene [98]. After this Mamada et al successfully synthesized syn- and anti-isomer of **12** and shown field-effect mobility of anti-isomer is higher than that of syn-isomer [99].

K. Takimiya performed molecular orbital calculation over several linear thiophene(sexithiophene) and thiophene fused with benzene (BDT, **10** and BTBT, **13**), they showed that there is no contribution of sulfur atom to the HOMO of linear thiophene indicating zero contribution of S-atom to intermolecular HOMO overlap [90, 100]. On the other hand, there is large involvement of sulfur atom to HOMO of BTBT molecule showing effective contribution of sulfur atom. They reported diphenyl derivative of [1]benzothieno[3,2-b][1]benzothiophene (BTBT, **13**) used for working of OFETs which is showing mobility upto  $2.0\text{cm}^2\text{V}^{-1}\text{s}^{-1}$ . After that they synthesized various  $\pi$ -extended BTBT derivatives and estimated as OSCs for OFETs devices. Dinaphtho[2,3-b:2',3'-f]thieno[3,2-b]thiophene (DNTT, **14**) having six aromatic ring gave high performance OFETs with mobilities of  $3.0\text{cm}^2\text{V}^{-1}\text{s}^{-1}$  [91]. Further when long alkyl chain (dodecyl,  $\text{C}_{10}\text{H}_{21}$ ) is attached to this molecule results in stable skeleton with further high hole mobility of  $7.9\text{cm}^2\text{V}^{-1}\text{s}^{-1}$  [93].

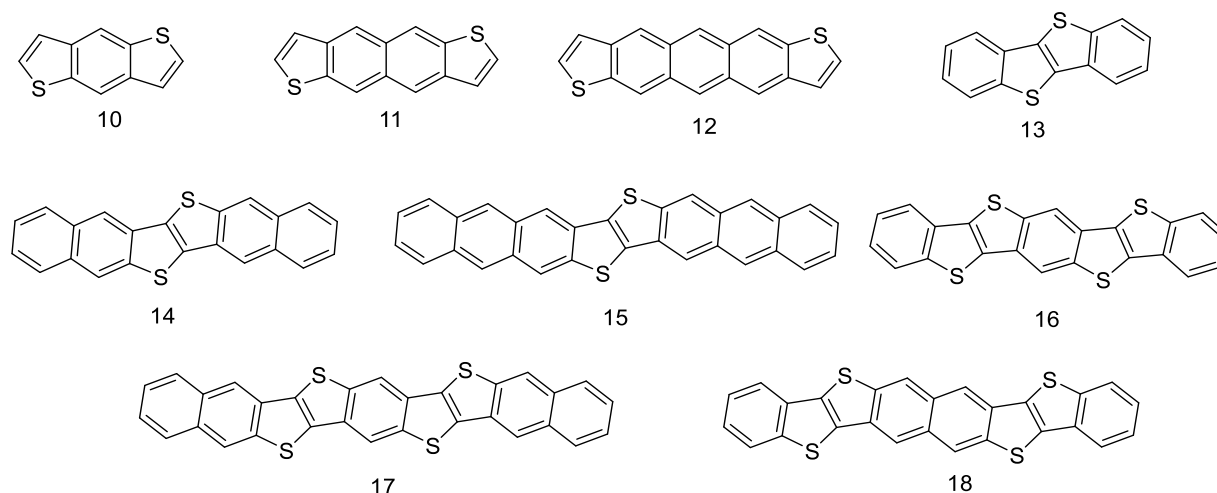


Figure 1.9: Thiophene based fused acene molecules reported by Takimiya group

Neckers et al. reported heteropentacene with sulphur as heteroatom for organic transistor (**19-20** in figure 1.10) [101]. They specifically synthesized thieno bis(benzothiophene) along with their full characterization for materials. Crystallographic analysis of **20** shows molecule crystallize in coplanar arrangement and its observed FET mobility is  $0.12 \text{ cm}^2\text{V}^{-1}\text{s}^{-1}$ . However, its isomer i.e. molecule **19** is showing smaller mobility due to difference in grain size observed upon AFM analysis, molecule **19** is having large grain and poorer surface coverage. Further they also successfully synthesized sulphur containing stable unsubstituted heptacene namely Dianthra-[2,3-b;2',3'-d]-thiophene(DAT-2,3) (**21**) and Dianthra-[1,2-b;1',2'-d]-thiophene (DAT-1,2) (**22**) shown in figure 1.10 with a high degree of charge carrier mobility when assemble with organic transistors. The observed HOMO-LUMO gap for compound **21** and **22** are 2.38eV and 2.26eV respectively which is comparable to pentacene [102].

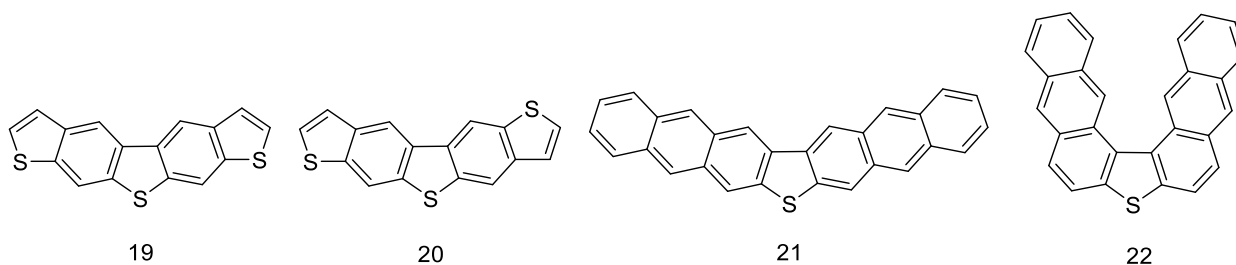


Figure 1.10: Thiophene based pentacene and heptacene molecules reported by Neckers group

In addition to experimental work on thiophene fused heteroacene, a majority of theoretical studies are also performed which give valuable information that compliments the experimental findings. These studies also provide background for the understanding of electronic structures and optoelectronic properties of materials. Sokolov et al [89] consider dinaphtho[2,3-b;2',3'-f]thieno[3,2-b]thiophene (**14**) above as base molecule which is showing high hole mobility and air stability can be used as high performance semiconductor and designed derivatives (**23-28**) of it shown in figure 1.11.

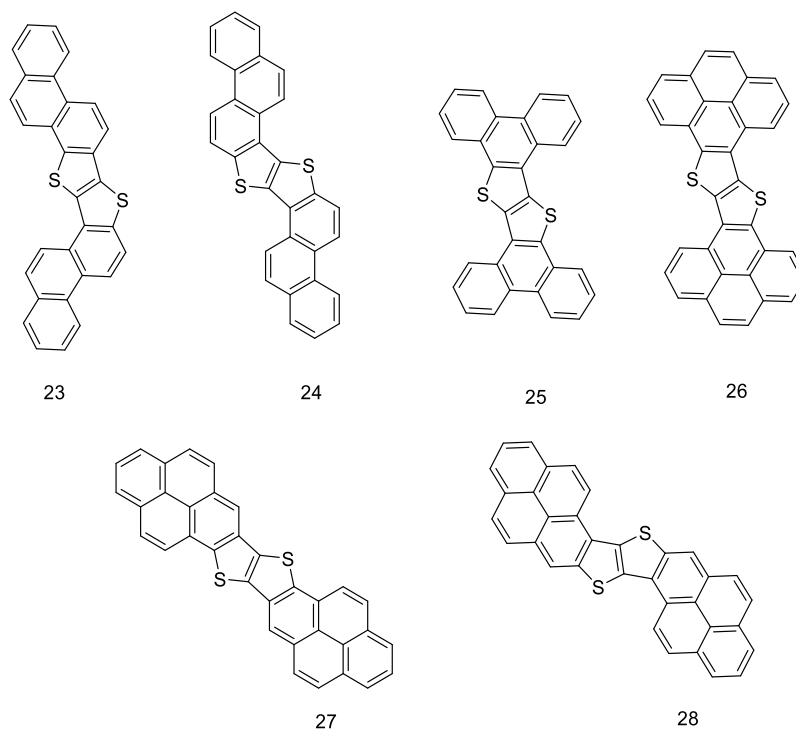


Figure 1.11: Thiophene based linear molecule showing high mobility

Thomas et al. executed computational studies on linear oligothiobenzenes, their positional isomers and shown that the presence of biradicaloid character in molecule possesses small value of hole and electron reorganization energies [103]. They consider positional isomer of thienoacenes (TT **1** and **2**), BDT (**10**), ADT (**11**) and tetradithiophene and also compare their studies with structural analogues of linear oligoacene (**6**, **7** and **9**).

### 1.6.3. Star-Shaped Thiophene based organic materials

Star-shaped organic molecules have number of advantage over linear oligomer and polymer organic molecules including capability of determine multifunctionality and multidimensionality in a molecule. Also solubility problem is totally solved under star shaped framework which is one of the major problems in linear oligothiophene. Recent progress in OSCs shows that star-shaped molecules are promising class of semiconducting materials. Ponomarenko et al. for the first time reported synthesis of star shaped oligothiophene having three armed structure shown in figure 1.12. They well described semiconducting characteristics for solution processible OFETs. Though these star shaped materials are showing lower



mobility than linear analogs but better solubility and film forming properties lead to improve spin coating process in OFETs [104].

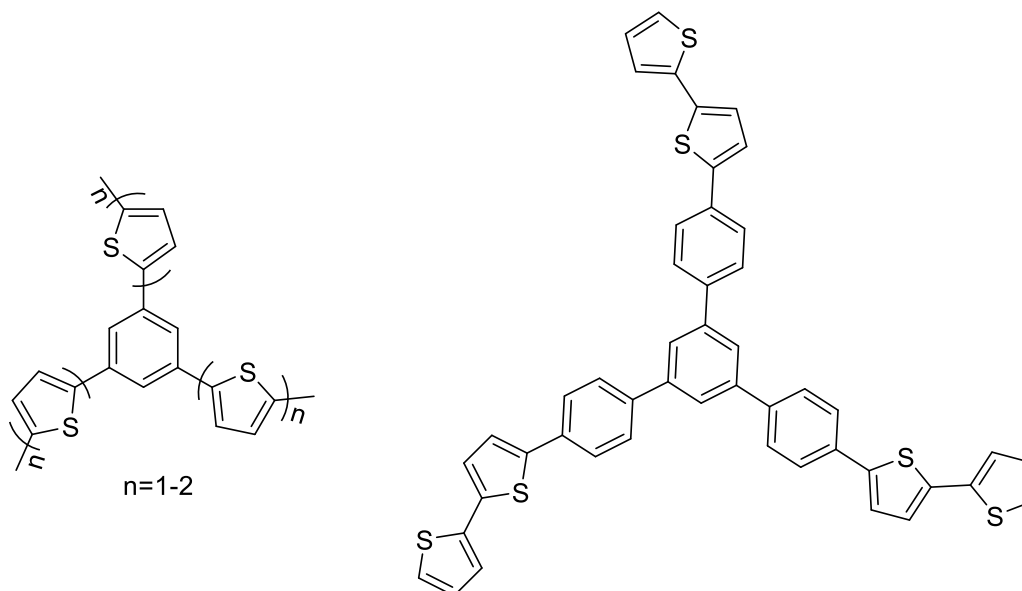


Figure 1.12: Star-shaped oligothiophene synthesized by *Ponomarenko et al.*

In another report Pie et al. reported facile synthesis a number of  $C_3$ -symmetric star-shaped polycyclic based on truxene core (shown in figure 1.13) [105]. They successfully synthesized long branches up to four thiophene ring in truxene core via Suzuki cross coupling and yield of the products is excellent. They reported absorption and emission properties of synthesized compounds and can be further tuned by introduction of thiophene rings [105]. In continuation to Pie work, Sun et al. reported OFETs devices performances to these truxene derivatives. They presented that there is significant change in OFETs characteristics with increase in thiophene ring in branch which not only extends delocalization but also lead to high mobility than previous reports of Ponomarenko on star-shaped molecule [106]. In this perspective, Roncali and their coworkers synthesized new series of star-shaped oligothiophenes having short linear oligothiophene branch connected to central benzotrithiophene (BTT) core (shown in figure 1.13). They compare electronic properties of synthesized compounds with linear analogues and other know star-shaped oligothiophene and showed use of BTT as central core allows evolution of new planar star-shaped conjugated system with greater  $\pi$ -electron delocalization [107]. Kim et al. synthesized three star-shaped thiophene based molecule having good

solubility and good self-film-forming properties. The synthesized molecules are showing high carrier mobility in solution processed OSCs for OFETs (shown in figure 1.13) [108].

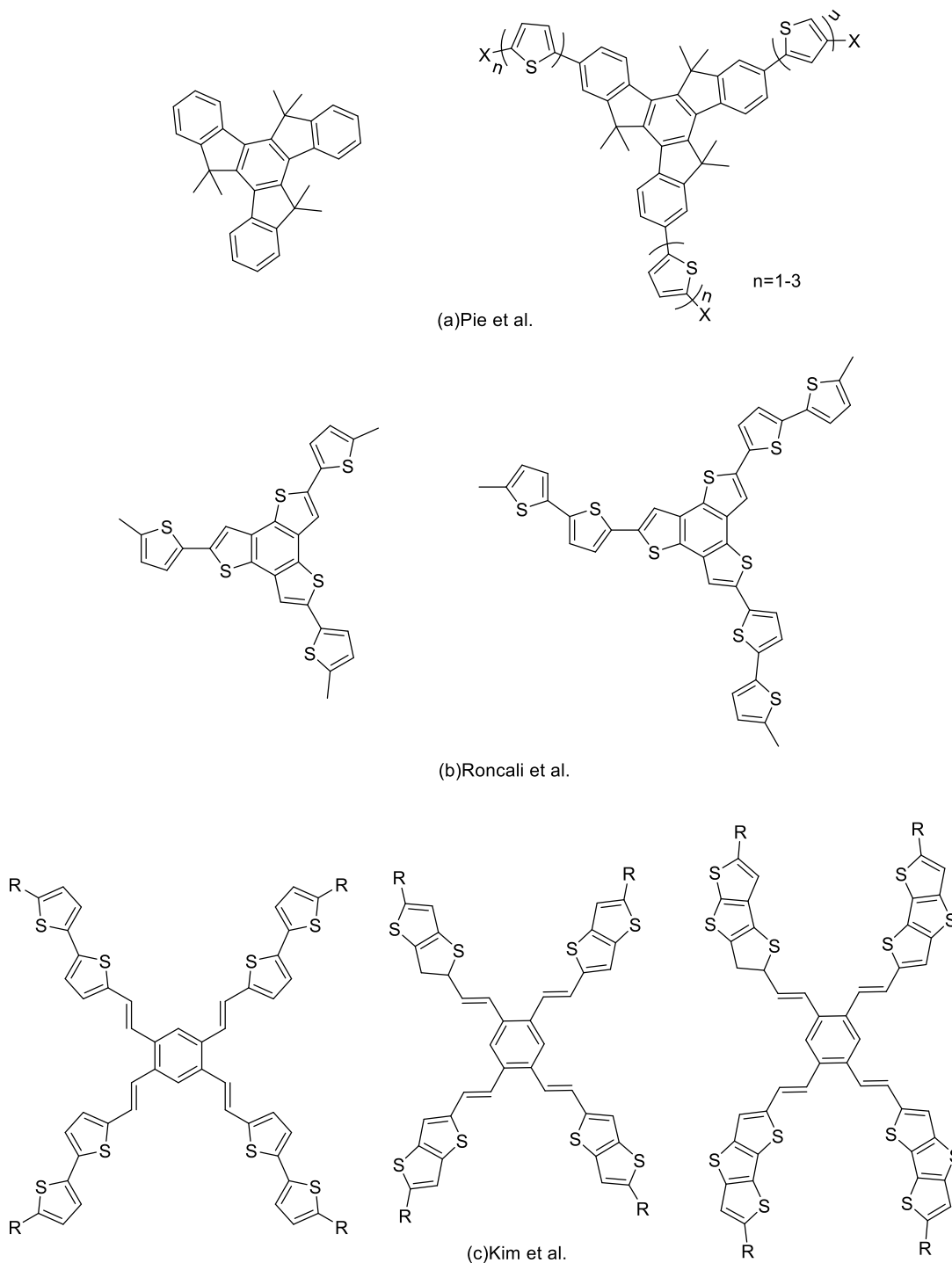


Figure 1.12: Reported star-shaped thiophene based molecules by (a) Pie; (b) Roncali; and (c) Kim

In addition to experimental results, many theoretical studies on thiophene based star-shaped molecules are also available in literature. Ruifa Jin a theoretical and computational chemist while working on series of D- $\pi$ -A type star-shaped molecules reveal that properties designed molecules finds applications in OLEDs and solar cells [109-110]. The various properties of designed molecules like optical, electronic and charge transport are investigated by using DFT methodology. They designed D- $\pi$ -A type molecule with triazine as central core, thiophene and furan as  $\pi$ -spacer and used various aromatic derivative as end group (shown in figure 1.14). Their results disclose that aimed molecules are better for hole and electron transport materials and work for donor material in organic solar cells and also luminescent material for OLEDs [111]. In one of their other reports for star-shape molecule they selected triphenylamine as core with different  $\pi$ -conjugated spacers having naphthalimide as end group (figure 1.14) [112].

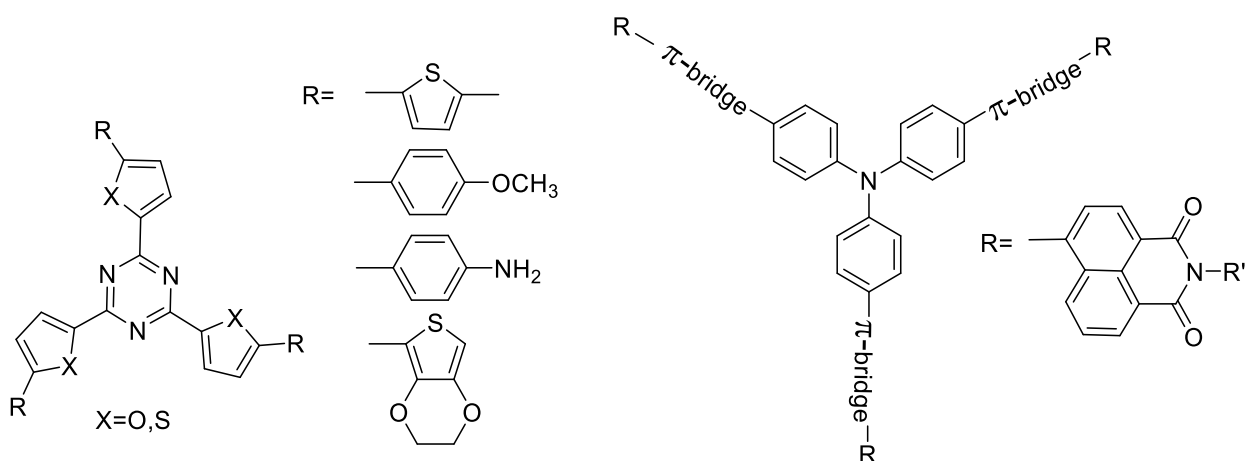


Figure 1.13: Designed star-shaped thiophene based molecules by R. Jin for organic solar cells and OLEDs

### 1.7. Theoretical methods

In recent times theoretical and computational methods has attracted researchers and scientists in order to search for low band gap materials which are applicable for OSCs devices. These theoretical techniques help to explore new methodologies in pushing the efficiency further toward the theoretical limit. The one of the main advantage of theoretical methods are these models are good enough to rule out those molecular systems which are incompatible for future use. This information from these models are very useful as synthesis of any compound/molecule/polymer material involve raw materials and months of labor of

researchers. Hence theoretical method will provide essential information and methodology for careful designing of materials for various applications with desirable optical and electronic properties.

Today there are number of quantum chemical methods are available to find out total energy to predict molecular structures. The well-known quantum methods are *Ab initio* methods, Semi-empirical and empirical methods, molecular mechanics, molecular and chemical dynamics, Density functional methods etc. are shown in fig. 1.15, among various methods reported above density functional theory (DFT) is the most used and useful method for organic molecules

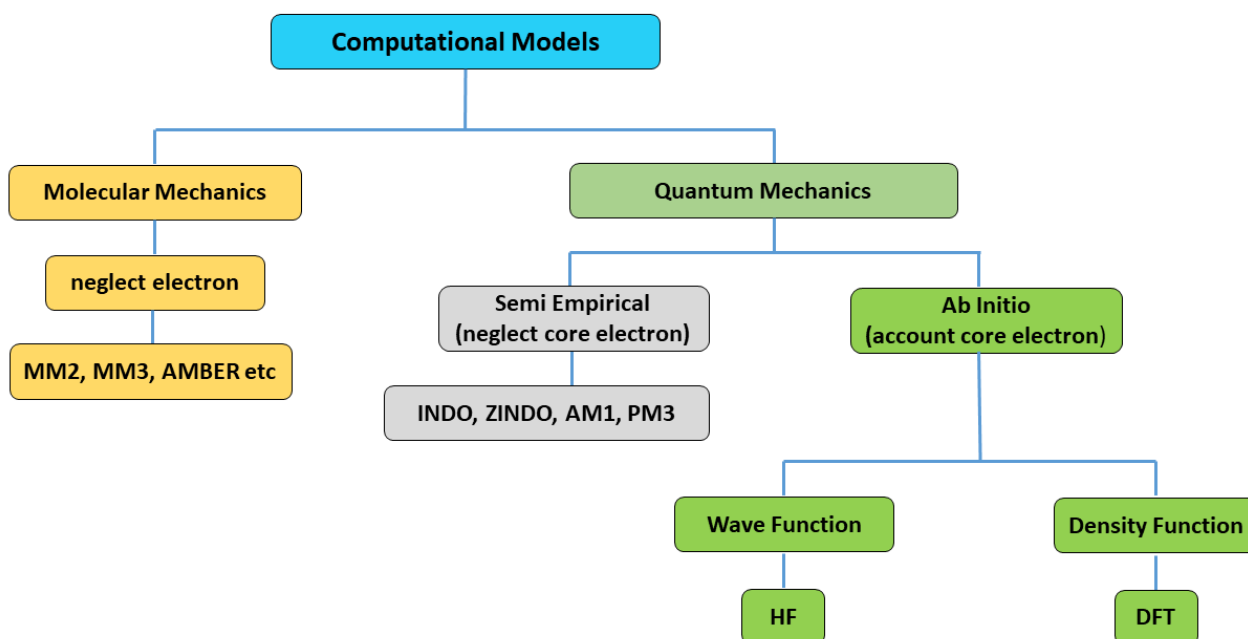


Figure 1.14: Flowchart for different Computational approaches

### 1.8. Density Functional Theory (DFT)

DFT define the electronic structure of connected many body systems. It is based on principle that property of system can be seen as functional of ground state electron density. By knowing exact functional, DFT can predict an exact solution for ground state energy. However, for a system with more than one electron there are no exact functional are known but work of Kohn and Sham has acceptable ground state functionals of many electrons to be estimated [113].

Before DFT came into existence, energies of the molecules are calculated by Hartree Fock (HF) and post Hartree Fock methods in quantum mechanics. These methods are time consuming as first they need to solve Schrodinger equation and to over-come these problems DFT methods are introduced based on electron density rather than wave function [114].

The time dependent Schrödinger equation for ground state  $\Psi_0$  in operator form written as

$$(\hat{T} + \hat{E}_{en} + \hat{V}_{ee} + E_{nn})\psi_0 = E_0\psi_0 \dots \dots \dots .1.21$$

Here, T is kinetic energy operator,  $E_{en}$  and  $V_{ee}$  are electron-nuclear and electron-electron interaction operator and  $E_{nn}$  is nuclear-nuclear interaction energy.

In DFT electron density is defined as

$$n(r) = \int |\psi(r_1, r_2, \dots, r_N)|^2 \sum_i \delta(r - r_i) dr_1 dr_2 \dots dr_N \dots \dots \dots .1.22$$

According to variational principle for the minimum value of energy functional, electron density  $n(r)$  is equal to ground state electron density  $n_0(r)$  and hence ground state energy functional is ground state electron density i.e.

$$E_0 = E[n_0] = \text{Min}\langle\psi|E|\psi\rangle = \langle\psi_0|E|\psi_0\rangle \dots \dots \dots .1.23$$

Hohenberg and Kohn in 1964 gave the theorem which provides the existence of exact DFT, which states that the electronic density uniquely determines the ground state energy of a molecule. After this, Kohn and Sham introduced the equation which gives the exact wave function. In Kohn Sham methodology energy functional is defined as [115]

$$E[n] = T[n] + E_H[n] + E_{en}[n] + E_{nn} + E_{xc}[n] \dots \dots \dots .1.24$$

Where

- $T[n]$  is KE functional and is ground state KE of gas of non-interacting electron.
- $E_H[n]$  is Hartree energy functional which is average field energy of electron.
- $E_{en}[n]$  is electron-nuclear functional.
- $E_{nn}$  is nuclear interaction energy.
- $E_{xc}[n]$  is exchange correlation functional, and origin of this term due to fact that for given electron at position  $r_0$ , other electrons are kept away because of both the

necessary antisymmetric of wave function (exchange) and Coulomb repulsion (correlation).

Among above mentioned five term, four are calculated exactly, but fifth term i.e. exchange-correlation functional due to many-body system must be approximated. For the correctness of ground state energy and density is estimated from the exchange-correlation functional are introduced.

## 1.9. Outline of Thesis

In this dissertation, a computational study on optoelectronic and charge transport properties of thiophene based linear and star shaped organic materials with the help of DFT methodology. Further to make study broader, comparison of optical and transport properties is done with their heteroatomic (NH, O, Si and Se) analogues (wherever possible). Principally, chapters are divided on the basis of number of heterocycle (mainly thiophene) fused with benzene, starting with dithiophene in chapter 2, trithiophene in chapter 3 and 4 and tetrathiophene in chapter 5. All the calculation part in the thesis, like geometry optimization, TDDFT calculations and calculation of charge transport properties are performed by using **GAUSSIAN 16** package [116].

In **Chapter 2**, study start with linear thiophene based acene and their heteroatomic (O and Se) based acene molecules. Results shows in chalcogen based acene molecules, there is improvement in charge transport properties with thiophene and selenophene based acene molecule as compare to furan based acene molecule.

**Chapter 3** is subdivided into two subchapters, in first part of chapter i.e. **Chapter3A**, DFT study on optical and charge transport properties of seven possible isomers of benzotrithiophene (BTT) has been performed. In second part of chapter i.e. **Chapter 3B**, computational study of the star-shaped oligomer of most stable isomer of BTT has been consider for study.

**Chapter 4** is extension of chapter 3 and is further subdivided into two subchapters. **Chapter 4A** deals with comparative study of heteroatomic analog of BTT isomers i.e. benzotripyrrole (BTP), benzotrifuran (BTF) and benzotriselenophene (BTSe) isomers. Here comparative study of optical and charge transport properties of heteroanalog i.e. BTP, BTF and BTSe isomers with BTT isomers are done with the help of computational methods. In second part i.e.

**Chapter 4B**, comparative study of star-shape thiatruxene, truxene and their heteroatomic (O, Si and NH) analog has been done using computational methods.

Lastly, **Chapter 5** deals with influence of heteroatom on electronic excitations and charge transport properties of Anthratetrathiophene (ATT) and Anthratetrathiazole (ATTz) isomers. Additionally, effect of thiophene and thiazole moiety having different arrangements at the periphery on various properties are also studied in this chapter.

---

**References**

1. J. Zaumseil, H. Sirringhaus, *Chem. Rev.* **2007**, 107, 1296.
2. A. Facchetti, *Mater. Today* **2013**, 16, 123.
3. C. J. Brabec, *Sol. Energy Mater. Sol. Cells* **2004**, 83, 273.
4. D. Elkington, N. Cooling, W. Belcher, P.C. Dastoor, X. Zhou, *Electronics* **2014**, 234.
5. Y. Ohmori, M. Uchida, K. Muro, K. Yoshino, *Solid State Commun.* **1991**, 80, 605.
6. Q. D. Liu, R. X. Peng, S. J. Chen, L. Ai, S. Y. Wang, Z. Y. Liu, Z. Y. Ge, *Macromol. Chem. Phys.* **2014**, 215, 1287.
7. A. Facchetti, *Mater. Today* **2007**, 10, 28.
8. S. R. Forrest, *Nature* **2004**, 428, 911.
9. M. M. Torrent, C. Rovira, *Chem. Rev.* **2011**, 111, 4833.
10. O. Ostroverkhova, *Chem. Rev.* **2016**, 116, 13279.
11. H. Sirringhaus, T. Kawase, R. H. Friend, T. Shimoda, M. Inbasekaran, W. Wu, E. P. Woo, *Science* **2000**, 290, 2123.
12. B. Valeur, *Molecular Fluorescence: Principles and Applications*. Wiley-VCH, **2002**.
13. T. Itoh, *Chem. Rev.* **2012**, 112, 4541.
14. M. Kasha, *Discuss. Faraday Soc.* **1950**, 9, 14.
15. M. Pope, C. E. Swenberg, “*Electronic Processes in Organic Crystals and Polymers*” **1999**.
16. S. A. Choulis, J. Nelson, Y. Kim, D. Poplavskyy, T. Kreouzis, J. R. Durrant, D. D. C. Bradley, *Appl. Phys. Lett.* **2003**, 83, 183812.
17. G. Horowitz, *J. Mat. Chem.* **1999**, 9, 2021.
18. Z. Bao, A. Dodabalapur, A. J. Lovinger, *Appl. Phys. Lett.* **1996**, 69, 4108.
19. Y. Liu, X. Wan, B. Yin, J. Zhou, G. Long, S. Yin, Y. Chen, *J. Mat. Chem.* **2010**, 20, 2464.
20. M. Funahashi, J. I. Hanna, *Adv. Mater.* **2005**, 17, 594.
21. A. Einstein, *Annalen der Physik* **1905**, 322, 1521.
22. A. Troisi, G. Orlandi *J. Phys. Chem. B* **2005**, 109, 1849.
23. Y. C. Cheng, R. J. Silbey, D. A. Da Silva Filho, J. P. Calbert, J. Cornil, J. L. Bredas, *J. Chem. Phys.* **2003**, 118, 3764.



- 
24. A. Kadashchuk, F. Tong, R. Janneck, I. I. Fishchuk, A. Mityashin, E. Pavlica, A. Kohler, P. Heremans, C. Rolin, G. Bratina, J. Genoe, *Phys. Rev. B* **2017**, 125202, 1.
  25. J. L. Bredas, D. Beljonne, V. Coropceanu, J. Cornil, *Chem. Rev.* **2004**, 104, 4971.
  26. R. A. Marcus, *Annu. Rev. Phys. Chem.* **1964**, 15, 155.
  27. R. A. Marcus, *J. Chem. Phys.* **1956**, 24, 979.
  28. R. A. Marcus, N. Sutin, *Biochim. Biophys. Acta Rev. Bioenergy*, **1985**, 811, 265.
  29. K. F. Freed, J. Jortner, *J. Chem. Phys.* **1970**, 52, 6272.
  30. E. Fermi, *Nuclear Physics. Chicago: University of Chicago Press*, **1950**.
  31. S. F. Nelsen, F. Blomgren, *J. Org. Chem.* **2001**, 66, 6551.
  32. S. F. Nelsen, D. A. Trieber II, R. F. Ismagilov, Y. Teki, *J. Am. Chem. Soc.* **2001**, 123, 5684.
  33. C. Poelking, E. Cho, A. Malafeev, V. Ivanov, K. Kremer, C. Risko, J. L. Bredas, D. Andrienko, *J. Phys. Chem. C* **2013**, 117, 1633.
  34. S. Athanasopoulos, J. Kirkpatrick, D. Martinez, J. M. Frost, C. M. Foden, A. B. Walker, J. Nelson, *Nano Lett.* **2007**, 7, 1785.
  35. R. P. Fornari, A. Troisi, *Phys. Chem. Chem. Phys.* **2014**, 21, 9997.
  36. J. Wade, F. Steiner, D. Niedzialek, D. T. James, Y. Jung, D.J. Yun, D. D. C. Bradley, J. Nelson, J. S. Kim, *J. Mater. Chem. C* **2014**, 2, 10110.
  37. S. H. Wen, A. Li, J. Song, W. Q. Deng, K. L. Han, W. A. Goddard, *J. Phys. Chem. B* **2009**, 113, 8813.
  38. Y. Liu, X. Liu, J. Huang, J. Liu, S. Xie, Y. Zheng, *J. Mol. Model.* **2016**, 22, 2.
  39. J. J. Kwiatkowski, J. Nelson, H. Li, J. L. Bredas, W. Wenzel, C. Lennartz, *Phys. Chem. Chem. Phys.* **2008**, 10, 1852.
  40. F. Steiner, S. Foster, A. Losquin, J. Labram, T. D. Anthopoulos, *Mater. Horiz.* **2014**, 2, 113.
  41. K. Senthilkumar, F. C. Grozema, C. F. Guerra, F. M. Bickelhaupt, F. D. Lewis, Y. A. Berlin, M. A. Ratner, L. D. A. Siebbeles, *J. Am. Chem. Soc.* **2005**, 127, 14894.
  42. D. P. McMahon, A. Troisi, *J. Phys. Chem. Lett.* **2010**, 1, 941.
  43. K. Sakanoue, M. Motoda, M. Sugimoto, S. Sakaki, *J. Phys. Chem.* **1999**, 103, 5551.
  44. K. Takimiya, M. Nakano, H. Sugino, I. Osaka, *Synth. Met.* **2016**, 217, 68.
  45. J.H. Jou, S. Kumar, A. Agrawal, T.H. Li, S. Sahoo, *J. Mater. Chem. C* **2015**, 3, 2974.
-

- 
46. M. Malagoli, J. L. Bredas, *Chem. Phys. Lett.* **2000**, 327, 13.
  47. B.C. Lin, C.P. Cheng, Z.Q. You, C.P. Hsu, *J. Am. Chem. Soc.* **2005**, 127, 66.
  48. A. Irfan, R. Cui, J. Zhang, *J. Mol. Struct. Theochem.* **2010**, 956, 61.
  49. M. E. Cinar, T. Ozturk, *Chem. Rev.* **2015**, 9, 3036.
  50. E. J. Dell, B. Capozzi, J. Xia, L. Venkataraman, L. M. Campos, *Nat. Chem.* **2015**, 7, 209.
  51. G. Barbarella, M. Zambianchi, L. Antolini, A. Bongini, *Adv. Mater.* **1993**, 5, 834.
  52. G. Barbarella, F. D. Maria, *Acc. Chem. Res.* **2015**, 48, 2230.
  53. I. F. Perepichka, D. F. Perepichka, “*Handbook of thiophene-based materials: applications in organic electronics and photonics*”. Wiley, Chichester, **2009**.
  54. J. Roncali, *Chem. Rev.* **1992**, 92, 711
  55. R. D. McCullough, *Adv. Mater.* **1998**, 10, 93.
  56. M. Mazzeo, D. Pisignano, L. Favaretto, G. Barbarella, R. Cingolani, G. Gigli, *Synth. Met.* **2003**, 139, 671.
  57. A.W. Hains, C. Ramanan, M.D. Irwin, J. Liu, M.R. Wasielewski, T. J. Marks, *ACS Appl. Mater. Interfaces* **2010**, 2,175.
  58. Y. Kunugi, K. Takimiya, N. Negishi, T. Otsubo, Y. Aso, *J. Mater. Chem.* **2004**, 14, 2840.
  59. E.A. Marseglia, F. Grepioni, E. Tedesco, D. Braga, *Mol. Cryst. Liq. Cryst.* **2000**, 348, 137.
  60. F. Zhang, D. Wu, Y. Xua, X. Feng, *J. Mater. Chem.* **2011**, 21,17590.
  61. T. Lei, J. Pei, *J. Mater. Chem.* **2012**, 22, 785.
  62. X-D. Tang, Y. Liao, H. Geng, Z. G. Shuai, *J. Mater. Chem.* **2012**, 22, 18181.
  63. T. Vehoff, B. Baumeier, A. Troisi, D. Andrienko, *J. Am. Chem. Soc.* **2010**, 132, 11702.
  64. X. Yang, L. Wang, C. Wang, W. Long, Z. Shuai, *Chem. Mater.* **2008**, 20, 3205.
  65. M-X. Zhang, G-J Zhao, *J. Phys. Chem. C* **2012**, 116, 19197.
  66. C. Zhang, X. Zhu, *Acc. Chem. Res.* **2017**, 50, 1342.
  67. X.C. Li, H. Sirringhaus, F. Garnier, A.B. Holmes, S. C. Moratti, N. Feeder, W. Clegg, S. J. Teat, R. H. Friend, *J. Am. Chem. Soc.* **1998**, 120, 2206.
  68. T. Ozturk, E. Ertas, O. Mert, *Tetrahedron*, **2005**, 61, 11055.
  69. Y. Zhang, X. Cai, Y. Bian, X. Li, J. Jiang, *J. Phys. Chem. C* **2008**, 112, 5148.
-

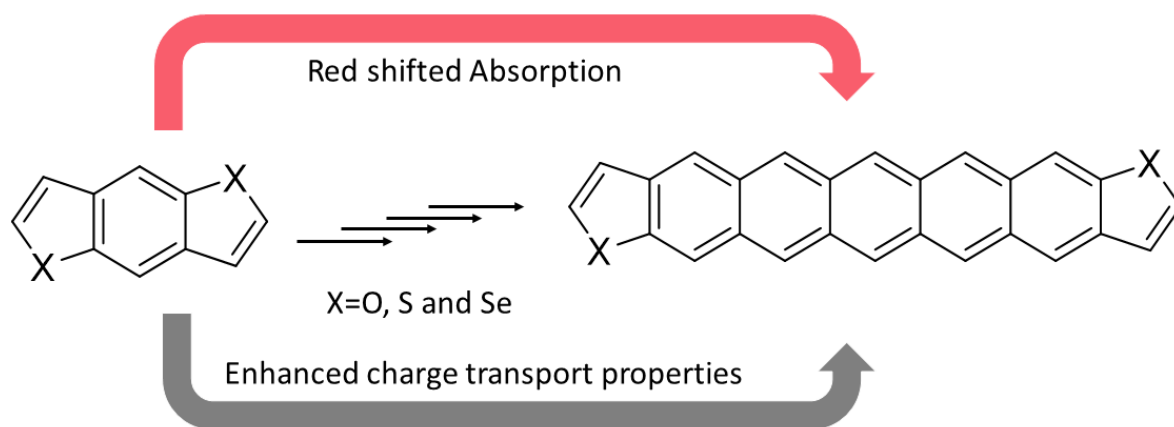
- 
70. S Ando, J. I. Nishida, E. Fujiwara, H. Tada, Y. Inoue, S. Tokito, Y. Yamashita, *Chem. Mater.* **2005**, 17, 1261.
  71. J. Shi, C. W. Tang, *Appl. Phys. Lett.* **2002**, 80, 3201.
  72. H. M. Duong, M. Bendikov, D. Steiger, Q. Zhang, G. Sonmez, J. Yamada, F. Wudl, *Org. Lett.* **2003**, 5, 4433.
  73. N. S. Stutzmann, E. Smits, H. Wondergem, C. Tanase, P. Blom, P. Smith, D. de Leeuw, *Nat. Mater.* **2005**, 4, 601.
  74. Y. Y Lin, D. J Gundlach, S. Nelson T. N. Jackson, *IEEE Trans. Electron Devices* **1997**, 44, 1325.
  75. T.W. Kelley, D. V. Muryres, P. F. Baude, T. P. Smith, T. D. Jones, *Mater. Res. Soc. Symp. Proc.* **2003**, 771, L6.5.1.
  76. E. J. Meijer, D. M. D. Leeuw, S. Setayesh, E. V. Veenendaal, B. H. Huisman, P.W. M. Blom, J.C. Hummelen, U. Scherf, T. M. Klapwijk, *Nat. Mater.* **2003**, 2, 678.
  77. S. Yoo, B. Domercq, B. Kippelen, *Appl. Phys. Lett.* **2004**, 85, 5427.
  78. R. Mondal, B. K. Shah, D. C. Neckers, *J. Am. Chem. Soc.* **2006**, 128, 9612.
  79. C. Tonshoff, H. F. Bettinger, *Angew. Chem., Int. Ed.* **2010**, 49, 412.
  80. M. Yamada, I. Ikemoto, H. Kuroda, *Bull. Chem. Soc. Jpn.* **1988**, 61, 1057.
  81. P. Coppo, S. G. Yeates, *Adv. Mater.* **2005**, 17, 3001.
  82. P. K. De, D. C. Neckers, *Org. Lett.* **2012**, 14, 78.
  83. J. E. Anthony J. S. Brooks, D. L. Eaton, S. R. Parkin, *J. Am. Chem. Soc.* **2001**, 123, 9482.
  84. M. M. Payne, S. R. Parkin, J. E. Anthony, *J. Am. Chem. Soc.* **2005**, 127, 8028.
  85. C. Wang, H. Dong, W. Hu, Y. Liu, D. Zhu, *Chem. Rev.* **2012**, 112, 2208.
  86. T. Lei, J. Pei, *J. Mater. Chem.* **2012**, 22, 785.
  87. X. Yang, L. Wang, C. Wang, W. Long, Z. Shuai, *Chem. Mater.* **2008**, 20, 3205.
  88. K. Takimiya, S. Shinamura, I. Osaka, E. Miyazaki, *Adv. Mater.* **2011**, 23, 4347.
  89. A. N. Sokolov, S. A. Evrenk, R. Mondal, H.B. Akkerman, R. S. S. Carrera, S. G. Focil, J. Schier, S. C. B. Mannsfeld, A. P. Zoombelt, Z. Bao, A. A. Guzik, *Nat. Commun.* **2011**, 2, 437.
  90. K. Takimiya, I. Osaka, T. Mori, M. Nakano, *Acc. Chem. Res.* **2014**, 47, 1493.
-

- 
91. K. Takimiya, H. Ebata, K. Sakamoto, T. Izawa, T. Otsubo, Y. Kunugi, *J. Am. Chem. Soc.* **2006**, 128, 12604.
  92. K. Takimiya, T. Yamamoto, H. Ebata, T. Izawa, *Sci. and Technol. Adv. Mater.* **2007**, 8, 273.
  93. K. Niimi, S. Shinamura, I. Osaka, E. Miyazaki, K. Takimiya, *J. Am. Chem. Soc.* **2011**, 133, 18732.
  94. T. Mori, T. Nishimura, T. Yamamoto, I. Doi, E. Miyazaki, I. Osaka, K. Takimiya, *J. Am. Chem. Soc.* **2013**, 135, 13900.
  95. S. Shinamura, I. Osaka, E. Miyazaki, K. Takimiya, *Heterocycle*, **2011**, 83, 1187.
  96. M. Nakano, K. Niimi, E. Miyazaki, I. Osaka, K. Takimiya, *J. Org. Chem.* **2012**, 77, 8099.
  97. S. Shinamura, I. Osaka, E. Miyazaki, A. Nakao, M. Yamagishi, J. Takeya, K. Takimiya, *J. Am. Chem. Soc.* **2011**, 133, 5024.
  98. J. H. Schon, Ch. Kloc, T. Siegrist, J. G. Laquindanum, H. E. Katz, *Org. Electron.* **2001**, 2, 165.
  99. M. Mamada, H. Katagiri, M. Mizukami, K. Honda, T. Minamiki, R. Teraoka, T. Uemura, S. Tokito, *ACS Appl. Mater. Interfaces* **2013**, 5, 9670.
  100. K. Takimiya, S. Shinamura, I. Osaka, E. Miyazaki, *Adv. Mater.* **2011**, 23, 4347.
  101. B. Wex, B. R. Kaafarani, R. Schroeder, L. A. Majewski, P. Burckel, M. Grell, D. C. Neckers, *J. Mater. Chem.* **2006**, 16, 1121.
  102. K. D. Puran, D. C. Neckers, *Org. Lett.* **2012**, 14, 78.
  103. A. Thomas, R. K. Chitumalla, A. L. Puyad, K. V. Mohan, J. Jang, *Comput. Theor. Chem.* **2016**, 1089, 59.
  104. S. A. Ponomarenko, S. Kirchmeyer, A. Elschner, B. H. Huisman, A. Karbach, D. Drechsler, *Adv. Funct. Mater.* **2003**, 13, 591.
  105. J. Pie, J. L. Wang, X. Y. Cao, X. H. Zhou, W. B. Zhang, *J. Am. Chem. Soc.* **2003**, 125, 9944.
  106. Y. Sun, K. Xiao, Y. Liu, J. Wang, J. Pie, G. Yu, D. Zhu, *Adv. Funct. Mater.* **2005**, 15, 818.
  107. Y. Nicolas, P. Blanchard, E. Levillan, M. Allain, N. Mercier, J. Roncali, *Org. Lett.* **2004**, 6, 273.
-

- 
- 108.K. H. Kim, Z. Chi, M. J. Cho, J. I. Jin, M. Y. Cho, S. J. Kim, J. S. Joo, D. H. Choi, *Chem. Mater.* **2007**, 19, 4925.
- 109.D. Luo, R. Jin, *Mol. Phys.* **2019**, 117, 1825.
- 110.F. Sun, R. Jin, *J. Lumin.* **2014**, 149, 125.
- 111.R. Jin, *C. R. Chimie*, **2015**, 18, 954.
- 112.R. F. Jin, Y. F. Chang, *Phys. Chem. Chem. Phys.* **2015**, 17, 2094.
- 113.R. M. Martin, “*Electronic Structure: Basic Theory and Practical Methods*”. Cambridge University Press, **2004**.
- 114.T. Ziegler, *Chem. Rev.* **1991**, 91, 651.
- 115.W. Kohn, L. J. Sham, *Phys. Rev.* **1965**, 140, A 1133.
- 116.M. J. Frisch, G. W. Trucks, H. B. Schlegel, G.E. Scuseria, M. A. Robb, J. R. Cheeseman, G. Scalmani, V. Barone, B. Mennucci, G. A. Petersson, H. Nakatsuji, M. Caricato, X. Li, H. P. Hratchian, A. F. Izmaylov, J. Bloino, G. Zheng, J. L. Sonnenberg, M. Hada, M. Ehara, K. Toyota, R. Fukuda, J. Hasegawa, M. Ishida, T. Nakajima, Y. Honda, O. Kitao, H. Nakai, T. Vreven, J.A. Montgomery Jr., J.E. Peralta, F. Ogliaro, M. Bearpark, J. J. Heyd, E. Brothers, K. N. Kudin, V. N. Staroverov, R. Kobayashi, J. Normand, K. Raghavachari, A. Rendell, J. C. Burant, S. S. Iyengar, J. Tomasi, M. Cossi, N. Rega, J. M. Millam, M. Klene, J. E. Knox, J. B. Cross, V. Bakken, C. Adamo, J. Jaramillo, R. Gomperts, R. E. Stratmann, O. Yazyev, A. J. Austin, R. Cammi, C. Pomelli, J. W. Ochterski, R. L. Martin, K. Morokuma, V. G. Zakrzewski, G. A. Voth, P. Salvador, J.J. Dannenberg, S. Dapprich, A.D. Daniels, O. Farkas, J. B. Foresman, J. V. Ortiz, J. Cioslowski, D. J. Fox, Gaussian 16, Revision E.01; Gaussian, Inc.: Wallingford, CT, **2016**.

# Chapter 2

## Lowest Electronic Excitations and Charge Transport Properties of Chalcogen (O, S and Se) based Linear Acenes



*Results of this chapter published in J Mol. Struct. 2020, 1203, 127397*







## 2.1. Introduction

Organic semiconductors are needed for this generation as they are having several advantages over inorganic semiconductors. Though power conversion efficiency of organic semiconductors is smaller than inorganic semiconductors but these limitations can be overcome with the low cost, lightweight and producing flexible and large-area devices makes organic semiconductors a better alternative for inorganic materials [1-2]. Between the number of molecular classes reported so far, acenes and heteroacenes are examined as promising candidates for organic semiconductors and find applications in organic photovoltaics (OPVs) and organic field-effect transistors (OFETs) [3-6]. Among acenes, pentacene is well-known p-type organic semiconductor material with a high hole mobility of  $5\text{cm}^2\text{V}^{-1}\text{s}^{-1}$  [7]. But pentacene was suffered from the drawbacks as oxidative instability and poor solubility under ambient conditions [8-9]. The synthetic reports on higher homologous members of pentacene i.e. hexacene, heptacene, octacene, nonacene, decacene and undecacene by different groups have been reported but their applications are still not explored in the field of material chemistry as charge transport materials [10-13]. To overcome these limitations different schemes have been applied by substrate variation and functionalization of the molecular structure [14-16]. It is evident from the literature that fused thiophenes are the most extensively studied heteroatomic compounds due to their stability, electron-donating capability and the possibility to form intermolecular interactions such as S...S bonds [17-21]. Among them benzodithiophene (BDT) and their isomers equivalent to anthracene (three-ring system) are one of the simplest and most studied fused thiophenes. D. C. Neckers et al. synthesized a series of well-defined isomer of pure fused ring system of alternating benzene and thiophene moieties [22-24]. The photophysical properties of synthesized molecules have been reported by using steady-state absorption, fluorescence and phosphorescence spectroscopy [24]. The molecules having S-atom are on the same side (syn-isomer) are showing longer phosphorescence lifetime and higher phosphorescence quantum yield [24]. In recent times, thiophene comprising heteroacene with minor change in the molecular structure of pentacene has been studied intensively due to their potential applications in high-performance organic semiconductor devices like OFETs, OTFTs and OLEDs [25-27]. The design of isostructural and isoelectronic analogues of pentacene such as anthradithiophene, thiotetracene and benzothienobenzothiophene has been reported [28-30]. Katz et al. shown anthradithiophene

(ADT) and its alkyl derivatives are more soluble and stable than pentacene and exhibit hole mobility like pentacene [28]. Further, they also studied the charge transport properties in ADT crystal and compared it with pentacene and  $\alpha$ -sexithiophene to show noticeable two dimensionalities is related to the importance of molecular orbital of sulfur atom obstructing charge transport [31]. M. Mamada et al. successfully synthesized syn- and anti-isomer of ADT and shown field-effect mobility of anti-ADT is higher than that of syn-ADT [32]. K. Takimiya gave direct synthetic route for linear and angular shaped naphthodithiophene (NDT) and showed their applicability in OFETs. It is also found that the linear-shaped NDTs are showing lower oxidation potentials and show red-shifted absorption compared to their angular shaped NDTs and hence promising candidates for organic semiconductors [33]. The direct synthetic route for pure anti-isomer of ADT, anthradifuran (ADF) and anthradiselenophene (ADSe) from dimethoxyanthracene have been reported and verified that isomerically pure anti isomer of ADT shows higher mobility than mixed ADT [34]. Anti-isomers of ADF, ADT and ADSe are shown as an active material for OFET devices which showed mobility up to  $1.3 \text{ cm}^2\text{V}^{-1}\text{s}^{-1}$  [34]. J. E. Anthony group, first time synthesized silylethynyl substituent of acene-thiophene from anthradithiophene to pentadithiophene [35]. Though thiophene and its derivatives are made solid progress and their power conversion efficiency reached up to 10%, but furan and its derivatives are also coming up with promising performance in OPVs due to their low cost and structural specialties [36-38]. Because of smaller size of oxygen than sulfur atom, furan-based polymers show less steric hindrance to adjacent molecule than thiophene based polymer [39]. Further, furan-based oligomers are more electron-rich than corresponding thiophene based oligomers and show a blue shift in absorption [39]. N. Hayashi and coworkers synthesized syn and anti-isomers of BDF and performed a comparative study of their electronic spectra along with their redox behavior and showed that oxidation potential of anti-isomers is significantly higher than corresponding syn-isomers [40]. Recently Thomas et al. executed computational studies on linear oligothienoacenes, their positional isomers and shown that the presence of biradicaloid character in molecule possesses small value of hole and electron reorganization energies [41]. As there are numerous reports on thiophene based acene molecules, yet higher members of thiophene, furan and selenophene based acenes are not investigated for materials applications and because of same basic property, these molecules likewise have same or better (tunable) optical and charge transport properties.

Here in this chapter, we are interested to see the effect of heteroatoms (O and Se) on linearly fused acenothiophenes, starting from three-membered to seven-membered rings. The two possible isomers of each molecule are syn and anti, are considered for the present study shown in scheme 2.1 (S- and A- are used for syn and anti-molecules respectively). The main interest is to study how the electronic and charge transport properties are varying with increasing the size of acenes and also by introducing the heteroatom (O, S and Se).

The nomenclature considered here (scheme 2.1) for thiophene based acenes are; syn- and anti-isomers of benzodithiophene (S-BDT and A-BDT) followed by naphthodithiophene (S-NDT and A-NDT), anthradithiophene (S-ADT and A-ADT), tetracenedithiophene (S-TDT and A-TDT) and pentacenedithiophene (S-PDT and A-PDT). For furan based acenes; syn- and anti-isomers of benzodifuran (S-BDF and A-BDF) followed by naphthodifuran (S-NDF and A-NDF), anthradifuran (S-ADF and A-ADF), tetracenedifuran (S-TDF and A-TDF) and pentacenedifuran (S-PDF and A-PDF). Similarly, for selenophene based acenes: syn- and anti-isomers of benzodiselenophene (S-BDSe and A-BDSe) followed by naphthodiselenophene (S-NDSe and A-NDSe), anthradiselenophene (S-ADSe and A-ADSe), tetracenediselenophene (S-TDSe and A-TDSe) and pentacenediselenophene (S-PDSe and A-PDSe).

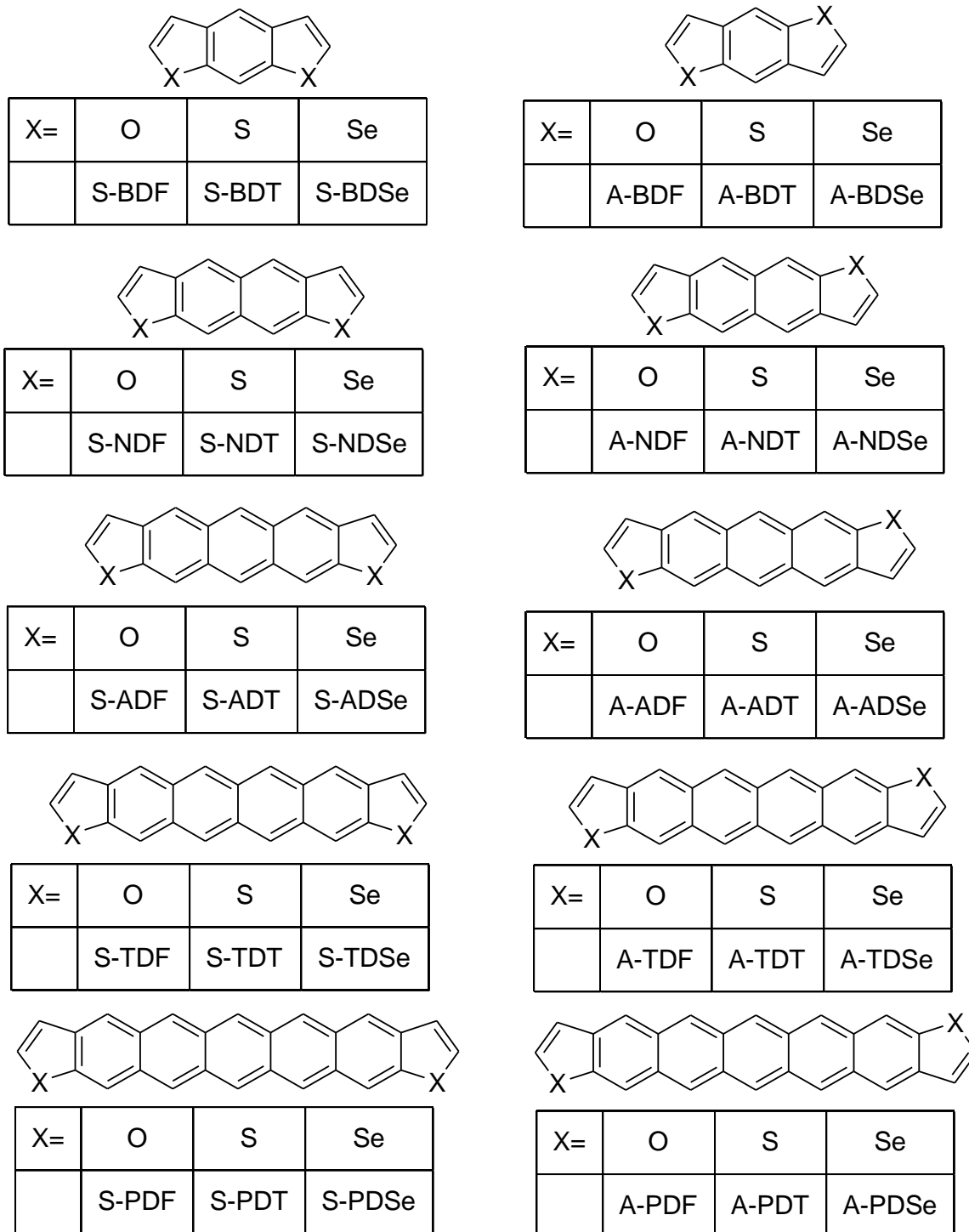
## 2.2. Computational Methodology

All the quantum chemical calculations are performed by using Gaussian16 package (Frisch et al.) [42]. All the molecules considered here were optimized at the DFT level with B3LYP functional and 6-311+G (d, p) basis set. The non-negative frequency of the optimized structures ensures that molecules are at their lowest energy state and hence characterized as true minima state. TDDFT calculations are performed on B3LYP/ 6-311+ G (d, p) optimized geometries to get the absorption energies for the studied molecules.

The calculation of charge transport property is done by using the Marcus theory and Hopping model. This model is known to be suitable for prediction of carrier mobilities of triisopropylsilylethynyl-anthradithiophene (TIPS-ADF) and triisopropylsilylethynyl-anthradithiophene (TIPS-ADT) derivatives along with triisopropylsilyl-ethynylpentacene (TIPS-PENT) [43].

The calculation of hole ( $\lambda_h$ ) and electron ( $\lambda_e$ ) reorganization energies are done by using *equation 1.14* and *1.15* respectively (in chapter 1). Also the calculation of charge injection

parameters i.e. ionization potential (IP) and electron affinity (EA) are done by using *equations 1.17* and *1.18* respectively. Further hole and electron extraction potentials are calculated by *equations 1.19* and *1.20* respectively.



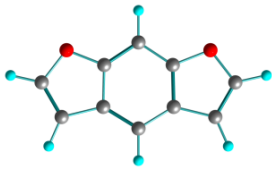
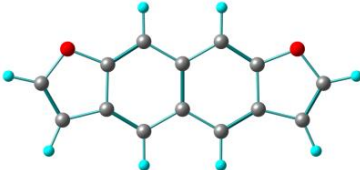
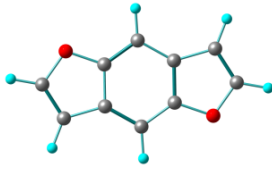
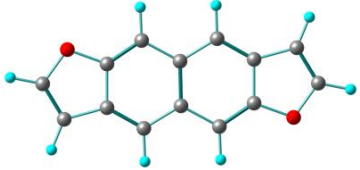
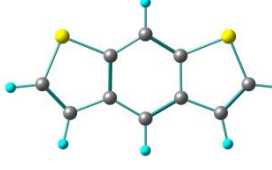
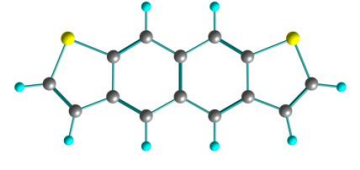
Scheme 2.1: Molecular structures of chalcogen (O, S and Se) based acene molecules

## 2.3. Results and Discussion

### 2.3.1. Geometry and Structures

All the studied molecules are optimized by using B3LYP/6-311+ G (d, p) level of theory shows these molecules possess planar geometry in its ground state (structures of optimized geometries are shown in table 2.1-2.4). Syn-isomers are with  $C_{2h}$  symmetry while anti isomers are with  $C_{2v}$  symmetry. However, the energy difference between both the isomers is very small and both syn- and anti-isomers are approximate of the same energy (less than 1 kcal). S-BDF is 0.39 kcal less stable than A-BDF while for thiophene based acene A-BDT is 0.19 kcal more stable than S-BDT (Table 2.1).

Table 2.1: Optimized Structures and relative energy (RE in Kcal) of benzene and naphthalene based hetero acenes

Name	Structures	RE	Name	Structures	RE
S-BDF		0.40	S-NDF		0.08
A-BDF		<b>0.00</b>	A-NDF		<b>0.00</b>
S-BDT		0.20	S-NDT		0.04

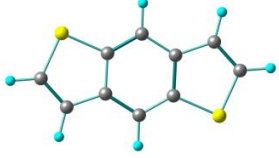
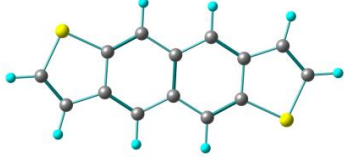
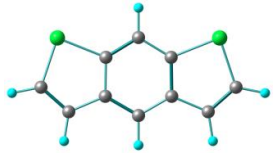
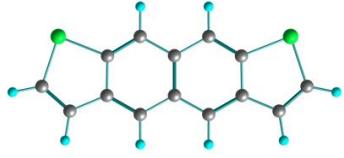
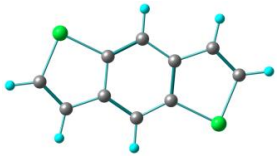
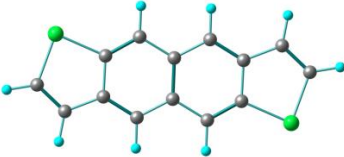
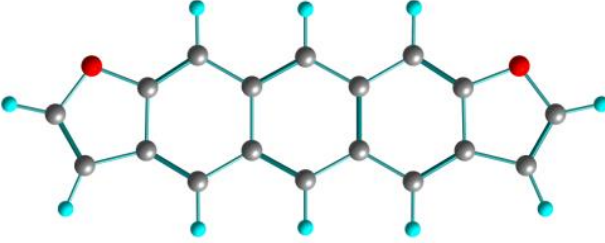
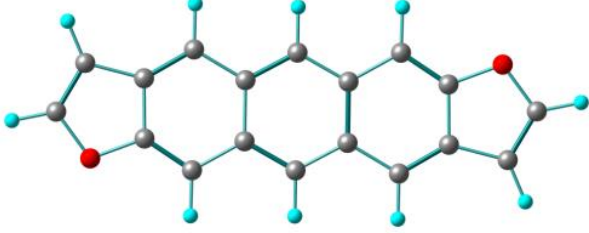
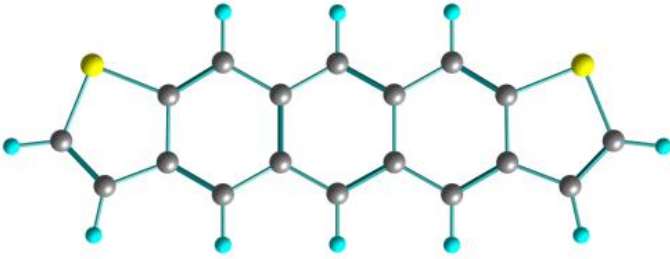
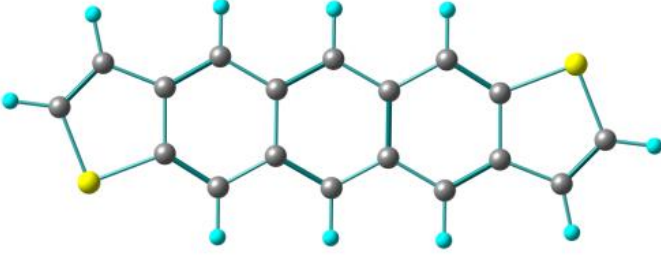
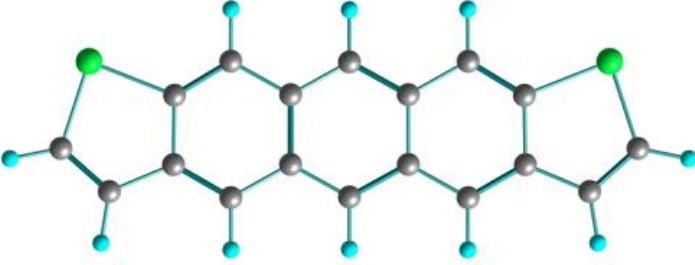
A-BDT		<b>0.00</b>	A-NDT		<b>0.00</b>
S-BDSe		0.16	S-NDSe		0.04
A-BDSe		<b>0.00</b>	A-NDSe		<b>0.00</b>

Table 2.2: Optimized Structures and relative energy (RE in Kcal) of anthracene based heteroacenes

Molecules	Structures	RE
S-ADF		0.04

A-ADF		0.00
S-ADT		0.01
A-ADT		0.00
S-ADSe		0.01

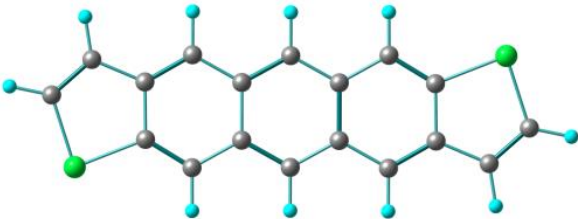
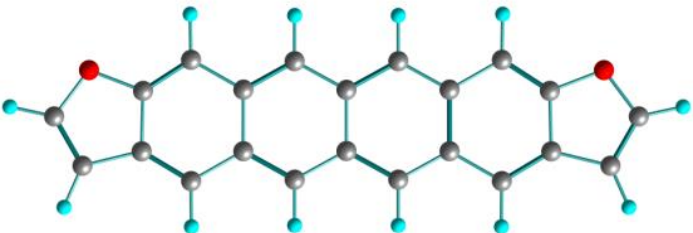
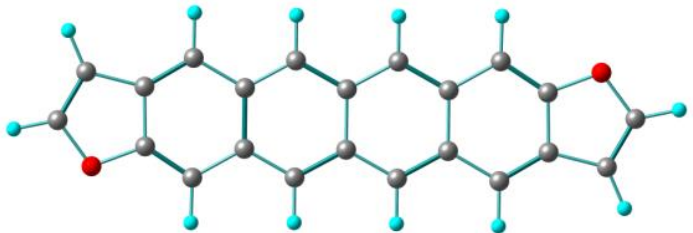
A-ADSe		<b>0.00</b>
--------	--	-------------

Table 2.3: Optimized Structures and relative energy (RE in Kcal) of tetracene based heteroacenes.

Molecules	Structures	RE
S-TDF		0.01
A-TDF		<b>0.00</b>
S-TDT		<b>0.00</b>



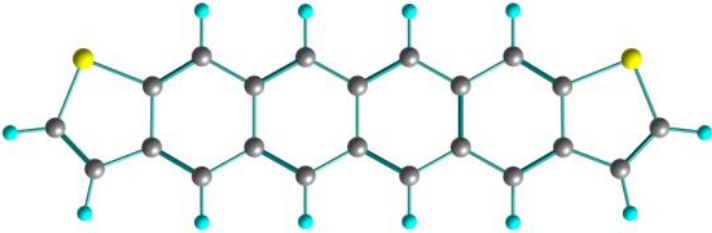
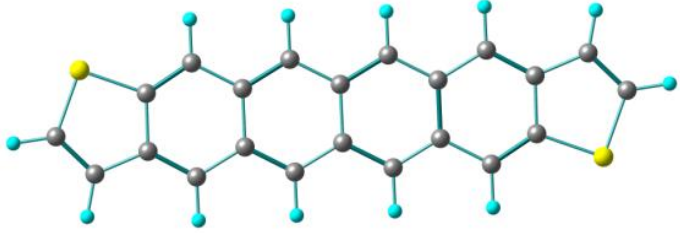
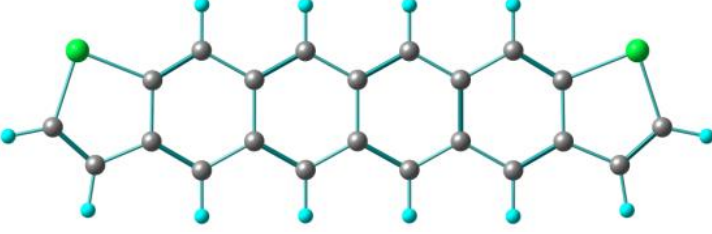
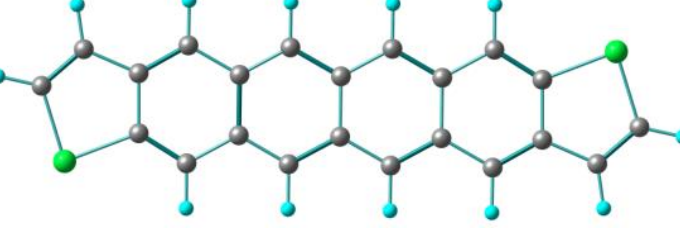
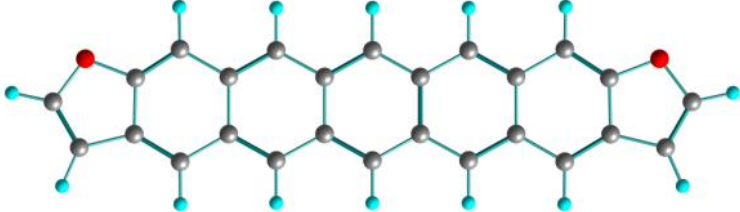
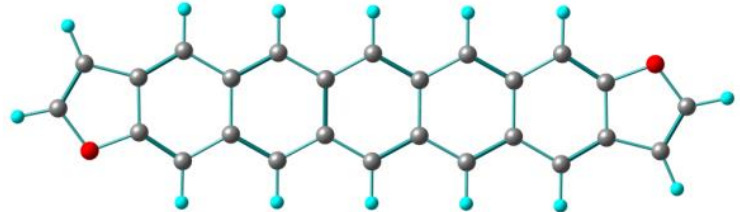
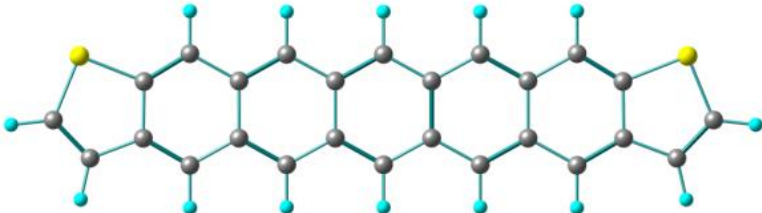
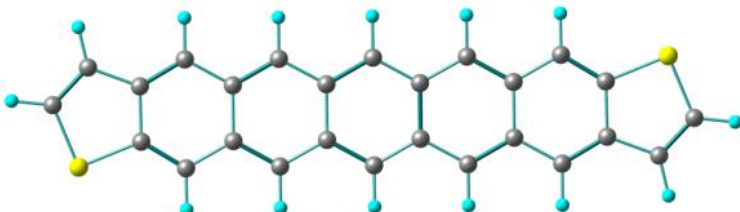
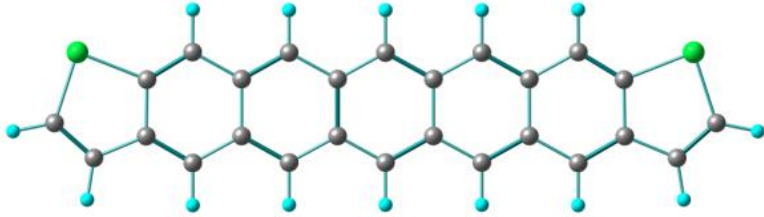
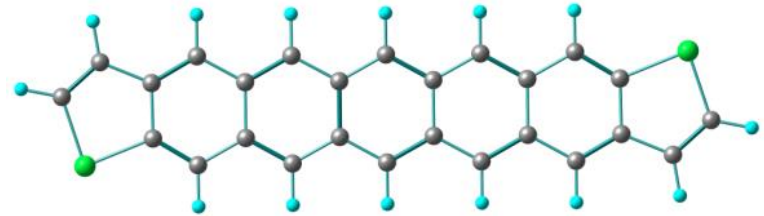
		
A-TDT		0.02
S-TDSe		<b>0.00</b>
A-TDSe		0.02

Table 2.4: Optimized Structures and relative energy (RE in Kcal) of pentacene based heteroacenes.

Molecules	Structures	RE
S-PDF		0.00
A-PDF		0.02
S-PDT		0.02
A-PDT		0.00

S-PDSe		0.03
A-PDSe		<b>0.00</b>

### 2.3.2. Absorption properties

To see the electronic excitations in these molecules, the quantum chemical calculations were performed with TDDFT methodology using TD-B3LYP/6-311+G (d, p) level. In table 2(a and b), tabulated the absorption maxima, oscillator strength, major transitions along with % weight contributions for syn- and anti-isomers. In addition to B3LYP, calculations are also performed with different functionals namely PBE0, BHandHLYP, M062X, B3P86, CAM-B3LYP and WB97XD to see the effect of functional on absorption energies of the studied molecules (shown in table 2.5). Absorption energies from different functionals show that B3P86 and PBE0 are giving similar results like B3LYP and are in agreement with experimental absorption energies, our further discussion of electronic excitations is based on B3LYP functional with 6-311+ G (d, p) basis set.

Table 2.5: Computed lowest electronic excitations ( $\lambda_{\text{CAL}}$  in nm) of anti-isomers with different functionals calculated at B3LYP/6-311+G (d, p) optimized geometries

Molecules	$\lambda_{\text{EXP}}$	$\lambda_{\text{CAL}}$						
		B3LYP	B3P86	PBE0	M062X	BHHLYP	CAM-B3LYP	WB97XD
A-BDF	302, 295 <sup>a</sup>	282	279	275	261	262	265	263
A-BDT	336 <sup>b</sup>	319	317	310	291	285	292	290
A-BDSe	357	333	332	324	302	295	302	301
A-NDF	364 <sup>d</sup>	365	363	355	327	324	330	327
A-NDT	405 <sup>c</sup>	403	402	391	357	351	356	352
A-NDSe	401 <sup>d</sup>	410	409	397	359	352	357	353
A-ADF	453 <sup>d</sup>	475	473	460	415	413	417	410
A-ADT	489 <sup>d</sup> , 488 <sup>e</sup>	514	512	497	444	439	441	432
A-ADSe	481 <sup>d</sup>	515	514	497	441	435	436	427
A-TDF		608	607	587	518	517	516	502
A-TDT		649	649	626	546	544	539	523
A-TDSe		644	644	621	539	535	530	515
A-PDF		768	767	737	636	637	627	603
A-PDT		812	812	779	663	665	649	622
A-PDSe		802	802	769	652	652	637	611

<sup>a</sup> *J. Phys. Chem. A* **2009**, 113, 5342.

<sup>b</sup> *J. Phys. Chem. A* **2006**, 110 13754.

<sup>c</sup> *J. Am. Chem. Soc.* **2011**, 133, 5024.

<sup>d</sup> *J. Org. Chem.* **2012**, 77, 8099.

<sup>e</sup> *ACS Appl. Mater. Interfaces* **2013**, 5, 9670.

Table 2.6: Computed lowest electronic excitations ( $\lambda_{\text{CAL}}$  in nm) of syn-isomers with different functionals calculated at B3LYP/6-311+G (d, p) optimized geometries

Molecules	$\lambda_{\text{EXP}}$	$\lambda_{\text{CAL}}$						
		B3LYP	B3P86	PBE0	M062X	BHHLYP	CAM-B3LYP	WB97XD
S-BDF	305, 299, 292 <sup>a</sup>	276	274	270	256	256	262	260
S-BDT		308	307	299	278	274	279	277
S-BDSe	328 <sup>b</sup>	316	314	306	286	280	288	287
S-NDF		361	359	351	322	320	326	323
S-NDT		399	398	387	352	347	352	348
S-NDSe	410 <sup>c</sup>	404	403	391	352	346	350	346
S-ADF		473	471	458	413	410	415	408
S-ADT	489 <sup>e</sup>	512	512	496	442	438	439	431
S-ADSe		512	512	495	438	433	433	425
S-TDF		607	605	586	512	516	515	501
S-TDT		648	648	625	546	543	538	522
S-TDSe		643	643	619	538	534	529	514
S-PDF		767	766	737	635	636	627	602
S-PDT		811	812	778	663	664	649	621
S-PDSe		801	802	768	651	652	636	610

<sup>a</sup> *J. Phys. Chem. A* **2009**, 113, 5342

<sup>b</sup> *J. Phys. Chem. A* **2006**, 110, 13754

<sup>c</sup> *J. Am. Chem. Soc.* **2011**, 133, 5024

<sup>e</sup> *ACS Appl. Mater. Interfaces* **2013**, 5, 9670

---

It is clear from the table 2.5 and 2.6; anti-isomers of BDF, BDT and BDSe are showing higher absorption (~10-15 nm) than their corresponding syn-isomers. With an increase in the number of benzene rings in heteroacene, the difference in absorption maxima of syn and anti-isomers are close to zero. TDDFT results with B3LYP functional are reproducing the experimental results and hence our further discussion is based on with B3LYP functional. The calculated absorption maxima, oscillator strength, major transitions and % contribution for anti and syn-isomers with B3LYP functional are shown in table 2.7 and 2.8 respectively. The absorption maxima of anti and syn-isomers of NDT are at 403nm and 399 nm respectively and both are arising due to HOMO to LUMO transitions. With the addition of each benzene ring, the absorption maximum shifts drastically towards higher wavelength region. The calculated absorption maximum for A-BDT is 319 nm while A-NDT is at 403nm, there is almost 85nm redshift in absorption with the addition of one benzene ring to BDT. Further addition of one more benzene ring to A-NDT, the absorption maximum red-shifted to 109 nm (i.e. A-ADT, 512nm). Similarly, on moving from A-ADT to A-TDT and A-TDT to A-PDT the difference in absorption maxima are 137nm and 163nm respectively. Similar trends are observed in both furan and selenophene based acene molecules. The absorption spectra for anti-isomers of thiophene, furan and selenophene based acene molecules are shown in figure 2.1-2.3. With the replacement of thiophene with furan ring, a blue shift of approximately 30 nm is the result while replacement of thiophene with selenophene ring results in approximately the same absorption. In figure 2.4, comparative absorption maxima of anti-isomer ADT, ADF and ADSe and PDT, PDF and PDSe are shown.

Table 2.7: Computed lowest electronic excitations ( $\lambda_{\text{CAL}}$  in nm) Oscillator strength ( $f$ ) major transitions (MT) and % weight (%Ci) of anti-isomers at TD-B3LYP/6-311+G (d, p) method.

NAME	$\lambda_{\text{EXP}}$	$\lambda_{\text{CAL}}$	$f$	MT	%Ci
A-BDF	302, 295 <sup>a</sup>	282	0.309	H→L	94
A-BDT	336 <sup>b</sup>	319	0.135	H→L	89
A-BDSe	357	333	0.150	H→L	91
A-NDF	364 <sup>d</sup>	365	0.134	H→L	96
A-NDT	405 <sup>c</sup>	403	0.088	H→L	97
A-NDSe	401 <sup>d</sup>	410	0.088	H→L	97
A-ADF	453 <sup>d</sup>	475	0.087	H→L	99
A-ADT	488 <sup>d</sup> , 489 <sup>e</sup>	514	0.061	H→L	99
A-ADSe	481 <sup>d</sup>	515	0.058	H→L	99
A-TDF		608	0.061	H→L	100
A-TDT		649	0.047	H→L	100
A-TDSe		644	0.045	H→L	100
A-PDF		768	0.045	H→L	99
A-PDT		812	0.037	H→L	100
A-PDSe		802	0.036	H→L	100

<sup>a</sup> *J. Phys. Chem. A* **2009**, 113, 5342

<sup>b</sup> *J. Phys. Chem. A* **2006**, 110, 13754

<sup>c</sup> *J. Am. Chem. Soc.* **2011**, 133, 5024

<sup>d</sup> *J. Org. Chem.* **2012**, 77, 8099

<sup>e</sup> *ACS Appl. Mater. Interfaces* **2013**, 5, 9670

Table 2.8: Computed lowest electronic excitations ( $\lambda_{\text{CAL}}$  in nm) Oscillator strength ( $f$ ) major transitions (MT) and % weight (%Ci) of syn-isomers at TD-B3LYP/6-311+G (d, p) method.

NAME	$\lambda_{\text{EXP}}$	$\lambda_{\text{CAL}}$	$f$	MT	%Ci
S-BDF	305, 299, 292 <sup>a</sup>	276	0.106	H-1→L	75
				H→L+1	23
S-BDT	328 <sup>b</sup>	308	0.037	H→L	95
S-BDSe		316	0.026	H→L	95
S-NDF		361	0.067	H→L	97
S-NDT	410 <sup>c</sup>	399	0.044	H→L	98
S-NDSe		404	0.036	H→L	98
S-ADF		473	0.055	H→L	99
S-ADT	489 <sup>e</sup>	512	0.042	H→L	99
S-ADSe		512	0.036	H→L	99
S-TDF		607	0.045	H→L	100
S-TDT		648	0.036	H→L	100
S-TDSe		643	0.034	H→L	100
S-PDF		767	0.036	H→L	100
S-PDT		811	0.031	H→L	100
S-PDSe		801	0.030	H→L	100

<sup>a</sup> *J. Phys. Chem. A* **2009**, 113, 5342

<sup>b</sup> *J. Phys. Chem. A* **2006**, 110, 13754

<sup>c</sup> *J. Am. Chem. Soc.* **2011**, 133, 5024

<sup>e</sup> *ACS Appl. Mater. Interfaces* **2013**, 5, 9670



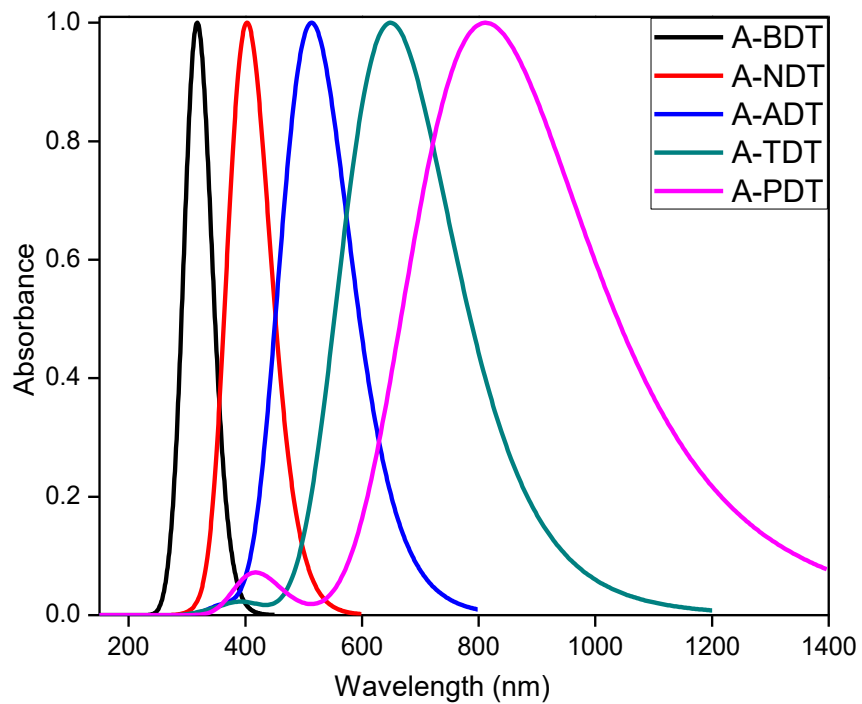


Figure 2.1: Normalized absorption spectra of anti-isomers of thiophene based acenes

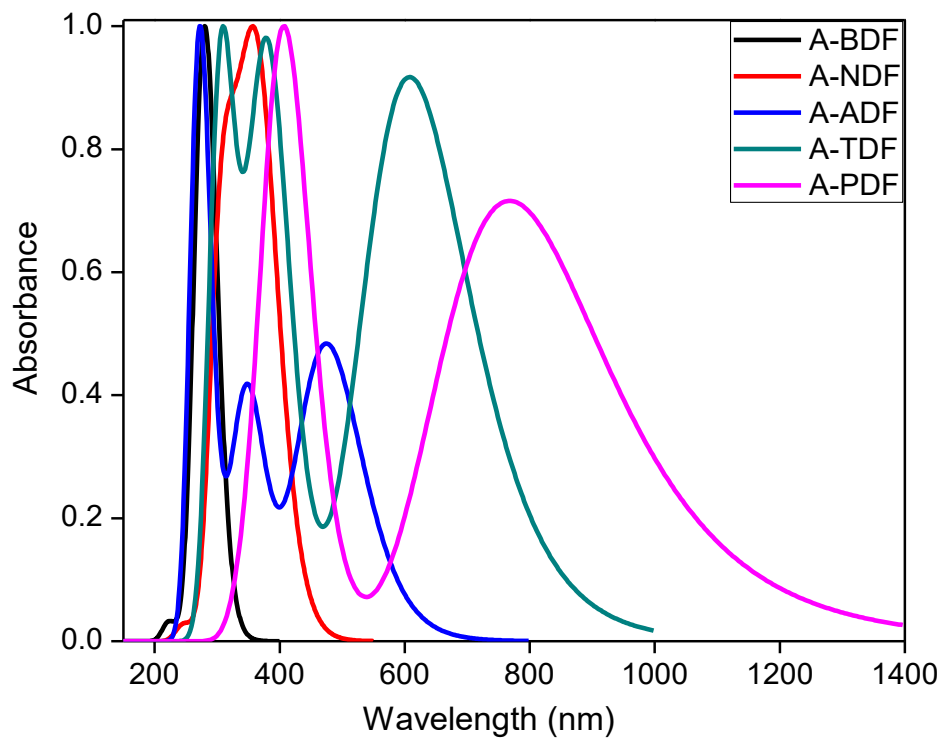


Figure 2.2: Normalized absorption spectra of anti-isomers of furan based acenes

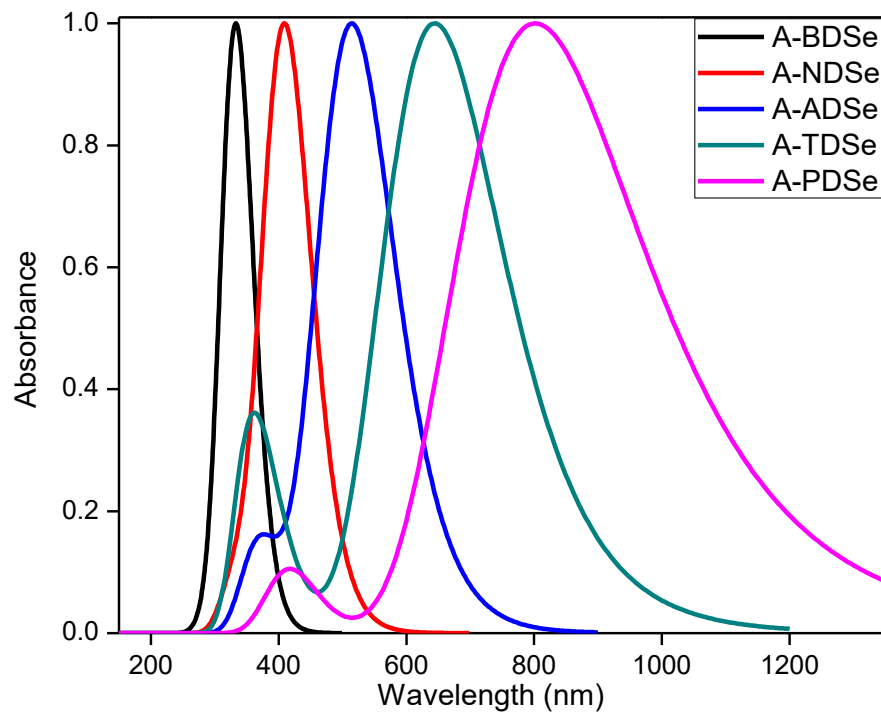


Figure 2.3: Normalized absorption spectra of anti-isomers of selenophene based acenes

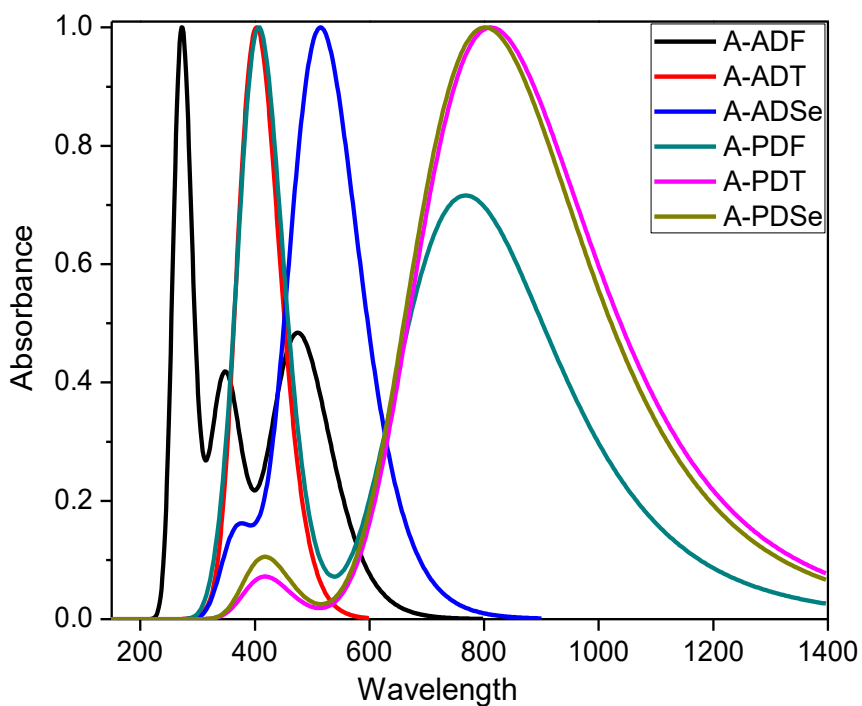


Figure 2.4: Comparative normalized absorption spectra of anti-isomer of anthracene and pentacene based hetero acenes

### 2.3.3. Molecular orbital energies

HOMO, LUMO energies and their HOMO-LUMO gap (HLG) for all the molecules are calculated and tabulated in table 2.9. HLG is higher in the case of furan based acenes as compared to corresponding thiophene or selenophene based acenes. In figure 2.5, comparative HLG for A-ADF, A-ADT and A-ADSe are shown with their molecular orbital pictures. For A-ADF the HOMO and LUMO energies are -5.12 eV and -2.20eV and their corresponding HLG is 2.92eV while a decrease in HLG is observed in case of A-ADT and A-ADSe due to destabilization of HOMO and stabilization LUMO levels. Further, in figure 2.6 molecular orbital pictures with energies of HOMO and LUMO for anti-isomers of thiophene based acenes are shown. On moving from, A-BDT to A-NDT, there is destabilization and stabilization of HOMO and LUMO levels respectively. Similar is the case for A-NDT to A-PDT, and decrease in HLG with the addition of successive benzene rings. It is also noticed from the table syn-isomers are always showing higher or comparable HLG as compared to their corresponding anti-isomers. The molecular orbital pictures anti and syn-isomers of all the molecules are shown in table 2.10 and 2.11 respectively.

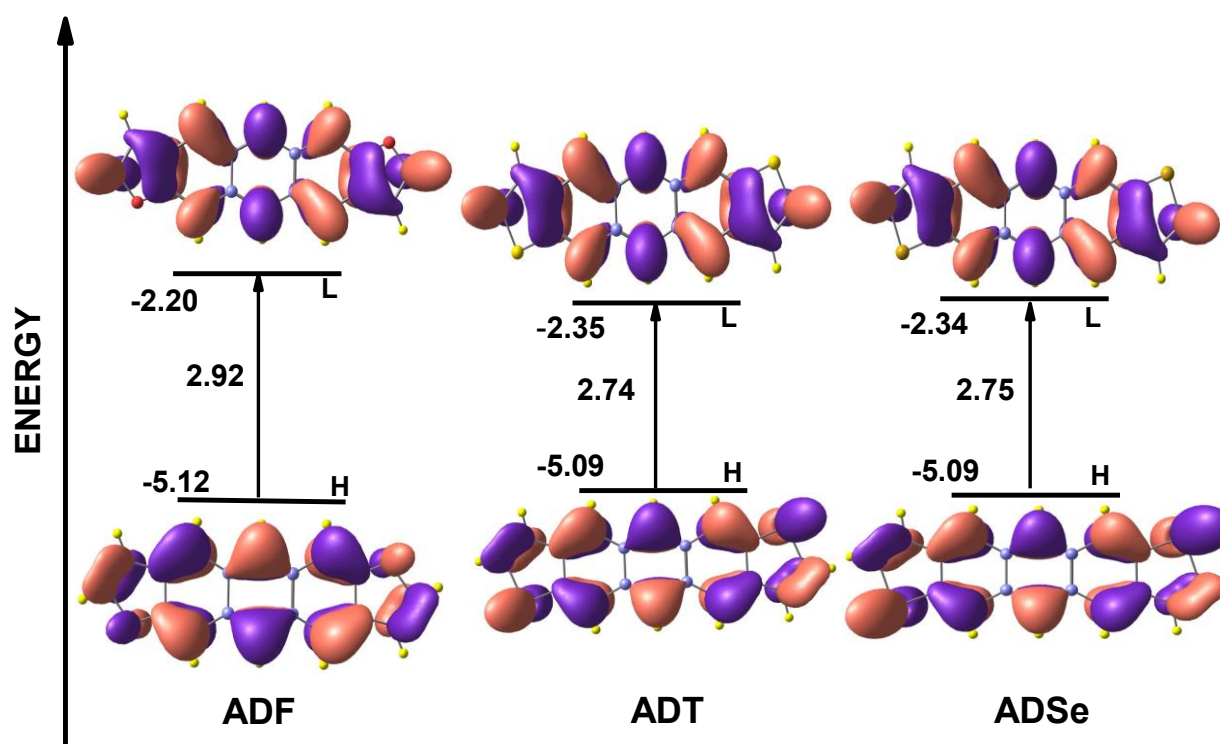


Figure 2.5: HOMO and LUMO gap with their molecular orbital pictures of anti-isomer of ADF, ADT and ADSe

Table 2.9: Calculated HOMO, LUMO energies (in eV) and HOMO-LUMO gap (HLG) of syn-isomers and anti-isomers

NAME	HOMO	LUMO	HLG	NAME	HOMO	LUMO	HLG
S-BDF	-6.07	-1.17	4.90	A-BDF	-5.92	-1.28	4.64
S-BDT	-5.76	-1.28	4.48	A-BDT	-5.74	-1.45	4.29
S-BDSe	-5.67	-1.24	4.43	A-BDSe	-5.66	-1.50	4.16
S-NDF	-5.50	-1.74	3.76	A-NDF	-5.48	-1.78	3.70
S-NDT	-5.38	-1.90	3.48	A-NDT	-5.37	-1.34	4.03
S-NDSe	-5.35	-1.88	3.47	A-NDSe	-5.35	-1.93	3.42
S-ADF	-5.12	-2.13	2.99	A-ADF	-5.12	-2.20	2.92
S-ADT	-5.09	-2.34	2.75	A-ADT	-5.09	-2.35	2.74
S-ADSe	-5.09	-2.33	2.76	A-ADSe	-5.09	-2.34	2.75
S-TDF	-4.86	-2.52	2.34	A-TDF	-4.86	-2.53	2.33
S-TDT	-4.87	-2.66	2.21	A-TDT	-4.87	-2.66	2.21
S-TDSe	-4.89	-2.65	2.24	A-TDSe	-4.88	-2.66	2.22
S-PDF	-4.67	-2.78	1.89	A-PDF	-4.67	-2.78	2.89
S-PDT	-4.70	-2.89	1.81	A-PDT	-4.70	-2.90	1.80
S-PDSe	-4.72	-2.89	1.83	A-PDSe	-4.72	-2.89	1.83

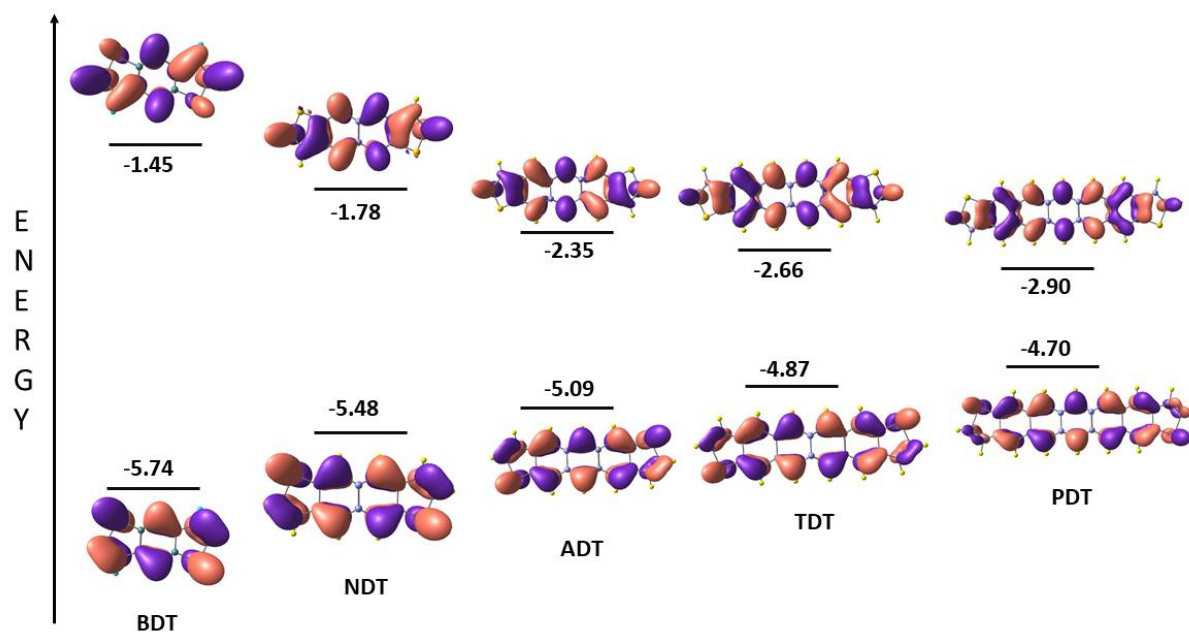
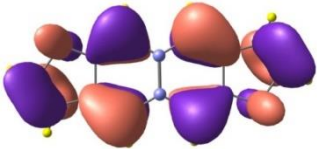
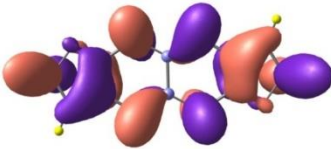
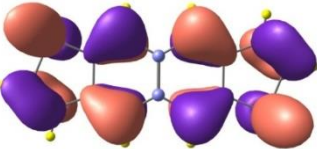
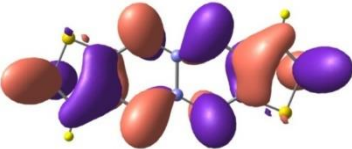
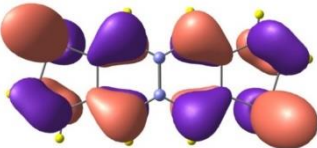
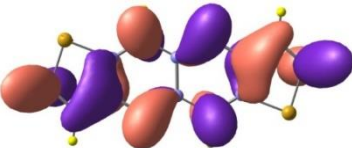
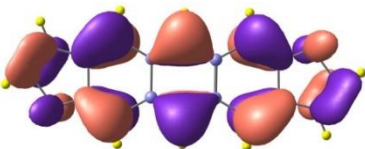
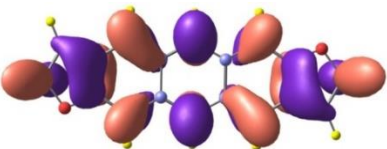
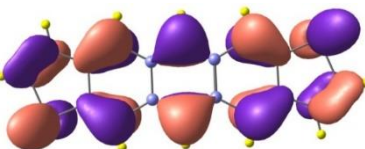
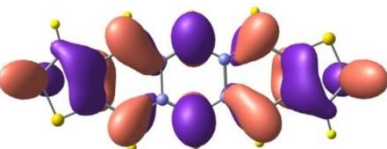
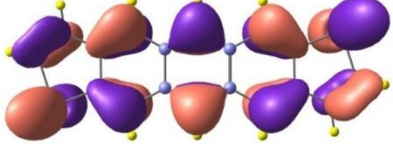
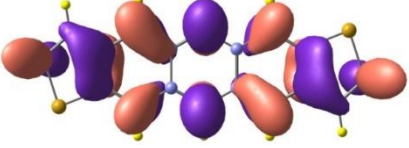
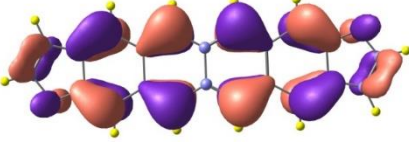
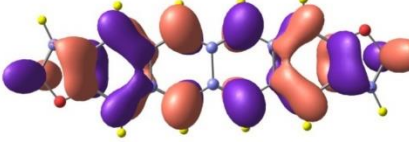
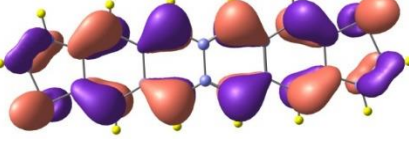
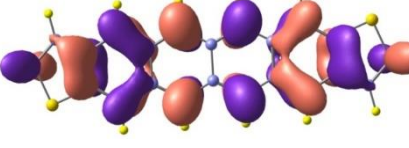
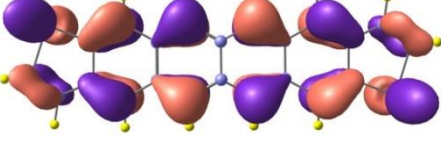
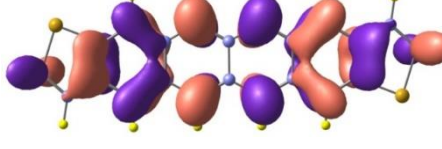
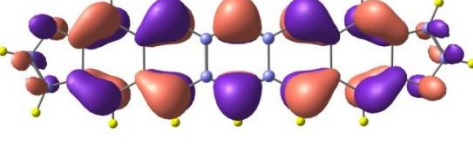
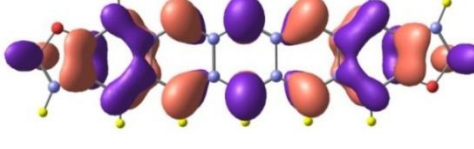
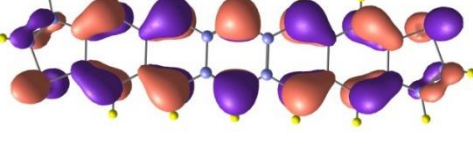
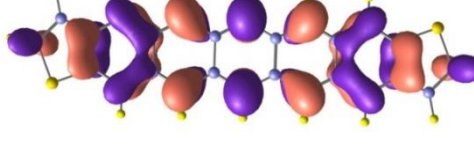


Figure 2.6: HOMO and LUMO energies with their molecular orbital pictures Anti isomers of thiophene based acenes

Table 2.10: Molecular orbital pictures of anti-isomers

Molecule	HOMO	LUMO
A-BDF		
A-BDT		
A-BDSe		

A-NDF		
A-NDT		
A-NDSe		
A-ADF		
A-ADT		
A-ADSe		

		
A-TDF		
A-TDT		
A-TDSe		
A-PDF		
A-PDT		



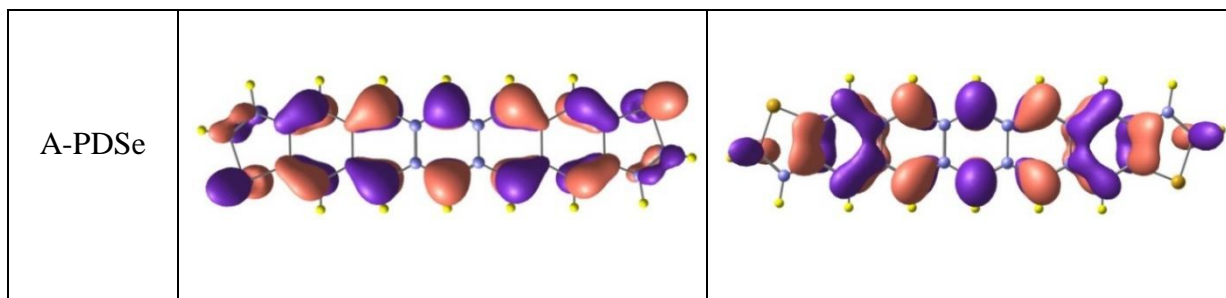
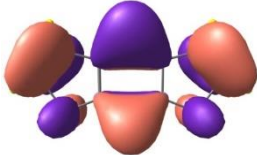
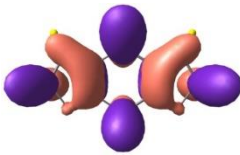
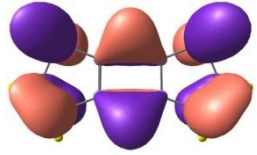
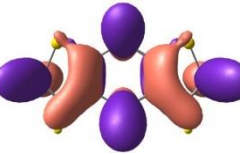
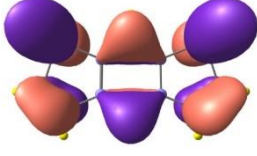
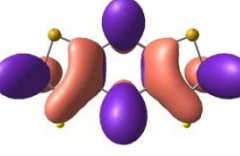
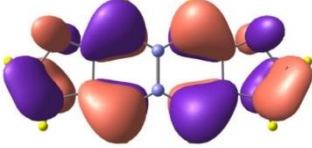
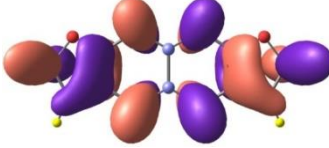
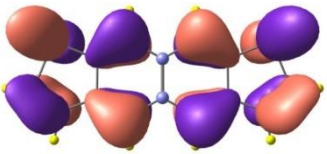
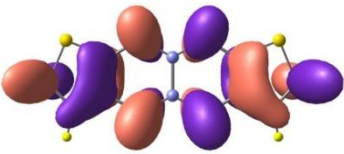
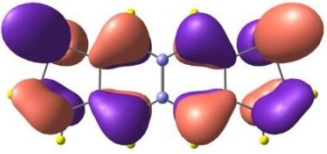
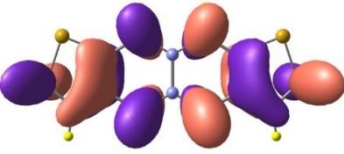
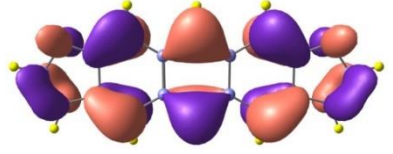
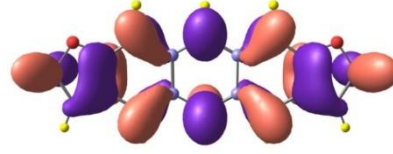
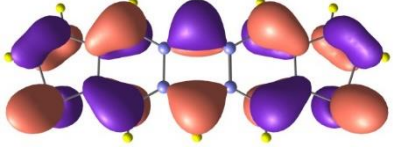
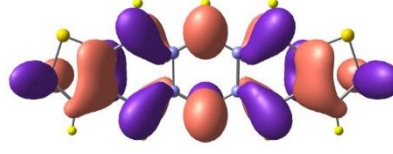
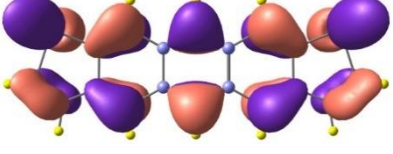
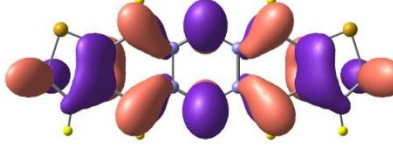
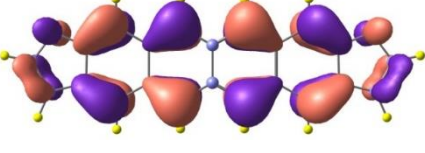
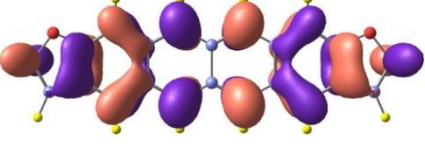
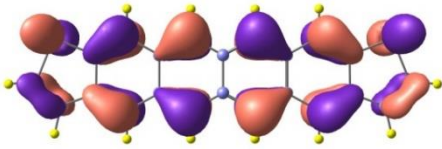
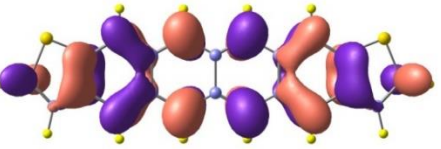
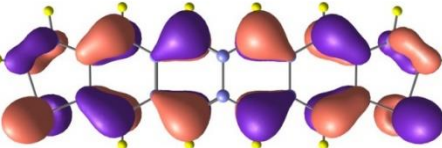
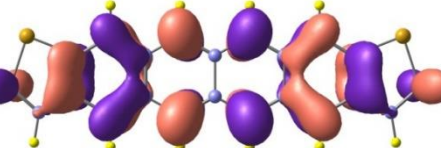
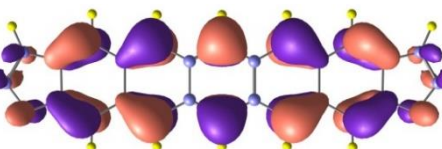
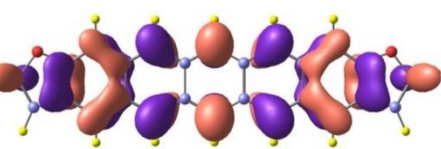
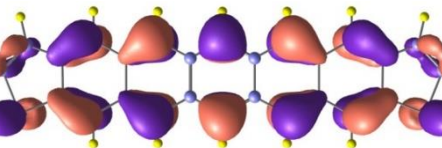
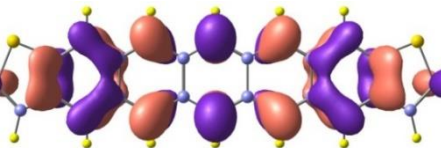
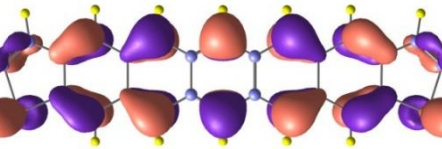
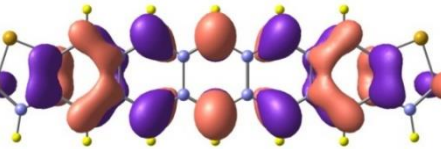


Table 2.11: Molecular orbital pictures of syn-isomers

Molecule	HOMO	LUMO
S-BDF		
S-BDT		
S-BDSe		
S-NDF		



S-NDT		
S-NDS <sub>e</sub>		
S-ADF		
S-ADT		
S-ADSe		
S-TDF		

S-TDT		
S-TDSe		
S-PDF		
S-PDT		
S-PDSe		

---

### 2.3.4. Ionization potential (*IP*) and Electron affinity (*EA*)

IP and EA are the key parameters for charge injection phenomenon in organic semiconductors. The lower IP and higher EA revealed that material would be a better hole and electron transporter, respectively. The calculated IP and EA of all the molecules are tabulated in table 2.12 and 2.13. IP values are decreasing while EA values are increasing continuously with an increase in the size of acenes. However, for syn and anti-isomers there is not much difference in IP and EA values. Furan based acene molecules are always showing higher IP than corresponding thiophene and selenophene based molecules. Among all studied molecules A-PDT and A-PDSe are showing smallest IP and highest EA values, suggesting it is easy to inject hole into the HOMO and electron into the LUMO of these molecules. Thus, thiophene and selenophene based pentacene molecules are showing better hole and electron transport property than another studied molecule.

### 2.3.5. Hole extraction potential (HEP) and electron extraction potential (EEP)

The calculation of HEP and EEP are also done and are tabulated in table 2.12 and 2.13. There is a decrease in HEP and increase in EEP with an increase in the size of acene backbone. Among studied molecules, furan based acenes are showing higher HEP values in case of first three molecules (i.e. BDF, NDF and ADF) than their corresponding thiophene and selenophene (BDT, NDT, ADT, BDSe, NDSe and ADSe) based acene isomers. While higher members of furan based acenes (TDF and PDF) are showing almost comparable HEP values as that of thiophene and selenophene based acene molecules. Therefore, it is easy to extract hole from thiophene and selenophene based acene molecules compared to furan based acene molecules. Moreover, PDT and PDSe are showing the smallest HEP values suggesting with increase in size of acenes hole extraction is easy. On the other hand, EEP values are smaller for furan based acenes as compared to their thiophene and selenophene based acene molecules. EEP values are highest for A-PDT (S-PDT) and A-PDSe (S-PDSe) and therefore it is easy to extract electron from these molecules.

### 2.3.6. Reorganization energy ( $\lambda$ )

As mentioned in equation 1.10 (chapter 1) smaller the value of reorganization energies, higher will be the rate constant for charge transfer reaction. The calculated hole ( $\lambda_h$ ) and electron ( $\lambda_e$ ) reorganization energies for anti and syn-isomers are given in table 2.12 and 2.13 respectively. With the increase in the size of the acene molecule, both  $\lambda_h$  and  $\lambda_e$  energies are decreasing which increases the rate constant and hence the rate of charge transfer increases in a molecule. It is observed from the table, furan based acenes molecules are showing higher  $\lambda_h$  values than the corresponding thiophene based acenes molecule. Among all, selenophene based acene molecules are showing smallest  $\lambda_h$ . For most of the molecules syn-isomers are showing smaller  $\lambda_h$  and  $\lambda_e$  energies than their corresponding anti-isomers (shown in figure 2.7 and 2.8). The  $\lambda_h$  energies for syn-isomer for furans (thiophenes) based acene molecules are in order of: S-BDF (S-BDT) > S-NDF (S-NDT) > S-ADF (S-ADT) > S-TDF (S-TDT) > S-PDF (S-PDT) having  $\lambda_h$  values 362 meV (100 meV), 117 meV (95 meV), 109 meV (92 meV), 100 meV (87 meV) and 90 meV (79 meV) respectively. Similar trends are obtained for selenophene-based acene molecules, S-PDSe is showing the smallest  $\lambda_h$  of 75 meV among all studied molecules. Similarly, the same trend is observed for anti-isomers of furan, thiophene and selenophene based acene molecules. The  $\lambda_h$  calculated for all molecules (except BDF) are smaller than that of N,N'-diphenyl-N,N'-bis(3-methylphenyl)-(1,1'-biphenyl)-4,4'-diamine (TPD) which is typical hole transport material ( $\lambda_h=290$  meV) [44]. The smallest  $\lambda_h$  is for syn and anti-isomer of pentacene selenophene i.e. S-PDSe and A-PDSe. Moreover, the calculated  $\lambda_e$  for most of the molecules is smaller than tris(8-hydroxyquinolato)aluminum(III) (Alq3) which is considered as typical electron transport material ( $\lambda_e=276$  meV) [45]. Additionally, all molecules are showing  $\lambda_h < \lambda_e$ , which represents the studied molecules are better for hole-transporting materials.

Table 2.12: Calculated hole and electron ( $\lambda_h$  and  $\lambda_e$ ) reorganization energy (in meV), Ionization Potential (IP), Electron Affinity (EA), HEP and EEP (in eV) of anti-isomers at B3LYP/6-311+G (d, p) level of theory

Name	IP <sub>A</sub>	IP <sub>V</sub>	EA <sub>A</sub>	EA <sub>V</sub>	HEP	EEP	$\lambda_h$	$\lambda_e$
A-BDF	7.55	7.71	-0.24	-0.37	7.39	-0.12	318	250
A-BDT	7.32	7.40	-0.02	-0.12	7.24	-0.16	157	292
A-BDSe	7.21	7.26	0.12	-0.03	7.17	-0.27	110	305
A-NDF	6.99	7.05	0.38	0.28	6.92	0.48	137	207
A-NDT	6.79	6.84	0.61	0.50	6.74	0.71	101	210
A-NDSe	6.73	6.77	0.64	0.53	6.69	0.75	84	222
A-ADF	6.48	6.53	0.91	0.83	6.42	1.00	109	169
A-ADT	6.37	6.42	1.11	1.03	6.32	1.20	93	165
A-ADSe	6.35	6.39	1.13	1.05	6.31	1.22	83	168
A-TDF	6.10	6.15	1.33	1.26	6.05	1.40	100	143
A-TDT	6.05	6.10	1.51	1.44	6.01	1.58	87	135
A-TDSe	6.04	6.09	1.52	1.45	6.00	1.59	81	137
A-PDF	5.82	5.86	1.66	1.60	5.77	1.72	89	121
A-PDT	5.80	5.84	1.81	1.75	5.76	1.87	79	114
A-PDSe	5.80	5.84	1.82	1.77	5.77	1.88	76	115

Table 2.13: Calculated hole and electron ( $\lambda_h$  and  $\lambda_e$ ) reorganization energy (in meV), Ionization Potential (IP), Electron Affinity (EA), HEP and EEP (in eV) of syn-isomers at B3LYP/6-311+G (d, p) level of theory

Name	IP <sub>A</sub>	IP <sub>V</sub>	EA <sub>A</sub>	EA <sub>V</sub>	HEP	EEP	$\lambda_h$	$\lambda_e$
S-BDF	7.78	8.06	-0.37	-0.49	7.70	0.24	362	238
S-BDT	7.36	7.39	-0.17	-0.30	7.31	0.05	100	249
S-BDSe	7.23	7.28	-0.17	-0.39	7.20	0.04	76	258
S-NDF	7.01	7.07	0.33	0.23	6.95	0.43	117	202
S-NDT	6.79	6.84	0.56	0.46	6.75	0.66	95	197
S-NDSe	6.74	6.78	0.57	0.47	6.70	0.67	80	201
S-ADF	6.48	6.53	0.90	0.81	6.42	0.98	109	169
S-ADT	6.37	6.42	1.10	1.02	6.33	1.18	92	161
S-ADSe	6.35	6.39	1.12	1.03	6.31	1.20	83	164
S-TDF	6.10	6.15	1.33	1.26	6.05	1.40	100	144
S-TDT	6.05	6.10	1.51	1.44	6.01	1.57	87	134
S-TDSe	6.05	6.09	1.52	1.45	6.00	1.59	80	136
S-PDF	5.82	5.86	1.66	1.60	5.77	1.72	90	123
S-PDT	5.80	5.84	1.81	1.75	5.76	1.87	79	115
S-PDSe	5.81	5.84	1.82	1.77	5.77	1.88	75	115

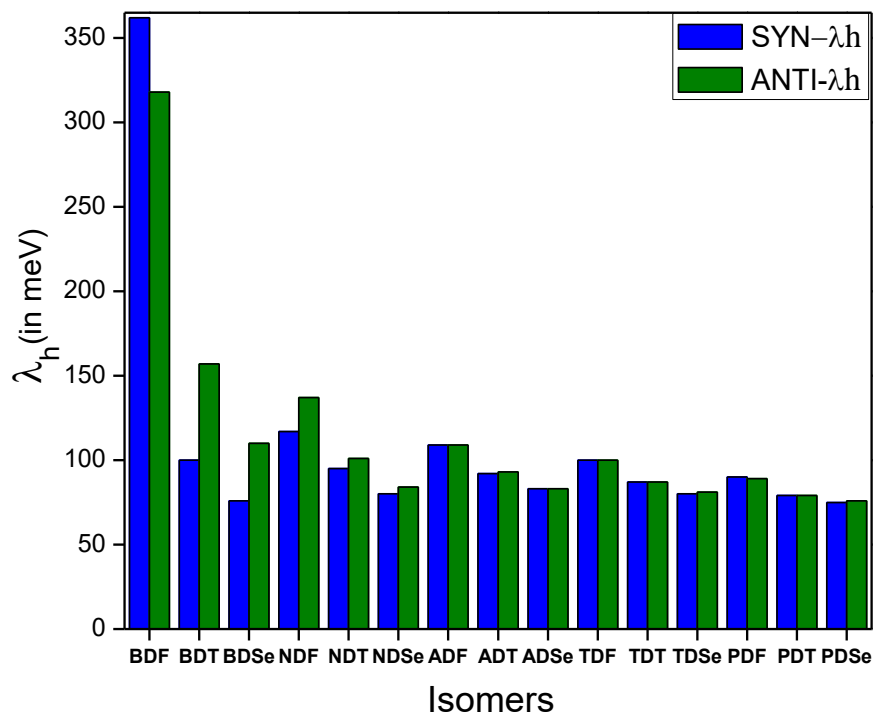


Figure 2.7: Hole reorganization energies of syn and anti-isomers

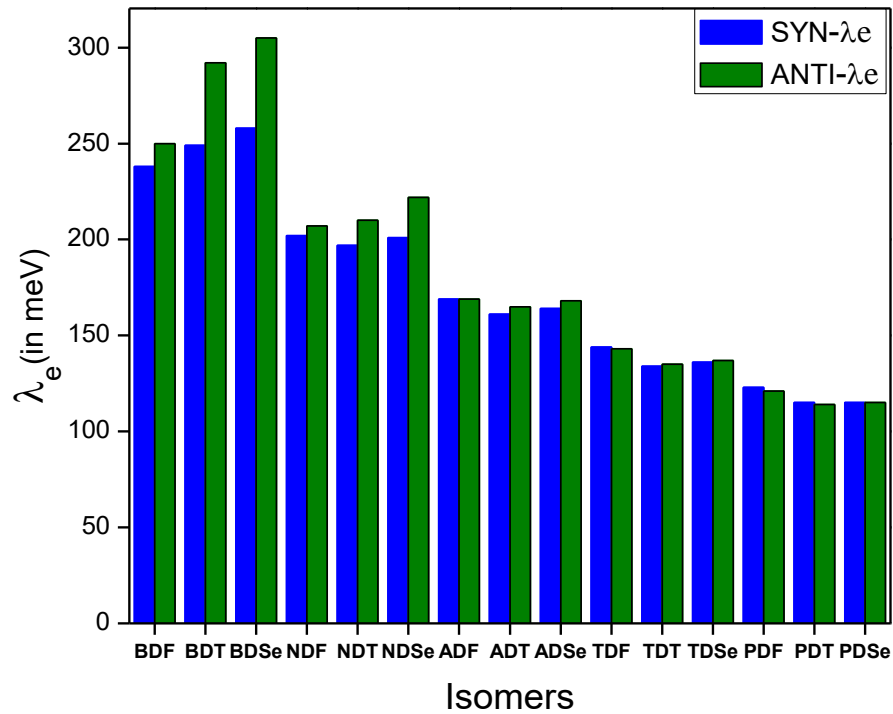


Figure 2.8: Electron reorganization energies of syn and anti-isomers

Further to see the trend in  $\lambda_h$  and  $\lambda_e$  values, calculations are also performed with different functionals (PBE0, B3P86 and B3LYP) (shown in figure 2.9 and 2.10). The similar trends in  $\lambda_h$  and  $\lambda_e$  are obtained with B3LYP, PBE0 and B3P86 functionals (table 2.14 and 2.15).

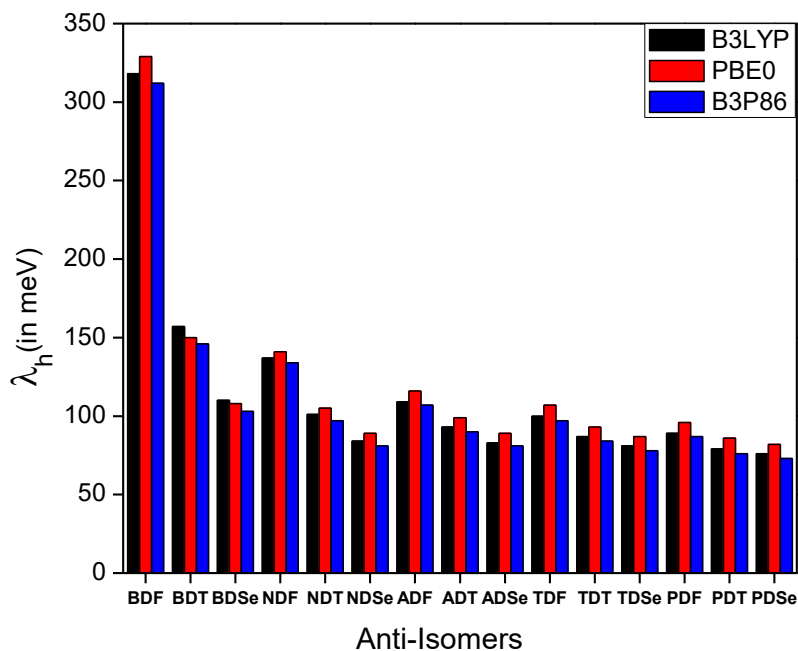


Figure 2.9: Calculated hole reorganization energies of anti-isomers with different functionals

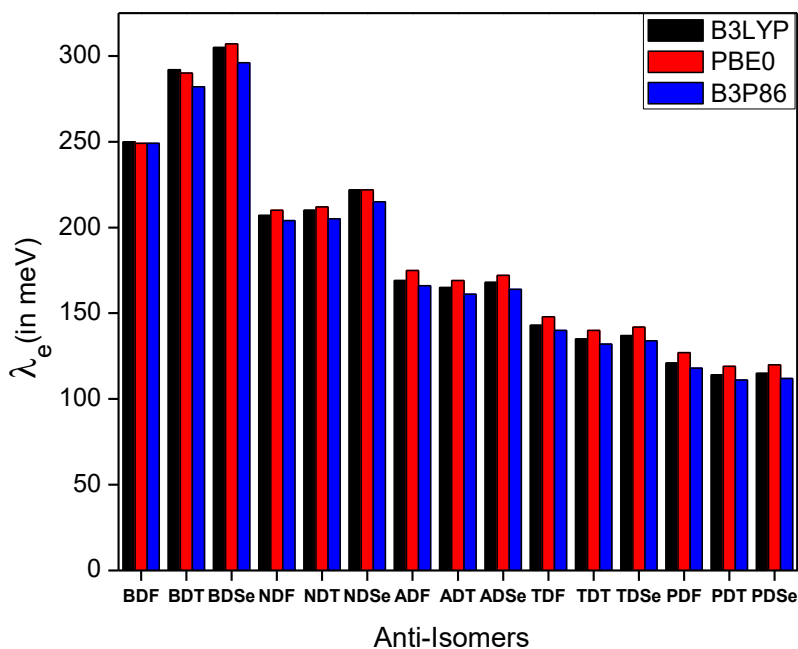


Figure 2.10: Calculated electron reorganization energies of anti-isomers with different functionals



Table 2.14: Calculated hole and electron ( $\lambda_h$  and  $\lambda_e$ ) reorganization energy (in meV) using functionals for anti and syn-isomers

Anti isomers	B3LYP		PBE0		B3P86		Syn isomers	B3LYP		PBE0		B3P86	
	$\lambda_h$	$\lambda_e$	$\lambda_h$	$\lambda_e$	$\lambda_h$	$\lambda_e$		$\lambda_h$	$\lambda_e$	$\lambda_h$	$\lambda_e$	$\lambda_h$	$\lambda_e$
BDF	318	250	329	249	312	249	BDF	362	238	356	242	366	241
BDT	157	292	150	290	146	282	BDT	100	249	103	251	98	248
BDSe	110	305	108	307	103	296	BDSe	76	258	80	262	74	256
NDF	137	207	141	210	134	204	NDF	117	202	125	207	116	200
NDT	101	210	105	212	97	205	NDT	95	197	101	202	93	194
NDSe	84	222	89	222	81	215	NDSe	80	201	86	205	78	198
ADF	109	169	116	175	107	166	ADF	109	169	116	175	107	167
ADT	93	165	99	169	90	161	ADT	92	161	99	167	89	158
ADSe	83	168	89	172	81	164	ADSe	83	164	89	169	80	160
TDF	100	143	107	148	97	140	TDF	100	144	107	150	97	140
TDT	87	135	93	140	84	132	TDT	87	134	93	141	84	131
PDSe	81	137	87	142	78	134	TDSe	80	136	87	142	78	134
PDF	89	121	96	127	87	118	PDF	90	123	96	130	87	120
PDT	79	114	86	119	76	111	PDT	79	115	86	121	76	112
PDSe	76	115	82	120	73	112	PDSe	75	115	82	121	72	113

---

## 2.4. Conclusion

In summary, here we investigated structures, electronic and charge transport properties of syn- and anti-isomers of BDT, NDT, ADT, TDT and PDT and their hetero analogues (O and Se) by means of DFT calculations. The calculated results show that with the introduction of heteroatom (O and Se) affects the absorption and charge transport property of the molecule. The furan based acene molecules are always shown a blue shift in absorption compared to corresponding thiophene and selenophene based acene molecules due to stabilization of HOMO and destabilization of LUMO levels. It is concluded that an increase in the number of benzene rings in the backbone of the acene molecule results in smaller hole and electron reorganization energies. The syn-isomers are always showing smaller hole and electron reorganization energies compared to their corresponding anti-isomers. All the studied molecules are showing smaller  $\lambda_h$  compared to  $\lambda_e$  suggesting studied molecules are better for hole-transporting materials.

---

**References**

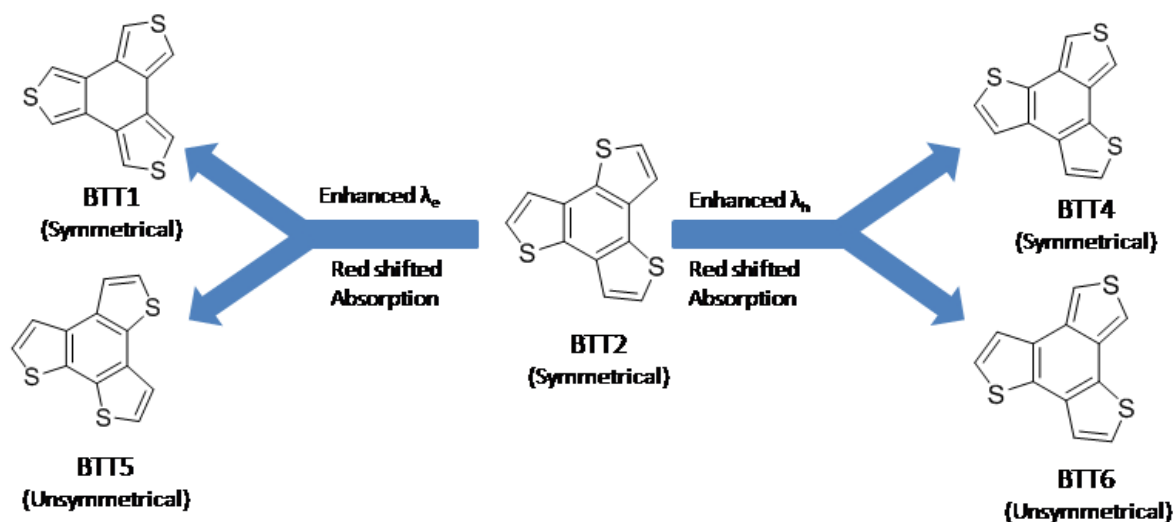
1. S. R. Forrest, *Nature* **2004**, 428, 911.
2. M. M. Torrent, C. Rovira, *Chem. Rev.* **2011**, 111, 4833.
3. Q-D. Liu, R-X. Peng, S-J. Chen, L. Ai, S-Y. Wang, Z-Y. Liu, Z-Y. Ge, *Macromol. Chem. Phys.* **2014**, 215, 1287.
4. M. Nakano, H. Mori, S. Shinamura, K. Takimiya, *Chem. Mater.* **2012**, 24, 190.
5. M. Nakano, K. Niimi, E. Miyazaki, I. Osaka, K. Takimiya, *J. Org. Chem.* **2012**, 77, 8099.
6. S. Arulmozhiraja, T. Ohno, *J. Phys. Chem. C* **2008**, 112, 16561.
7. J. E. Anthony, *Chem. Rev.* **2006**, 106, 5028.
8. M. Yamada, I. Ikemoto, H. Kuroda, *Bull. Chem. Soc. Jpn.* **1988**, 61, 1057.
9. P. Coppo, S. G. Yeates, *Adv. Mater.* **2005**, 17, 3001.
10. R. Mondal, B. K. Shah, D. C. Neckers, *J. Am. Chem. Soc.* **2006**, 128, 9612.
11. C. Tonshoff, H. F. Bettinger, *Angew. Chem. Int. Ed.* **2010**, 49, 4125.
12. J. Kruger, F. Gracia, F. Eisenhut, D. Skidin, J. Alonso, D. Perez, G. Cuniberti, D. Pena, *Angew. Chem. Int. Ed.* **2017**, 56, 11945.
13. B. Purushothaman, M. Bruzek, S. R. Parkin, A. F. Miller, J. E. Anthony, *Angew. Chem. Int. Ed.* **2011**, 50, 7013.
14. P. K. De, D. C. Neckers, *Org. Lett.* **2012**, 14, 78.
15. J. E. Anthony, J. S. Brooks, D. L. Eaton, S. R. Parkin, *J. Am. Chem. Soc.* **2001**, 123, 9482.
16. M. M. Payne, S. R. Parkin, J. E. Anthony, *J. Am. Chem. Soc.* **2005**, 127, 8028.
17. C. Wang, H. Dong, W. Hu, Y. Liu, D. Zhu, *Chem. Rev.* **2012**, 112, 2208.
18. T. Lei, J. Pei, *J. Mater. Chem.* **2012**, 22, 785.
19. X. Yang, L. Wang, C. Wang, W. Long, Z. Shuai, *Chem. Mater.* **2008**, 20, 3205.
20. K. Takimiya, S. Shinamura, I. Osaka, E. Miyazaki, *Adv. Mater.* **2011**, 23, 4347.
21. B. Wex, B. R. Kaafarani, R. Schroeder, L. A. Majewski, P. Burckel, M. Grell, D. C. Neckers, *J. Mater. Chem.* **2006**, 16, 1121.
22. B. Wex, B. R. Kaafarani, R. K. Kirschbaum, D. C. Neckers, *J. Org. Chem.* **2005**, 70, 4502.
23. B. Wex, B. R. Kaafarani, D. C. Neckers, *J. Org. Chem.* **2004**, 69, 2197.

- 
24. B. Wex, B. R. Kaafarani, E. O. Danilov, D. C. Neckers, *J. Phys. Chem. A* **2006**, 110, 13754.
  25. M. L. Tang, T. Okamoto, Z. Bao, *J. Am. Chem. Soc.* **2006**, 128, 16002.
  26. M. M. Payne, S.R. Parkin, J. E. Anthony, C. C. Kuo, T. N. Jackson, *J. Am. Chem. Soc.* **2005**, 127, 4986.
  27. L. Wang, L. Wang, L. Zhang, *Mater. Chem. Phys.* **2018**, 212, 155.
  28. J. G. Laquindanum, H. E. Katz, A. J. Lovinger, *J. Am. Chem. Soc.* **1998**, 120, 664
  29. M. L. Tang, A. D. Reichardt, T. Siegrist, S. C. B. Mannfeld, Z. Bao, *Chem. Mater.* **2008**, 20, 4669.
  30. K. Takimiya, I. Osaka, T. Mori, M. Nakano, *ACC. Chem. Res.* **2014**, 47, 1493.
  31. J. H. Schon, Ch. Kloc, T. Siegrist, J. G. Laquindanum, H. E. Katz, *Org. Elec.* **2001**, 2, 165.
  32. M. Mamada, H. Katagiri, M. Mizukami, K. Honda, T. Minamiki, R. Teraoka, T. Uemura, S. Tokito, *ACS Appl. Mater. Interfaces* **2013**, 5, 9670.
  33. S. Shinamura, I. Osaka, E. Miyazaki, A. Nakao, M. Yamagishi, J. Takeya, K. Takimiya, *J. Am. Chem. Soc.* **2011**, 133, 5024.
  34. M. Nakano, K. Niimi, E. Miyazaki, I. Osaka, K. Takimiya, *J. Org. Chem.* **2012**, 77, 8099.
  35. M. M. Payne, S. A. Odom, S. R. Parkin, J. E. Anthony, *Org. Lett.* **2004**, 6, 3325.
  36. P. Huang, J. Du, M. C. Biewer, M. C. Stefan, *J. Mater. Chem. A*, **2015**, 3, 6244.
  37. L. Huo, Y. Huang, B. Fan, X. Guo, Y. Jing, M. Zhang, Y. Li, J. Huo, *Chem. Commun.* **2012**, 48, 3318.
  38. Y. Zhang, L. Gao, C. He, Q. Sun, Y. Li, *Polym. Chem.* **2013**, 4, 1474.
  39. U. H. F. Bunz, *Angew. Chem. Int. Ed.* **2010**, 49,5037.
  40. N. Hayashi, Y. Saito, H. Higuchi, K. Suzuki, *J. Phys. Chem. A* **2009**, 113, 5342.
  41. A. Thomas, R. K. Chitumalla, A. L. Puyad, K. V. Mohan, J. Jang, *Comput. Theor. Chem.* **2016**, 1089, 59.
  42. M. J. Frisch, Gaussian 16, Revision E.01; Gaussian, Inc.: Wallingford CT, **2016**.
  43. R. M. Wu, H. X. Liu, M. Z. Ao, D. Y. Wu, X. Wang, *Comp. Theor. Chem.* **2014**, 1046, 107.
  44. M. Malagoli, J. L. Bredas, *Chem. Phys. Lett.* **2000**, 327,13.
-

45. B. C. Lin, C. P. Cheng, Z. Q. You, C. P. Hsu, *J. Am. Chem. Soc.* **2005**, 127, 66

# Chapter 3A

## Optoelectronic and Charge Transport Properties of Benzotrithiophene (BTT) isomers



*Results of this chapter published in J. Chin. Chem. Soc. 2019, 66, 891*







### 3A.1. Introduction

Recently, in the field of material science, organic materials have showed a remarkable progress in terms of their use as an alternative to inorganic materials. Though their electronic properties are not as efficient as inorganic materials, but manufacturing of organic materials is superior as they have relatively low cost, lightweight and have the possibility of producing flexible and large area devices [1-2]. In developing new technology and designing new molecular structures and methods for fabricating devices, the power conversion efficiency of organic materials has reached up to 10% [3]. The wide range of applications of organic materials in the fields of organic solar cells [4-5], organic photovoltaic cells (OPVs) [6-7], organic light emitting diodes (OLEDs) [8], organic field effect transistors (OFETs) [9-10], etc. make them a promising area of research. In recent years, many research articles have been published on 'thiophene based organic materials' due to their remarkable optoelectronic and electrochemical properties [11-13].

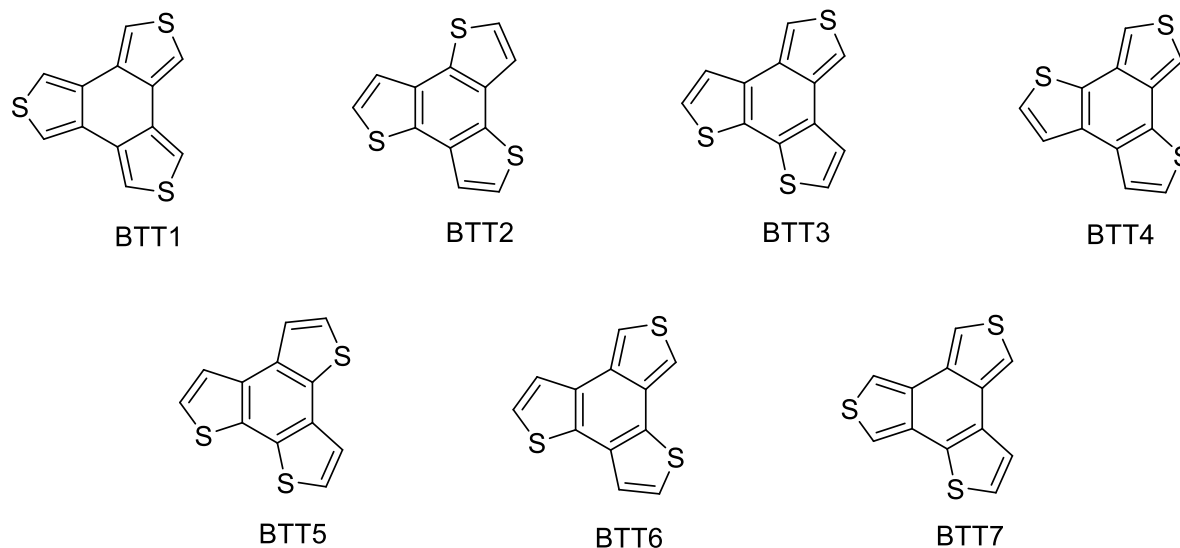
Thiophene compounds are one of the most studied optoelectronic materials due to their reasonable chemical stability, ease of processing and applications in optoelectronic device technology [14]. Thiophene, when combined with benzene or other aromatic rings, becomes an excellent donor unit and acts as a perfect donor in a donor-acceptor polymer system [15]. Within thiophene materials, multi-thiophene fused-aromatic compounds are drawing attention as potential optoelectronic materials in the field of organic semiconductors [16-17]. A large amount of literature on star-shaped thiophene with one or more thiophene/ oligothiophene chains attached with benzene, truxene and triazine as a central aromatic core was published in recent years [18-22]. In this context, Benzotrithiophene (BTT) emerged as a potential  $\pi$ -core of a new class of organic semiconductor. The planar and rigid  $\pi$ -framework of BTT promotes strong intermolecular interactions which are suitable for developing organic semiconducting materials [4-7].

BTT structure is with three identical thiophene moieties at the periphery of the benzene ring and the dihedral angle between two consecutive thiophene rings is close to zero. these properties create a high possibility of building a planar star-shaped molecule with enhanced  $\pi$ -electron delocalization [23-24]. BTT is a derivative of the well-known and most useful donor moieties in photovoltaic devices with fullerene acceptor which is known as benzodithiophene

(BDT) [25]. The third fused thiophene ring in BTT contributes extra electron density to the aromatic backbone and this extended aromatic core is an advantage for intermolecular  $\pi$ -stacking and charge transport. BTT being an electron rich molecule can act as a suitable donor constituent in D-A copolymer system as it can be used in organic electronics [26-27].

Proetzsch et al. reported the first synthesis of BTT in 1972 [28]. Later on, an efficient method for preparation of symmetrical BTT (BTT1; Scheme 3A.1) with its electronic excitations, similar to triphenylene and with the absorption maxima of 320 nm was reported by Hart and Sasaoka in 1978 [29]. Next, symmetrical and unsymmetrical BTT (BTT2 and BTT5 in scheme 3A.1) have been successfully prepared by Jayasuriya and Kagan in 1989 [30]. Roncali et al. have demonstrated remarkable applications of star-shaped fused oligothiophene based BTT-core compounds in photovoltaic devices. They also observed that the performance of the BTT-core compounds is superior to linear benzothiophene analogs and other tri-branched oligothiophenes due to BTT-core characteristics of enhanced  $\pi$ -electron delocalization [24]. Takimiya et al. reported the utilization of fused BTT-core in creating co-planarity and effective intermolecular  $\pi$ -stacking structure for developing new  $\pi$ -conjugated functional materials [23]. BTT is itself a strong electron donor; however, the substitution of long alkyl chain can increase electron donor property significantly and become an ideal material for construction of donor-acceptor (D-A) copolymers, which are popular materials for applications in OPVs, OFETs, OLEDs [16, 26-27]. Side chains also play an essential role in improving the solubility of the conjugated polymer, impacting the molecular interaction, thin film packing order and charge carrier transport [32]. Conjugated side chain substitutions in BTT based polymers have proven to improve the thermal stability of molecules [32].

Based on the connectivity of thiophene moiety with the benzene core, BTT has seven possible isomers (Scheme 3A.1), in which the first four are symmetrical while the last three are unsymmetrical isomers. Best of our knowledge and currently available literature, only four out of seven possible isomers have reports with successful route of synthesis, and the remaining three are yet to be synthesized. Here in this chapter, a computational study of possible seven isomers of BTT was performed. DFT and TDDFT computational methods are used to find out stability, electronic excitations along with ionization potentials ( $IP$ ), electron affinity ( $EA$ ) and reorganization energies ( $\lambda$ ) for all the isomers of BTT.



Scheme 3A.1: The Possible symmetric (BTT1-BTT4) and asymmetric (BTT5-BTT7) isomers of Benzotrithiophene (BTT)

### 3A.2. Computational Methodology

The geometries of all the BTT isomers were fully optimized employing the Gaussian16 package (Frisch et al.) [33]. Becke's three-parameter hybrid exchange functional and the Lee-Yang-Parr correlation functional (LYP) were utilized in the calculation with 6-311+G (d, p) basis set [34-35]. All the isomers were examined for frequency check to ensure that optimized geometries correspond to true minima. TDDFT calculations were carried out in hexane, chloroform, methanol, and DMSO using the polarizable continuum model (PCM) to check the effect of various solvents on electronic excitations. The frontier molecular orbitals which are responsible for the excitations leading to the absorption maximum, were pictorially visualized from the population analysis.

Further, calculation of hole ( $\lambda_h$ ) and electron ( $\lambda_e$ ) reorganization energies are done by using *equation 1.14* and *1.15* respectively (in chapter 1). Also the calculation of charge injection parameters i.e. ionization potential (IP) and electron affinity (EA) are done by using equations *1.17* and *1.18* respectively.

---

### 3A.3. Results and Discussions

#### 3A.3.1. Geometry and Structural parameters

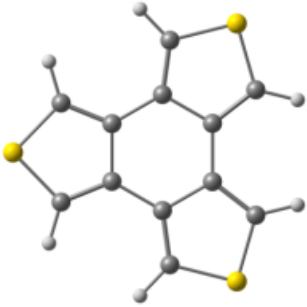
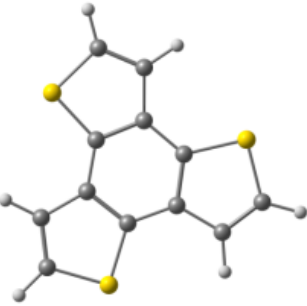
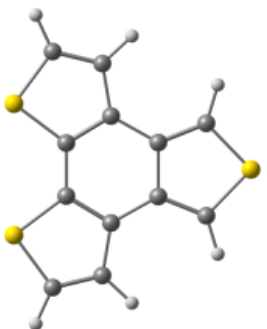
To study the stability of BTT isomers, symmetrical BTTs (BTT1, BTT2, BTT3, and BTT4) and unsymmetrical BTTs (BTT5, BTT6, and BTT7) have been optimized at B3LYP/ 6-311+G (d, p) level of theory (symmetry and relative energies of BTT isomers are shown in table 3A.1). A molecule with higher symmetry may be more stable; however, one cannot predict the stability of molecule by its symmetry only and also one should consider other factors such as bond length, bond angles,  $\pi$ -electron delocalization, etc.,. Among BTT isomers, BTT1 is more symmetrical with point group  $D_{3h}$ , but BTT1 has the highest energy than other isomers. These results suggest that the symmetry is not the only factor in deciding the stability of the molecules.

We further investigated the geometries of all the BTT isomers and compared their bond lengths & bond angles and the results are summarized in table 3A.2 and table 3A.3 for symmetrical isomers (BTT1-BTT4) and for unsymmetrical isomers (BTT5-BTT7) respectively. In BTT1 the thiophene ring attached to central benzene is of radialene like structure, which is non-aromatic and its six exocyclic C-C bonds (2 C-C bonds from each thiophene) are with the double bond characteristics (1.372 Å). The C-S bond length is of 1.727 Å and the central benzenic core bond length is 1.460 Å and 1.446 Å alternately (table 3A.2) [36]. Therefore, these bond length data shows that non-delocalization of electrons did not resonate throughout the molecule which reflects non-aromatic characteristics of the central benzene core in BTT1. In the case of BTT2, the central benzene ring has bond lengths of 1.418 Å and 1.406 Å alternately; this resembles a benzene-like aromatic structure. Further, the C-C bond lengths of thiophene moieties at the periphery of benzene are 1.437 Å and 1.357 Å and the C-S bond length is ~1.750 Å [24]. Thus, it indicated that the delocalization of  $\pi$ -electrons over an aromatic sextet in BTT2, while delocalization of  $\pi$ -electrons is observed only over thiophene moiety in the case of BTT1, as a result of which stability of BTT2 is greater than BTT1.

The relative energy difference between BTT2 and BTT5 is less than 1 kcal per mole (table 3A.1) and the  $\pi$ -electron delocalization in both the molecules are also similar. All the BTT isomers (except BTT1 and BTT7) are with more  $\pi$ -electron delocalization in its ground state from one thiophene to another thiophene through benzene either by 1-dimension or 2-dimensional conjugation. The calculated bond lengths and bond angles of isomers BTT1 and

BTT2 compared with their crystal data and are tabulated in table 3A.4 and table3A.5 respectively [24, 41]. Based on calculated results, there is hardly any significant change in bond lengths and bond angles of experimentally reported data in both BTT1 and BTT2 isomers.

Table 3A.1: Optimized structure, Symmetry and Relative energy (RE, in Kcal) of isomers calculated at B3LYP/6-311+G (d, p) level.

Name	Structure	Symmetry	RE (in Kcal)
BTT1		D <sub>3h</sub>	13.37
BTT2		C <sub>3h</sub>	<b>0.00</b>
BTT3		C <sub>2v</sub>	7.47

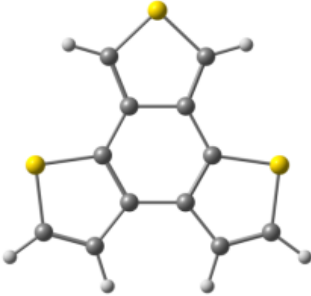
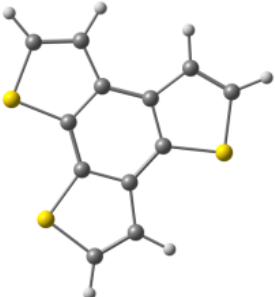
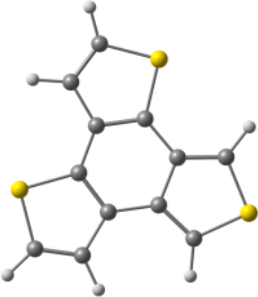
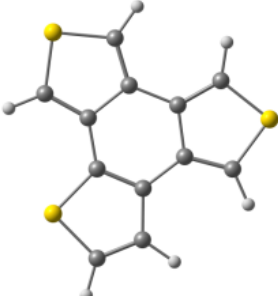
BTT4		$C_{2v}$	7.40
BTT5		$C_s$	0.56
BTT6		$C_s$	7.15
BTT7		$C_s$	10.73

Table 3A.2: Calculated bond length (in Å) and bond angles (in degree (°)) for the symmetrical BTTs (BTT1, BTT2, BTT3, and BTT4) isomers obtained at B3LYP/6-311+ G (d, p) level of theory.

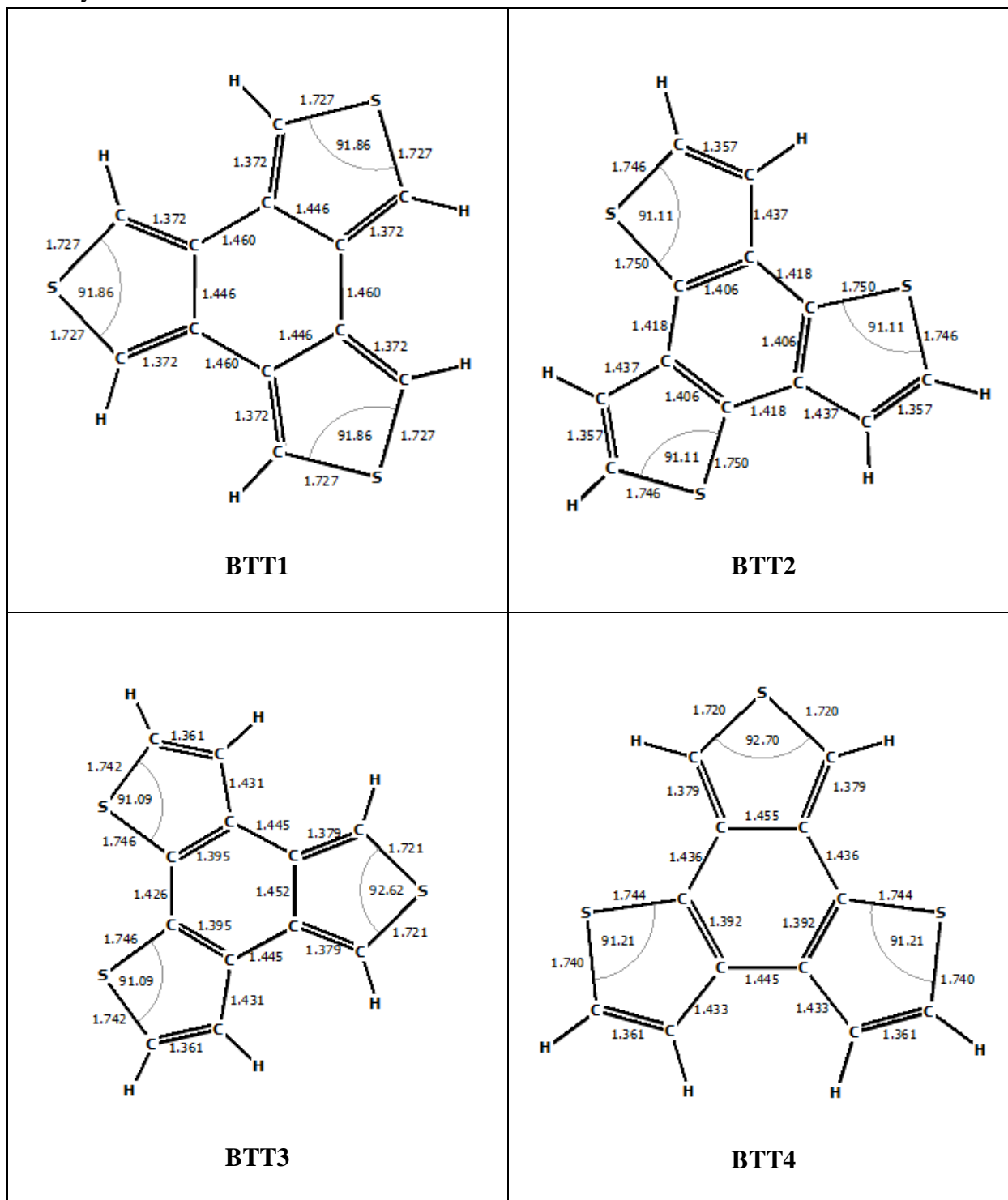


Table 3.A.3: Calculated bond length (in Å) and bond angles (in degree (°)) for the unsymmetrical BTTs (BTT5, BTT6, and BTT7) isomers obtained at B3LYP/6-311+ G (d, p) level of theory.

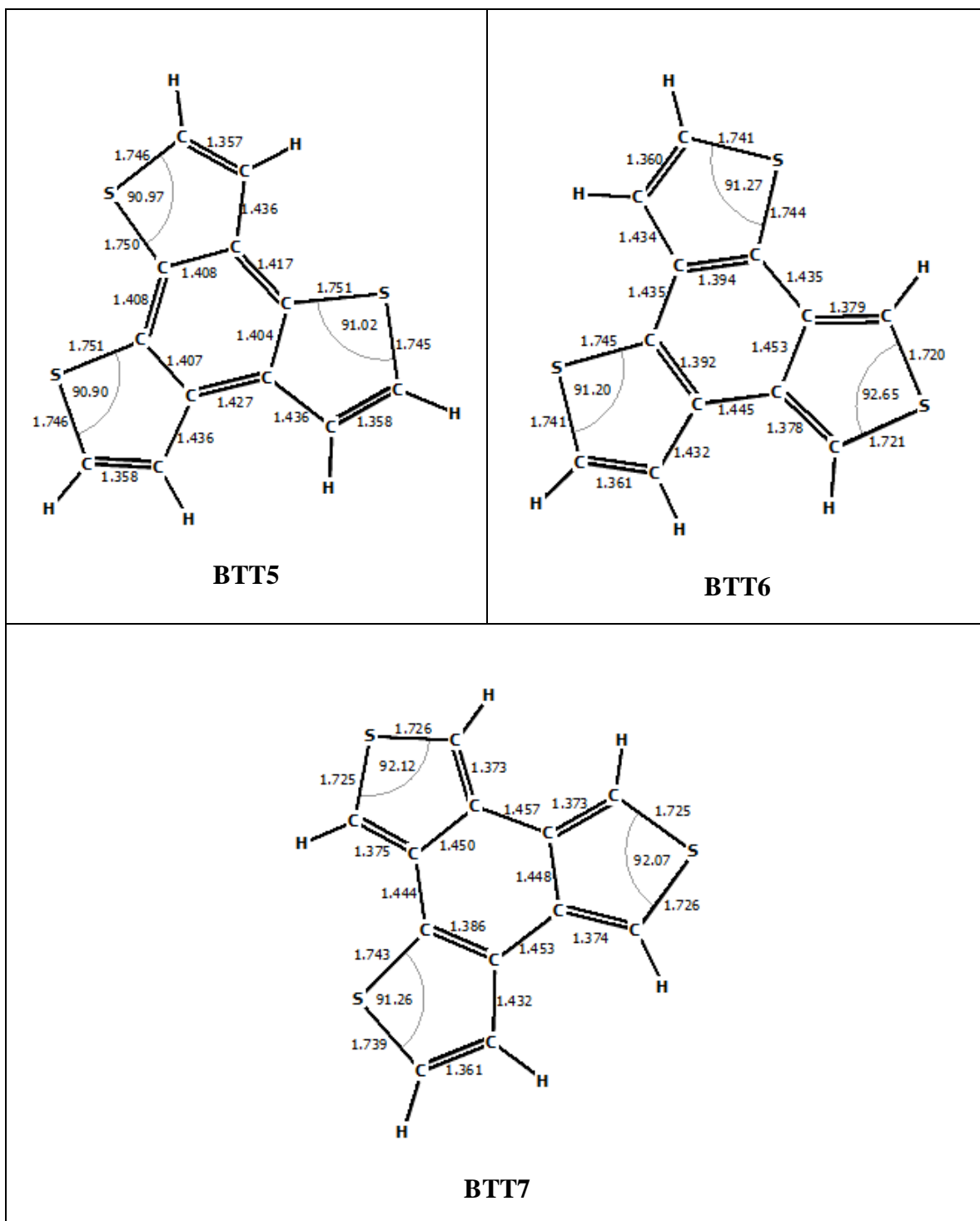
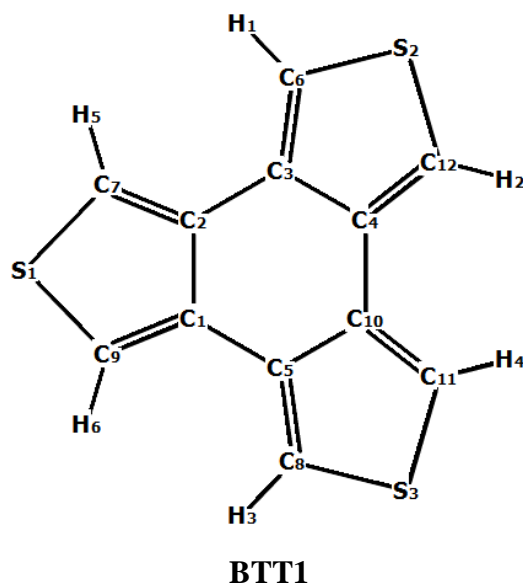




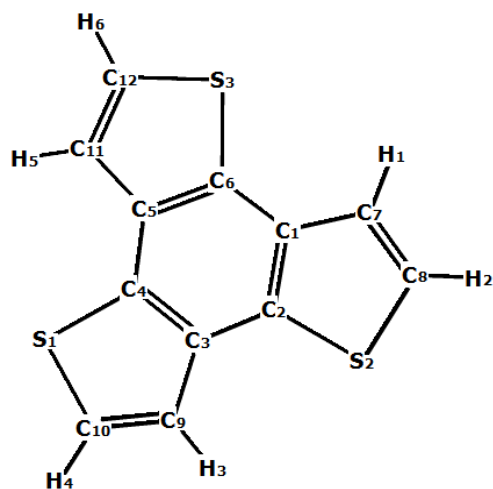
Table3A.4 : Bond lengths ( $BL^{\text{cal}}$  and  $BL^{\text{exp}}$  in Å) and Bond angles ( $BA^{\text{cal}}$  and  $BA^{\text{exp}}$  in degree ( $^{\circ}$ )) of optimized structure of BTT1 calculated at B3LYP/6-311+ G (d, p) level.



<b>BL</b>	<b>BL<sup>cal</sup></b>	<b>BL<sup>exp*</sup></b>	<b>BA</b>	<b>BA<sup>cal</sup></b>	<b>BA<sup>exp*</sup></b>
<b>C1-C2</b>	1.446	1.420	C7-S1-C9	91.86 <sup>o</sup>	93.20 <sup>o</sup>
<b>C2-C3</b>	1.460	1.444	C6-S2-C12	91.86 <sup>o</sup>	92.70 <sup>o</sup>
<b>C3-C4</b>	1.446	1.428	C8-S3-C11	91.86 <sup>o</sup>	93.60 <sup>o</sup>
<b>C3-C6</b>	1.372	1.364			
<b>C1-C5</b>	1.460	1.455			
<b>C2-C7</b>	1.372	1.376			
<b>C1-C9</b>	1.372	1.377			
<b>C5-C8</b>	1.372	1.365			
<b>C5-C10</b>	1.446	1.434			
<b>C4-C12</b>	1.372	1.365			
<b>C4-C10</b>	1.460	1.462			
<b>C10-C11</b>	1.372	1.366			
<b>C9-S1</b>	1.727	1.703			
<b>C7-S1</b>	1.727	1.700			
<b>C6-S2</b>	1.727	1.710			
<b>C12-S2</b>	1.727	1.708			
<b>C8-S3</b>	1.727	1.706			
<b>C11-S3</b>	1.727	1.715			

\* *Bull. Chem. Soc. Jpn.* 1988, 61, 2303

Table 3A.5: Bond lengths ( $BL^{cal}$  and  $BL^{exp}$  in Å) and Bond angles ( $BA^{cal}$  and  $BA^{exp}$  in degree ( $^{\circ}$ )) of optimized structure of BTT2 calculated at B3LYP/6-311+G (d, p) level.



**BTT2**

BL	$BL^{cal}$	$BL^{exp*}$	BA	$BA^{cal}$	$BA^{exp*}$
<b>C1-C2</b>	1.406	1.378	C4-S1-C10	$91.11^{\circ}$	$89.80^{\circ}$
<b>C2-C3</b>	1.418	1.383	C2-S2-C8	$91.11^{\circ}$	$90.70^{\circ}$
<b>C3-C4</b>	1.406	1.396	C6-S3-C12	$91.11^{\circ}$	$90.80^{\circ}$
<b>C4-C5</b>	1.418	1.411			
<b>C5-C6</b>	1.406	1.396			
<b>C6-C1</b>	1.418	1.393			
<b>C1-C7</b>	1.437	1.466			
<b>C7-C8</b>	1.357	1.322			
<b>C5-C11</b>	1.437	1.443			
<b>C11-C12</b>	1.357	1.354			
<b>C3-C9</b>	1.437	1.457			
<b>C9-C10</b>	1.357	1.350			
<b>C4-S1</b>	1.750	1.737			
<b>C10-S1</b>	1.745	1.673			
<b>C2-S2</b>	1.750	1.747			
<b>C8-S2</b>	1.745	1.619			
<b>C6-S3</b>	1.750	1.739			
<b>C12-S3</b>	1.745	1.631			

\* *Org. Lett.* 2004, 6, 273

### 3A.3.2. Linear Optical Properties

For an understanding of the electronic excitations in these BTT isomers, the quantum chemical calculations in gaseous and solvent phase (DMSO, methanol, chloroform and hexane) has been performed with TDDFT methodology using B3LYP/6-311+G (d, p) level. Further, to check whether the change of functional would effect on absorption maxima, TDDFT calculations were also carried out with different functional such as M06 [37], BLYP [34-35], CAM-B3LYP [38] and WB97XD [39] with 6-311 + G (d, p) basis set (shown in table 3A.6). In this analysis, B3LYP functional gave best results which are in good agreement with the experimental result (table 3A.7). Calculated absorption energies ( $\lambda_{\max}$ ), oscillator strength ( $f$ ), major transitions (MT), and % weight (%  $C_i$ ) are listed in table 3A.7. The calculated absorption maxima for all BTT isomers are in the range of 280-360 nm, which is originated from localized  $\pi$ - $\pi^*$  transition of conjugated backbone. The absorption maxima of BTT1 calculated by TDDFT method was at 311 nm with the major transition from HOMO to LUMO (figure 3A.1) and is very close to the experimentally reported longest wavelength absorption, 320 nm [29]. In the case of BTT2 molecule, experimentally reported absorption was at 260 nm and a weaker vibronic peak at 288 nm, and an extra 50 nm blue shift was observed than in BTT1 [31]. TDDFT calculated absorption for BTT2 was at 268 nm which is also in good agreement with the experimental result. The TDDFT calculated absorption shows two transitions: one from HOMO-1 to LUMO and other from HOMO to LUMO+1 (figure 3A.1). Both, BTT3 and BTT4 exhibit  $C_{2v}$ -symmetry and experimentally reported absorption of BTT3 was at 360 nm [27]. TDDFT calculations for both BTT3 and BTT4 show almost similar absorption maxima at 362 and 359 nm respectively and also depict transitions from HOMO to LUMO (figure 3A.2). In the case of unsymmetrical BTTs, experimentally reported absorption for BTT5 was at 335 nm and TDDFT calculated value was 314 nm [30]. The major transitions in BTT5 molecule were from HOMO-1 to LUMO, HOMO to LUMO and HOMO to LUMO+1 (figure 3A.3). Experimentally reported absorption data is not available yet for BTT6 and BTT7 isomers (not synthesized yet), however TDDFT calculated absorption for BTT6 portrays absorption maxima at 357 nm and shows transition from HOMO to LUMO. On the other hand ,BTT7 shows absorption maxima at 332 nm with three major transitions from HOMO-1 to LUMO, HOMO to LUMO and HOMO to LUMO+1(figure 3A.4). The normalized absorption spectra of BTT isomers are shown in figure 3A.5. Further to study the effect of solvents on absorption

maxima, the absorption energies were calculated with various solvents. Calculated absorption energies for different solvents (DMSO, methanol, chloroform and hexane) showed that there is no significant effect of solvents on absorption maxima (table 3A.8).

Table 3A.6: Absorption energies ( $\lambda_{\text{max}}$  in nm) calculated at TDDFT method 6-311+G (d, p) basis set with different functional.

Name	$\lambda_{\text{exp}}$	B3LYP	BLYP	M06	WB97XD	CAM- B3LYP
BTT1	320	311	361	304	264	269
BTT2	288	268	304	265	242	243
BTT3	360	362	394	361	329	333
BTT4	--	359	393	357	324	328
BTT5	335	314	349	313	286	287
BTT6	--	357	391	356	323	327
BTT7	--	332	383	326	296	299

Table 3A.7: Calculated absorption maxima  $\lambda_{\text{max}}$  (nm), Oscillator strength ( $f$ ), Major Transitions (MT), and %weight (% $C_i > 10$ ) at TD-B3LYP method using 6-311+G (d, p) basis sets.

Name	$\lambda_{\text{exp}}^{\text{max}}$ (in nm)	$\lambda_{\text{max}}$ (in nm)	$f$	MT	% $C_i$
BTT1	320 <sup>a</sup>	311	0.024	H $\rightarrow$ L	90
BTT2	288, 260 <sup>b</sup>	268	0.350	H-1 $\rightarrow$ L H $\rightarrow$ L+1	34 34
BTT3	360 <sup>c</sup>	362 302	0.167 0.180	H $\rightarrow$ L H-1 $\rightarrow$ L	98 88
BTT4	--	359	0.030	H $\rightarrow$ L	98
BTT5	335 <sup>d</sup>	314	0.041	H-1 $\rightarrow$ L H $\rightarrow$ L H $\rightarrow$ L+1	61 13 23
BTT6	--	357 315	0.091 0.077	H $\rightarrow$ L H-1 $\rightarrow$ L H $\rightarrow$ L+1	98 70 20

BTT7	--	332	0.039	H-1 →L	10
				H →L	50
				H →L+1	33

<sup>a</sup> *J. Am. Chem. Soc.* **1978**, 17, 4326

<sup>b</sup> *Org. Lett.* **2009**, 11, 3230

<sup>c</sup> *Org. Lett.* **2011**, 13, 6062

<sup>d</sup> *J. Org. Chem.* **1989**, 54, 4203

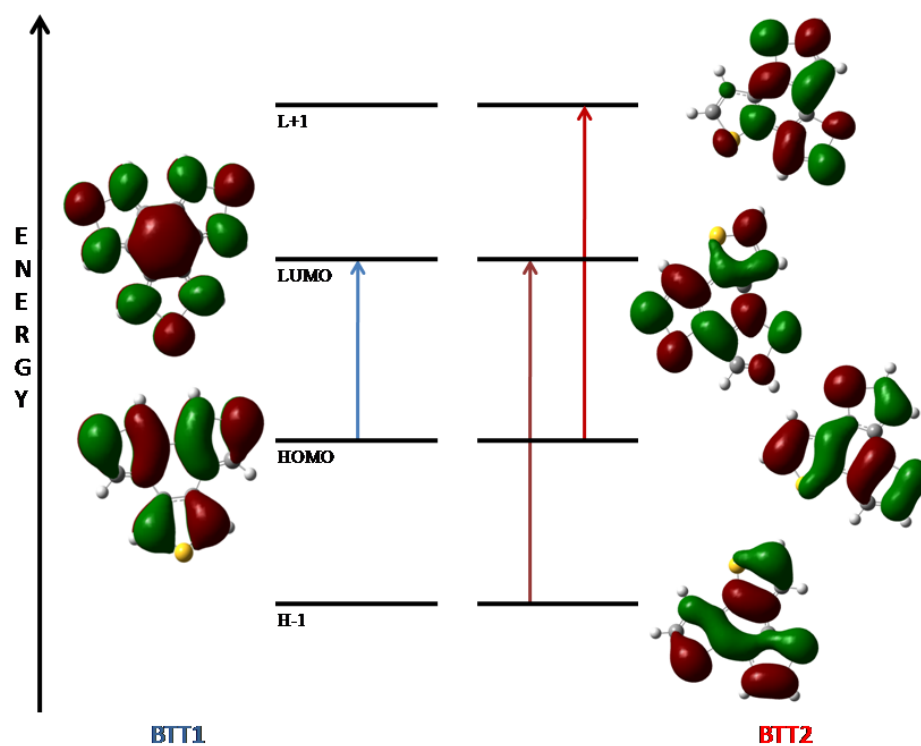


Figure 3A.1: Electronic excitations with their molecular orbitals of **BTT1** and **BTT2**

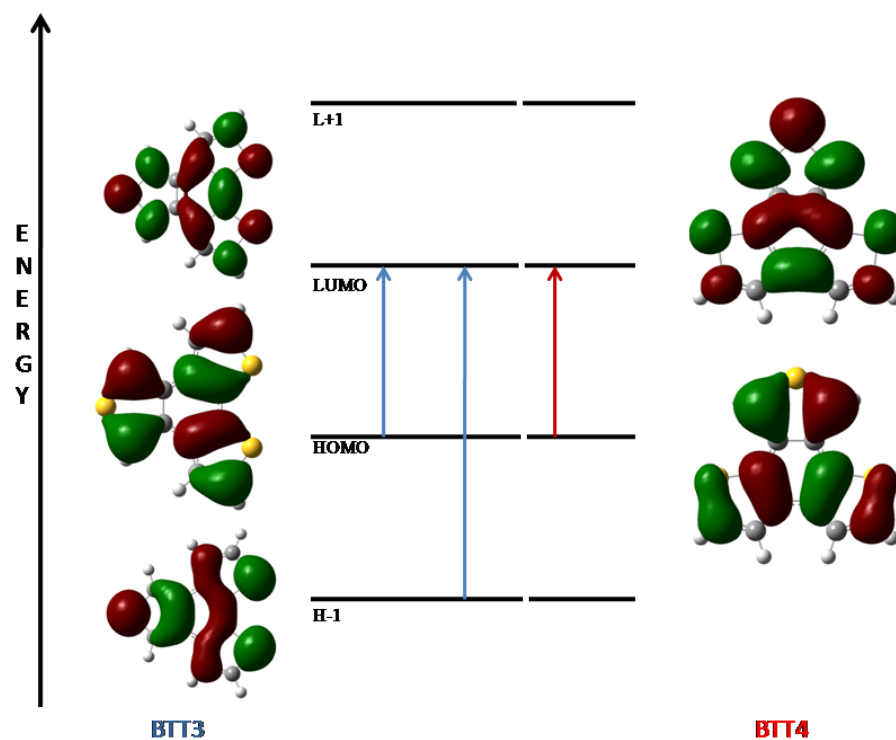


Figure 3A.2: Electronic excitations with their molecular orbitals of **BTT3** and **BTT4**

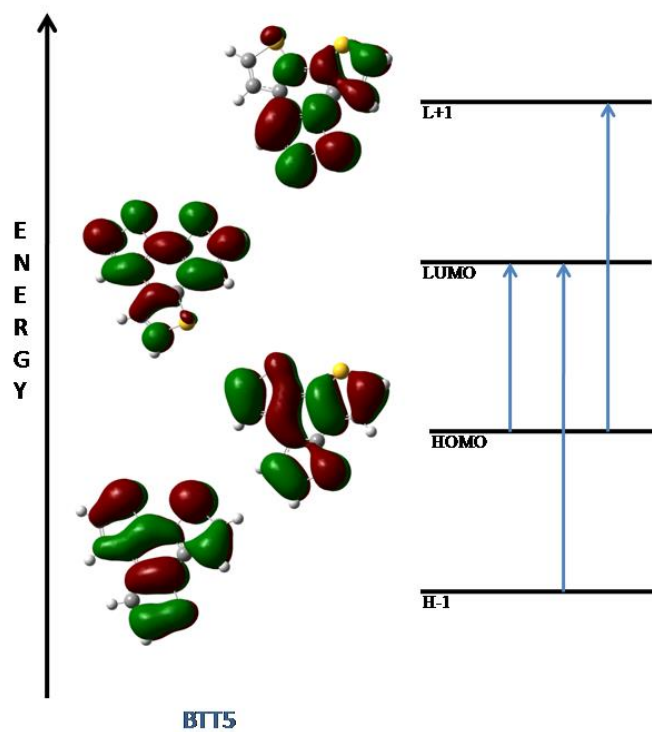


Figure 3A.3: Electronic excitations with their molecular orbitals of **BTT5**

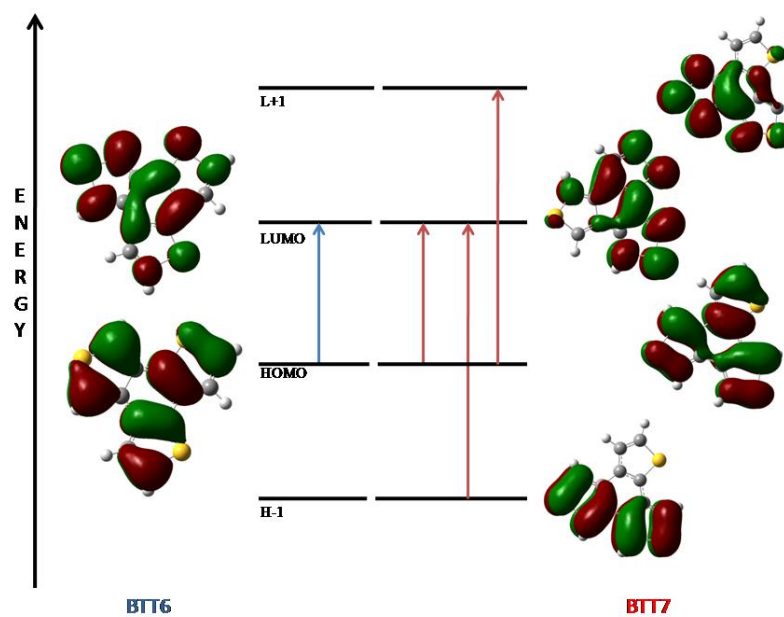


Figure 3A.4: Electronic excitations with their molecular orbitals of **BTT6** and **BTT7**

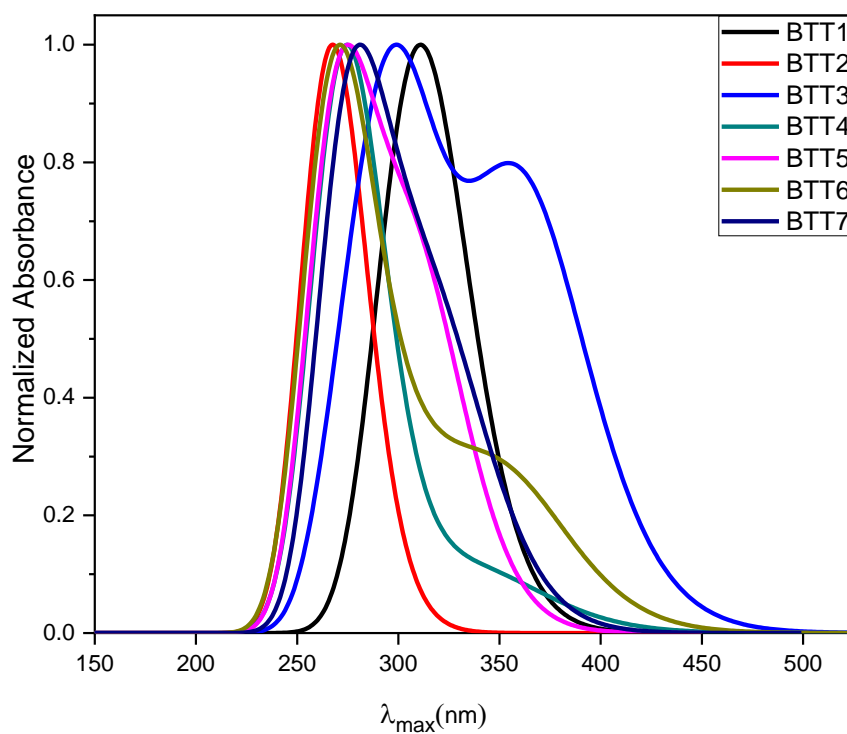


Figure 3A.5: Normalized spectra of all the isomers of BTT calculated at B3LYP/6-311+G (d, p) level.

Table 3A.8: Absorption ( $\lambda_{\max}$  in nm) of isomers in different solvents

BTT isomers	Gas phase	DMSO	Methanol	Chloroform	Hexane
BTT1	311	311	311	311	311
BTT2	309	310	310	309	309
BTT3	362	362	362	362	362
BTT4	359	360	360	360	359
BTT5	314	314	314	314	314
BTT6	357	358	358	358	357
BTT7	332	332	332	332	332

The major excitations for all the isomers BTTs with their molecular orbital pictures obtained at B3LYP/6-311 + G (d, p) level are shown in Figure 3A.1-3A.4. To the best of our knowledge and available literature on BTTs, there are very few articles published on electrochemical characterization (experimental energy gap) of core BTTs. The experimentally determined HOMO and LUMO energy for BTT3 are -5.30 eV and -1.99 eV respectively and corresponding HOMO-LUMO energy gap (HLG) is 3.31eV [27]. Nazeeruddin et al. also reported substituted BTTs (substitution on BTT2, BTT3 and BTT5) as hole transporting materials [39-40] and experimentally determined energy gap for these substituted derivatives of BTT were also compared with DFT methodology along with core BTT structures (BTT2, BTT3 and BTT5) [39-40]. Further, they also showed a smaller HLG for BTT3 (3.80eV) as compared to BTT2 (4.91eV) and BTT5 (4.45eV), which results in destabilization of HOMO and stabilization of LUMO level of BTT3. Our findings are also in line with the reported results and continuation to the above results HOMO LUMO energy levels for all the BTT isomers were computed to find out HLG. The calculated values of HOMO and LUMO for BTT1 are -6.07 eV and -1.57 eV respectively and the corresponding HLG is 4.49 eV. The computed value of HOMO and LUMO energies and HLG are shown in table3A.9. On moving to BTT2, though both HOMO and LUMO get destabilized, destabilization of LUMO was relatively higher and increased HLG (4.82 eV). Further, BTT3 shows smallest HLG gap shifts of 3.80 eV among all BTT isomers. Conversely, HOMO was more destabilized and LUMO was stabilized in BTT3 isomer resulting in an overall decrease in HLG gap. Similar to BTT3 isomer, BTT4 isomer



showed HLG gap shifts of 3.86 eV due to more stabilization of HOMO. In the case of unsymmetrical BTTs, HLG of BTT5 was 4.39 eV and HOMO and LUMO energies were -5.89 eV and -1.49 eV, respectively. The calculated HLG for BTT6 is 3.87 eV, which was the result of destabilization of HOMO and stabilization of LUMO. The isomer BTT6 showed the highest decrease in HLG gap shift among other unsymmetrical BTTs. HOMO and LUMO energies of BTT7 were -5.76eV and 1.58eV respectively and the corresponding energy difference was 4.18eV. An increasing order of HLG gap shifts for all BTT isomers are BTT3 <BTT4 <BTT6 <BTT7 <BTT5 <BTT1 <BTT2 and a reciprocal order of isomers follows for wavelength. The energy gap between the HOMO-LUMO and their energies are shown in figure 3A.6.

Table 3A.9: Computed HOMO and LUMO energies and Energy Gap (in eV)

Name	HOMO	LUMO	H-L gap
BTT1	-6.06	-1.57	4.49
BTT2	-5.99	-1.16	4.82
BTT3	-5.60	-1.80	3.80
BTT4	-5.70	-1.84	3.86
BTT5	-5.89	-1.49	4.39
BTT6	-5.65	-1.78	3.87
BTT7	-5.76	-1.58	4.18

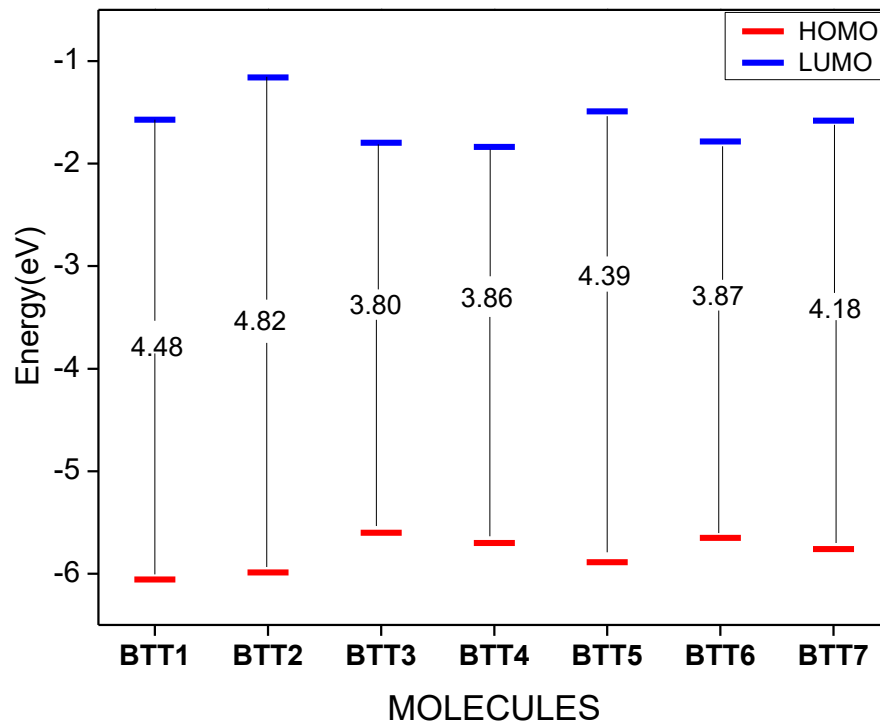


Figure 3A.6. HOMO, LUMO energy levels and HOMO-LUMO gap of all the isomers of BTT

### 3A.3.3. Ionization potential (*IP*), electron affinity (*EA*)

Efficient hole and electron injection are prerequisites for better performance of an optoelectronic device. The molecular ionization potential (*IP*) and electron affinity (*EA*) are key parameters for deciding hole and electron injection ability by reducing the barrier of a molecule. The *IP* and *EA* can predict the ability of devices to transport holes and electrons. *IP* is the energy needed by a molecule when an electron is removed; for efficient hole injection into the HOMO of the molecule, it should be minimum. *EA* indicates the energy of the molecule on the capability of obtaining electrons; the more significant the *EA* is, the easier it becomes for a molecule to get electron. Therefore, adiabatic and vertical *IP*, *EA* and  $\lambda$  for all BTT isomers were calculated and are shown in table 3A.10. Among all isomers of BTT, BTT3 had minimum adiabatic and vertical *IP* values of 7.01eV and 7.11eV respectively (table 3A.10). The calculated *IP* values suggest that it is easy to create a hole in isomer BTT3 than in other isomers of BTT. Among all BTT isomers, BTT4 showed the higher value of adiabatic and vertical *EA* of 0.45eV and 0.36eV, respectively. BTT3 isomer also has a similar value of

adiabatic electron affinity as that of BTT4 isomer. However, there was a small variation in their vertical electron affinity ( $\sim 0.03\text{eV}$ ). This variation can be due to easy electron injection capability into the LUMO of BTT3 and BTT4 than in other isomers. Thus, it concluded that the isomers BTT3 and BTT4 are having the better hole and electron injection ability than other isomers and are applicable in charge transport materials.

### 3A.3.4. Reorganization energy ( $\lambda$ )

Since  $\lambda$  is inversely proportional to the rate constant of charge transport, it implies that smaller the value of  $\lambda$  higher will be the charge transfer rate. The calculated reorganization energies for hole and electron are listed in table 3A.10. All isomers of BTTs show smaller  $\lambda_h$  values (except BTT5) than a well-known hole transport material N,N'-diphenyl-N,N'-bis(3-methylphenyl)-(1,1'-biphenyl)-4,4'-diamine (TPD; 290meV), [42], indicating that the hole transfer rate is higher in BTT isomers than in TPD. Interestingly, BTT4 has  $\lambda_h$  value of 172 meV which is smaller than other BTT isomers, which implies that it can be considered as the best hole transport materials among the studied molecule. Further, all BTT isomers also showed smaller  $\lambda_e$  values than a typical well-known electron transport material tris(8-hydroxyquinolato) aluminum(III)(Alq<sub>3</sub>; 276 meV) [43], which indicates that the electron transfer rate of BTT isomers is higher than Alq<sub>3</sub>. Remarkably, BTT1 has the smallest  $\lambda_e$  value; therefore, it can be the best electron transport material among all BTT isomers.

Table3A.10: Calculated Ionization Potential (IP), Electron Affinity (EA) and reorganization energy ( $\lambda_h$  and  $\lambda_e$ ) in gas phase at B3LYP/6-311+ G (d,p) level of theory

Name	$\lambda_h$ (in meV)	$\lambda_e$ (in meV)	$IP_a$ (in eV)	$IP_v$ (in eV)	$EA_a$ (in eV)	$EA_v$ (in eV)
BTT1	206	143	7.48	7.58	0.21	0.14
BTT2	224	239	7.41	7.52	-0.19	-0.31
BTT3	194	241	7.01	7.11	0.45	0.33
BTT4	172	194	7.13	7.22	0.45	0.36
BTT5	453	272	7.29	7.63	0.15	0.02
BTT6	187	231	7.07	7.17	0.42	0.30
BTT7	250	268	7.15	7.28	0.24	0.11

---

### 3A.4. Conclusion

In summary here in this chapter, electronic excitations, ionization potentials ( $IP$ ), electron affinities ( $EA$ ) and reorganization energies ( $\lambda$ ) for seven isomers of benzotrithiophene (BTT) have been calculated by using the density functional theory (DFT) methods. Structures of all the BTTs are planar with a dihedral angle almost equal to zero; making it the ideal backbone for high charge mobility. The calculated results of the absorption wavelength for all the isomers are in the range of 280-360nm. Among all isomers, BTT3 shows longer wavelength absorption at 362 nm which is also follows experimental results. All molecules are having deep HOMO levels (-5.60 to -6.06eV) and the HOMO-LUMO gap was in the range of 3.80 to 4.82eV. Smallest HOMO-LUMO gap was observed for BTT3 (3.80eV). Based on calculations of IP and EA, BTT3 isomer has shown a greater hole creating ability. BTT3 and BTT4 isomers have shown greater electron injection ability among all BTT isomers. Relatively, all BTT isomers showed low hole/electron reorganization energies, which is an indication of a better hole/electron transporting material. BTT1 and BTT5 isomers show smaller reorganization energies and are better electron transport materials among all BTT isomers. On the other hand,  $\lambda_h < \lambda_e$  for BTT2, BTT3, BTT4, BTT6 and BTT7 and are better for hole transporting materials. Furthermore, most of the BTT isomers show a difference of less than 50 meV between  $\lambda_h$  and  $\lambda_e$ , which is an indication of the ambipolar characteristics and may find application in organic electronic materials.

---

**References**

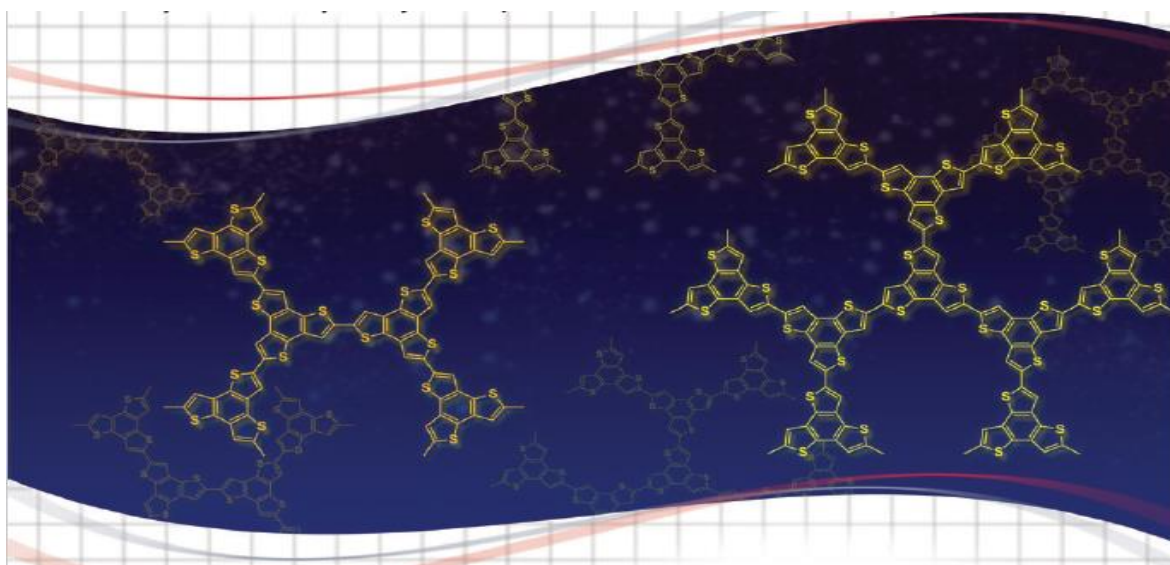
1. S. R. Forrest, *Nature* **2004**, 428, 911.
2. M. M. Torrent, C. Rovira, *Chem. Rev.* **2011**, 111, 4833.
3. J. You, L. Dou, K. Yoshimura, T. Kato, K. Ohya, T. Moriarty, K. Emery, C. C. Chen, J. Gao, G. Li, Y. Yang, *Nat. Commun.* **2013**, 4, 1446.
4. M. L. Keshtov, S. A. Kuklin, V. S. Kochurov, I. O. Konstantinov, M. M. Krayushkin, N. A. Radychev, A. A. R. Khokhlov, *Doklady Chemistry* **2014**, 454, 25.
5. X. Zhao, D. Yang, H. Lv, L. Yin, X. Yang, *Polym. Chem.* **2013**, 4, 57.
6. C. B. Nielsen, R. S. Ashraf, S. Rossbauer, T. Anthopoulos, *Macromolecules*, **2013**, 46, 7727.
7. M. L. Keshtov, Y. Geng, S. A. Kuklin, A. R. Khokhlov, E. N. Koukaras, G. D. Sharma, *Org. Electron.* **2015**, 17, 167.
8. M. X. Chen, E. Perzon, N. Robisson, S. K. M. Jonsson, M. R. Andersson, M. Fahlman, M. Berggren, *Synth. Met.* **2004**, 146, 233.
9. C. Videlot, J. Ackermann, P. Blanchard, J. M. Raimundo, P. Frere, M. Allain, R. D. Bettignies, E. Levillain, J. Roncali, *Adv. Mater.* **2003**, 15, 306.
10. C. Wang, H. Dong, W. Hu, Y. Liu, D. Zhu, *Chem. Rev.* **2012**, 112, 2208.
11. X. Guo, M. Baumgarten, K. Mullen, *Prog. Polym. Sci.* **2013**, 38, 1832.
12. K. Takimiya, S. Shinamura, I. Osaka, E. Miyazaki, *Adv. Mater.* **2011**, 23, 4347.
13. M. Bourass, A. T. Benjelloun, M. Benzakour, M. Mcharfi, M. Hamidi, S. M. Bouzzine, F. S. Spirau, T. Jarroson, J. M. Sotiropoulos, M. Bouachrine, *C. R. Chimie* **2017**, 20, 461.
14. G. Barbarella, M. Melucci, G. Sotgiu, *Adv. Mater.* **2005**, 17, 1581.
15. X. Guo, S. R. Puniredd, M. Baumgarten, W. Pisula, K. Mullen, *J. Am. Chem. Soc.* **2012**, 134, 8404.
16. R. D. Bettignies, Y. Nicolas, P. Blanchard, E. Levillain, J. M. Nunzi, J. Roncali, *Adv. Mater.* **2003**, 15, 1939.
17. T. A. Liu, C. Prabahakar, J. Y. Yu, C. H. Chen, H. H. Huang, J. S. Yang, *Macromolecules* **2012**, 45, 4529.
18. F. Cherioux, L. Guyard, *Adv. Funct. Mater.* **2001**, 11, 305.

19. J. Pei, J. L. Wang, X. Y. Cao, X. H. Zhou, W. B. Zhang, *J. Am. Chem. Soc.* **2003**, 125, 9944.
20. M. Chahma, J. B. Gilroy, R. G. Hicks, *J. Mater. Chem.* **2007**, 17, 4768.
21. R. Jin, *C.R. Chimie* **2015**, 18, 954.
22. Y. Geng, A. Fechtenkotter, K. Mullen, *J. Mater. Chem.* **2001**, 11, 1634.
23. T. Kashiki, M. Kohara, I. Osaka, E. Miyazaki, K. Takimiya, *J. Org. Chem.* **2011**, 76, 4061.
24. Y. Nicolas, P. Blanchard, E. Levillain, M. Allain, N. Mercier, J. Roncali, *Org. Lett.* **2004**, 6, 273.
25. H. Zhou, L. Yang, A. C. Stuart, S.C. Price, S. Liu, W. You, *Angew. Chem. Int. Ed.* **2011**, 50, 2995.
26. C. B. Nielsen, J. M. Fraser, B. C. Schroeder, J. Du, A. J. P. White, W. Zhang, I. McCulloch, *Org. Lett.* **2011**, 13, 2414.
27. X. Guo, S. Wang, V. Enkelmann, M. Baumgarten, K. Mullen, *Org. Lett.* **2011**, 13, 6062.
28. R. Proetzsch, D. Bieniek, F. Korte, *Tetrahedron Lett.* **1972**, 6, 543.
29. H. Hart, M. Sasaoka, *J. Am. Chem. Soc.* **1978**, 100, 4326.
30. N. Jayasuriya, J. Kagan, *J. Org. Chem.* **1989**, 54, 4203.
31. T. Taerum, O. Lukoyanova, R. G. Wylie, D. F. Perpitchka, *Org. Lett.* **2009**, 11, 3230.
32. G. Zhang, M. Zhu, J. Guo, J. Ma, X. Wang, H. Lu, L. Qiu, *Org. Electron.* **2014**, 15, 2608.
33. M. J. Frisch, Gaussian 16, Revision E.01; Gaussian, Inc.: Wallingford CT, **2016**.
34. A. D. Becke, *J. Chem. Phys.* **1993**, 98, 5648.
35. C. Lee, W. Yang, R. G. Parr, *Phys. Rev. B* **1988**, 37, 785.
36. T. Sugano, T. Hashida, A. Kobayashi, H. Kobayashi, *Bull. Chem. Soc. Jpn.* **1988**, 61, 2303.
37. Y. Zhao, D. G. Truhlar, *Theor. Chem. Acc.* **2008**, 120, 215.
38. T. Yanai, D. P. Tew, N. C. Handy, *Chem. Phys. Lett.* **2004**, 393, 51.
39. J. D. Chai, M.H. Gordon, *J. Chem. Phys.* **2008**, 128, 084106.
40. I. G. Benito, I. Zimmermann, J. U. Mora, J. Arago, A. M. Ontoria, E. Orti, N. Martin, M.K. Nazeeruddin, *J. Mater. Chem. A* **2017**, 5, 8317.

41. A. M. Ontoria, I. Zimmermann, I. G. Benito, P. Gratia, C. R. Carmona, S. Aghazada, M. Graetzel, M. K. Nazeeruddin, N. Martin, *Angew. Chem.* **2016**, 128, 6378.
42. M. Malagoli, J.L. Bredas, *Chem. Phys. Lett.* **2000**, 327, 13.
43. B.C. Lin, C.P. Cheng, Z-Q You, C-P Hsu, *J. Am. Chem. Soc.* **2005**, 127, 66.

# Chapter 3B

## *Tuning of Optoelectronic and Charge Transport Properties in Symmetrical Benzotrithiophene (BTT) and its Oligomers*



*Results of this chapter published in J. Phys. Org. Chem. 2020, 33, e4037 as cover page article*







### 3B.1. Introduction

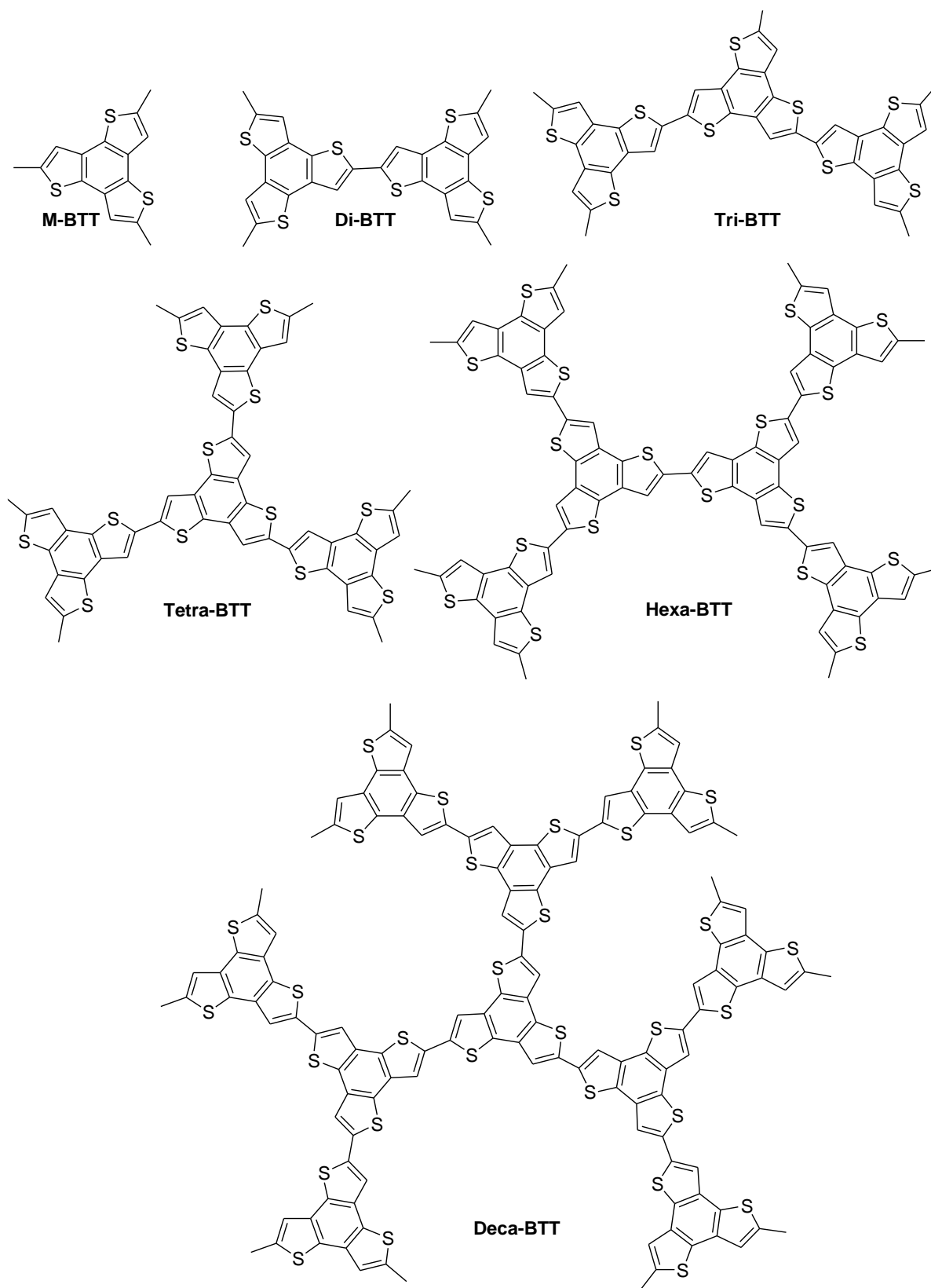
In recent studies have shown that the thiophene-based  $\pi$ -conjugated organic materials are promising candidates for semiconductors [1-2]. These  $\pi$ -conjugated molecules found various optoelectronic applications in organic light-emitting diodes (OLEDs) [3], organic field-effect transistors (OFETs) [4-5] and organic photovoltaics (OPVs) [6-7]. The electron-donating capability of thiophene and their derivatives make them a donor unit in donor-acceptor (D-A) copolymer system [8]. Within thiophene compounds, fused-aromatic compounds with multi-thiophenes are drawing attention as optoelectronic materials in the field of organic semiconductors [9-10]. Further, with an increase in dimensionality (2D or 3D) in conjugated oligomers and polymers results in new opportunities that can manage the morphology of material in thin-film devices and building of nanostructured materials [11]. Branching (dimensionality) in the polymer backbone permits a better  $\pi$ -stacking and charge transport properties. The star-shaped oligothiophenes are consisting of benzene, triazine, truxene and isotruxene as central core unit and are showing better optoelectronic properties [12-14, 9]. M Y Cho group reported soluble star-shaped molecules with benzene as central core unit and used for the fabrication of organic thin-film transistors (OTFTs). They showed that the observed photosensitivity of the device is higher than Si-based phototransistors [15]. J Pie et al., synthesized star-shaped polycyclic aromatic functionalized oligothiophene compounds with a truxene core in excellent yields and shown that the presence of long alkyl chain prevents self-association through  $\pi$ - $\pi$  stacking, which provides a versatile strategy for controlling the morphology of truxene derivatives [16]. RuifaJin, theoretically investigated the electronic excitations and charge transport properties in triazine core-based star-shaped molecules for the application of OLEDs and OSCs [17].

Benzotrithiophene (BTT) emerged as a potential  $\pi$ -core of a new class of organic semiconductor. Its rigid  $\pi$ -framework and planarity promote strong intermolecular interactions, which are appropriate for developing organic semiconducting materials [18]. BTT structure contains three identical thiophene moieties at the periphery of the benzene ring with the dihedral angle between two successive thiophene rings is close to zero (figure 3B.1) and the properties creating a great possibility of building the star-shaped planar molecule with improved  $\pi$ -electron delocalization. Depending on the connectivity of thiophene ring to the central benzene ring, there are seven isomers are possible for BTT, among them; four are

symmetrical while other three are asymmetrical isomers. To the best of our knowledge and available literature on BTT, out of these seven isomers, only four isomers are synthesized while the remaining three are still a challenge for a synthetic chemist [19-21]. In previous chapter 3A, we performed computational studies of all the possible isomers of BTTs for their optoelectronic properties and shown that they may find applications in organic semiconductors as hole/electron transport materials. From the optimized structures of BTT-isomers, BTT2 i. e., benzo[1,2-b:3,4-b':5,6-b'']trithiophene is the most stable among all possible seven isomers (BTT isomers along with relative energies are shown in Table 3A.1). It is evident from the literature BTT2 is one of the most studied isomers among all and act as a core unit for the building of star-shaped oligomer and polymer system [18, 21, 22-26]. Roncali et al. reported the synthesis of star-shaped oligothiophenes based on BTT core and outstanding performance of these molecules in photovoltaic devices [22]. It is also showed that the performance of the BTT-core compounds is superior to linear benzothiophene analogs and other tri-branched oligothiophenes due to BTT-core characteristics of enhanced  $\pi$ -electron delocalization [22]. BTT is an electron-rich molecule with electron donor capability, with the substitution of long alkyl chains in place of branching alkyl chains in BTT, there will be reduction in steric hindrance and further increases its electron donor capability, which helps to construct donor-acceptor (D-A) copolymer systems used in OPVs, OFETs, OLEDs, etc. [24-26]. K. Takimiya group synthesized BTT oligomers and showed that fused BTT-core is a useful unit for coplanarity and effective intermolecular  $\pi$ -stacking structure for developing new  $\pi$ -conjugated functional materials [23].

From the literature reports and encouraged by the fact, the design of the new molecular structure is the key to the development of a planar and  $\pi$ -conjugated framework, which promotes strong molecular interactions suitable for organic semiconducting materials.

In this chapter, we performed DFT and TDDFT studies to investigate the electronic excitations and charge transport properties in benzo[1,2-b:3,4-b':5,6-b'']trithiophene (BTT) molecule and its di-, tri-, tetra- hexa- and deca-oligomers (shown in scheme 3B.1).



Scheme 3B.1: Structure of BTT and its oligomers

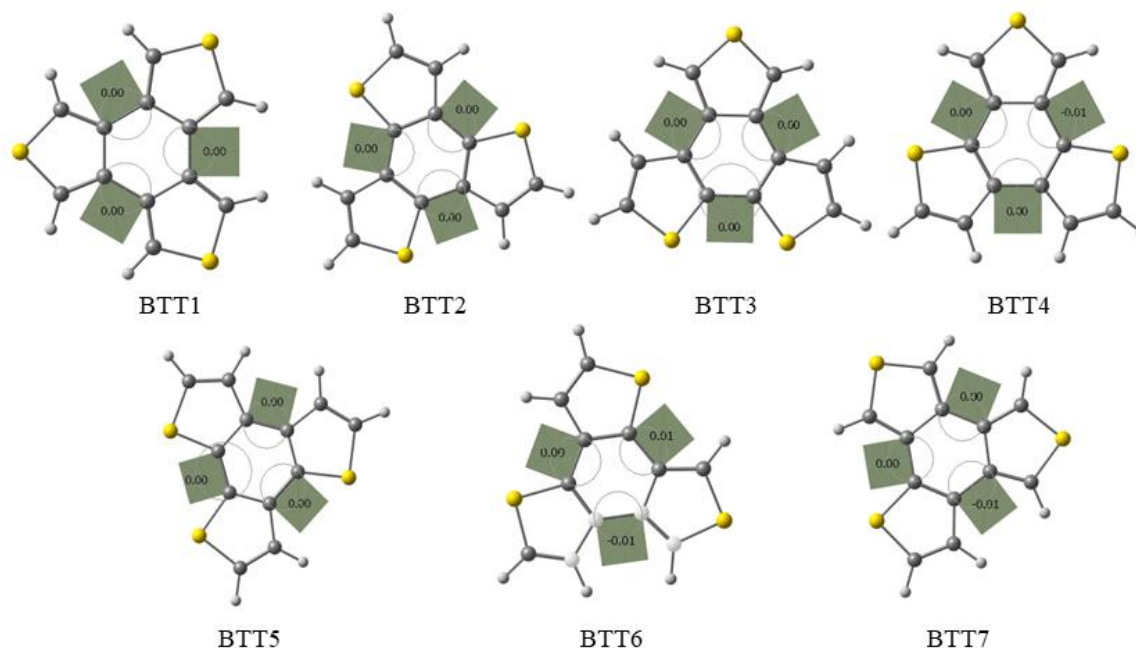


Figure 3B.1: Seven possible isomers of Benzotrithiophene (BTT); Symmetrical (BTT1-BTT4) and Asymmetrical (BTT5-BTT7) isomers (with dihedral angle between two thiophene ring)

### 3B.2. Computational Methodology

The geometry of all the BTT oligomers are shown in scheme 3B.1 and are fully optimized using Gaussian software (Frisch et al.)[27]. All the molecules are optimized using B3LYP functional and with 6-31G (d, p) basis set. Further, all the frequency calculations were carried out to check the imaginary frequencies to ensure that optimized geometries correspond to the true minima. Further diffused basis sets with B3LYP functionals are also considered to see their effect on geometries of oligomers. TDDFT methodology is used to calculate lowest electronic excitations for all the oligomer with different functionals specifically B3LYP, M06, PBE0, BHandHLYP, CAM-B3LYP and WB97XD with 6-311++G (d, p) basis set.

The calculation of hole ( $\lambda_h$ ) and electron ( $\lambda_e$ ) reorganization energies are done by using *equations 1.14* and *1.15* respectively (in chapter 1). Also the calculation of charge injection parameters i.e. ionization potential (IP) and electron affinity (EA) are done by using *equations 1.17* and *1.18* respectively. Further hole and electron extraction potentials are calculated by *equations 1.19* and *1.20* respectively.

---

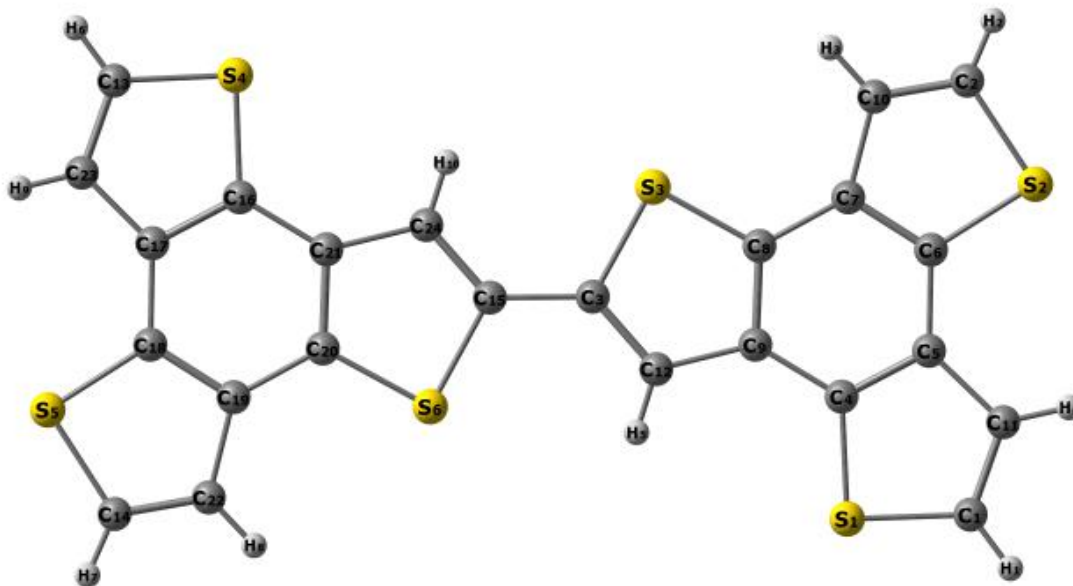
### 3B.3. Results and Discussions

#### 3B.3.1. Geometry and structures

Out of six molecules considered in this study, five are known for its synthetic routes (except Tri-BTT) [23]. Molecular geometry of all the molecules are optimized in its ground state. The bond length (BL) and bond angle (BA) of the available crystal structure of Di-BTT are compared with its optimized geometry and are shown in table 3B.1. It is clear from the table 3B.1, the bond lengths and bond angles of the crystal structure (experimentally reported crystal is without any substitution) and DFT (B3LYP/6-31G (d, p)) optimized structure are in good agreement.

To check the effect of basis set on the geometry of BTT-oligomers, four isomers namely M-BTT, Di-BTT, Tri-BTT and Tetra-BTT are optimized by using the higher basis set 6-311+ G (d, p) at B3LYP method. In table 3B.2, comparison of bond lengths and bond angles are shown for the optimized Di-BTT with 6-31G (d, p) and 6-311+ G (d, p) basis set. It is clear from table 3B.2 that there is a negligible change in bond length and bond angles on increasing the size of the basis set. Since there is no considerable difference in geometry with 6-31G (d, p) and 6-311+ G (d, p) basis sets, our further discussions are based on B3LYP/6-31G (d, p) optimized geometries.

Table 3B.1: Comparative study of Bond lengths (BL) and Bond angles (BA) of Crystal structure and Optimized geometry at B3LYP/6-31 G (d, p) level for the molecule Di-BTT.

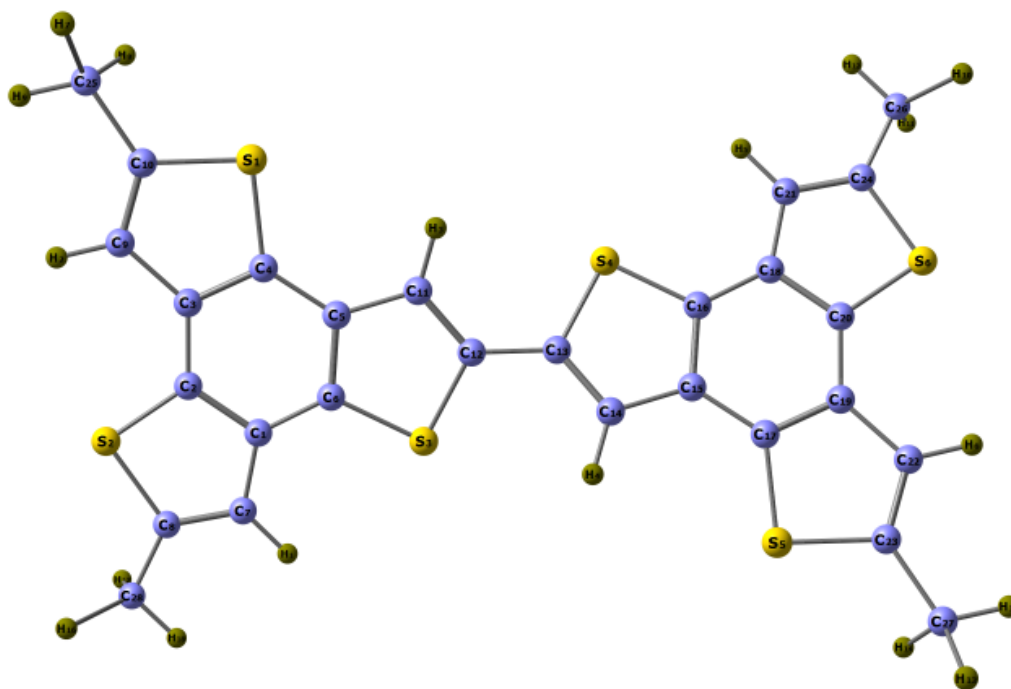


BL/BA	Crystal	Calculated		BL/BA	Crystal	Calculated
C <sub>1</sub> C <sub>11</sub>	1.375	1.358		C <sub>19</sub> C <sub>22</sub>	1.457	1.438
C <sub>11</sub> C <sub>5</sub>	1.426	1.437		C <sub>22</sub> C <sub>14</sub>	1.337	1.359
C <sub>5</sub> C <sub>6</sub>	1.423	1.418		C <sub>1</sub> S <sub>1</sub>	1.723	1.751
C <sub>6</sub> C <sub>7</sub>	1.382	1.409		C <sub>4</sub> S <sub>1</sub>	1.718	1.747
C <sub>7</sub> C <sub>8</sub>	1.427	1.416		C <sub>2</sub> S <sub>2</sub>	1.741	1.751
C <sub>8</sub> C <sub>9</sub>	1.392	1.408		C <sub>6</sub> S <sub>2</sub>	1.723	1.748
C <sub>9</sub> C <sub>12</sub>	1.443	1.431		C <sub>3</sub> S <sub>3</sub>	1.753	1.780
C <sub>12</sub> C <sub>3</sub>	1.355	1.371		C <sub>8</sub> S <sub>3</sub>	1.716	1.769
C <sub>7</sub> C <sub>10</sub>	1.457	1.438		C <sub>13</sub> S <sub>4</sub>	1.723	1.751
C <sub>10</sub> C <sub>2</sub>	1.337	1.358		C <sub>16</sub> S <sub>4</sub>	1.718	1.747
C <sub>3</sub> C <sub>15</sub>	1.449	1.447		C <sub>14</sub> S <sub>5</sub>	1.741	1.751
C <sub>15</sub> C <sub>24</sub>	1.355	1.371		C <sub>18</sub> S <sub>5</sub>	1.723	1.748
C <sub>24</sub> C <sub>21</sub>	1.443	1.430		C <sub>15</sub> S <sub>6</sub>	1.753	1.769
C <sub>21</sub> C <sub>20</sub>	1.392	1.409		C <sub>20</sub> S <sub>6</sub>	1.716	1.751



<b>C<sub>20</sub>C<sub>19</sub></b>	1.428	1.416	<b>C<sub>4</sub>S<sub>1</sub>C<sub>2</sub></b>	90.09	91.09
<b>C<sub>19</sub>C<sub>18</sub></b>	1.382	1.409	<b>C<sub>6</sub>S<sub>2</sub>C<sub>3</sub></b>	89.12	91.13
<b>C<sub>18</sub>C<sub>17</sub></b>	1.423	1.418	<b>C<sub>8</sub>S<sub>3</sub>C<sub>13</sub></b>	90.12	91.43
<b>C<sub>17</sub>C<sub>16</sub></b>	1.389	1.408	<b>C<sub>13</sub>S<sub>4</sub>C<sub>16</sub></b>	90.09	91.09
<b>C<sub>16</sub>C<sub>21</sub></b>	1.419	1.419	<b>C<sub>14</sub>S<sub>5</sub>C<sub>18</sub></b>	89.11	91.14
<b>C<sub>17</sub>C<sub>23</sub></b>	1.425	1.438	<b>C<sub>15</sub>S<sub>6</sub>C<sub>20</sub></b>	90.12	91.43
<b>C<sub>23</sub>C<sub>13</sub></b>	1.375	1.359			

Table 3B.2: Comparison of Bond lengths(BL) and Bond angles (BA) of Di-BTT optimized by using B3LYP functionals with 6-311+G (d, p) and 6-31G (d, p) basis set



<b>BL</b>	<b>6-311+G (d, p)</b>	<b>6-31G (d, p)</b>	<b>BL/BA</b>	<b>6-311+G (d, p)</b>	<b>6-31G (d, p)</b>
<b>C<sub>1</sub>C<sub>2</sub></b>	1.406	1.408	<b>C<sub>19</sub>C<sub>22</sub></b>	1.437	1.438
<b>C<sub>2</sub>C<sub>3</sub></b>	1.415	1.416	<b>C<sub>22</sub>C<sub>23</sub></b>	1.359	1.361
<b>C<sub>3</sub>C<sub>4</sub></b>	1.405	1.407	<b>C<sub>18</sub>C<sub>21</sub></b>	1.438	1.438
<b>C<sub>4</sub>C<sub>5</sub></b>	1.416	1.417	<b>C<sub>21</sub>C<sub>24</sub></b>	1.359	1.361
<b>C<sub>5</sub>C<sub>6</sub></b>	1.408	1.410	<b>C<sub>24</sub>C<sub>26</sub></b>	1.496	1.498

<b>C<sub>1</sub>C<sub>7</sub></b>	1.438	1.438		<b>C<sub>23</sub>C<sub>27</sub></b>	1.497	1.498
<b>C<sub>7</sub>C<sub>8</sub></b>	1.358	1.360		<b>C<sub>4</sub>S<sub>1</sub></b>	1.752	1.752
<b>C<sub>3</sub>C<sub>9</sub></b>	1.437	1.438		<b>C<sub>10</sub>S<sub>1</sub></b>	1.762	1.765
<b>C<sub>9</sub>C<sub>10</sub></b>	1.359	1.361		<b>C<sub>2</sub>S<sub>2</sub></b>	1.752	1.753
<b>C<sub>5</sub>C<sub>11</sub></b>	1.430	1.431		<b>C<sub>8</sub>S<sub>2</sub></b>	1.763	1.765
<b>C<sub>11</sub>C<sub>12</sub></b>	1.368	1.370		<b>C<sub>6</sub>S<sub>3</sub></b>	1.750	1.752
<b>C<sub>10</sub>C<sub>25</sub></b>	1.497	1.497		<b>C<sub>12</sub>S<sub>3</sub></b>	1.768	1.771
<b>C<sub>8</sub>C<sub>28</sub></b>	1.497	1.497		<b>C<sub>13</sub>S<sub>4</sub></b>	1.768	1.771
<b>C<sub>12</sub>C<sub>13</sub></b>	1.447	1.447		<b>C<sub>16</sub>S<sub>4</sub></b>	1.750	1.752
<b>C<sub>13</sub>C<sub>14</sub></b>	1.368	1.370		<b>C<sub>17</sub>S<sub>5</sub></b>	1.752	1.752
<b>C<sub>14</sub>C<sub>15</sub></b>	1.430	1.431		<b>C<sub>23</sub>S<sub>5</sub></b>	1.762	1.765
<b>C<sub>15</sub>C<sub>16</sub></b>	1.408	1.410		<b>C<sub>20</sub>S<sub>6</sub></b>	1.752	1.753
<b>C<sub>15</sub>C<sub>17</sub></b>	1.416	1.417		<b>C<sub>24</sub>S<sub>6</sub></b>	1.763	1.765
<b>C<sub>16</sub>C<sub>18</sub></b>	1.413	1.414		<b>C<sub>4</sub>S<sub>1</sub>C<sub>10</sub></b>	91.639	91.605
<b>C<sub>17</sub>C<sub>19</sub></b>	1.405	1.407		<b>C<sub>2</sub>S<sub>2</sub>C<sub>8</sub></b>	91.682	91.651
<b>C<sub>18</sub>C<sub>20</sub></b>	1.406	1.409		<b>C<sub>6</sub>S<sub>3</sub>C<sub>12</sub></b>	91.454	91.427
<b>C<sub>19</sub>C<sub>20</sub></b>	1.415	1.416		<b>C<sub>13</sub>S<sub>4</sub>C<sub>16</sub></b>	91.454	91.427
				<b>C<sub>17</sub>S<sub>5</sub>C<sub>23</sub></b>	91.639	91.605
				<b>C<sub>20</sub>S<sub>6</sub>C<sub>24</sub></b>	91.682	91.651

### 3B.3.2. Electronic excitations

To know the nature of electronic excitations in these oligomers, the quantum chemical calculations were performed with TDDFT methodology at 6-311++ G (d, p) basis set. To obtain the absorption energies, the low-lying fifteen electronic excitations are considered for the calculations. Further, to see the effect of different functionals on electronic excitations, TDDFT calculations have been performed with various functionals namely B3LYP, M06, PBE0, BHandHLYP, CAM-B3LYP and WB97XD. Among all the functional, PBE0 is in good agreement with the experimental absorption energies (shown in Figure 3B.2) and further

discussions are based on the results obtained at PBE0/6-311++ G (d, p) level. The calculated absorption with different functionals are shown in table 3B.3.

Table 3B.3: Calculated Absorption ( $\lambda$ ) and Oscillator strength ( $f$ ) with different functionals using 6-311++G(d,p) at B3LYP/6-31G(d,p) optimized geometry

BTT-Oligomers	B3LYP		BHHLYP		PBE0		M06		CAM-B3LYP		WB97XD	
	$\lambda$	$f$	$\lambda$	$f$	$\lambda$	$f$	$\lambda$	$f$	$\lambda$	$f$	$\lambda$	$f$
M-BTT	275	0.437	246	0.705	267	0.502	267	0.427	250	0.716	248	0.752
Di-BTT	395	0.977	352	1.073	382	1.027	391	0.991	352	1.065	346	1.093
Tri-BTT	410	0.537	358	1.897	392	1.371	400	1.555	347	2.017	351	1.938
Tetra-BTT	403	1.480	357	1.851	393	1.652	400	1.604	358	1.834	346	1.886
Hexa-BTT	429	0.001	364	2.658	407	0.003	411	2.278	365	2.628	358	2.707
Deca-BTT	429	0.004	366	2.254	408	2.025	414	2.006	366	2.241	359	2.301

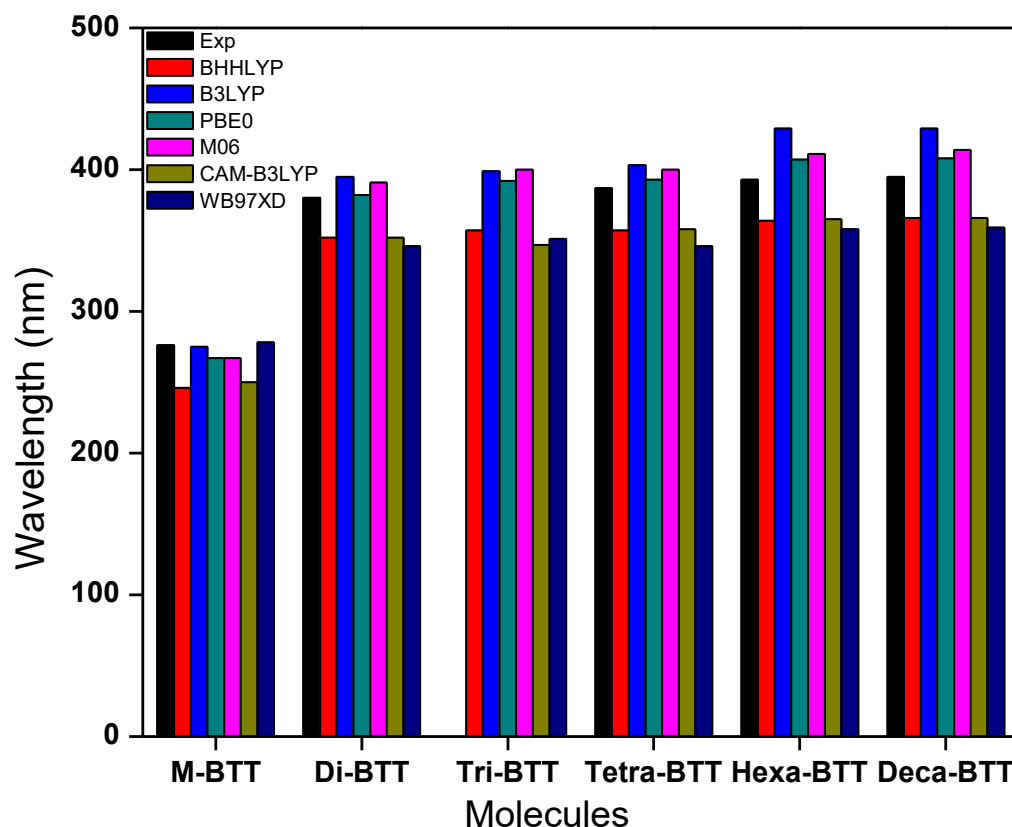


Figure 3B.2: Calculated absorption energies with different functionals

K. Takimiya et. al. showed that the increasing number of BTT units in the molecules, results in destabilization of HOMO level and the HOMO-LUMO energy gap becomes smaller. However, the extent of destabilization of HOMO and reduction in the HOMO-LUMO gap are not significant [23]. Further, they also performed theoretical calculations using DFT method at B3LYP/6-31 G (d) level for unsubstituted M-BTT, Di-BTT and Tetra-BTT. It has shown that M-BTT and Tetra-BTT possess doubly degenerate frontier molecular orbitals. However, Di-BTT has non-degenerated levels with electron density delocalized over the whole molecule [23]. The same trend is followed in our calculations and further, we extended the study up to Deca-BTT.

The experimentally observed absorption maximum ( $\lambda_{\max}$ ) for M-BTT is at 276 nm while its dimer Di-BTT is showing 100 nm red-shifted with the  $\lambda_{\max}$  at 380 nm. Similarly, observed  $\lambda_{\max}$  for Tetra-BTT, Hexa-BTT and Deca-BTT are at 387 nm, 393 nm and 395 nm respectively. TDDFT calculated  $\lambda_{\max}$  for M-BTT is at 267 nm, and the main transitions are from

HOMO→LUMO, HOMO→LUMO+1, HOMO-1→LUMO and HOMO-1→LUMO+1 with the oscillator strength of 0.502. The  $\lambda_{\max}$  for Di-BTT is at 382 nm, which is associated with the HOMO→LUMO transition. Around 100 nm red shift in absorption was observed while moving from M-BTT to Di-BTT but on the addition of one more BTT unit (from Di-BTT to Tri-BTT), there is hardly redshift of 10 nm. The  $\lambda_{\max}$  for Tri-BTT is at 392 nm that arises due to HOMO→LUMO+1 transition. Tri-BTT and Tetra-BTT are showing close absorption maxima; the calculated  $\lambda_{\max}$  for Tetra-BTT is at 393 nm. The main transitions are from HOMO→LUMO+2 and HOMO→LUMO. Few minor transitions are also involved along with the main transitions, which are from HOMO→LUMO+1, HOMO-1→LUMO+1 and HOMO-1→LUMO. Hexa-BTT is showing  $\lambda_{\max}$  at 407 nm with low intensity (0.003) with the transition from HOMO→LUMO and HOMO-1→LUMO+1; the intense peak is at 405 nm with HOMO-2→LUMO+1 and HOMO-1→LUMO and HOMO→LUMO+1 transitions. Similar is the case for Deca-BTT there is a negligible difference in  $\lambda_{\max}$  when comparing with the Hexa-BTT and showing absorption at 408 nm. Normalized absorption energies for all the molecules are shown in figure 3B.3. As the absorption energies are shown in table 3B.4, after Di-BTT, there is no appreciable change in  $\lambda_{\max}$  of BTT oligomers with the addition of further BTT units. This may be due to the deviation in its planarity in Tri-BTT- Deca-BTT (table 3B.5). Deviation in planarity affects the effective delocalization of electron and hence there is a minor change in the absorption properties with the further addition of BTT units. It is evident from the molecular orbital pictures that the electron density is confined within two or three BTT parts in each orbital for the Tetra-BTT, Hexa-BTT and Deca-BTT. As discussed above except Di-BTT, all the oligomers are having more than one transition.

The HOMO and LUMO energies, and corresponding HOMO-LUMO energy gap (HLG) for each oligomer are calculated and tabulated in table 3B.6. The calculated HOMO and LUMO energy for M-BTT is -5.39 eV and -0.59 eV respectively and corresponding HLG is 4.80eV. There is a decrease in HLG (3.57eV) of Di-BTT when compared with M-BTT, which is due to the stabilization of LUMO and destabilization of HOMO levels. The calculated HOMO and LUMO energies for Di-BTT are -5.10eV and -1.53eV, respectively. On further increasing the branching on Di-BTT, i.e. for Tri-BTT, Tetra-BTT and Hexa-BTT, HOMO energy (-5.15 eV) are almost the same. The LUMO level in the case of Tri-BTT and Tetra-BTT is also degenerate (-1.67eV). However, there is a decrease in HLG for Hexa-BTT due to more stabilization of

LUMO level (-1.76 eV) and the resulting energy gap is 3.40 eV. In the case of Deca-BTT, a small destabilization of HOMO and stabilization of LUMO level results in a further decrease in HLG (3.37eV) as compared to Hexa-BTT. The HOMO, LUMO levels and HLG for all the molecules are shown in Figure 3B.4 (HOMO, LUMO energies of oligomers are shown in table 3B.6).

In M-BTT, HOMO and HOMO-1 energy levels are almost degenerate (-5.39eV) and LUMO and LUMO+1 are also doubly degenerate with the energy of -0.59 eV and electron density are delocalized throughout the molecule (figure 3B.5). Di-BTT shows non-degenerate HOMO and LUMO levels (figure 3B.6). However, in other oligomers, Tri-BTT, Tetra-BTT, Hexa-BTT and Deca-BTT all are having doubly degenerate frontier molecular orbitals and are shown in figure 3B.7 to figure 3B.10. The experimentally reported HOMO, LUMO energies and their corresponding energy gap for alkylated (octyl-substituted) BTT and their oligomers show that, on moving from M-BTT to Deca-BTT destabilization of HOMO and stabilization of LUMO level taking place. This destabilization of HOMO and stabilization of LUMO level results in a decrease in energy gap [23]. The trend observed from theoretical calculations is in accordance with the experimental results that with addition of BTT unit destabilization of HOMO and stabilization of LUMO level takes place and hence there is decrease in HLG.

Table 3B.4: Experimental ( $\lambda^{\text{Exp}}$  in nm) and Calculated absorption maxima ( $\lambda^{\text{Cal}}$  in nm), Oscillator strength ( $f$ ), Major Transitions (MT), % weight (%  $C_i$ , contributions >10% are shown) at PBE0 method using 6-311++G (d, p) basis sets.

BTT-oligomers	$\lambda^{\text{Exp}}$	$\lambda^{\text{Cal}}$	$f$	MT	% $C_i$
M-BTT	276 <sup>a</sup>	267	0.502	H-1→L+1	40
				H→L	40
		256	0.013	H→L+2	94
		239	0.216	H-2→L+1	90
Di-BTT	380 <sup>a</sup>	382	1.027	H→L	97
		349	0.048	H→L+2	84
		303	0.155	H→L+2	75
Tri-BTT	--	393	1.371	H→L+1	89

		384	0.507	H-1→L+1	68
				H→L	21
		380	0.302	H→L	70
Tetra-BTT	387 <sup>a</sup>	393	1.652	H→L	20
				H-1→L+1	17
				H→L+2	25
		369	0.026	H-1→L+2	69
		356	0.020	H-3→L	15
			H-4→L+1	12	
Hexa-BTT	393 <sup>a</sup>	407	0.003	H→L	52
		405	1.788	H-2→L	27
				H-1→L	17
				H→L+1	15
				H-2→L+2	12
404	0.566	H-1→L+2	28		
			H-2→L	31	
			H-1→L	14	
Deca-BTT	395 <sup>a</sup>	408	1.852	H-3→L	12
				H-4→L+1	12
		406	0.008	H-1→L	27
				H→L+1	26
405	0.302	H-2→L	18		

<sup>a</sup> *J. Org. Chem.* **2011**, 76, 4061

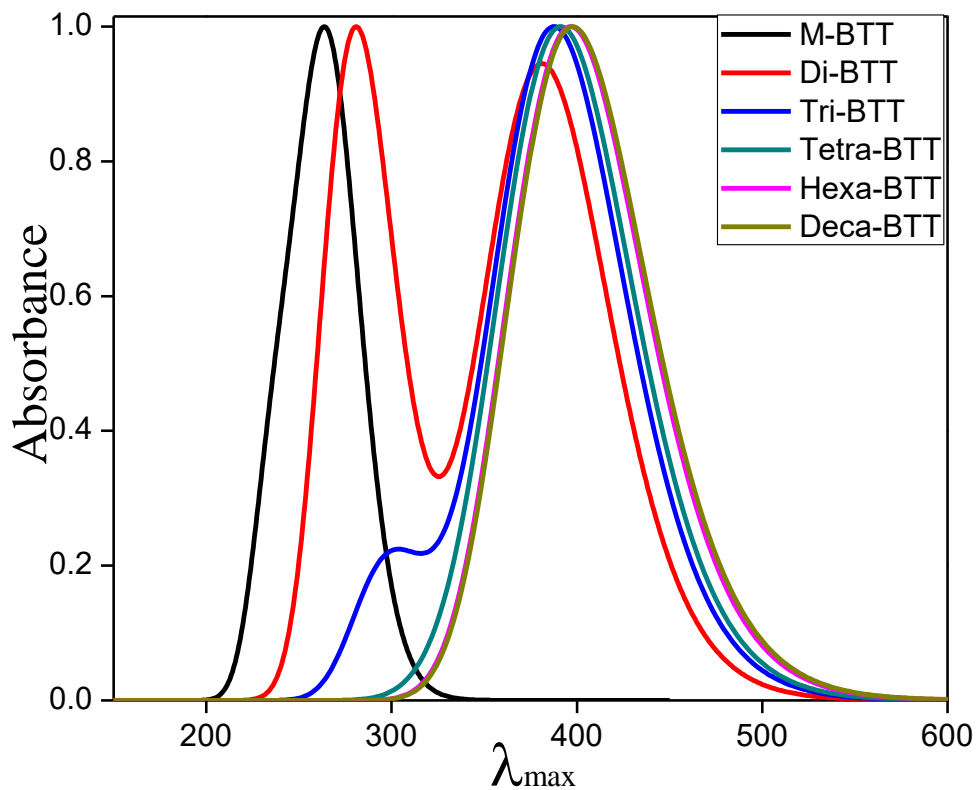


Figure 3B.3: Normalized absorption spectra of BTT and its oligomers

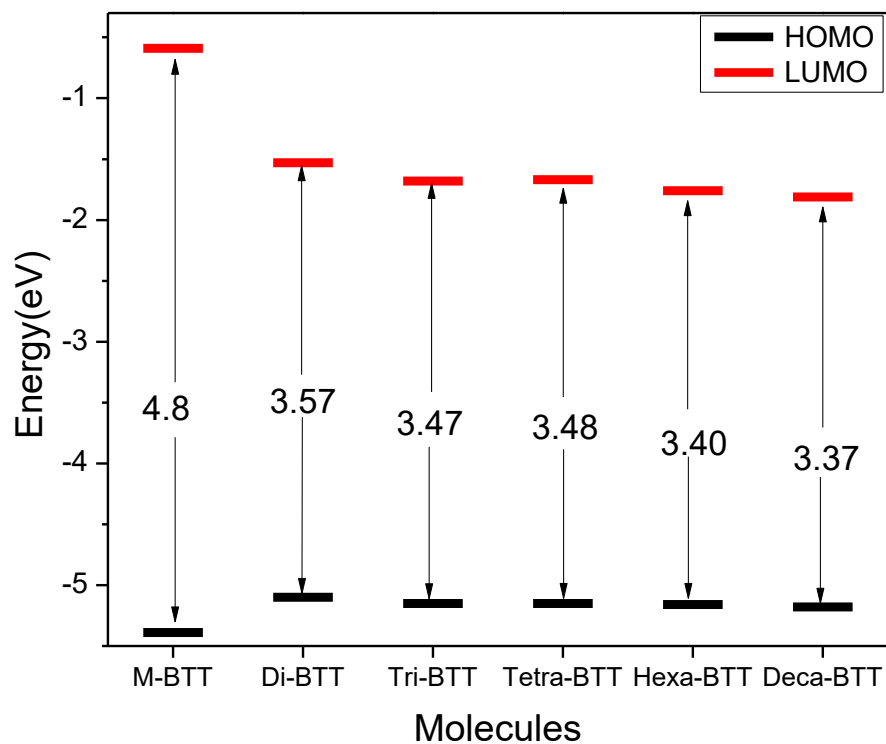
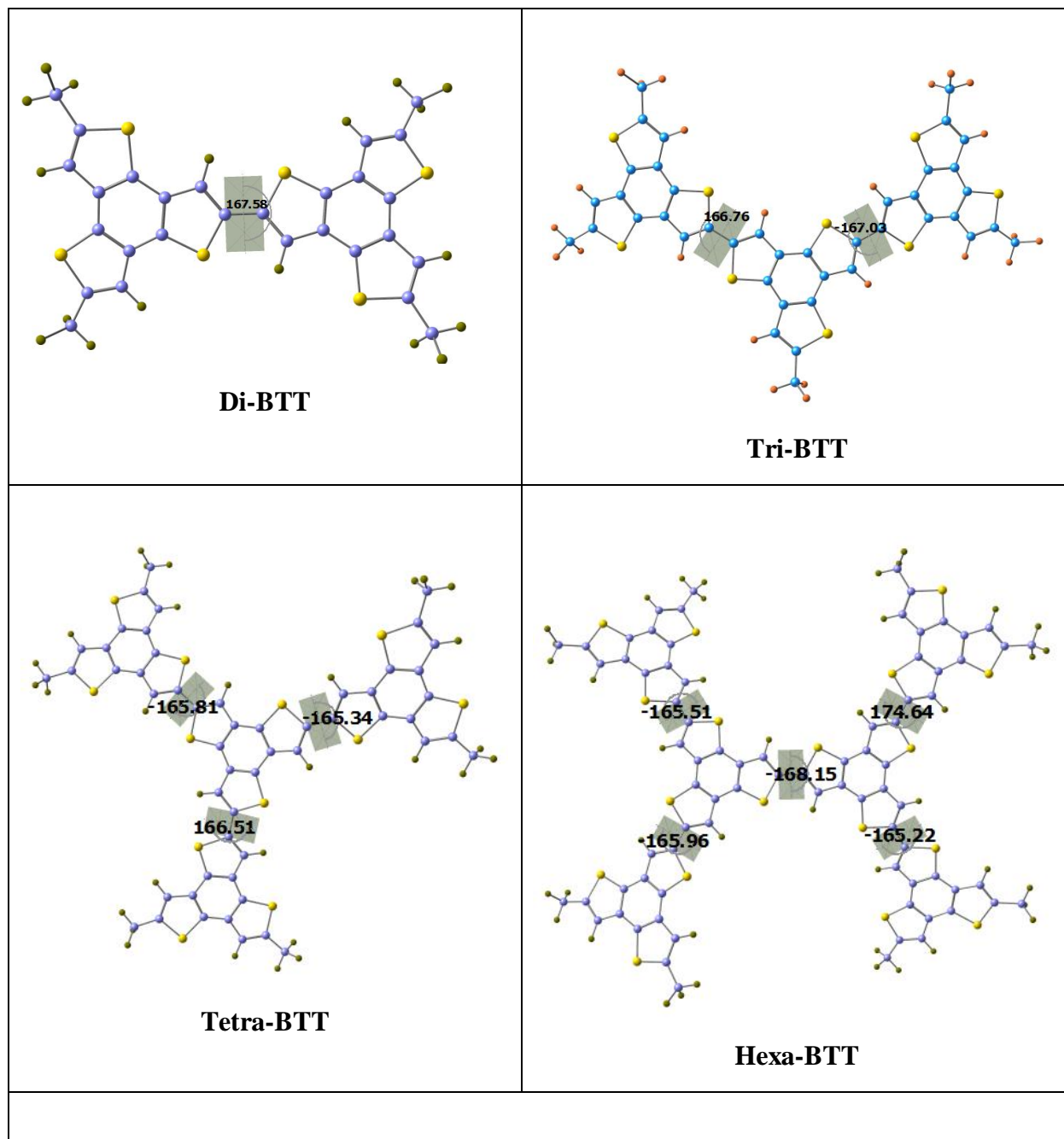


Figure 3B.4: HOMO-LUMO levels and energy gap (in eV) of BTT and its oligomers



Table 3B.5: Optimized geometries with dihedral angles.



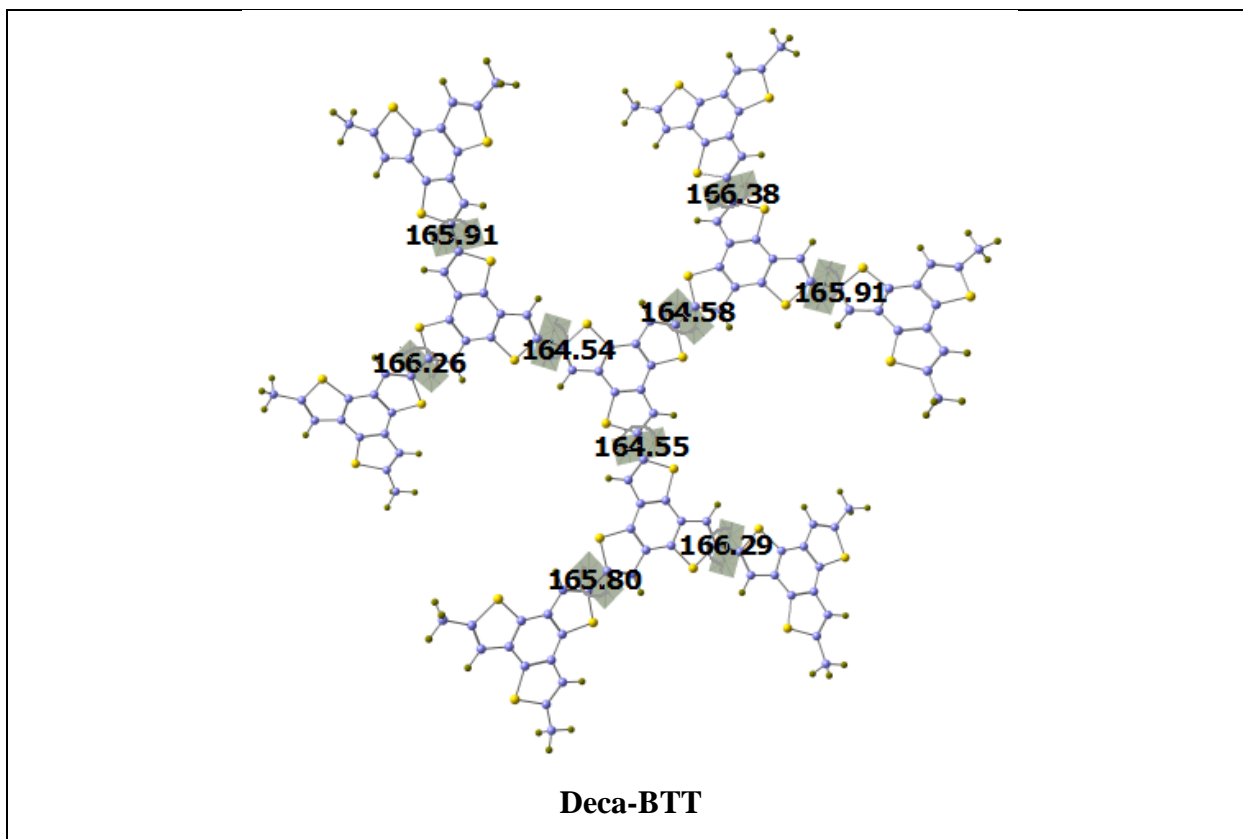


Table 3B.6: HOMO, LUMO energies and corresponding HOMO-LUMO gap (in eV)

BTT-oligomers	HOMO	LUMO	H-L gap
M-BTT	-5.39	-0.59	4.8
Di-BTT	-5.10	-1.53	3.57
Tri-BTT	-5.15	-1.68	3.47
Tetra-BTT	-5.15	-1.67	3.48
Hexa-BTT	-5.16	-1.76	3.40
Deca-BTT	-5.18	-1.81	3.37

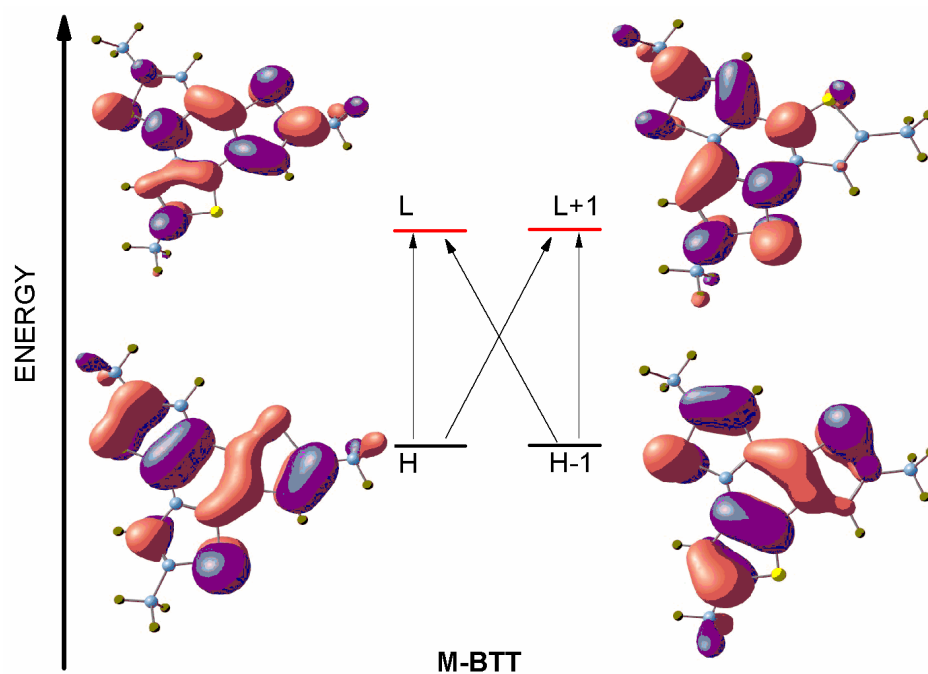


Figure 3B.5: Major electronic excitations and molecular orbital pictures of **M-BTT**

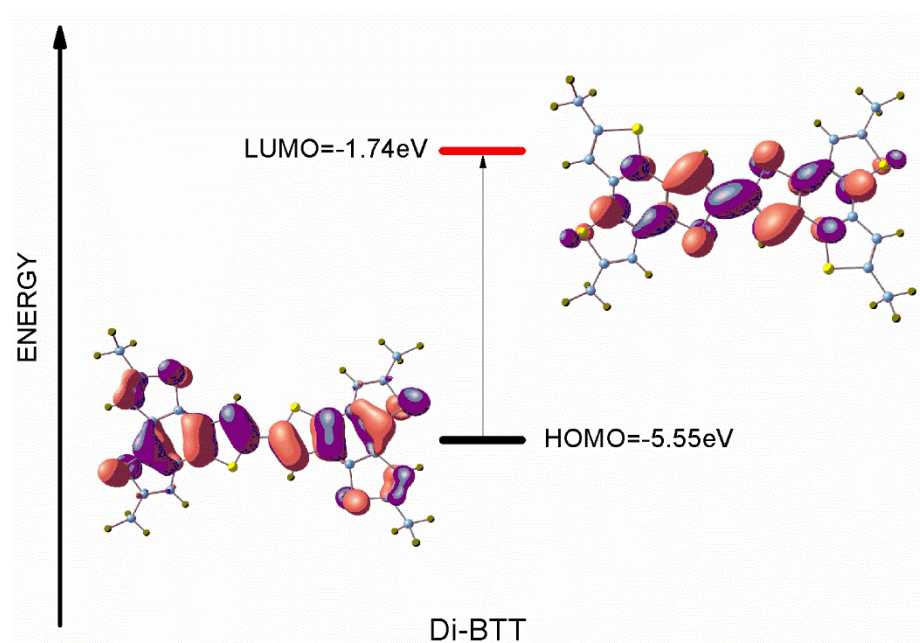


Figure 3B.6: Major electronic excitations and molecular orbital pictures of **Di-BTT**

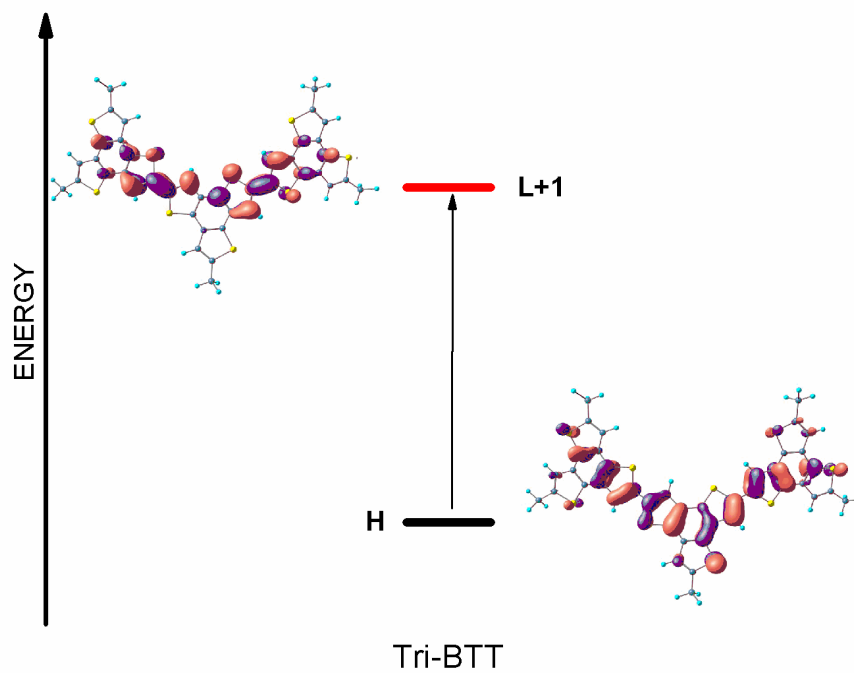


Figure 3B.7: Major electronic excitations and molecular orbital pictures of **Tri-BTT**

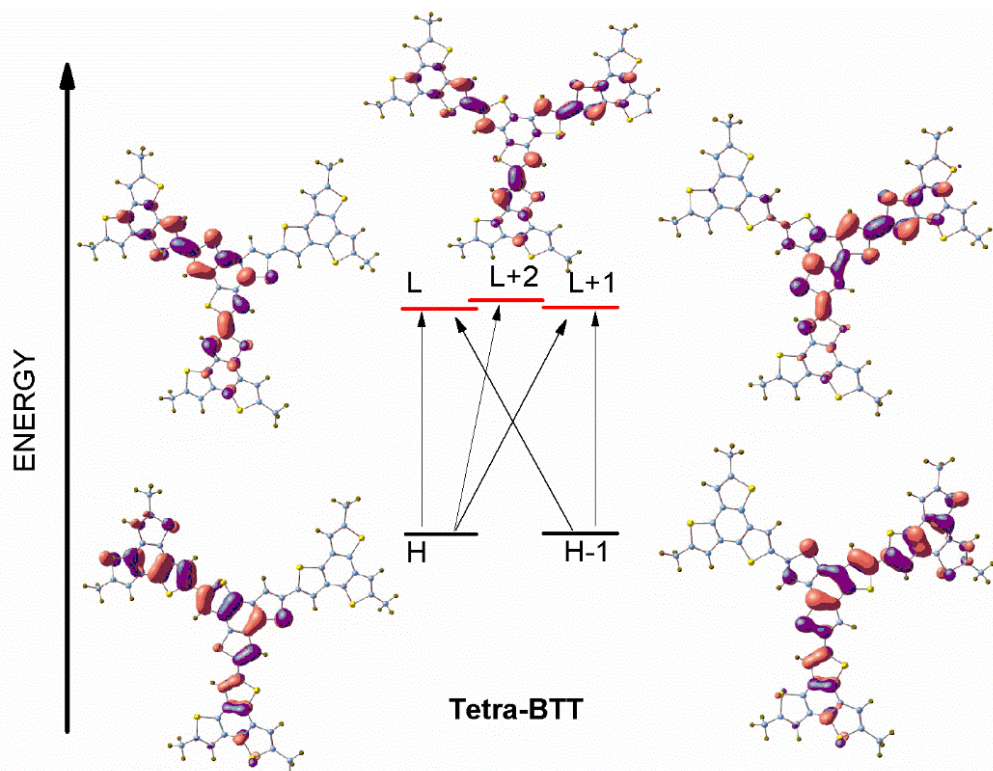


Figure 3B.8: Major electronic excitations and molecular orbital pictures of **Tetra-BTT**



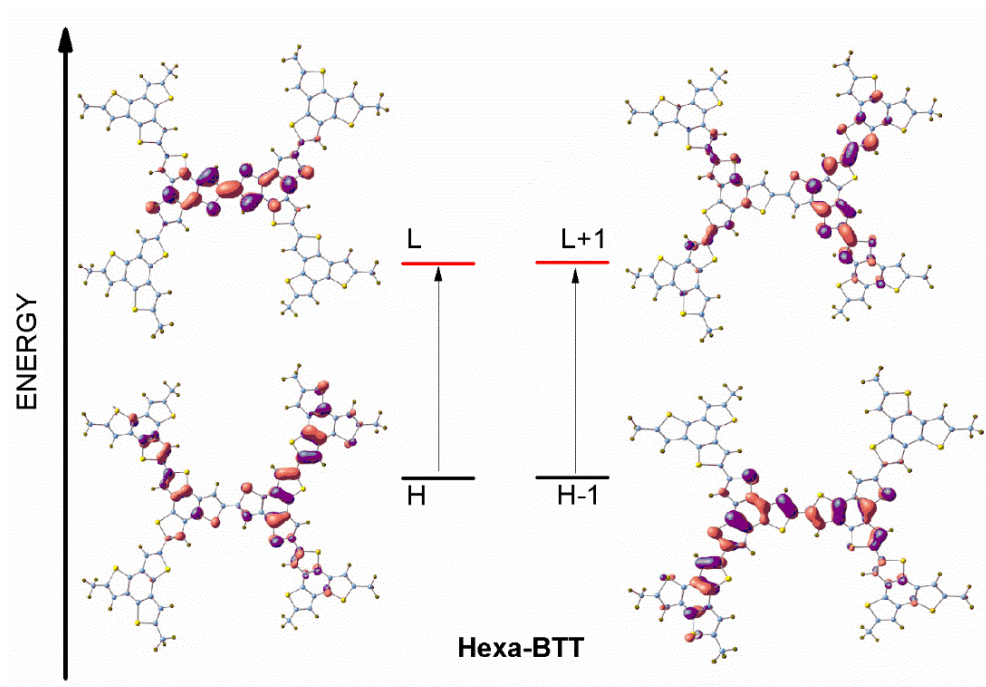


Figure 3B.9: Major electronic excitations and molecular orbital pictures of **Hexa-BTT**

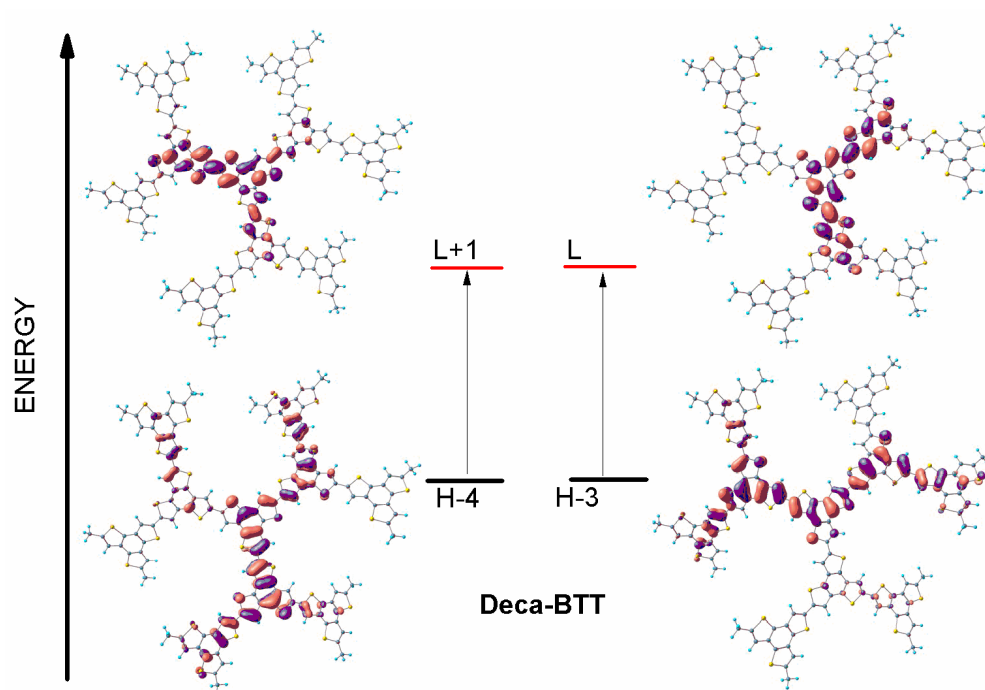


Figure 3B.10: Major electronic excitations and molecular orbital pictures of **Deca-BTT**

### 3B.3.3. Ionization potentials (IP) and electron affinities (EA)

IP and EA are the key parameters for supporting the charge injection mechanism for compounds. IP defined as the energy required by the system when an electron separated from the molecule and it must be small so that there is an efficient injection of the hole into the HOMO of the molecule. EA is defined as the energy departures while an electron is imparted to the system and it must be elevated to allow an efficient injection of an electron into LUMO level of the molecule. The calculated values of adiabatic (a) and vertical (v) IP & EA are shown in figure 3B.11 and 3B.12 (values are shown in Table 3B.7). It is understandable table 3B.7; the IP is decreasing with an increase in the number of BTT units. M-BTT has the adiabatic (vertical) IP value of 6.76 eV (6.87 eV) which decreases with the addition of further one more BTT unit to M-BTT (i.e. Di-BTT) and the adiabatic (vertical) IP values are 6.10 eV (6.21 eV).

Similarly, the IP values are decreasing in Tri-BTT, Tetra-BTT, Hexa-BTT and Deca-BTT when compared to the M-BTT. The energy obligatory to create a hole in the oligomer decreases with an increased number of BTT-units. The IP is smallest for Deca-BTT having adiabatic and vertical IP of 5.64 eV and 5.67 eV respectively, resulting it is easy to inject a hole in Deca-BTT than other oligomers. EA is increasing with an increase in the number of BTT units (Figure 3B.11 and 3B.12). The EA value is highest for Deca-BTT having values of 1.24 eV ( $EA_a$ ) and 1.19 eV ( $EA_v$ ), showing it is easy to inject an electron into LUMO of Deca-BTT. From these outcomes, it is apparent that with an increase in BTT-units, the oligomer becomes more and more appropriate for hole and electron transport materials.

Table 3B.7: Calculated reorganization energy ( $\lambda_h$ , and  $\lambda_e$ ) (in meV), Ionization Potential (IP), Electron Affinity (EA), HEP and EEP (in eV) at B3LYP/6-31G (d, p) level of theory

BTT-oligomers	$\lambda_h$	$\lambda_e$	$IP_a$	$IP_v$	$EA_a$	$EA_v$	HEP	EEP
M-BTT	230	242	6.76	6.87	-0.74	-0.86	6.65	-0.62
Di-BTT	222	295	6.10	6.21	0.51	0.36	5.99	0.66
Tri-BTT	152	176	5.94	6.02	0.76	0.66	5.86	0.84
Tetra-BTT	142	149	5.92	5.99	0.87	0.80	5.85	0.95
Hexa-BTT	124	99	5.76	5.85	1.07	1.02	5.73	1.12
Deca-BTT	66	83	5.64	5.67	1.24	1.19	5.61	1.28

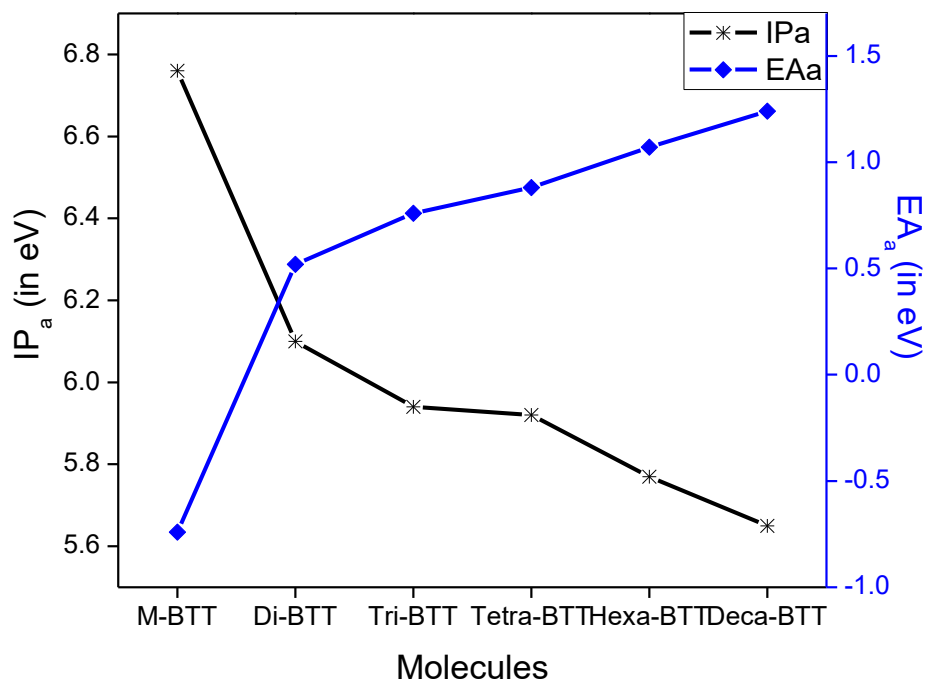


Figure 3B.11: Graphical representation of Adiabatic Ionization Potentials (IP<sub>a</sub>) and Electron Affinities (EA<sub>a</sub>) of all the oligomers

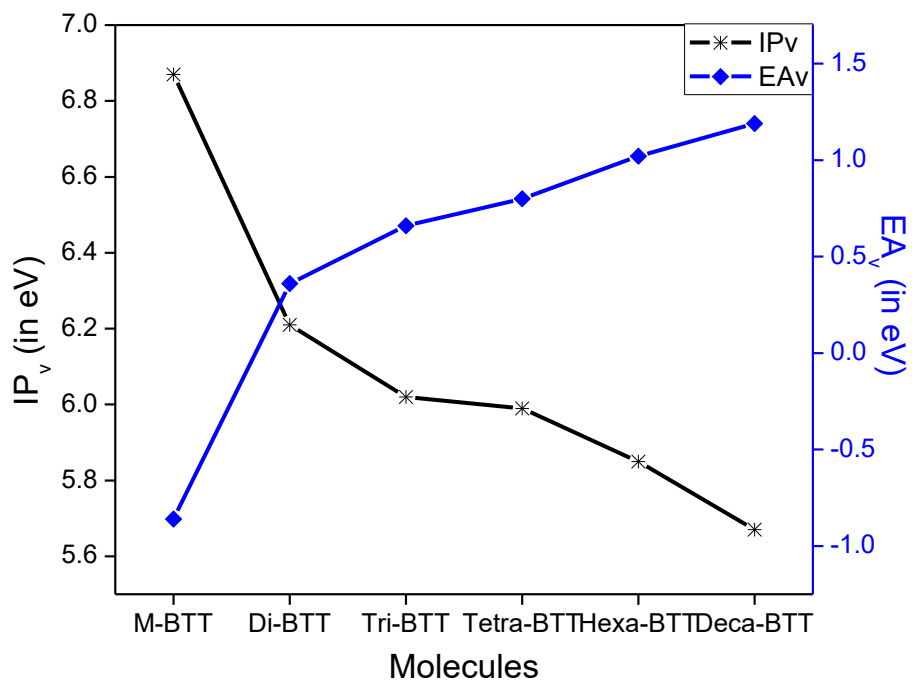


Figure 3B.12: Graphical representation of Vertical Ionization Potentials (IP<sub>v</sub>) and Electron Affinities (EA<sub>v</sub>) of all the oligomers.

### 3B.3.4. Hole extraction potentials (HEP) and electron extraction potentials (EEP)

In addition to IP and EA, we also calculated HEP and EEP for all the molecules and are shown in figure 3B.13. There is a decrease in HEP and increase in EEP with the increase in the number of BTT units. The HEP of M-BTT is 6.65 eV on adding one more BTT-unit (i.e., Di-BTT) the HEP value decreases to 5.99eV. This value further reduces to 5.86 eV, 5.85 eV, 5.73 eV and 5.61 eV for Tri-BTT, Tetra-BTT, Hexa-BTT and Deca-BTT, respectively ((shown in figure 3B.13). On the other hand, EEP of M-BTT is -0.62 eV while in the addition of another BTT-unit, it increases to 0.66 eV (Di-BTT). EEP of Tri-BTT, Tetra-BTT, Hexa-BTT and Deca-BTT are 0.84 eV, 0.95 eV, 1.12 eV and 1.28 eV respectively (shown in Figure 3B.13 and table 3B.7). The smaller HEP and higher EEP of Deca-BTT suggests that it is easy to extract either hole or electron from this oligomer.

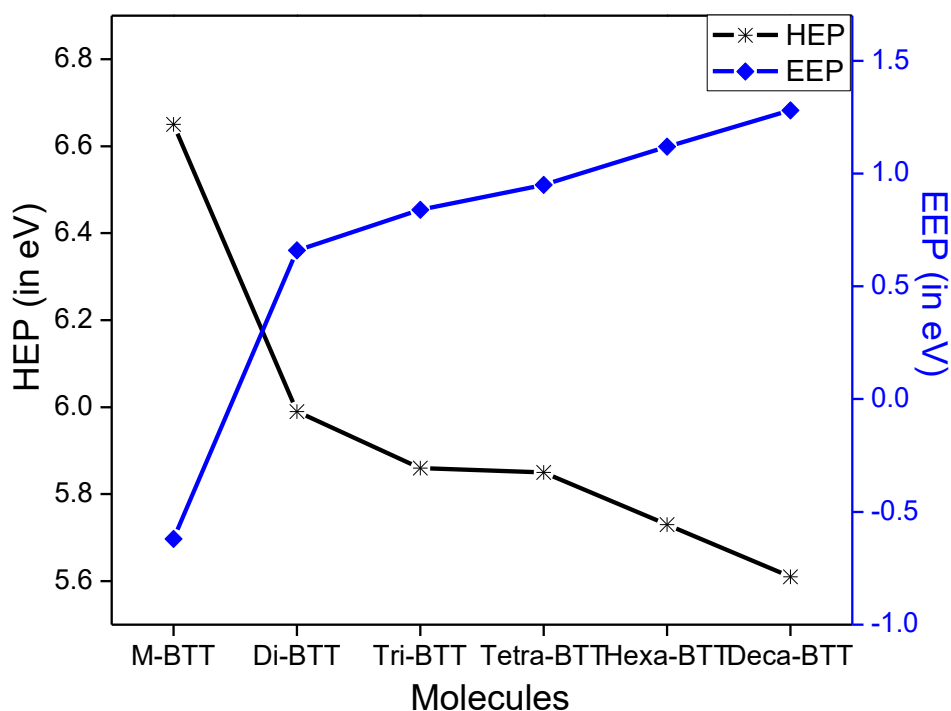


Figure 3B.13: Graphical representation of Hole Extraction Potentials (HEP) and Electron Extraction Potentials (EEP) of all the oligomers



### 3B.3.5. Reorganization energies ( $\lambda$ )

The charge transport rate in an organic molecule is inversely proportional to  $\lambda$ . For a molecule to be better carrier (either hole or electron), its  $\lambda$  should be small enough. Here we calculated  $\lambda$  for all the molecules and are shown in figure 3B.14 and table 3B.7. The hole reorganization energies ( $\lambda_h$ ) are lesser than their corresponding electron reorganization energies ( $\lambda_e$ ) except for oligomer Hexa-BTT where  $\lambda_h > \lambda_e$  (shown in Figure 3B.14). The  $\lambda_h$  value for M-BTT is 230meV and its  $\lambda_e$  value is 242meV, which is slightly higher than  $\lambda_h$  value. As we increase the number of BTT-units,  $\lambda_h$  and  $\lambda_e$  values are decreasing. For Di-BTT, Tri-BTT, Tetra-BTT, Hexa-BTT, and Deca-BTT,  $\lambda_h$  values are 222, 152, 142, 124 and 66 meV, respectively (Table 3B.7). From Figure 3B.14 and Table 3B.7 it is clear that Deca-BTT is with smaller  $\lambda_h$  value (66 meV) which indicates Deca-BTT is a better hole transporting material among all studied molecules. In all the molecules, the calculated  $\lambda_h$  values are lesser than N,N'-diphenyl-N,N'-bis(3-methylphenyl)-(1,1'-biphenyl)-4,4'-diamine (TPD) which is well known hole transport material (290 meV) suggesting that the studied molecules are superior for hole transport materials since hole reorganization energies are smaller than that of TPD [28]. The calculated  $\lambda_e$  for all the molecules (shown figure 3B.14 and table 3B.7) are lesser than tris(8-hydroxyquinolato)aluminium(III)(Alq<sub>3</sub>) which is a characteristic electron transport material (276 meV) [29]. Particularly Deca-BTT has  $\lambda_e$  value of 83 meV, which is much smaller than the standard Alq<sub>3</sub>. This smaller  $\lambda_e$  value shows that Deca-BTT is also a better electron transporting material. The increasing order of  $\lambda_e$  values are Deca-BTT < Hexa-BTT < Tetra-BTT < Tri-BTT < Di-BTT < M-BTT. For all the molecules, the difference between the  $\lambda_h$  and  $\lambda_e$  (except Di-BTT) are less than 30 meV, showing that the studied molecules are ambipolar in nature.

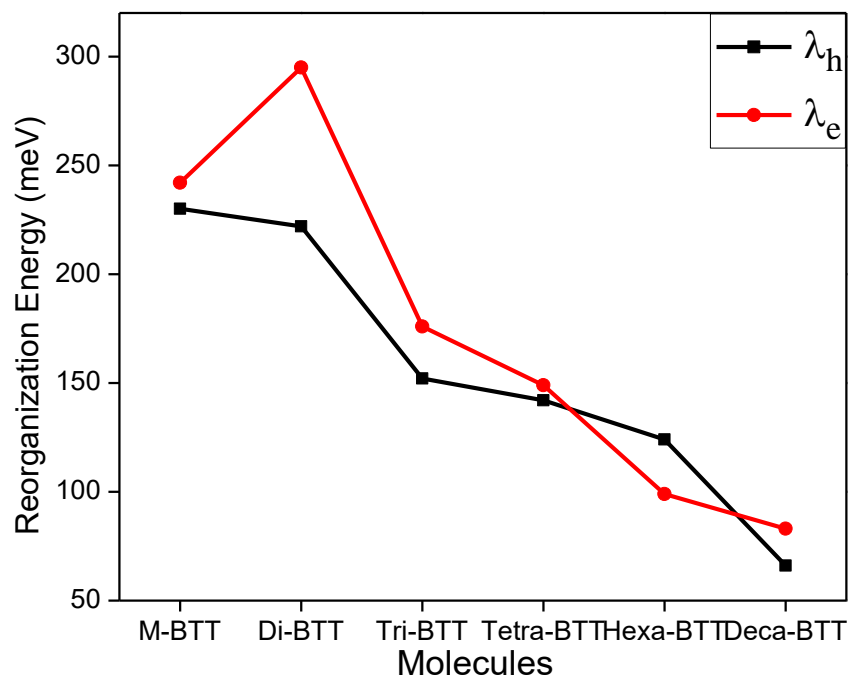


Figure 3B.14: Hole and Electron reorganization energies of BTT and its oligomers

### 3B.4. Conclusion

Here in this work, optical and electronic properties along with reorganization energies of BTT-oligomers are explored through DFT and TDDFT computational studies. Addition of BTT unit to M-BTT (i. e. Di-BTT) shows a drastic enhancement in its absorption due to more  $\pi$ -delocalization in the backbone of the molecule. The successive addition of further BTT units to Di-BTT (i. e. Tri-BTT, Tetra-BTT, Hexa-BTT and Deca-BTT), the effect on absorption energies are minimal but shows enhancement in its hole and electron reorganization energies. Deca-BTT has the smallest hole and electron reorganization energy among all oligomers and may use as better hole/ electron charge transport material. The studied molecules are with small difference in their  $\lambda_h$  and  $\lambda_e$  reorganization energies and are ambipolar, which is useful in both hole as well as electron transport materials.

---

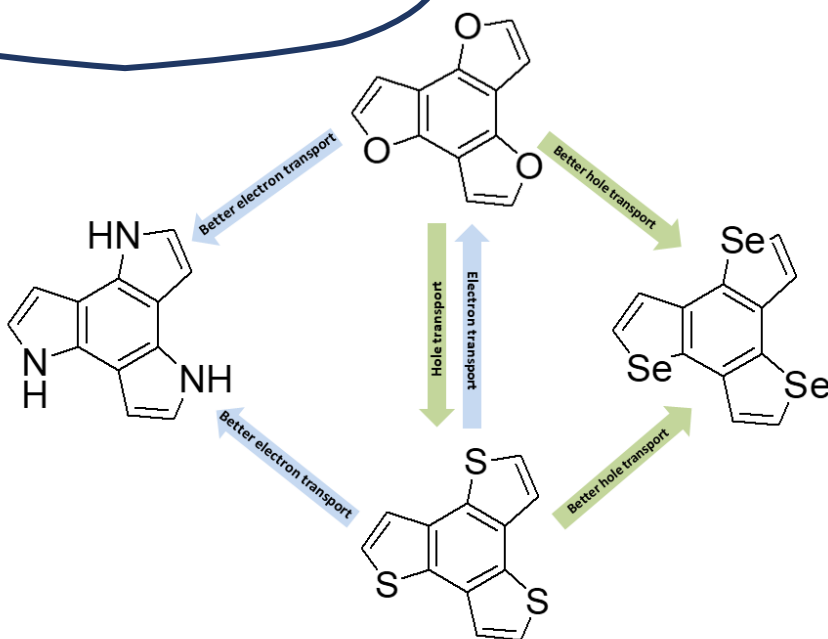
**References**

1. G. Barbarella, M. Melucci, G. Sotgiu, *Adv. Mater.* **2005**, 17, 1581.
2. R. D. Bettignies, Y. Nicolas, P. Blanchard, E. Levillain, J. -M. Nunzi, J. Roncali, *Adv. Mater.* **2003**, 15, 1939.
3. M. X. Chen, E. Perzon, N. Robisson, S. K. M. Jonsson, M. R. Andersson, M. Fahlman, M. Berggren, *Synth. Met.* **2004**, 146, 233.
4. C. Vidélot, J. Ackermann, P. Blanchard, J. -M. Raimundo, P. Frere, M. Allain, R. D. Bettignies, E. Levillain, J. Roncali, *Adv. Mater.* **2003**, 15, 306.
5. C. Wang, H. Dong, W. Hu, Y. Liu, D. Zhu, *Chem. Rev.* **2012**, 112, 2208.
6. C. B. Nielsen, R. S. Ashraf, S. Rossbauer, T. Anthopoulos, I. McCulloch, *Macromolecules* **2013**, 46, 7727.
7. M. L. Keshotov, Y. Geng, S. A. Kuklin, A. R. Khokhlov, E. N. Koukaras, G. D. Sharma, *Org. Electron.* **2015**, 17, 167.
8. C. B. Nielsen, R. S. Ashraf, B. C. Schroeder, P. D. Angelo, S. E. Watkins, K. Song, T. D. Anthopoulos, I. McCulloch, *Chem. Comm.* **2012**, 48, 5832.
9. T. -A. Liu, C. Prabhakar, J. -Y. Yu, C. H. Chen, H. -H. Huang, J. -S. Yang, *Macromolecules* **2012**, 45, 4529.
10. B. S. Ong, Y. Wu, P. Liu, S. Gardner, *J. Am. Chem. Soc.* **2004**, 126, 3378.
11. J. M. Tour, *Chem. Rev.* **1996**, 96, 537.
12. F. Cherioux, L. Guyard, *Adv. Funct. Mater.* **2001**, 11, 305.
13. M. Chahma, J. B. Gilroy, R. G. Hicks, *J. Mater. Chem.* **2007**, 17, 4768.
14. Y. Geng, A. Fechtenkötter, K. Mullen, *J. Mater. Chem.* **2001**, 11, 1634.
15. M. Y. Cho, S. J. Kim, Y. D. Han, D. H. Park, K. H. Kim, D. H. Choi, J. Joo, *Adv. Funct. Mater.* **2008**, 18, 2905.
16. J. Pei, J. L. Wang, X. Y. Cao, X. -H. Zhou, W. -B. Zhang, *J. Am. Chem. Soc.* **2003**, 125, 9944.
17. R. Jin, *C. R. Chimie*, **2015**, 18, 954.
18. X. Guo, S. R. Puniredd, M. Baumgrten, W. Pisula, K. Mullen, *J. Am. Chem. Soc.* **2012**, 134, 8404.
19. N. Jayasuriya, J. Kagan, *J. Org. Chem.* **1989**, 54, 4203.

- 
20. T. Sugano, T. Hashida, A. Kobayashi, H. Kobayashi, *Bull. Chem. Soc. Jpn.* **1988**, 61, 2303.
  21. X. Guo, S. Wang, V. Enkelmann, M. Baumgarten, K. Mullen, *Org. Lett.* **2011**, 13, 6062.
  22. Y. Nicolas, P. Blanchard, E. Levillain, M. Allain, N. Mercier, J. Roncali, *Org. Lett.* **2004**, 6, 273.
  23. T. Kashiki, M. Kohara, I. Osaka, E. Miyazaki, K. Takimiya, *J. Org. Chem.* **2011**, 76, 4061.
  24. C. B. Nielsen, J. M. Fraser, B. C. Schroeder, J. Du, A. J. P. White, W. Zhang, I. McCulloch, *Org. Lett.* **2011**, 13, 2414.
  25. C. B. Nielsen, E. H. Sohn, D. J. Cho, B. C. Schroeder, J. Smith, M. Lee, T. D. Anthopoulos, I. McCulloch, *ACS Appl. Mater. Interfaces* **2013**, 5, 1806.
  26. B. C. Schroeder, S. Rossbauer, R. J. Kline, L. Biniek, S. E. Watkins, T. D. Anthopoulos, I. McCulloch, C. B. Nielsen, *Macromolecules* **2014**, 47, 2883.
  27. M. J. Frisch, Gaussian 16, Revision E.01; Gaussian, Inc.: Wallingford CT, **2016**.
  28. M. Malagoli, J. L. Bredas, *Chem. Phys. Lett.* **2000**, 327, 13.
  29. B. C. Lin, C. P. Cheng, Z.-Q. You, C.-P. Hsu, *J. Am. Chem. Soc.* **2005**, 127, 66.

# Chapter 4A

*Electronic excitations, charge transport properties and nucleus independent chemical shift (NICS) studies of Benzotrithiophene (BTT) isomers and its Heteroatomic (NH, O, Se) Analogs*



Enhanced Charge Transport Properties with change in Heteroatom

*Results of this chapter published in Mol. Simul. 2020, 46, 548*





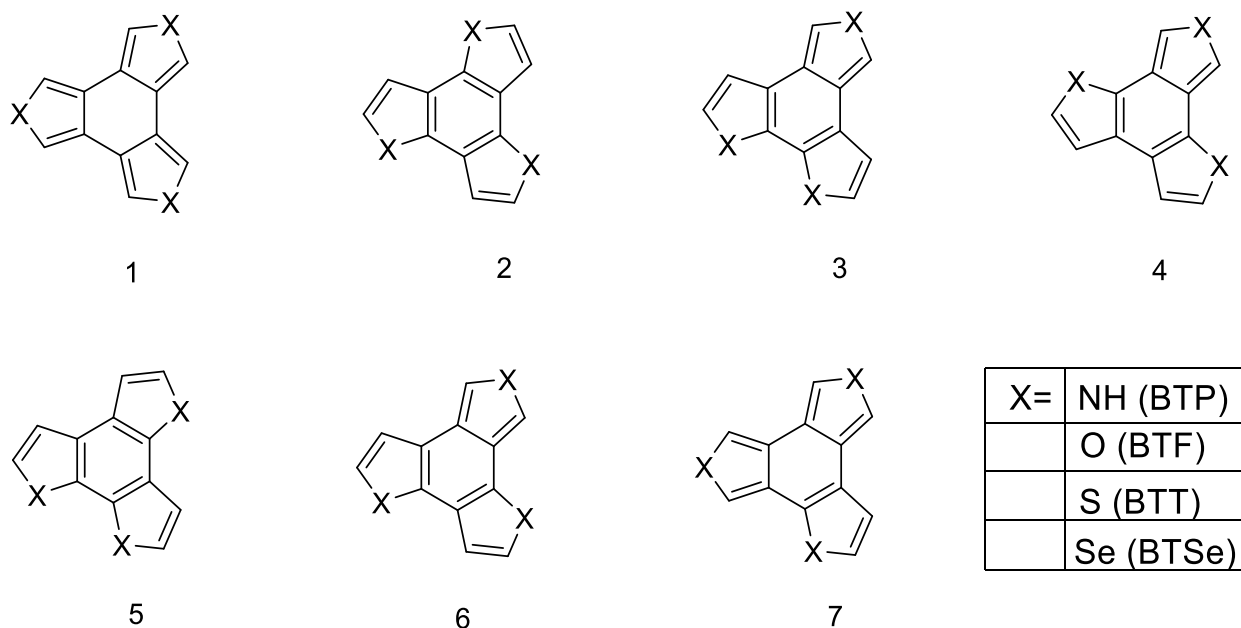


## 4A.1 Introduction

With continuous progress in organic electronics, it has encouraged researchers to innovate or design new organic materials which are applicable in electronic devices. It is familiar that the properties of organic materials are prominently depend on pi-conjugation of the molecules [1-2]. However electronic properties of these organic materials are still not up to the mark that achieved by inorganic materials, but this drawback can be overcome by the manufacturability, low cost, and possibility of producing flexible and large-area devices [3-4]. In this context, organic conjugated materials have received significant attention due to their potential applications in organic light-emitting diodes (OLEDs) [5-6], organic solar cells [7], organic field-effect transistors (OFETs)[8], organic photovoltaics (OPVs), etc. [9-10]. Among organic pi-conjugated materials, linear acenes (e.g., pentacene and their derivatives) are considered as promising candidates due to their high hole mobilities ( $5.5\text{cm}^2\text{V}^{-1}\text{s}^{-1}$ ) [11-12]. But these linear acenes (like pentacene) have some drawbacks like instability and poor solubility under ambient conditions; restrict them for further applications [13-15]. Various schemes have been adopted to increase the stability and solubility of the molecules, such as introducing different substituents and  $\pi$ -conjugated units, changing the position of heteroatom and so on [16-18]. K. Takimiya group synthesized number of benzothiophene derivatives which find applications in high-performance field-effect transistors [19-22]. When three thiophene rings added to the benzene ring, i.e., benzotrithiophene (BTT), the molecule becomes an excellent donor and used in donor-acceptor copolymer system and also finds applications in various organic semiconductor devices [23-28]. In BTT, when sulfur atom replaced by oxygen and nitrogen then molecule become benzotrifuran (BTF) and benzotripyrrole (BTP) respectively. M B Stringer gave the very first synthesis of benzotrifuran (BTF1 in scheme 4A.1) in 1980 after the synthesis of benzotrithiophene (BTT1 in scheme 4A.1) [29-30]. Recently, T. Fallon et al. synthesized oligomers of furans along with BTF1 (scheme 4A.1) with good yield (89 %) using 3,4-disubstituted furan and also reported electronic excitations of the said compounds [31]. R K Castellano group synthesized  $C_{3h}$  symmetric isomer of BTF (BTF2 in scheme 4A.1) for the first time in good yield. The absorption properties, electrochemistry and DFT calculations of BTF isomer have shown that this isomer (BTF2) is having similar optical and electronic properties to their corresponding BTT isomer and is a building unit for the  $\pi$ -conjugated system [32]. J H Gall in 1979 reported the synthesis of tripyrrole derivative having

trisazahexaradialene system and these tripyrrole derivative shows high reactivity towards dienophile than corresponding benzotrithiophene (BTT1) [33]. Further, H Tsuji et al. synthesized  $C_{3h}$  symmetric isomer of both BTF and BTP (BTF2 and BTP2 in scheme 4A.1) from 1,3,5-triethynyl-2,4,6-trifluorobenzenes in good yields [34]. Benzotriselenophenes (BTSe1 and BTSe2) are also synthesized independently by two different groups along with corresponding BTT isomers [35-36]. Recently, Nazeeruddin et al. synthesized three new star-shaped hole transport materials based on  $C_{3h}$  symmetric BTP2, BTF2 and BTSe2 core for highly effective perovskite solar cells. They find heteroatomic core (N, O, S, Se) has relevant effect on optical and electrochemical properties of hole transporting materials [37]. While working on BTT (in chapter 3A), it is shown that all the isomers of BTT are planar with a dihedral angle of almost zero. In addition to this, the smaller hole and electron reorganization energies in BTT isomers, suggesting these are better for charge transport properties. Though BTP, BTF and BTSe are not well explored like BTT but due to similarity in its structures, they may find potential applications in optoelectronic devices.

Here in this chapter, systematic study of the relationship between the structures and properties (electronic excitations, charge transport properties and NICS studies) of isomers of BTF, BTP, BTT and BTSe are carried out by using quantum chemical calculations. All the molecules considered in this study are shown in scheme 4A.1.



Scheme 4A.1: Structures of seven possible isomers of BTP, BTF, BTT and BTSe

## 4A.2 Materials and Methods

The geometries of all the isomers of each series were fully optimized using Gaussian16 package with B3LYP hybrid functional in combination with 6-311+G (d, p) basis set (Frisch et al.) [38]. The absorption spectra of all the molecules have been calculated by time-dependent density functional theory (TDDFT) using B3LYP functional by adopting 6-311+G (d, p) basis set.

The calculation of hole ( $\lambda_h$ ) and electron ( $\lambda_e$ ) reorganization energies are done by using *equation 1.14* and *1.15* respectively (in chapter 1). Also the calculation of charge injection parameters i.e ionization potential (IP) and electron affinity (EA) are done by using *equations 1.17* and *1.18* respectively. Further hole and electron extraction potentials are calculated by *equations 1.19* and *1.20* respectively.

## 4A.3. Results and Discussions

### 4A.3.1. Geometry and Structures

Based on the connectivity of different heterocycles to the central benzene ring, there are seven possible isomers with each heteroatom. Among these seven isomers first four are symmetrical while the last three are unsymmetrical (scheme 4A.1).

All the optimized isomers of BTP, BTF, BTT and BTSe are planar with the dihedral angle of zero. Even though 1<sup>st</sup> isomer (BTX1 in each set, i.e. BTT1, BTP1, BTF1 and BTSe1) is more symmetric, has the highest energy among all; thus, it is not the stable isomer. However, the isomer having  $C_{3h}$  symmetry (isomer 2 in scheme 4A.1, BTX2) is stable among all studied molecules. Relative energies for each set, i.e., BTP, BTF, BTT and BTSe isomers are shown in figure 4A.1 and table 4A.1. The trend for the stability of these isomers is  $1 < 7 < 3 \sim 4 < 6 < 5 < 2$ . The isomer 2 in each set (BTP2, BTF2, BTT2 and BTSe2) is more stable than its corresponding other isomers. The calculated bond lengths, bond angles and dihedral angle of optimized structures of all the isomers of each series are shown in table 4A.2. It is clear from the table 4A.2, all the isomers are almost planar having dihedral angle nearly zero. The angle between carbon and heteroatom at the periphery of benzene ring decreases with the increase in the size of heteroatom (N, O, S and Se). For BTP2 the angle between carbon and heteroatom at the periphery of benzene ring is  $109.68^\circ$  which is reduces to  $106.41^\circ$ ,  $91.11^\circ$  and  $87.76^\circ$  for BTF2, BTT2 and BTSe2 respectively.

Table 4A.1: Relative energy (in kcal) of the isomers of BTP, BTF, BTT and BTSe

Molecule	Symmetry	BTP	BTF	BTT	BTSe
1	D <sub>3d</sub>	12.49	17.23	13.41	16.50
2	C <sub>3h</sub>	<b>0.00</b>	<b>0.00</b>	<b>0.00</b>	<b>0.00</b>
3	C <sub>2v</sub>	7.79	10.86	7.53	9.23
4	C <sub>2v</sub>	6.73	9.57	7.44	9.30
5	C <sub>s</sub>	2.80	1.86	0.61	0.53
6	C <sub>s</sub>	5.85	9.27	7.17	8.93
7	C <sub>s</sub>	9.65	13.68	10.75	13.16

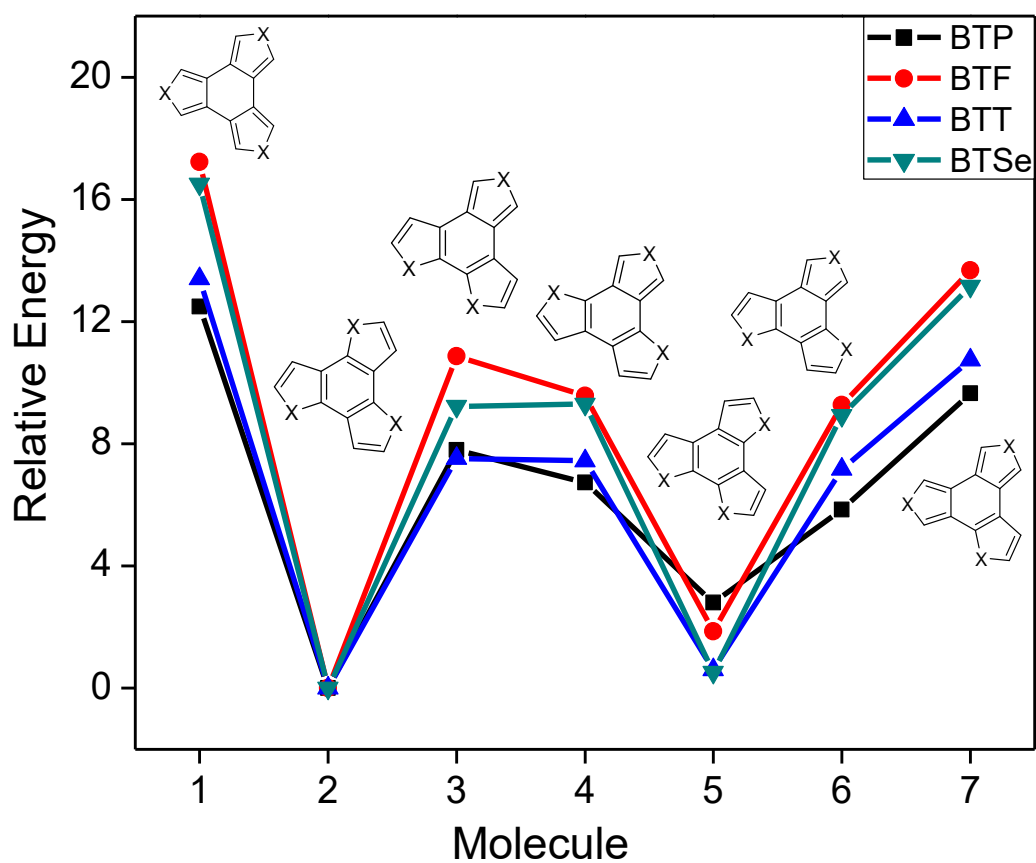
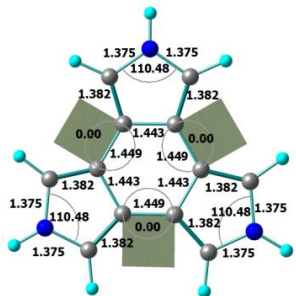
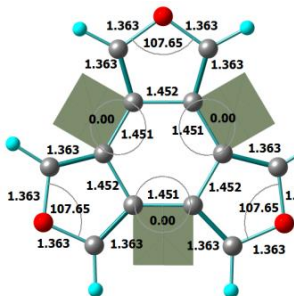
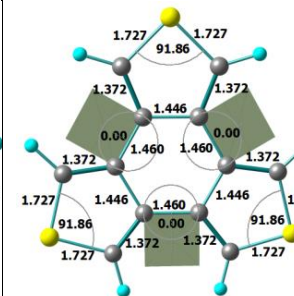
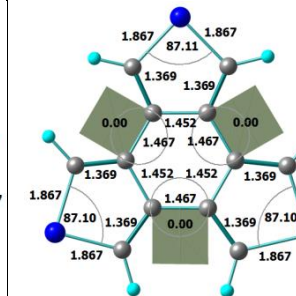
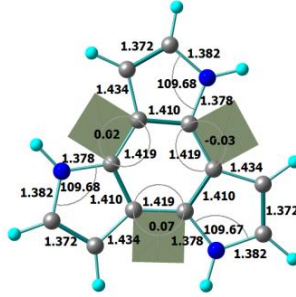
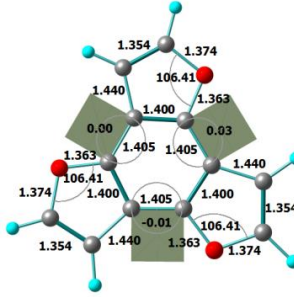
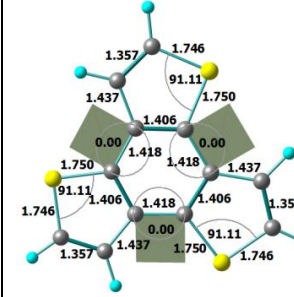
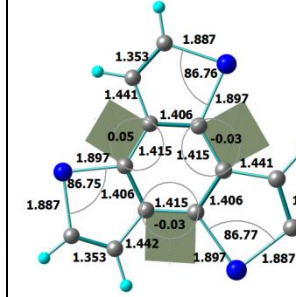
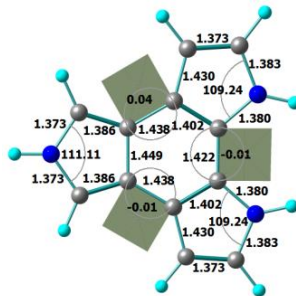
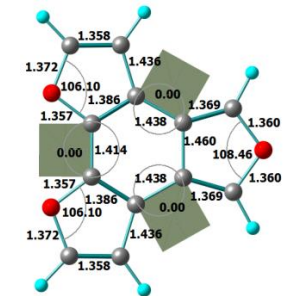
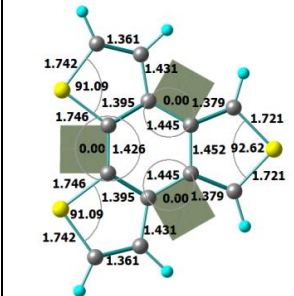
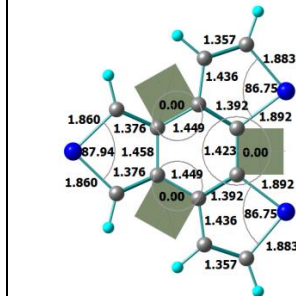


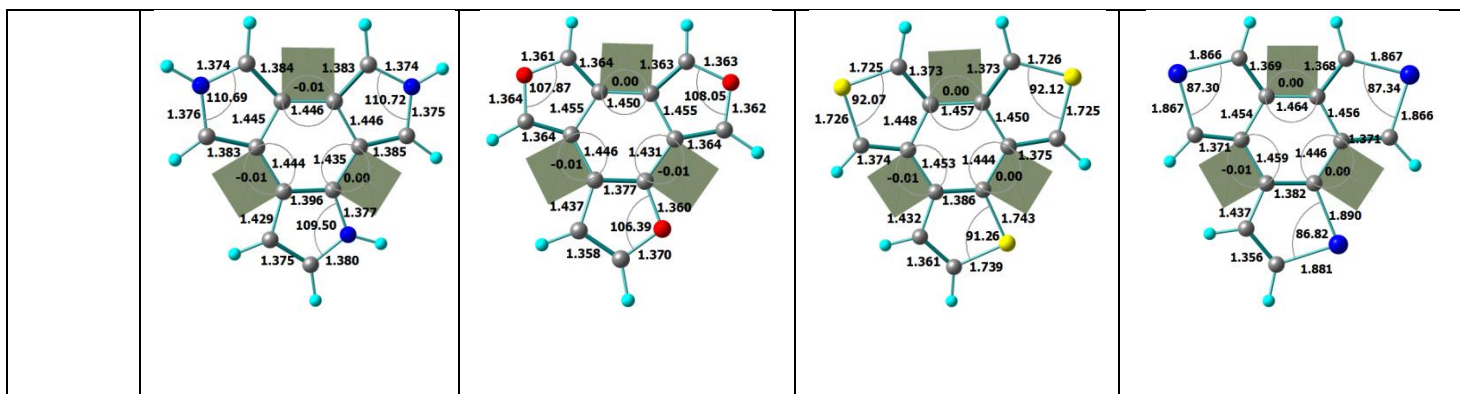
Figure 4A.1: Structures with their Relative energies

Table 4A.2: Bondlengths and Dihedral angles of the isomers of BTP, BTF, BTT and BTSe

Isomers	BTP	BTF	BTT	BTSe
1				
2				
3				

4				
5				
6				
7				





### 4A.3.2. NICS Calculation

Nucleus-independent chemical shift (NICS) calculations are performed on all the molecules to see the stability of isomers by considering their aromatic character. The stability of the molecule merely not depends on the symmetry of the molecule, but other factors are also responsible for stability (as shown in chapter 3A). The aromatic character is also one of the factors for deciding the stability of the molecule. NICS is a negative of magnetic shielding, a well-known property of the electronic system and it continues to gain popularity after its introduction by Schleyer et al. in 1996 [39]. It is one of the easy methods to compute aromaticity and antiaromaticity of rings, clusters and transition states [39]. One of the major advantages of NICS criteria of aromaticity over other methods available for aromaticity criteria is this method does not require any reference molecule, increment scheme, or adjusting equation for evaluation. According to NICS criterion, negative value signifies aromaticity while positive value denotes antiaromaticity and value close to zero for the non-aromatic character of the molecule. The magnitude of NICS indicates the degree of aromaticity, i.e., more negative the NICS value implies more aromatic character, which in turn gives stability to the system. The original NICS value was based on total isotropic shielding calculated at ring center i.e. NICS(0). However NICS(0) value is not considered as pure measure of  $\pi$ -aromaticity, as local contribution from  $\sigma$ -framework quite noticeable. It is well-known that C-H and C-C single bonds are also influences their magnetic environment and therefore due to these local effect results in non-zero NICS(0) value for non-aromatic rings. For planar molecules these local contributions fall off rapidly at points above the ring centers where  $\pi$ -contribution dominates. Hence NICS(1) values (i.e. 1Å above the ring center) were suggested as being better measure

of  $\pi$ -effect than NICS(0) values [40]. The calculated NICS(0) (i.e., at the center of the ring) values are shown in table 4A.3 for all the studied molecules. From table 4A.3, central benzene ring of isomer 1 (BTP1, BTF1, BTT1 and BTSe1) in each series is showing nearly zero or positive NICS(0) value indicates central ring of the molecule is either antiaromatic (for positive NICS value) or non-aromatic (for zero NICS value). The NICS(0) value for isomer 2 (BTP2, BTF2, BTT2 and BTSe2) and 5 (BTP5, BTF5, BTT5 and BTSe5) of each series are with higher negative value, indicates central benzene ring in these isomers are with more aromatic character. For isomer 2 of each set, the NICS(0) value of central ring for BTP2, BTF2, BTT2 and BTSe2 are -9.7, -12.1, -8.8 and -8.7 respectively, shows central ring is most aromatic in case of BTF2 and least in case of BTSe2. The NICS(0) value for isomer 1 i.e. BTP1 (-0.4), BTF1 (0.3), BTT1 (3.0) and BTSe1 (3.9) are either positive or close to zero shows central ring in isomer 1 is non-aromatic in character.

Additionally, NICS(1) (i.e., at 1 Å above the ring center) values are also calculated as local contributions from C-C and C-H single bonds are diminished relative to ring current effect [39] (Table 4A.4). It is also observed that NICS(1) value (given in Table S3) for six-membered central benzene ring is more as compared to their NICS(0) value, but the reverse is true for the five-membered heterocyclic ring, i.e. their NICS(0) value is more than NICS(1) values. Due to the more aromatic character of the central benzene ring in isomers 2 and 5 (evident from NICS(0) and NICS(1) values), these are the most stable among all the isomers. The five-membered heterocycle rings, i.e. pyrrole (in BTP), furan (in BTF), thiophene (in BTT) and selenophene (in BTSe) present at the periphery of benzene ring in all the isomers are showing negative NICS value and hence are also aromatic. Thus more aromatic character in central ring of isomers 2 and 5 as compared to other isomers make them stable, which is also evident from the optimized molecules (isomers 2 and 5 are more stable).

Table 4A.3: Nucleus Independent chemical shift NICS (0) at center (in ppm) for all the isomers obtained at B3LYP/6-311+ G (d, p) level

Molecule	Central Benzene Ring	Five membered rings		
BTP1	-0.4	-12.6	-12.6	-12.6
BTP2	-9.7	-12.4	-12.5	-12.5



BTP3	-5.9	-15.1	-11.9	-11.9
BTP4	-5.5	-11.9	-11.9	-15.1
BTP5	-9.9	-12.4	-12.4	-12.5
BTP6	-5.6	-14.9	-11.9	-11.9
BTP7	-2.5	-13.7	-13.6	-11.3
BTF1	0.3	-10.8	-10.7	-10.7
BTF2	-12.1	-10.3	-10.3	-10.3
BTF3	-5.7	-9.9	-14.1	-9.9
BTF4	-5.7	-14.3	-9.9	-9.9
BTF5	-12.3	-10.3	-10.4	-10.3
BTF6	-5.7	-9.9	-14.0	-9.9
BTF7	-1.6	-11.9	-9.3	-11.9
BTT1	3.0	-11.5	-11.9	-11.5
BTT2	-8.8	-17.7	-10.2	-10.3
BTT3	-3.3	-10.2	-10.1	-13.9
BTT4	-3.5	-10.1	-10.1	-13.9
BTT5	-9.2	-10.3	-10.1	-10.4
BTT6	-3.5	-10.3	-10.0	-13.9
BTT7	0.3	-12.3	-12.4	-9.7
BTSe1	3.9	-10.6	-10.7	-10.6
BTSe2	-8.7	-9.1	-9.0	-9.1
BTSe3	-2.4	-13.2	-9.0	-9.2
BTSe4	-2.6	-12.9	-9.1	-9.1
BTSe5	-8.8	-9.2	-9.2	-8.7
BTSe6	-2.7	-13.1	-8.9	-9.3
BTSe7	1.6	-11.5	-11.2	-8.7

Table4A.4: Calculated Nucleus Independent Chemical Shift at 1 Å above the ring center (in ppm) (i.e. NICS(1)) for all the isomers obtained at B3LYP/6-311+ G (d, p) level

Molecule	Central Benzene Ring	Five membered rings		
BTP1	-2.5	-9.3	-9.3	-9.3
BTP2	-9.7	-9.6	-9.2	-9.1
BTP3	-6.7	-11.4	-9.1	-9.1
BTP4	-6.5	-9.0	-9.0	-11.0
BTP5	-9.9	-9.3	-9.3	-9.5
BTP6	-6.5	10.9	-8.9	-8.7
BTP7	-4.1	-10.2	-9.9	-8.7
BTF1	-1.2	-8.5	-8.5	-8.5
BTF2	-11.6	-8.2	-8.5	-8.2
BTF3	-6.1	-8.2	-11.2	-8.2
BTF4	-6.1	-10.9	-8.1	-8.1
BTF5	-11.2	-8.3	-8.3	-8.3
BTF6	-6.1	-7.9	-10.9	-8.1
BTF7	-2.8	-9.4	-7.9	-9.2
BTT1	-0.7	-9.1	-9.2	-9.2
BTT2	-9.6	-10.6	-8.4	-8.4
BTT3	-5.5	-8.1	-8.1	-11.5
BTT4	-5.5	-8.2	-8.2	-11.1
BTT5	-10.0	-8.4	-8.2	-8.6
BTT6	-5.6	-8.5	-8.1	-11.3
BTT7	-2.8	-9.8	-9.9	-7.9
BTSe1	-0.2	-8.5	-8.1	-8.5
BTSe2	-9.8	-7.4	-7.3	-7.3
BTSe3	-4.9	-10.9	-7.1	-7.1

BTSe4	-5.0	-10.5	-7.2	-7.2
BTSe5	-9.8	-7.2	-7.5	-6.9
BTSe6	-5.1	-10.7	-7.0	-7.5
BTSe7	-1.9	-9.3	-9.0	-6.8

#### 4A.3.3. Electronic excitations

The calculated absorption ( $\lambda$ ), oscillator strength ( $f$ ), major transitions and %contributions for all the studied molecules calculated with B3LYP method using 6-311+G (d, p) basis set are shown in table 4A.5. In addition, to check the effect of different functionals on absorption energies, TDDFT calculations are also performed using different functionals namely BHandHLYP, PBE0, M06, M062X, B3P86, CAM-B3LYP and WB97XD at B3LYP optimized geometry and results are tabulated in table 4A.6. The calculated absorption energies have resulted from different functionals suggest that along with B3LYP functional, M062X, PBE0 and B3P86 are also giving close results to the experimentally observed absorption energies. Since these four functional (B3LYP, M062X, PBE0 and B3P86) are in good agreement with the experimental excitation energies, our further discussion of electronic excitations is based on B3LYP functional with 6-311+ G (d, p) basis set.

For BTT and their isomers, it is already discussed in our previous chapter 3A, here we focus mainly on BTP, BTF and BTSe and their isomers. For BTP1, the calculated absorption maximum is at 284nm while that of BTF1 is at 244nm. There is a 40nm blue shift observed on replacing NH with O atom. The major transitions in BTP1 are H-1→L and H→L+1 and in BTF1 are H-2→L and H→L+1. The experimentally observed and TDDFT calculated absorption maximum for BTSe1 are 337nm and 335nm, respectively. This absorption at 335nm is due to H-1→L transition having oscillator strength of 0.048. In the case of C<sub>3h</sub> symmetric isomers, i.e., BTP2, BTF2 and BTSe2, the calculated absorption maxima are at 282nm, 238 nm and 284nm, respectively. These absorptions are arising due to several transitions (shown in table 4A.5). However, the major transitions for BTP2 are H-1→L+2 and H-1→L, for BTF2 H-1→L+1 and H→L and for BTSe2 are H-1→L and H→L+1. The C<sub>2v</sub> symmetric molecules (isomer 3 and 4 in scheme 4A.1) are showing approximately the same absorption maxima, both BTP3 and BTP4 are showing absorption at 311nm having oscillator

strength of 0.248 and 0.012, respectively. These absorptions involve a single major transition; BTP3 is from  $H \rightarrow L+1$  and BTP4 is from  $H \rightarrow L+2$ . In the case for BTF3 (335nm) and BTF4 (325nm) there is 10nm difference in their absorption maxima and in both the cases; the major transition is from  $H \rightarrow L$ . BTSe3 and BTSe4 are showing absorption at 389nm and 390nm respectively which arises due to  $H \rightarrow L$  transition. Among unsymmetrical isomers (5, 6 and 7 in scheme 4A.1), isomer 6 is showing higher absorption (BTP6(330nm), BTF6(327nm) and BTSe6 (385nm)). For BTP5, the absorption is at 288nm and arises due to  $H-1 \rightarrow L+1$  and  $H \rightarrow L+1$  as major transitions. Similarly, for BTF5, the major transitions are  $H-1 \rightarrow L$ ,  $H \rightarrow L$  and  $H \rightarrow L+1$ , giving absorption at 281nm. BTSe5 shows absorption at 330nm due to excitation of an electron from  $H-1 \rightarrow L$ . The last isomer 7 of each series, showing absorption at 321nm(BTP7), 287nm(BTF7) and 353nm(BTSe7). On comparing with BTT isomers, corresponding isomers of BTF and BTP are always showing a blue shift in absorption while BTSe isomers are showing red-shifted absorption. The result indicates that with increase in size of the heteroatom increases the absorption maximum. In figure 4A.2, 4A.3 and 4A.4 the normalized absorbance spectra of all the isomers of BTP, BTF and BTSe respectively are shown.

Table 4A.5: Absorption maxima  $\lambda_{\max}$  (nm), Oscillator strength ( $f$ ), Major Transitions (MT) and % weight (% $C_i$ ) obtained at TD-B3LYP method using 6-311+G (d, p) basis sets.

Name	$\lambda_{\text{exp}}$	$\lambda$	$f$	MT	% $C_i$
BTP1		284	0.005	$H-1 \rightarrow L$	49
				$H \rightarrow L+1$	48
		246	0.032	$H-2 \rightarrow L+4$	84
BTP2		282	0.014	$H-1 \rightarrow L+2$	38
				$H \rightarrow L+1$	39
BTP3		311	0.248	$H \rightarrow L+1$	96
BTP4		311	0.012	$H \rightarrow L+2$	95
BTP5		288	0.041	$H-1 \rightarrow L+1$	54
				$H \rightarrow L+1$	26
				$H \rightarrow L+4$	15

BTP6		330	0.002	H→L	98
		309	0.101	H→L+1	96
BTP7		321	0.002	H→L	91
		301	0.024	H→+1	66
				H→+4	22
BTF1	222 <sup>a</sup> , 215 <sup>a</sup>	244	0.003	H-2→L	20
				H→L+1	69
		232	0.384	H-1→L+2	43
				H-2→L+1	43
		206	0.010	H-1→L+5	49
H-2→L+4	49				
BTF2	231 <sup>b</sup>	238	0.268	H-1→L+1	38
				H→L+2	15
				H→L	38
BTF3		335	0.235	H→L	99
BTF4		325	0.021	H→L	99
BTF5		281	0.066	H-1→L	49
				H→L	27
				H→L+1	20
BTF6		327	0.111	H→L	98
BTF7		302	0.009	H→L	26
				H→L+1	56
		287	0.210	H→L	65
				H→L+1	28
BTFSe1	337 <sup>c</sup>	335	0.048	H-1→L	93
BTFSe2		284	0.252	H-1→L	40
				H→L+1	40

BTSe3		389	0.138	H→L	98
BTSe4		390	0.033	H→L	98
BTSe5		330	0.060	H-1→L	68
				H→L+1	17
BTSe6		385	0.081	H→L	98
BTSe7		353	0.048	H→L	62
				H→L+1	25

<sup>a</sup> *Chem. Sci.* **2012**, 3, 2133

<sup>b</sup> *Chem. Comm.* **2017**, 53, 9590

<sup>c</sup> *Angew. Chem. Int. Ed.* **2007**, 46, 8814

Table 4A.6: Calculated absorption energies ( $\lambda_{\max}$  in nm) with different functional at B3LYP optimized geometries.

Molecule	$\lambda_{\text{exp}}$	B3LYP	BHand HLYP	PBE0	M06	M062X	B3P86	CAM- B3LYP	WB97XD
BTP1		284	249	266	331	256	270	245	238
BTP2		282	255	266	338	262	253	252	234
BTP3		311	289	302	347	283	308	288	285
BTP4		311	287	302	372	289	306	285	281
BTP5		288	264	279	327	267	285	264	263
BTP6		330	297	309	368	303	304	290	280
BTP7		321	289	301	384	296	295	284	266
BTF1	222 <sup>a</sup> ,	232	234	225	247	234	245	234	231
	215 <sup>a</sup>								
BTF2	231 <sup>b</sup>	238	216	231	251	217	236	219	217
BTF3		335	314	327	337	306	333	310	308
BTF4		325	305	318	327	297	323	301	299
BTF5		281	261	273	283	257	279	262	260
BTF6		327	306	319	329	299	325	302	300

BTF7		287	270	290	297	266	299	269	268
BTSe1	337 <sup>c</sup>	335	289	322	332	289	332	290	285
BTSe2		284	252	275	284	255	283	256	254
BTSe3		389	361	378	391	351	386	358	353
BTSe4		390	358	378	391	348	386	354	349
BTSe5		330	299	320	332	299	327	301	300
BTSe6		385	356	374	387	346	335	352	347
BTSe7		353	317	340	351	312	350	316	312

<sup>a</sup> *Chem. Sci.* **2012**, 3, 2133

<sup>b</sup> *Chem. Comm.* **2017**, 53, 9590

<sup>c</sup> *Angew. Chem. Int. Ed.* **2007**, 46, 8814

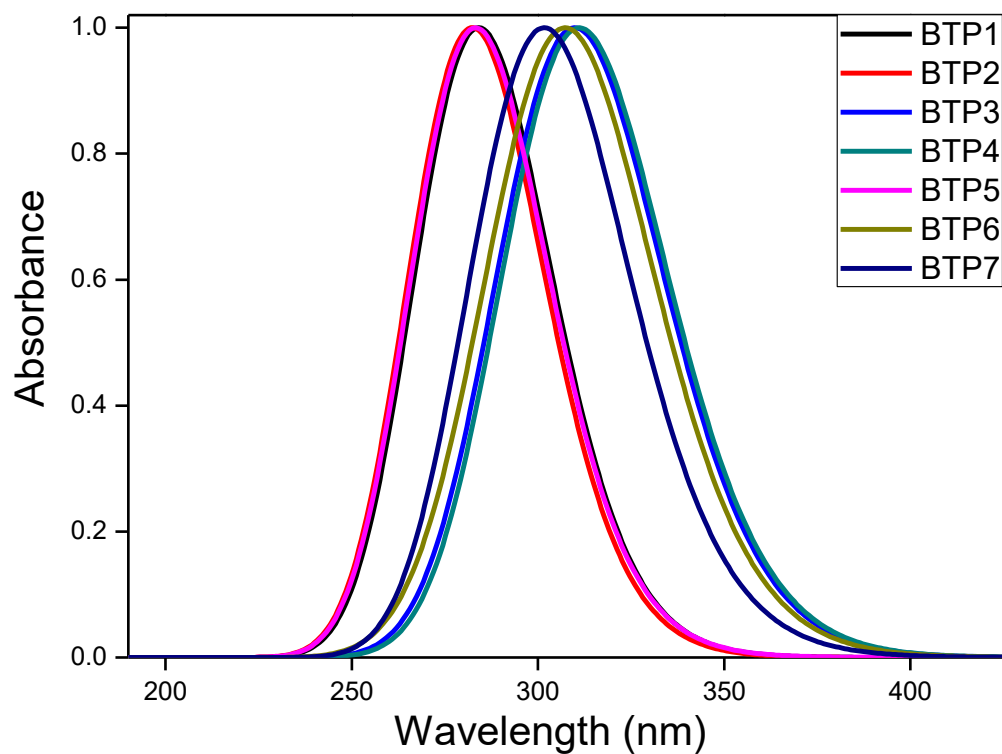


Figure 4A.2: Normalized Absorption spectra of BTP isomers

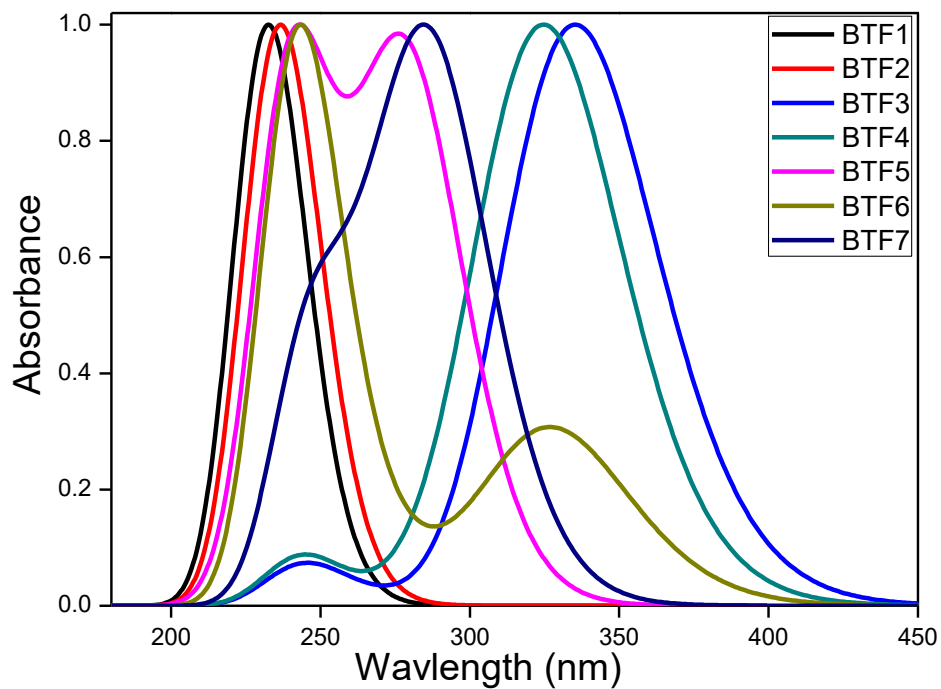


Figure 4A.3: Normalized Absorption spectra of BTF isomers

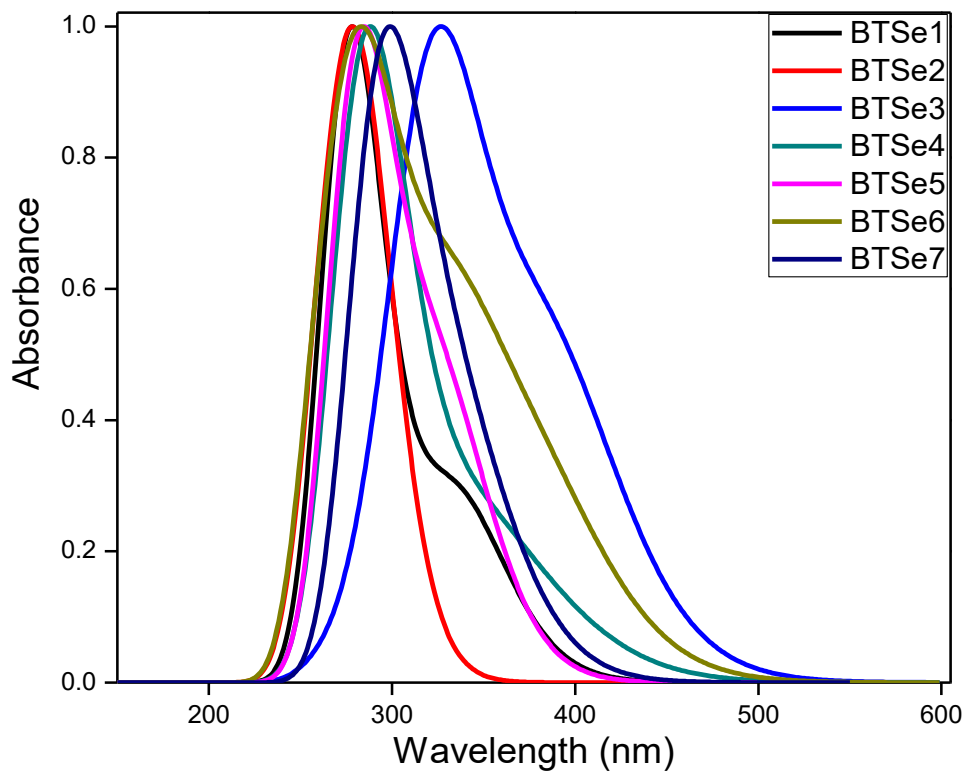


Figure 4A.4: Normalized Absorption spectra of BTSeisomers

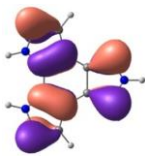
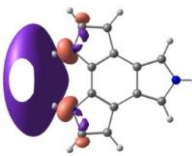
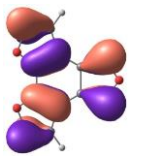
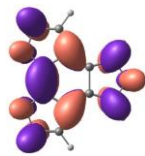
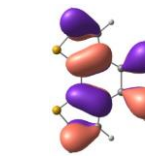
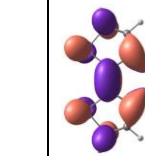
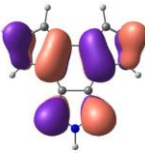
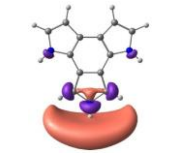
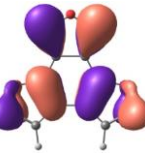
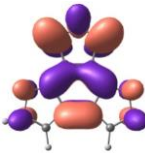
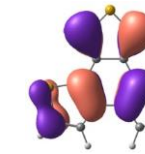
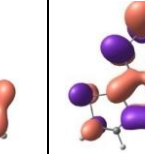
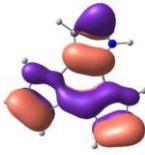
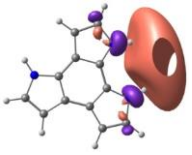
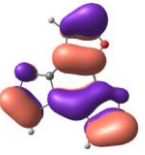
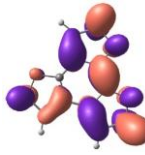
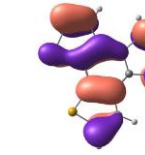
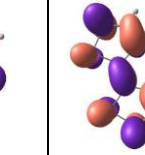
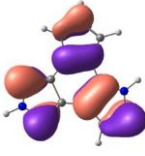
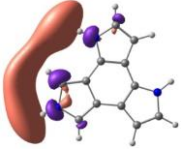
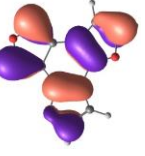
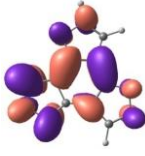
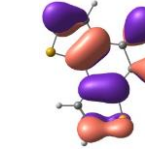
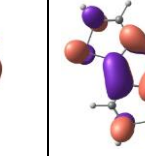
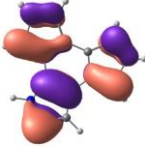
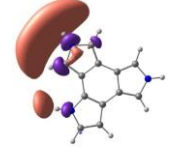
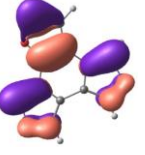
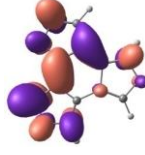
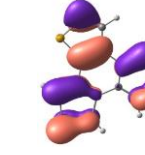
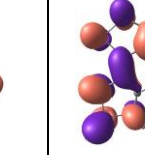


#### 4A.3.4. Frontier Molecular Orbitals (FMOs)

The frontier molecular orbital pictures, i.e., HOMO and LUMO of all the isomers of BTP, BTF and BTSe are shown in table 4A.7, 4A.8 and 4A.9 respectively. In each series of molecules, isomer 3 is showing the smallest HOMO-LUMO gap (HLG) among seven possible isomers (table 4A.10). In BTP series, the HOMO and LUMO energies of isomer 1 (BTP1) are  $-4.97\text{eV}$  and  $-0.02\text{eV}$  respectively and corresponding HOMO-LUMO gap is  $4.95\text{eV}$ , which is highest among all the isomer of BTP. On the other hand, isomer 3, i.e. BTP3 shows HLG of  $4.12\text{eV}$  with HOMO and LUMO energies  $-4.57\text{eV}$  and  $-0.45\text{eV}$  respectively, which is lowest in BTP series (shown in figure 4A.5). Similar is the case for BTF and BTSe series, isomer 3 is showing HOMO(LUMO) energies of  $5.42\text{eV}$  ( $-1.37\text{eV}$ ) and  $5.54\text{eV}$  ( $-1.97\text{eV}$ ) respectively and the resulting HLG are  $-4.05\text{eV}$  and  $-3.57\text{eV}$  respectively (shown in figure 4A.6 and figure 4A.7). For comparison HOMO and LUMO levels and their energy gap for all the isomers of BTF, BTP, BTT are shown in figure 4A.8. Similar to absorption maxima, all the isomers of BTP and BTF are showing higher HLG than corresponding BTT isomers whereas BTSe isomers are showing smaller HLG than corresponding BTT isomers. This again shows that with increase in size of the heteroatom, stabilizing the HOMO and LUMO levels.

Table 4A.7: Molecular orbital pictures of BTP, BTF and BTSe isomers

Isomers	BTP		BTF		BTSe	
	HOMO	LUMO	HOMO	LUMO	HOMO	LUMO
1						
2						

3						
4						
5						
6						
7						

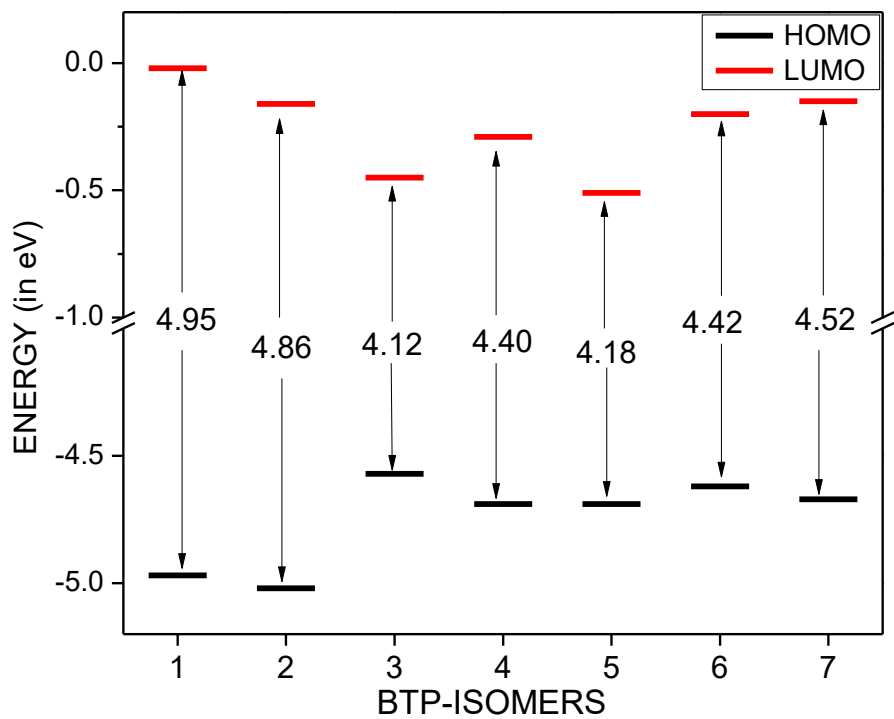


Figure 4A.5: HOMO, LUMO energy levels and energy gap of BTP isomers

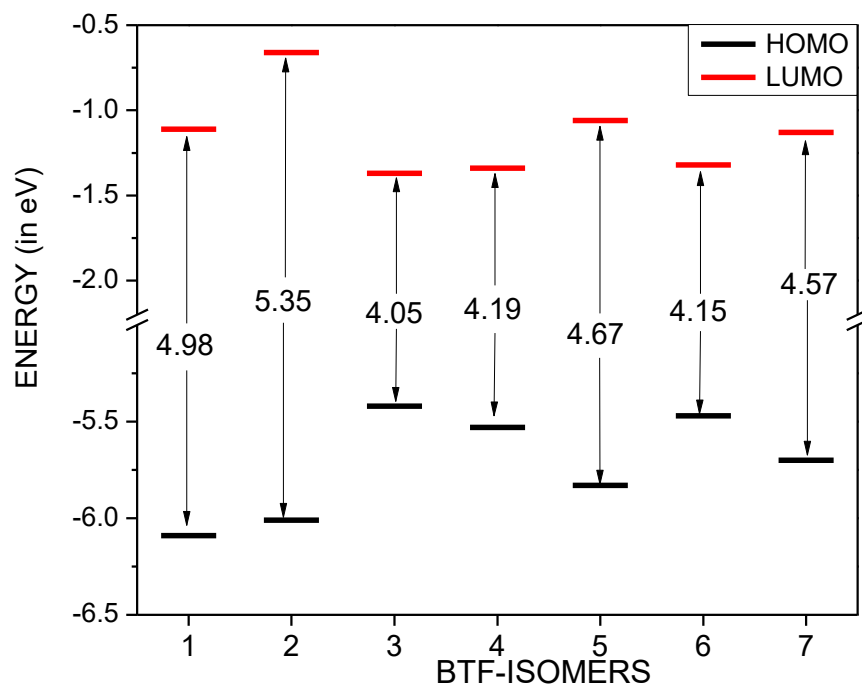


Figure 4A.6: HOMO, LUMO energy levels and energy gap of BTF isomers

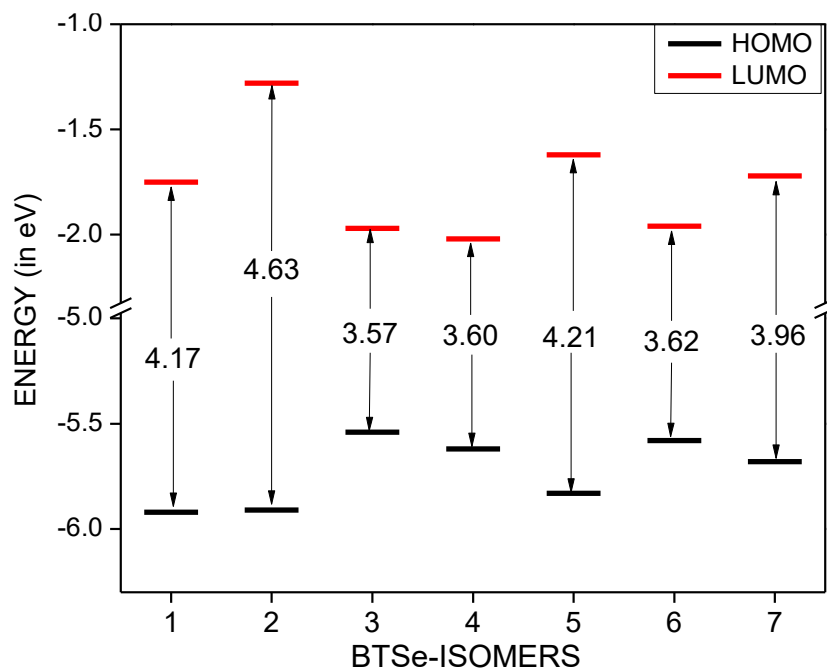


Figure 4A.7: HOMO, LUMO energy levels and energy gap of BTSe isomers

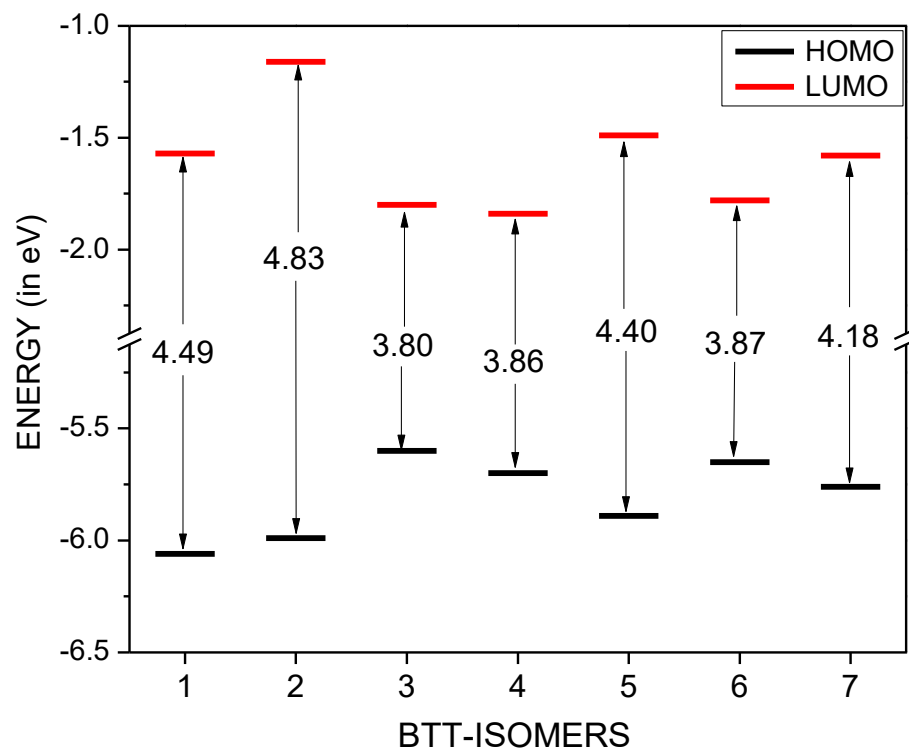


Figure 4A.8: HOMO, LUMO energy levels and energy gap of BTT isomers

Table 4A.8: Calculated HOMO and LUMO energies (in eV) and HOMO-LUMO gap (HLG in eV) for all the isomers

Isomer	BTP			BTF			BTT			BTSe		
	HOMO	LUMO	HLG	HOMO	LUMO	HLG	HOMO	LUMO	HLG	HOMO	LUMO	HLG
1	-4.97	-0.02	4.95	-6.09	-1.11	4.98	-6.06	-1.57	4.49	-5.92	-1.75	4.17
2	-5.02	-0.16	4.86	-6.01	-0.66	5.35	-5.99	-1.16	4.83	-5.91	-1.28	4.63
3	-4.57	-0.45	4.12	-5.42	-1.37	4.05	-5.60	-1.80	3.80	-5.54	-1.97	3.57
4	-4.69	-0.29	4.40	-5.53	-1.34	4.19	-5.70	-1.84	3.86	-5.62	-2.02	3.60
5	-4.69	-0.51	4.18	-5.83	-1.06	4.67	-5.89	-1.49	4.40	-5.83	-1.62	4.21
6	-4.62	-0.20	4.42	-5.47	-1.32	4.15	-5.65	-1.78	3.87	-5.58	-1.96	3.62
7	-4.67	-0.15	4.52	-5.70	-1.13	4.57	-5.76	-1.58	4.18	-5.68	-1.72	3.96

#### 4A.3.5. Ionization potentials (IP) and electron affinities (EA)

For a better quality of optoelectronic devices, there should be an efficient injection of hole and electron into an organic molecule. Here the calculation of adiabatic and vertical ionization potentials ( $IP_a$  and  $IP_v$ ) and electron affinities ( $EA_a$  and  $EA_v$ ) are done as they are important factors for charge injection phenomenon of hole and electron from source electrode into the semiconductor layer. IP defined as the energy supplied to the system to remove an electron and it must be low enough for efficient hole injection into the HOMO level of the molecule. On the other hand, EA defined as the energy released when an electron added to the system. EA must be high enough to allow an efficient electron injection into the LUMO level of the molecule. Calculation of IP, EA, HEP (hole extraction potential) and EEP (electron extraction potential) are carried out for all the molecules and are tabulated in table 4A.9. From the table 4A.9, it is clear that isomer 3 (BTP3, BTF3 and BTSe3) of each set is having the smallest IP and hence it is easy to create holes in these isomers compared to others. The  $IP_a$  ( $IP_v$ ) values for BTP3, BTF3 and BTSe3 are 6.08eV (6.16eV), 6.99eV (7.08eV) and 6.89eV (6.99eV) respectively. However, within these series, BTP isomers are showing smaller IP values than their corresponding BTF, BTT and BTSe isomers (shown in table 4A.9). HEP for isomer 3 in each series (BTP3, BTF3, BTT3 and BTSe3) also smallest and hence injection of the hole is easier in these molecules. In each series, isomer 3 and 4 are showing the highest EA, suggesting

there is an efficient electron injection in the HOMO level of this molecule as compared to others. Among all studied isomers of each series, isomer 3 and 4 also have the highest EEP. From these theoretical results one can predict that on replacing different heteroatoms in place of sulfur in BTT molecules, there is a noteworthy change in the electron-accepting, donating and transport properties.

#### 4A.3.6. Reorganization energies ( $\lambda$ )

The reorganization energy must be small enough for effective charge transfer in a molecule. The calculation of reorganization energies are carried out by the above formulae and are summarized in table 4A.9. With replacement of thiophene ring with pyrrole and selenophene ring at the periphery (i.e., BTT to BTP and BTSe) the electron reorganization energies become smaller and suggesting that BTP and BTSe isomers are better for the electron transporting material than its corresponding BTT isomers. On the other hand, BTF isomers (furan ring in place of thiophene ring) are showing smaller hole reorganization energies in most of the isomers (except for BTF2 and BTF7) showing BTF isomers are better for hole transporting material. The hole reorganization energies ( $\lambda_h$ ) calculated for most of the isomers in each series are smaller than that of typical hole transport material TPD (N,N'-diphenyl-N,N'-bis(3-methylphenyl)-(1,1'-biphenyl)-4,4'-diamine) ( $\lambda_h=290\text{meV}$ )[41]. In BTP series,  $\lambda_h$  is smallest for BTP3 (171 meV) suggesting among all BTP isomers, BTP3 is the best as hole transporting material. Similarly, BTF1 and BTSe1 are showing smaller  $\lambda_h$  values of 85meV and 168meV respectively in their respective series and are better for hole transporting materials (shown in figure 4A.9). Thus, the hole transfer rates for all the studied molecule are higher than that of TPD. The calculated electron reorganization energies ( $\lambda_e$ ) for most of the isomers are smaller than distinctive electron transport material Alq3 (tris(8-hydroxyquinolato)aluminum(III)) ( $\lambda_e= 276\text{meV}$ ) [42]. BTP series isomers are showing exceptionally small  $\lambda_e$  values (10-60meV), which means these isomers are better for electron transport materials (shown in figure 4A.10). However, BTF1 and BTSe1 isomers of BTF and BTSe are showing smaller  $\lambda_e$  values of 170meV and 115meV, respectively presenting these are better for electron transport materials in their respective series. Due to smaller  $\lambda_e$ , these BTP isomers can be utilized as electron-transporting materials in OLEDs.

Table 4A.9: Hole and electron ( $\lambda_h$  and  $\lambda_e$ ) reorganization energy (in meV), Ionization Potential (IP), Electron Affinity (EA), HEP and EEP (in eV) calculated at B3LYP/6-311+ G (d, p) level of theory

Molecule	$\lambda_h$	$\lambda_e$	IPa	IPv	EAA	EAv	HEP	EEP
BTP1	307	60	6.45	6.58	-0.78	-0.72	6.28	-0.78
BTP2	270	10	6.51	6.64	-0.62	-0.62	6.37	-0.61
BTP3	171	33	6.08	6.16	-0.49	-0.51	5.99	-0.48
BTP4	198	15	6.21	6.30	-0.56	-0.57	6.10	-0.55
BTP5	256	38	6.40	6.53	-0.46	-0.47	6.28	-0.43
BTP6	188	13	6.13	6.22	-0.64	-0.64	6.03	-0.63
BTP7	259	16	6.15	6.28	-0.63	-0.64	6.02	-0.62
BTF1	85	170	7.71	7.76	-0.31	-0.39	7.67	-0.22
BTF2	293	206	7.56	7.70	-0.76	-0.76	7.41	-0.55
BTF3	172	317	6.99	7.08	-0.07	-0.23	6.91	0.09
BTF4	167	280	7.12	7.20	-0.14	-0.27	7.03	0.01
BTF5	247	291	7.38	7.50	-0.36	-0.50	7.26	-0.21
BTF6	176	328	7.05	7.14	-0.13	-0.29	6.96	0.04
BTF7	300	375	7.23	7.39	-0.28	-0.47	7.09	-0.09
BTT1*	206	143	7.48	7.58	0.21	0.14	7.38	0.29
BTT2	224	239	7.41	7.52	-0.19	-0.31	7.30	-0.07
BTT3	194	240	7.01	7.11	0.45	0.33	6.92	0.57
BTT4	172	194	7.13	7.22	0.45	0.36	7.05	0.55
BTT5	453	272	7.29	7.63	0.15	0.02	7.18	0.29
BTT6	187	231	7.07	7.17	0.42	0.30	6.98	0.53
BTT7	250	268	7.15	7.28	0.24	0.11	7.03	0.38
BTSe1	168	115	7.30	7.38	0.43	0.37	7.21	0.49
BTSe2	203	215	7.29	7.39	-0.02	-0.13	7.18	0.09
BTSe3	202	209	6.89	6.99	0.66	0.56	6.78	0.77

BTSe4	178	165	7.00	7.09	0.68	0.60	6.91	0.77
BTSe5	223	262	7.20	7.31	0.33	0.20	7.09	0.46
BTSe6	194	200	6.94	7.04	0.64	0.54	6.84	0.74
BTSe7	250	243	7.01	7.14	0.43	0.31	6.89	0.55

\*BTT values are taken from Chapter 3A

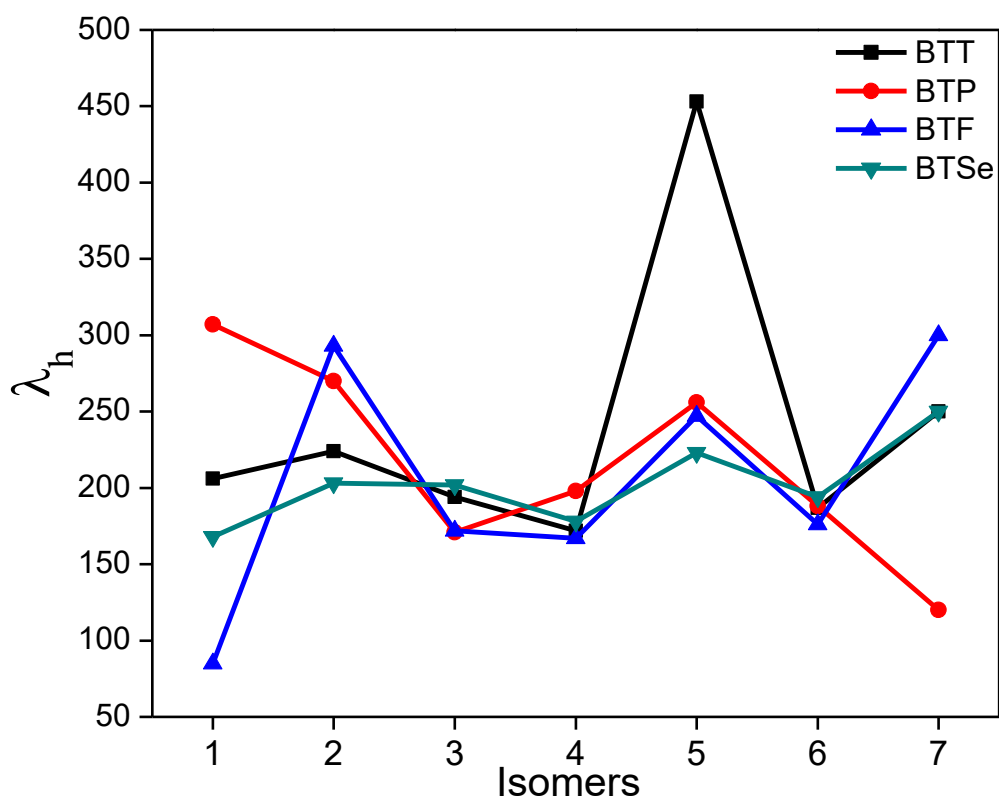


Figure 4A.9: Hole reorganization energies for BTP, BTF, BTSe and BTT isomers



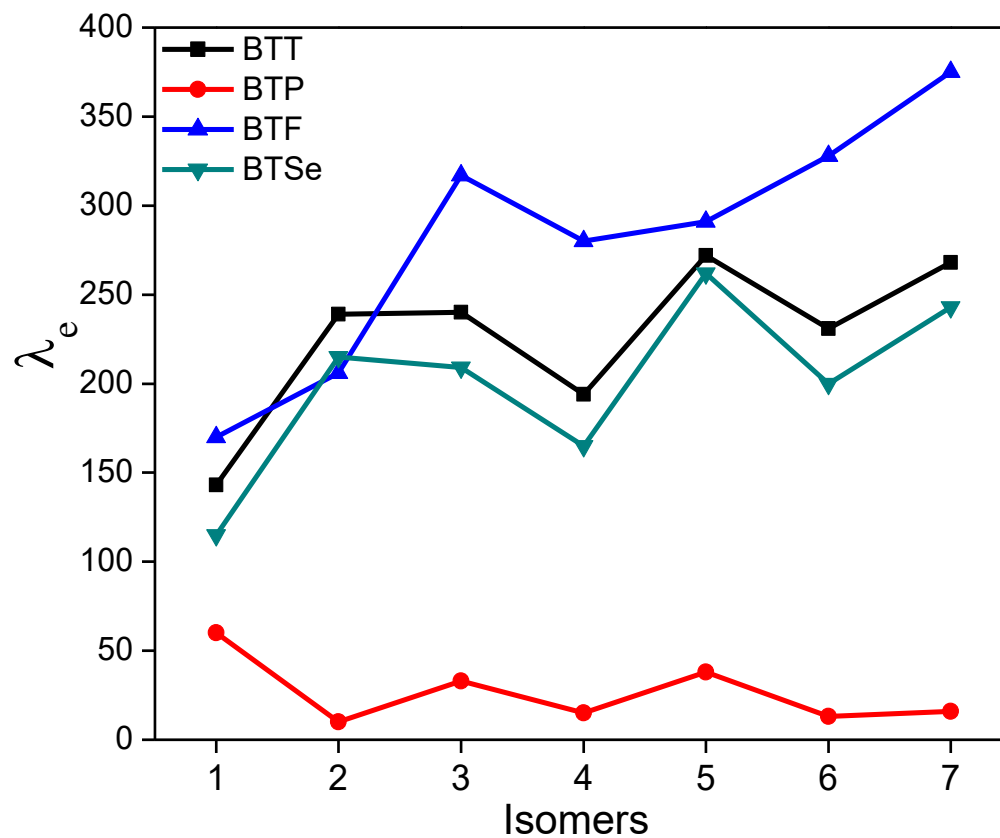


Figure 4A.10: Electron reorganization energies for BTP, BTF, BTSe and BTT isomers

---

#### 4A.4. Conclusion

In this paper, a comparative study of optoelectronic and charge transport properties along with the NICS studies in Benzotrithiophene (BTT) isomers and its heteroatomic analogues, i.e. Benzotripyrrole (BTP), Benzotrifuran (BTF) and Benzotriselenophene (BTSe) isomers are reported. The studied isomers are differing in the position of heteroatom (NH, O, and Se) results in diverse optoelectronic properties. NICS calculations are also in accordance with minimum energy geometries, showing  $C_{3h}$  symmetric isomer (isomer BTX2) in each series is more aromatic which in turn give stability to the molecule. The absorption energies are significantly affected by replacement of S with N, O, and Se. BTP and BTF isomers are showing blue-shifted absorption compared to their corresponding BTT isomers due to destabilization of both HOMO and LUMO levels. BTSe isomers are showing a red shift in absorption compared to their corresponding BTT isomers due to stabilization of both HOMO and LUMO levels. BTP isomers are with the smallest *IP* and *HEP* values suggesting among all series, and it is easy to create a hole in BTP isomers. On the other hand, BTSe isomers are showing the highest value for *EA* and *EEP*, implying BTSe isomers have greater electron injection ability than other studied set of molecules. Results of reorganization energies show BTP and BTSe isomers are better for electron transporting materials while BTF isomers are better for hole transporting material than corresponding BTT isomers. In addition, hole and electron reorganization energies for most of the studied molecules are smaller than a standard hole/ electron transport material and hence studied molecule may be useful as better hole and electron transporting materials. Moreover, electron reorganization energy for BTP isomers are minimal and are suitable candidates as electron transport materials.

---

**References**

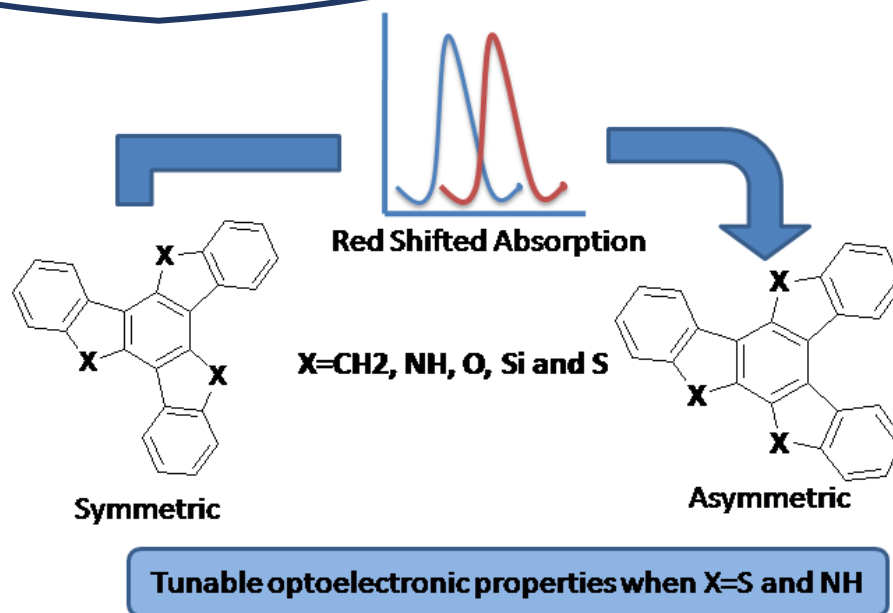
1. G. Barbarella, M. Melucci, G. Sotgiu. *Adv Mater.* **2005**, 17, 1581.
2. R.D. Bettignies, Y. Nicolas, P. Blanchard, E. Levillain, J. M. Nunzi, J. Roncali. *Adv Mater.* **2003**, 15, 1939.
3. S.R. Forrest. *Nature* **2004**, 428, 911.
4. M.M. Torrent, C. Rovira. *Chem Rev.* **2011**, 111, 4833.
5. J. Huang, J. H. Su, H. Tian. *J. Mat. Chem.* **2012**, 22, 10977.
6. Y.L. Liu, J.K. Feng, A.M. Ren. *J. Phys. Org. Chem.* **2007**, 20, 600.
7. S. Gunes, H. Neugebauer, N.S. Sariciiftci. *Chem Rev.* **2007**, 107, 1324.
8. C. Wang, H. Dong, W. Hu, Y. Liu, D. Zhu. *Chem. Rev.* **2012**, 112, 2208.
9. C.B. Nielsen, R.S. Ashraf, S. Rossbauer, T. Anthopoulos, I. McCulloch. *Macromolecules* **2013**, 46, 7727.
10. M.L. Keshtov, Y. Geng, S.A. Kuklin, A.R. Khokhlov, E.N. Koukaras, G.D. Sharma. *Org. Electron.* **2015**, 17, 167.
11. J.E. Anthony. *Chem. Rev.* **2006**, 106, 5028.
12. J.L. Brusso, O.D. Hirst, A. Dadvand, S. Ganeshan, F. Cicoira, C.M. Robertson, R.T. Oakley, F. Rosei, D.F. Perepichka. *Chem. Mater.* **2008**, 20, 2484.
13. M.M. Payne, S.R. Parkin, J.E. Anthony. *J. Am. Chem. Soc.* **2005**, 127, 8026.
14. R. Mondal, R.M. Adhikari, B.K. Shah, D.C. Neckers. *Org. Lett.* **2007**, 9, 2505.
15. B. Purushothaman, S.R. Parkin, J. E. Anthony. *Org. Lett.* **2010**, 12, 2060.
16. P.K. De, D.C. Neckers. *Org. Lett.* **2012**, 14, 78.
17. K. Xiao, Y. Lui, T. Qi, F. Wang, J. Gao, W. Qiu, Y. Ma, G. Cui, S. Chen, X. Zhan, G. Yu, J. Qin, W. Hu, D. Zhu. *J. Am. Chem. Soc.* **2005**, 127, 13281.
18. K. Niimi, S. Shinamura, I. Osaka, E. Miyazaki, K. Takimiya. *J. Am. Chem. Soc.* **2011**, 133, 8732.
19. K. Takimiya, T. Yamamoto, H. Ebata, T. Izawa. *Sci. Technol. Adv. Mater.* **2007**, 8, 273.
20. T. Yamamoto, K. Takimiya. *J. Am. Chem. Soc.* **2007**, 129, 2224.
21. H. Ebata, T. Izawa, E. Miyazaki, K. Takimiya, M. Ikeda, H. Kuwabara, T. Yui. *J. Am. Chem. Soc.* **2007**, 129, 15732.
22. T. Izawa, E. Miyazaki, K. Takimiya. *Adv. Mater.* **2008**, 20, 3388.

- 
23. X. Guo, S.R. Puniredd, M. Baumgarten, W. Pisula, K. Mullen. *J. Am. Chem. Soc.* **2012**, 134, 8404.
  24. Y. Nicolas, P. Blanchard, E. Levillian, M. Allain, N. Mercier, J. Roncali. *Org. Lett.* **2004**, 6, 273.
  25. T. Kashiki, M. Kohara, I. Osaka, E. Miyazaki, K. Takimiya. *J. Org. Chem.* **2011**, 76, 4061.
  26. C.B. Nielsen, J.M. Fraser, B.C. Schroeder, J. Du, A.J.P. White, W. Zhang, I. McCulloch. *Org. Lett.* **2011**, 13, 2414
  27. C.B. Nielsen, E. H. Sohn, D.J. Cho, B. C. Schroeder, J. Smith, M. Lee, T.D. Anthopoulos, I. McCulloch. *ACS Appl. Mater. Interfaces* **2013**, 5, 1806.
  28. B.C. Schroeder, S. Rossbauer, R.J. Kline, L. Biniek, S.E. Watkin, T.D. Anthopoulos, I. McCulloch, C.B. Nielsen. *Macromolecules* **2014**, 47, 2883.
  29. M.B. Stringer, D. Wege. *Tetrahedron Lett.* 1980, 21, 3831.
  30. H. Hart, M. Sasaoka. *J. Am. Chem. Soc.* 1978; 17: 4326.
  31. T Fallon, AC Willis, AD Rae, MNP Row, MS Sherburn. *Chem. Sci.* **2012**, 3, 2133.
  32. R.B. Ferreira, J.M. Figueroa, D.E. Fagnani, K.A. Abboud, R.K. Castellano, *Chem. Comm.* **2017**, 53, 9590.
  33. J.H. Gall, C.J. Gilmore, D.D. MacNicol. *J. Chem. Soc., Chem. Commun.* **1979**, 20, 927
  34. H. Tsuji, G. Cantagrel, Y. Ueda, T. Chen, L.J. Wan, E. Nakamura. *Chem. Asian J.* **2013**, 8, 2377.
  35. A. Patra, Y.H. Wijsboom, L.J.W. Shimon, M. Bendikov. *Angew. Chem. Int. Ed.* **2007**, 46, 8814
  36. T. Kashiki, S. Shinamura, M. Kohara, E. Miyazaki, K. Takimiya, M. Ikeda, H. Kuwabara. *Org Lett.* **2009**, 11, 2473
  37. I.G. Benito, I. Zimmermann, J.U. Mora, J. Arago, J. Calbo, J. Perles, A. Serrano, A.M. Ontoria, E. Orti, N. Martin, M. K. Nazeeruddin. *Adv. Funct. Mater.* **2018**, 1801734.
  38. M. J. Frisch, Gaussian 16, Revision E.01; Gaussian, Inc.: Wallingford CT, **2016**.
  39. P.V.R. Schleyer, C. Maerker, A. Dransfeld, H. Jiao, N. v. E. Hommes. *J. Am. Chem. Soc.* **1996**, 118, 6317.
  40. P.V.R. Schleyer, M. Manoharan, Z.X. Wang, B. Kiran, H. Jiao, R. Puchta, N. v. E. Hommes. *Org. Lett.* **2001**, 16, 2465.
-

41. M. Malagoli, J.L. Bredas. *Chem. Phys. Lett.* **2000**, 327, 13, 17.
42. B.C. Lin, C.P. Cheng, Z.Q. You, C.P. Hsu. *J. Am. Chem. Soc.* **2005**, 127,66.

# Chapter 4B

*Linear Optical and Charge Transport Properties of Truxene (isotruxene) and Thiatruxene (Isothiatruxene) and its Heteroatomic (N, O, and Si) analogs*



*Results of this chapter published in J. Phys. Org. Chem. 2019, 32, e3944*







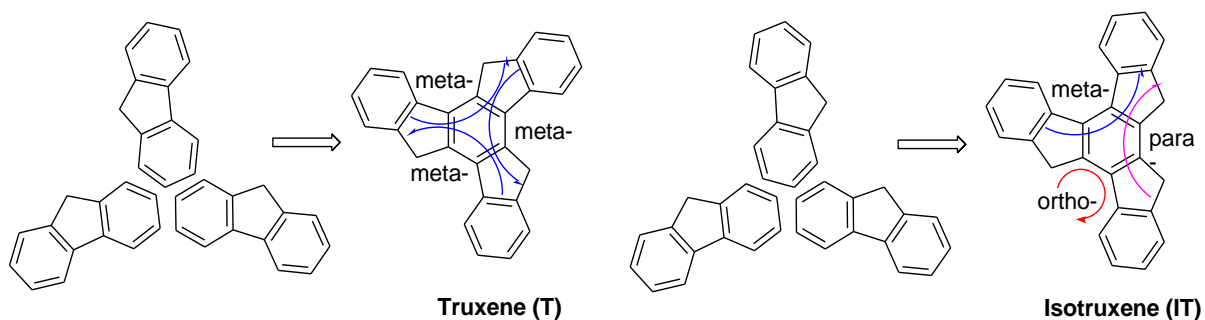
### 4B.1. Introduction

During the past few years, an intense research effort has made for the design, synthesis and application of organic materials. Nowadays, these organic materials are emerging as the best alternative for inorganic semiconductor materials and found applications in organic light emitting diodes (OLEDs) [1-2], organic photovoltaics (OPVs) [3-4], dye-sensitized solar cells (DSSCs) [5] and organic thin film transistors (OTFTs) [6]. A further advantage of these organic semiconductor materials is; low cost, light weight and possibility of producing bendable and great area devices make them best substituents for inorganic semiconductor materials [7-8]. Within the organic molecules, star-shaped  $\pi$ -conjugated molecules with large  $\pi$ -system are of considerable interest due to their potential applications in optoelectronic devices [9-11].

Recently developed star-shaped  $\pi$ -conjugated molecules with a Truxene (**T**) or isotruxene (**IT**) core became interested due to their remarkable photophysical properties (absorption and emission), high thermal stability and ease of synthesis which makes them a promising scaffold for future materials [9-18]. Truxene (10,15-dihydro-5H-diindeno[1,2-a;1',2'-c]fluorene) is a heptacyclic star-shaped  $\pi$ -conjugated polyarene produced by trimerization of indan-1-one. The **T** (scheme 4B.1) unit has a rigid, planar and  $C_{3h}$  symmetric structure and it can also be formally considered as a 1,3,5-triphenylbenzene derivative with three methylene clips so that all the four benzene rings are coplanar with  $\pi$ -conjugation. This results in a strong electron donating as well as strong  $\pi$ - $\pi$  stacking ability, which hints for the **T** utility as a building block in the development of advanced functional materials for various applications [12]. **IT** is an asymmetrical isomer of **T** with the difference in connectivity of fluorene moieties. In the case of **T**, there is meta-meta connectivity of three phenylene rings to the central core, while in **IT**, it is ortho-para connectivity (shown in scheme 4B.1). Yang et al. reported that ortho and para conjugate interactions are inherently stronger than meta interactions and this difference in connectivity to the central ring results in a different extent of electronic coupling between the three  $\pi$ -conjugated arms [13-14].

The very first report on the synthesis of **T** reported in 1894, where 3-phenyl propionic acid cyclized in-situ to indane-1-one under an acidic condition to give a mixture of **T** and **IT** [19]. However, the procedure of yielding specifically **IT** was established in 1960 [20]. Further, two groups Hartke et al. and Bergman et al. synthesized **T** using (3-methylthio) indene and indane-1-one respectively but the yield of the reaction is very low (~22%) [21-22]. For increasing the

yield of **T**, Huang-Minlon reduction procedure has been utilized, in which reduction of truxenone to **T** was established using Wolff-Kishner reagent and getting the product in 85% yield [23]. Jian Pie et al. synthesized various star-shaped  $\pi$ -conjugated molecules having the **T** core for OLED applications [24-25]. Derivatives with **T** core received more attention as a starting material for construction of large polyarene as analogous to the fullerene[26]. Since the previously known methods for the synthesis of **IT** required harsh conditions (20atm and 350°C) and yield of the product was also very low (18%) [13,20]. To overcome this problem, Yang et al. gave a facile multistep synthesis for **IT** with improved yield and minimized the effort in product purification [14]. The star-shaped  $\pi$ -conjugated system consisting of **IT** core and oligothiophene arms are showing a strong coupling in arms, which provide a new class of two-dimensional oligomer and polymer [27].

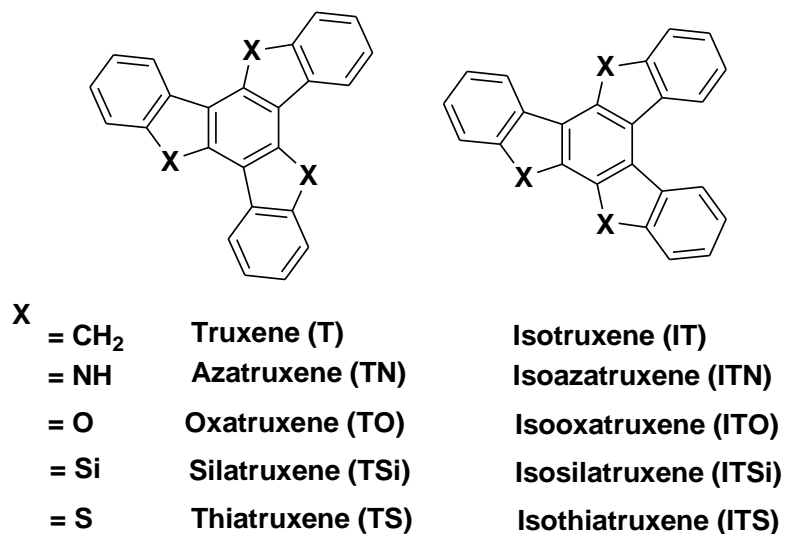


Scheme 4B.1: Structures of Truxene (**T**, meta-meta connectivity) and Isotruxene (**IT**, ortho-para connectivity)

Like **T**, another polycyclic aromatic compound azatruxene (**TN** in scheme 4B.2) or triindole (10,15-dihydro-5H-diindolo-[3,2-a:3',2'-c]carbazole) is also a planar  $\pi$ -extended conjugated structure that can be regarded as a cycle-trimer of indole. This polyarene (**TN**) also exists in two possible isomers namely **TN** and isoazatruxene (**ITN**) which differ only at the connectivity of carbazole moiety (shown in scheme 4B.2). **TN** was first synthesized by using an acidcatalyzed reaction between indole and 3-bromoindole but, it gives a combination of indole dimer, trimer, and tetramer [28]. After this, Gordon and Andrew performed electrochemical oxidation and polymerization of indole-5-carboxylic acid, and they found an insoluble unsymmetrical carboxylic acid derivative of **TN** and **ITN** [29]. Recently Rashatasakohn and co-workers derived a new synthetic route for the **TN** and **ITN** by using N-bromosuccinimide (NBS) as user-friendly reagent [30]. It also shown that **TN** based molecules are highly

promising hole selective materials with wide band gaps, high LUMO levels and high hole mobilities which make their use in organic electronic devices [31]. Further, Reghu et al. synthesized carbazole derivatives of both **TN** and **ITN**, shows that the reduction in the symmetry of the molecule results in a red-shifted absorption and it is unfavorable as a hole transport material in thin films [32]. Similar results obtained by Berta Gomez Lor group; they showed that by lowering in the symmetry of triindole, their photophysical and electronic properties can be tuned significantly and also there is an improvement in fluorescence quantum yield [33]. Wang et al. showed that **TN** is rich in electronic character and electron delocalization than **T** [34]. Both the above-studied molecules **T** and **TN** are planar  $\pi$ -extended electron-rich molecules which make these molecules having great potential application in DSSCs [35], field effect transistors (FET) [36], OLEDs [37-38], two-photon absorption (TPA) [39], organic laser and fluorescent sensors [33,40]. Other analogs of **T** are; oxatruxene (**TO**), silatruxene (**TSi**) and thiatruxene (**TS**) also synthesized, and its photophysical properties (except **TS**) are reported in the literature [41-42]. To the best of our knowledge, very few reports are available in the literature on **TO**, **TSi** & **TS** and these molecules not yet explored for materials properties, shown in scheme 4B.2 [41-42].

In the present chapter, the systematic studies were performed to analyze the effect of hetero-atom on photophysical and charge transport properties of **T** and **IT**. For this, we considered five sets of molecules (ten molecules) based on truxene & isotruxene and their analogs (**T**, **TN**, **TO**, **TSi**, and **TS** and their corresponding geometrical isomers **IT**, **ITN**, **ITO**, **ITSi**, and **ITS** respectively, shown in scheme 4B.2).

Scheme 4B.2: Structures of **T**, **IT** and its hetero-atomic (**N**, **O**, **Si** and **S**) analogs

#### 4B.2. Computational Methodology:

All the calculations have been performed in the gas phase with Gaussian 16 software package (Frisch et al.) [43]. The ground state geometries of neutral, cation and anion were fully optimized without symmetry constraints by using the DFT method with B3LYP functional and 6-311+G (d, p) basis set. TD-DFT has been used for the calculation of absorption energies by means of B3LYP functional with 6-311+G (d, p) basis set. Further, we employed different functionals (BLYP, BHandHLYP, M06, PBE0, LCWPBE, CAM-B3LYP, and WB97XD) to validate the best functional among all for the calculation of electronic excitations for all the molecules under study.

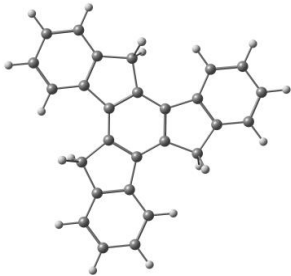
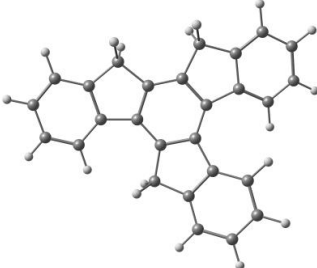
The calculation of hole ( $\lambda_h$ ) and electron ( $\lambda_e$ ) reorganization energies are done by using *equation 1.14* and *1.15* respectively (in chapter 1). For the calculation of reorganization energies, along with B3LYP, it is also performed with three more functionals, i.e. CAM-B3LYP, PBE0, and BHandHLYP. Also the calculation of charge injection parameters i.e. ionization potential (IP) and electron affinity (EA) are done by using formulae shown in *equations 1.17* and *1.18* respectively. Further hole and electron extraction potentials i.e. HEP and EEP are calculated by formulae shown in *equations 1.19* and *1.20* respectively.

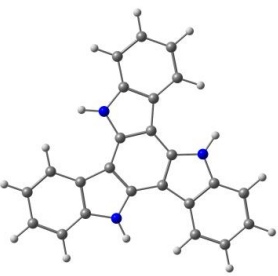
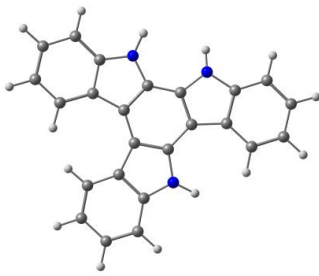
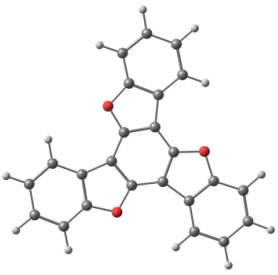
### 4B.3. Results and Discussions

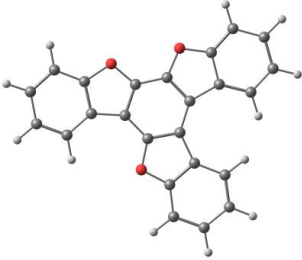
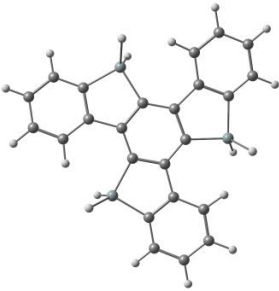
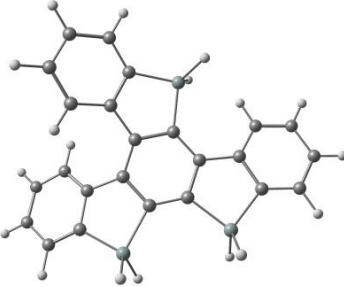
#### 4B.3.1. Molecular Structure and Geometries

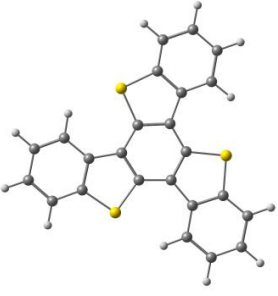
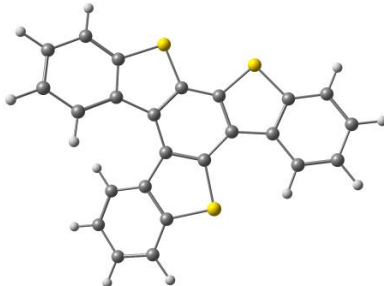
All the five sets of molecules are optimized in its ground state. For each set of the molecule, two major isomers (symmetrical and asymmetrical) are possible. It is well known that symmetrical isomers are more stable as compared to their asymmetrical one. It is found that iso-derivatives, i.e. asymmetric molecules are always 5~8 kcal less stable than their corresponding symmetric isomers. **T** is 4.72 kcal more stable than its corresponding asymmetrical isomer **IT**. Similar is the case for all the molecule, **TN**, **TO**, **TSi** and **TS** are 6.51 kcal, 4.22 kcal, 7.25 kcal and 7.64 kcal more stable than their corresponding asymmetrical isomers **ITN**, **ITO**, **ITSi** and **ITS** respectively. Molecular structures, symmetry and its relative energies for all the molecules are shown table 4B.1.

Table 4B.1: Structures, Relative Energy (RE) and Symmetry of studied molecules

Molecule	Structures	RE	Symmetry
<b>T</b>		<b>0.00</b>	<b>C<sub>3</sub></b>
<b>IT</b>		4.72	C <sub>s</sub>

TN		<b>0.00</b>	$C_3$
ITN		6.51	$C_s$
TO		<b>0.00</b>	$C_3$
ITO		4.22	$C_s$

			
TSi		<b>0.00</b>	$C_3$
ITSi		7.25	$C_s$
TS		<b>0.00</b>	$C_3$

			
ITS		7.64	C <sub>s</sub>

#### 4B.3.2. Linear optical properties (or Electronic Excitations)

The experimentally reported absorption maximum for **T** is 273 nm while its asymmetrical isomer **IT** is giving an intense peak at 337nm [44-45]. For the isomers **TN** and **ITN**, intense absorption peak were observed at 309 nm and 345 nm respectively [46-47]. These experimental results suggest that asymmetric isomers are always red-shifted than their corresponding symmetric isomers. Takuya Ogaki synthesized compounds **TO** and **TSi** by intramolecular triple cyclization of triphenylbenzene derivatives and they reported absorption for **TO** and **TSi** are at 293 nm and 310 nm respectively [42]. Best of our knowledge, there is no experimental report is available on photophysical properties of **ITO**, **ITSi**, **ITS**, and **TS**.

Further, to have a better understanding of reported absorption spectra in these molecules, the lowest electronic excitations of all the molecules have been calculated by means of TD-DFT methodology at B3LYP/6-311+ G (d, p) level.



In addition to this to see the effect of different functionals on absorption properties, various functionals are used to validate the best among all. Electronic excitations for all the molecules were computed with various functionals (BLYP, BHandHLYP, B3LYP, M06, PBE0, LCWPBE, CAM-B3LYP and WB97XD) at 6-311+ G (d, p) basis set based on B3LYP/6-311+ G (d, p) optimized geometries in order to verify the effect of functionals on the electronic excitations. Absorption energies calculated with various functionals are shown in figure 4B.1 and table 4B.2. It is clear from figure 4B.1 and table 4B.2, B3LYP, M06 and PBE0 functionals are showing good agreement with the experimentally reported excitation energies. Hence, our further discussion of electronic excitations is based on calculations at TD-B3LYP/6-311+ G (d, p) level.

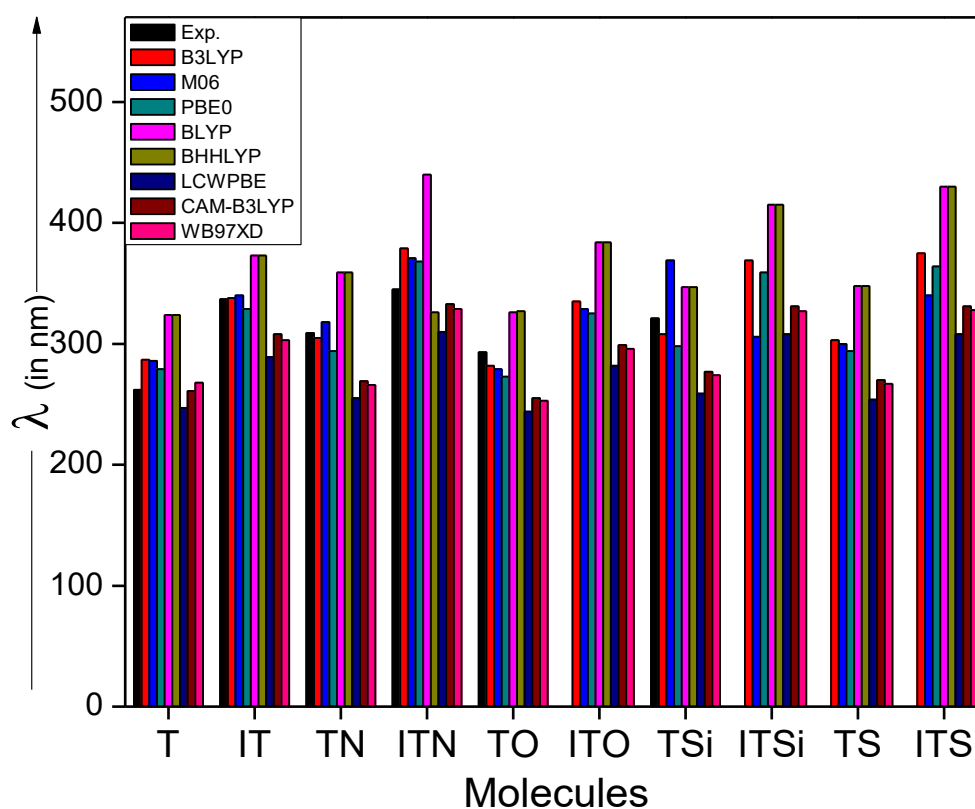


Figure 4B.1: Calculated absorption energies of the molecules using functionals B3LYP, BLYP, BHandHLYP, M06, PBE, LCWPBE, CAM-B3LYP and WB97XD at 6-311+G (d,p) level

Table 4B.2. Absorption maxima with different functionals calculated at B3LYP optimized geometries with 6-311+G (d, p) basis set

Molecules	$\lambda_{\text{Exp.}}$	B3LYP	BLYP	BHHLYP	M06	PBE0	LC-WPBE	CAM-B3LYP	WB97XD
<b>T</b>	273	287	324	324	286	279	247	261	258
<b>IT</b>	337	338	373	373	340	329	289	308	303
<b>TN</b>	309	305	359	359	318	294	255	269	266
<b>ITN</b>	345	379	440	326	371	368	310	333	329
<b>TO</b>	293	282	326	327	279	273	244	255	253
<b>ITO</b>	-	335	384	384	329	325	282	299	296
<b>TSi</b>	321	308	347	347	306	298	259	277	274
<b>ITSi</b>	-	369	415	415	369	359	308	331	327
<b>TS</b>	-	303	348	348	300	294	254	270	267
<b>ITS</b>	-	375	430	430	372	364	308	331	328

From TDDFT results, the lowest electronic excitation for **T** is at 287 nm with the oscillator strength 0.429. The major transitions for this excitation are HOMO-1→LUMO+1 and HOMO→LUMO. Molecule **IT** is showing absorption maximum at 338 nm, and this excitation is due to the transition from HOMO→LUMO. There is a good agreement between the experimental and calculated absorption energies for **T** and **IT**. The calculated electronic excitations, oscillator strength along with corresponding major orbital transitions are shown in table 4B.3. Normalized absorption spectra of symmetrical (**T-TS**) and asymmetrical (**IT-ITS**) isomers are shown in figure 4B.2 and figure 4B.3 respectively. Experimentally reported and theoretically calculated absorption maxima for the molecule **TN** are 309 nm and 305 nm respectively. Major transitions in case of **TN** are HOMO→LUMO and HOMO-1→LUMO+1. Along with these major transitions, other minor transitions from HOMO-1→LUMO+2 and HOMO→LUMO+2 with small contributions are also observed. The experimentally reported absorption maximum for **ITN** is showing a 36 nm red-shifted than **TN**(309 nm) with the intense peak at 345 nm. A similar trend is observed from TDDFT results, calculated absorption for **ITN** is showing 70 nm red-shift from **TN** which arises due to

transition from HOMO→LUMO (molecular orbital picture along with major transition for **TN** and **ITN** are shown in figure 4B.4). The calculated absorption maximum for **TO** is at 282 nm (observed absorption maximum is 293 nm) with the major transitions from HOMO-1→LUMO and HOMO→LUMO+1. Molecule **ITO** is showing absorption at 335 nm that is due to excitation from HOMO-1→LUMO (molecular orbital picture along with major transition for **TO** and **ITO** are shown in figure 4B.5). The molecule **TSi** shows an intense peak at 308 nm which is due to HOMO-1→LUMO and HOMO→LUMO+1 beside these major transitions, minor transitions are also involved and are shown in table 4B.3. Calculated absorption maximum for molecule **ITSi** is at 369 nm, which results the transition from HOMO→LUMO (molecular orbital picture along with major transition for **TSi** and **ITSi** are shown in figure 4B.6). From these results, we find that asymmetric molecules are always 50-70 nm red-shifted than their corresponding symmetrical isomers. **TS** is showing absorption at 303 nm which arises due to transitions from HOMO-1→LUMO and HOMO→LUMO+1. Other transitions are with minor contributions from HOMO-1→LUMO+1 and HOMO→LUMO. While in **ITS**, shows a red-shift in absorption compared to their respective isomer and wavelength observed for **ITS** is at 375 nm which is mainly due to transition HOMO→LUMO. Figure 4B.7 shows the major electronic excitations for molecules **T** and **TS** with their molecular orbital pictures and figure 4B.8 shows the major electronic excitations for molecules **IT** and **ITS** with their molecular orbital pictures. It is clear from table 4B.3, there is considerable variation in the absorption energies of the molecules with the change in hetero-atoms; for example, **TSi** shows a 26 nm red-shift compared to **TO**, **ITN** shows a 44 nm red-shift compared to **ITO**.

Table 4B.3: Computed lowest electronic excitations ( $\lambda_{\max}$  in nm), Oscillator strength ( $f$ ), Major Transitions (MT) and % weight (%  $C_i > 10\%$ ) at TD-B3LYP/6-311+G (d, p) method.

Molecules	$\lambda_{\text{exp}}$	$\lambda_{\text{max}}$	$f$	MT	% $C_i$
T	<sup>a</sup> 273	287	0.429	H-1→L	13
				H-1→L+1	32
				H→L	32
				H→L+1	13
IT	<sup>b</sup> 337	338	0.493	H→L	98
TN	<sup>c</sup> 309	305	0.281	H-1→L+1	15

				H-1→L+2	13
				H→L	29
				H→L+2	13
ITN	<sup>d</sup> 345	379	0.126	H→L	94
TO	<sup>e</sup> 293	282	0.573	H-1→L	45
				H→L+1	45
ITO		335	0.121	H-1→L	88
TSi	<sup>e</sup> 321	308	0.330	H-1→L	34
				H-1→L+1	13
				H→L	13
				H→L+1	34
ITSi		369	0.175	H→L	77
				H→L+1	17
TS		303	0.486	H-1→L	27
				H-1→L+1	18
				H→L	17
				H→L+1	27
ITS		375	0.110	H→L	92

<sup>a</sup> *J. Org. Chem.* **2006**, 71, 7858

<sup>b</sup> *Chem. Ber.* **1968**, 101, 212

<sup>c</sup> *Org. Lett.*, **2015**, 17, 4164

<sup>d</sup> *J. Chem. Soc. Perkin Trans.* **2000**, 2, 2337

<sup>e</sup> *Asian J. Org. Chem.* **2017**, 6, 290

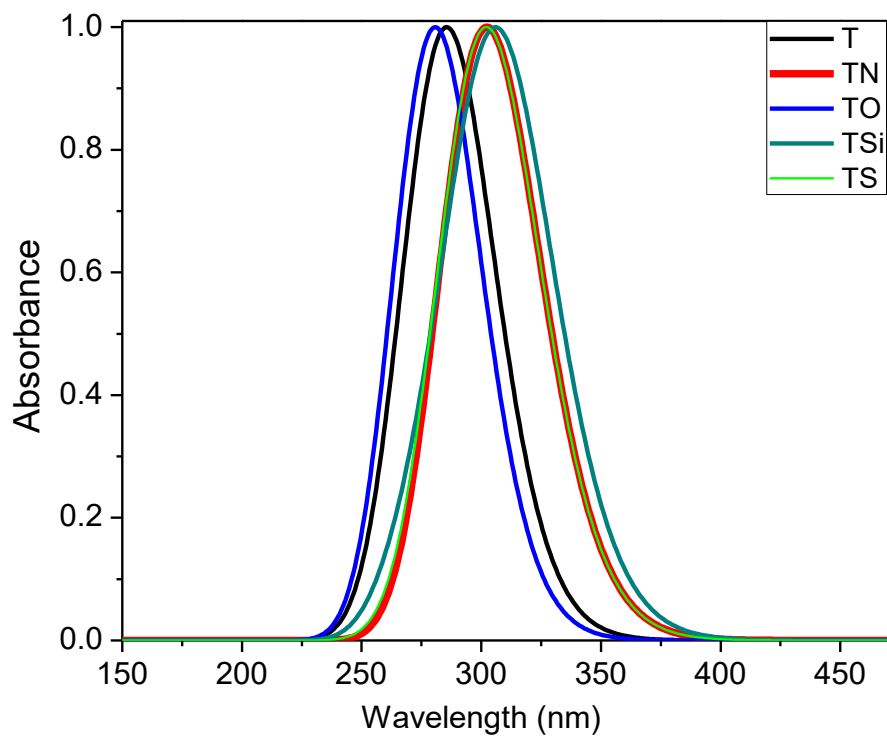


Figure 4B.2: Calculated Absorption spectra of symmetrical molecules, **T-TS**.

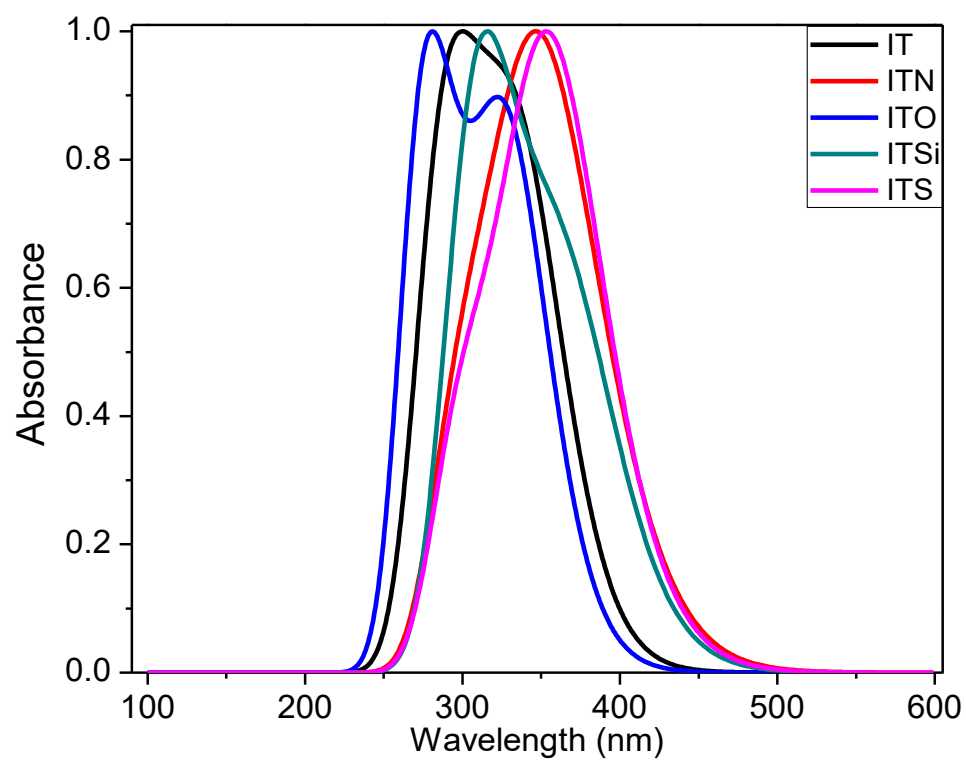


Figure 4B.3: Calculated Absorption spectra of asymmetrical molecules **IT-ITS**

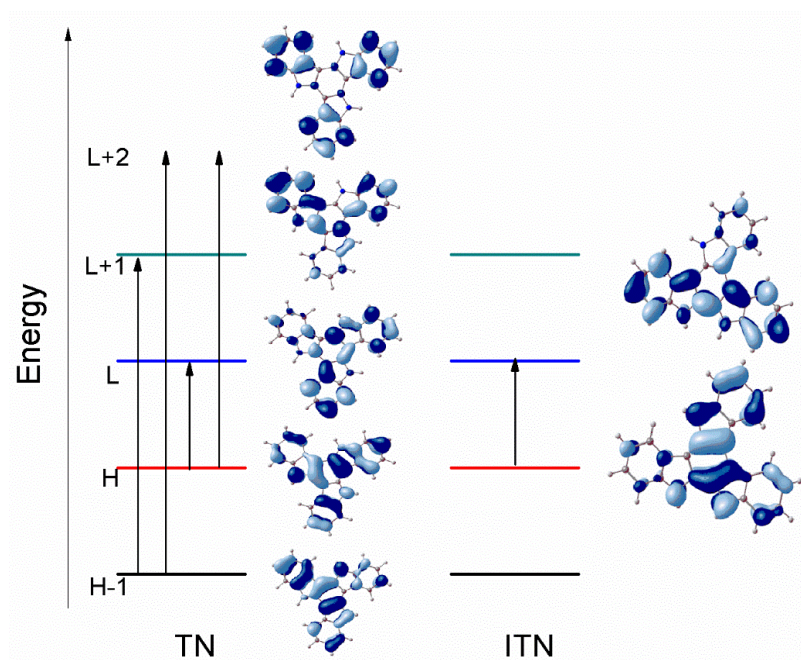


Figure 4B.4: Major Electronic transitions with their molecular orbitals for the molecules **TN** and **ITN**

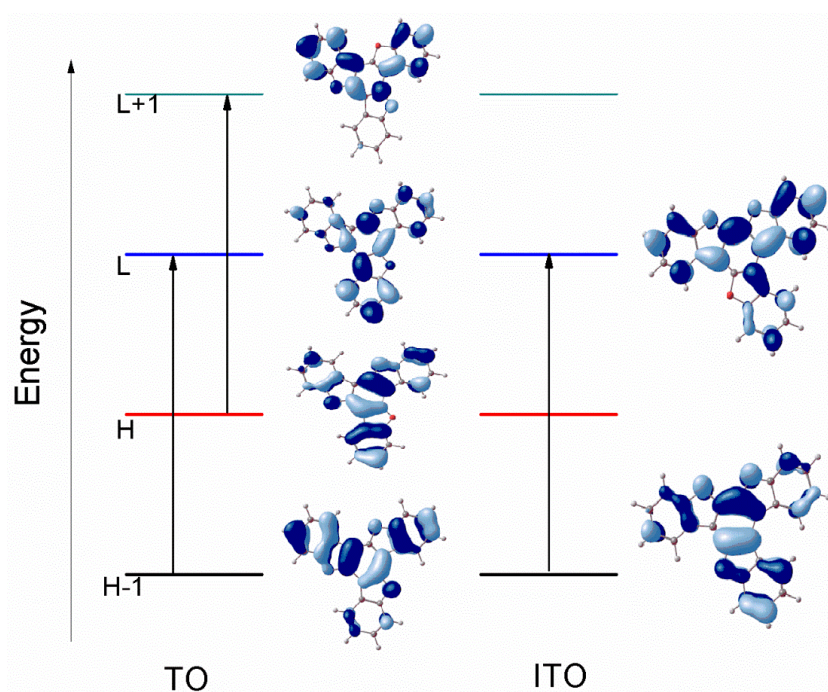


Figure 4B.5: Major Electronic transitions with their molecular orbitals for the molecules **TO** and **ITO**



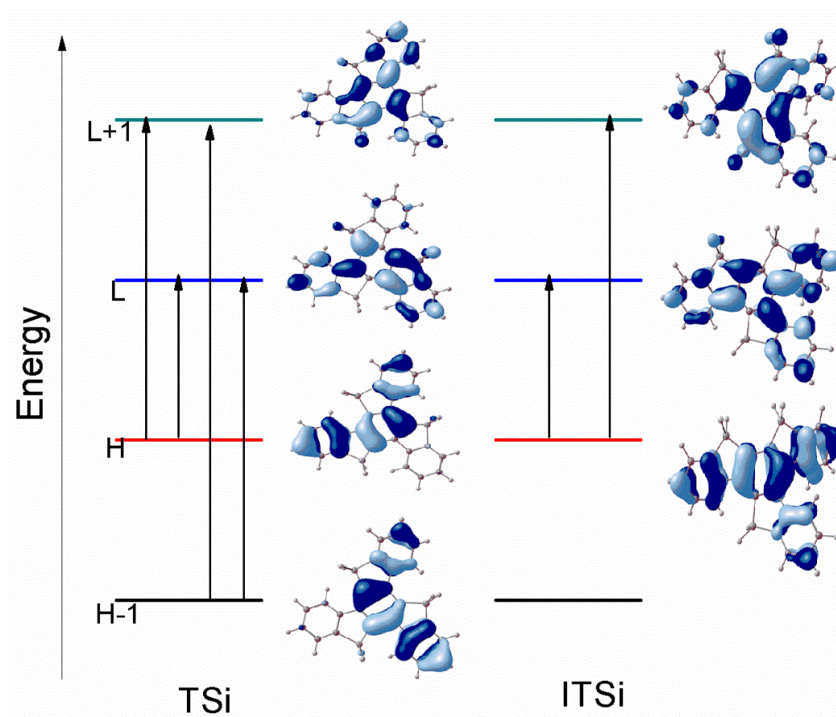


Figure 4B.6: Major Electronic transitions with their molecular orbitals for molecules **TSi** and **ITSi**

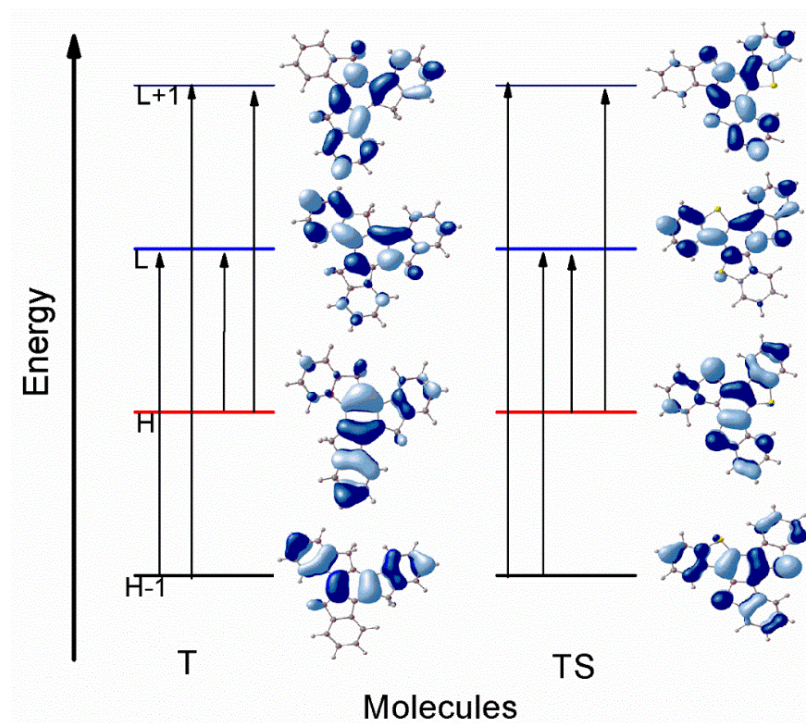


Figure 4B.7: Major Electronic transitions with their molecular orbitals for molecule **T** and **TS**

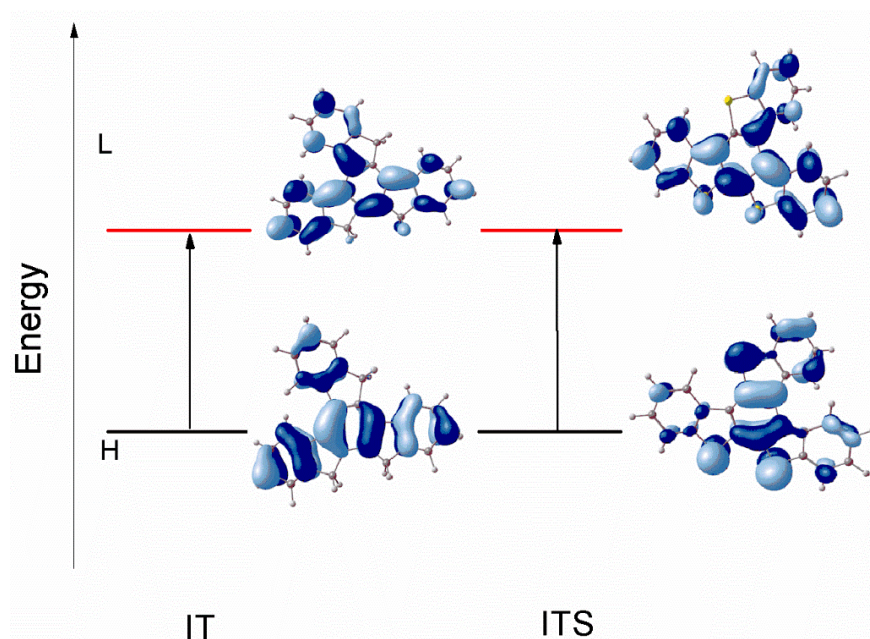


Figure 4B.8: Major Electronic transitions with their molecular orbitals for the molecules **IT** and **ITS**

Asymmetric isomers are showing smaller HOMO-LUMO gap as compared to their corresponding symmetric isomers, shown in figure 4B.9. For molecule **T**, HOMO and LUMO energies are at  $-5.90\text{eV}$  and  $-1.27\text{eV}$  respectively and corresponding HOMO-LUMO gap is  $4.63\text{ eV}$ , while in its asymmetric isomer, i.e. **IT**, is showing smaller HOMO-LUMO gap ( $4.02\text{ eV}$ ). This decrease in HOMO-LUMO gap in case of **IT** is due to destabilization of HOMO ( $-5.63\text{ eV}$ ) and stabilization of LUMO ( $-1.61\text{eV}$ ) levels, shown in figure 4B.9. Molecule **TN** is showing a HOMO-LUMO gap of  $-4.36\text{ eV}$  which is  $0.59\text{ eV}$  higher than its asymmetric isomer **ITN** ( $-3.77\text{ eV}$ ). In case of **TO** and **ITO**, the HOMO energies for both the isomers are approximately same but LUMO level for **ITO** gets stabilized to the greater extent which results in smaller HOMO-LUMO gap for isomer **ITO** ( $4.14\text{ eV}$ ) compared to **TO** ( $4.66\text{ eV}$ ). Molecule **TSi** is having deepest HOMO level among all studied molecule with the energy of  $-6.29\text{ eV}$ , while the LUMO level is at  $-1.90\text{ eV}$  and HOMO-LUMO energy gap is  $4.39\text{ eV}$ . Like other iso-derivative, **ITSi** is also showing smaller HOMO-LUMO gap ( $3.80\text{ eV}$ ) as compared to their corresponding isomer (**TSi**) with HOMO and LUMO energies of  $-5.86\text{ eV}$  and  $-2.05\text{ eV}$  respectively. A similar trend is followed for isomers **TS**, and **ITS**, HOMO energy of **TS** and



**ITS** are -5.89 eV and -5.81eV respectively, there is a destabilization of HOMO energy by an amount 0.08 eV from **TS** to **ITS**. Also, stabilization of LUMO by 0.41eV, on moving from **TS** to **ITS**, this destabilization of HOMO and stabilization of LUMO level lowers the HOMO-LUMO energy gap of **ITS** (3.84 eV) as compared to **TS** (4.36 eV). The calculated HOMO, LUMO energies with their HOMO-LUMO gap for all the studied molecules are tabulated in table 4B.4. The reason for the smaller HOMO-LUMO gaps for asymmetrical isomers than its corresponding symmetrical one is due to destabilization of HOMO and stabilization of LUMO levels (shown in figure 4B.9). Within the symmetrical molecules, **TS** and **TN** are showing the smallest HOMO-LUMO gap of 4.36 eV and 4.36 eV respectively while in asymmetric series, **ITN** is showing the smallest HOMO-LUMO gap with 3.77 eV.

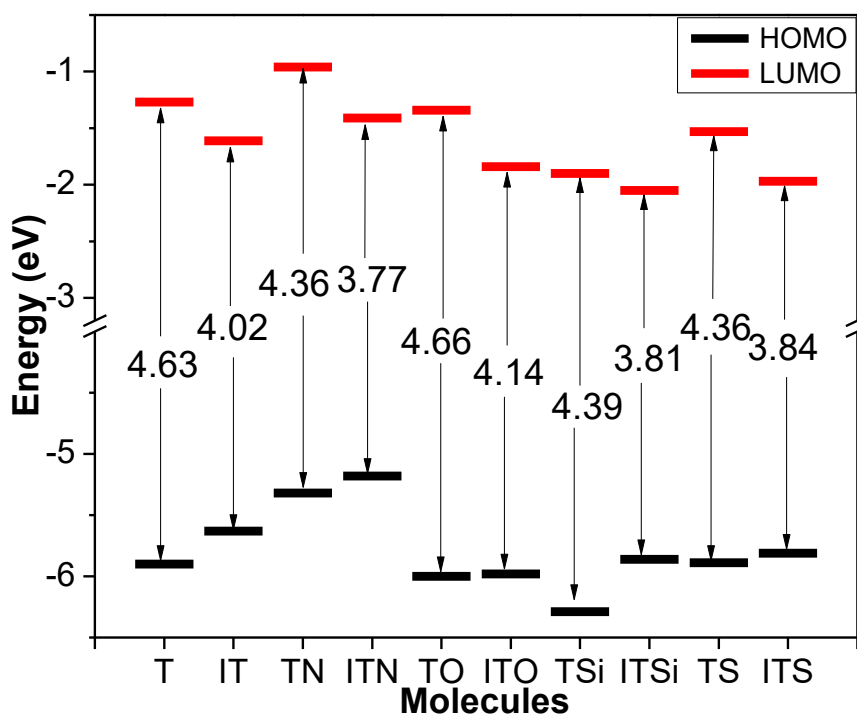


Figure 4B.9: Energy levels of HOMO, LUMO and HOMO-LUMO gap for all the molecules

Table 4B.4. HOMO, LUMO Energies and HOMO-LUMO Gap (HLG in eV)

Molecule	HOMO	LUMO	HLG
T	-5.90	-1.27	4.63
IT	-5.63	-1.61	4.02
TN	-5.32	-0.96	4.36
ITN	-5.18	-1.41	3.77
TO	-6.00	-1.34	4.66
ITO	-5.98	-1.84	4.14
TSi	-6.29	-1.90	4.39
ITSi	-5.86	-2.05	3.81
TS	-5.89	-1.53	4.36
ITS	-5.81	-1.97	3.84

#### 4B.3.3. Ionization Potential (IP) and Electron Affinity (EA), HEP and EEP

For the better performance of the optoelectronic device, there should be an efficient injection of hole and electron into an organic molecule. The energy barrier for the injection of the holes and electrons were evaluated by IP and EA. IP defined as the energy required by the system when an electron is removed, and it must be sufficiently low for efficient hole injection into the HOMO of the molecule. EA defined as the energy released when an electron is added to the system. EA must be high enough to allow an efficient electron injection into LUMO of the molecule. The lower the IP of the hole-transport layer (HTL), the easier will be the injection of holes from ITO (Indium tin oxide) to HTL, higher the EA of the electron-transport layer (ETL), and easier the injection of electrons from the cathode to ETL. Thus, calculation of IP, EA, HEP, and EEP are done by above-given formulae for all the molecules, and calculated results are shown in table 4B.5. Clemence Corminboeuf et al. reported that the truxene and its derivatives are promising dopant-free hole transporting materials and IP can be tuned with the alteration of a heteroatom in the truxene core [18]. From table 4B.5, it is clear that the IP and EA tuned with the alteration of heteroatom in the truxene core. Among symmetrical isomers (T-TS), TN is having smallest adiabatic and vertical IP of 6.50 eV and 6.59 eV while in

asymmetrical molecules **ITN** is showing smallest IP of 6.32 eV and 6.47 eV. Thus, it is easy to create a hole in molecules **TN** and **ITN** than other molecules. Also, asymmetrical molecules are always showing smaller IP (adiabatic or vertical) than their corresponding symmetrical isomers which result it is easy to create a hole in the asymmetrical molecule. Within all the studied molecules, **TN (ITN)** is also showing minimum HEP of 6.40 eV (6.18 eV) indicating that the injection of the hole is easier in these molecules. EA is highest for with the heteroatom Silicon, i.e., **TSi (ITSi)** and its vertical and adiabatic values are 0.86 eV (1.02 eV) and 0.72 eV (0.88 eV) respectively, signifying that there is an efficient electron injection in the HOMO level of this molecule as compared to others. Further, the energy required to extract electron (EEP) is highest for molecule **TSi (ITSi)** is 1.01 eV (1.15 eV), shown in table 4B.5.

Table 4B.5. Calculated ionization potentials (IP in eV), electron affinities (EA in eV), hole and electron extraction potentials (HEP and EEP in eV) and hole and electron reorganization energies ( $\lambda_h$ , and  $\lambda_e$  in meV) at B3LYP/6-311+ G (d, p) level of theory.

Molecule	$\lambda_h$	$\lambda_e$	$IP_a$	$IP_v$	$EA_a$	$EA_v$	HEP	EEP
T	182	200	7.08	7.17	0.14	0.04	6.99	0.24
IT	222	226	6.77	6.88	0.51	0.40	6.66	0.62
TN	186	144	6.50	6.59	-0.17	-0.24	6.40	-0.09
ITN	285	234	6.32	6.47	0.31	0.19	6.18	0.43
TO	220	187	7.19	7.30	0.19	0.10	7.08	0.29
ITO	305	213	7.17	7.38	0.70	0.59	7.07	0.81
TSi	244	289	7.39	7.51	0.86	0.72	7.27	1.01
ITSi	311	267	6.92	7.08	1.02	0.88	6.77	1.15
TS	147	180	7.06	7.14	0.42	0.33	6.99	0.51
ITS	167	231	6.99	7.07	0.89	0.77	6.90	1.00

#### 4B.3.4. Reorganization energy ( $\lambda$ )

The reorganization energy ( $\lambda$ ) values are used to evaluate charge-transport rate and balance between hole and electron injections. Reorganization energy ( $\lambda$ ) is a measure of change in energy of the system upon relaxation of the molecular structure due to excess of positive and negative charges. As stated in chapter 1, lower the  $\lambda$  value the higher is the charge-transport rate. Further smaller the difference between  $\lambda_h$  and  $\lambda_e$ , better the balance between hole transfer and electron transfer. The calculated reorganization energies are tabulated in table 4B.5 using B3LYP functional with 6-311+ G (d, p) basis set. Anup Thomas et al. reported that the reorganization energies obtained by Cam-B3LYP and BHandHLYP are higher than B3LYP predictions [48]. We also calculated the reorganization energies with different functionals (BHandHLYP, PBE0 and CAM-B3LYP) to see the effect of functionals and found that the reorganization energies with Cam-B3LYP and BHandHLYP are higher than B3LYP predictions [48] (shown in figure 4B.10 and figure 4B.11). The hole reorganization energy ( $\lambda_h$ ) calculated for all the molecules (except **ITO** and **ITSi**) are smaller than that of N,N'-diphenyl-N,N'-bis(3-methylphenyl)-(1,1'-biphenyl)-4,4'-diamine (TPD) which is typical hole transport material  $\lambda_h=290$  meV [49]. Further, hole ( $\lambda_h$ ) as well electron ( $\lambda_e$ ) reorganization energy of symmetrical molecules (**T-TSi**) are smaller than asymmetrical series (**IT-ITSi**) suggesting that the symmetrical isomers are better for the hole transporting material than asymmetrical isomers. Among symmetrical isomers the order of  $\lambda_h$  value **TS**<**T**<**TN**<**TO**<**TSi**, and molecule **TS** is showing smallest  $\lambda_h$  of 147meV thus, it behaves as the best hole transporting material among all studied symmetrical isomers. An asymmetrical isomer also follows similar trend, here the molecule **ITS** is showing the smallest  $\lambda_h$  value of 167 meV. In both the cases either symmetrical or asymmetrical, the presence of sulphur is the best (**TS**& **ITS**) for hole transporting materials. Also, the calculated electron reorganization energies,  $\lambda_e$  for all the molecules (except **TSi**) is smaller than tris(8-hydroxyquinolato) aluminium (III) (Alq3) which is considered as typical electron transport material  $\lambda_e= 276$  meV [50-51]. Order of  $\lambda_e$  values in case of symmetrical series is **TN**< **TS**< **TO**< **T**<**TSi**, which decides **TN** is better for the electron transporting material than other truxeneanalogs. The increasing order of  $\lambda_e$  in asymmetrical isomers are **ITO**<**IT**<**ITS**<**ITN**<**ITSi**, and shows **IT** is the better for electron transport materials. Within all studied molecules, in most of the cases, the difference between

the  $\lambda_h$  and  $\lambda_e$  energies are smaller than 40 meV which implies there is a good balance of hole and electron transfer rate in molecules and can behave as ambipolar molecules.

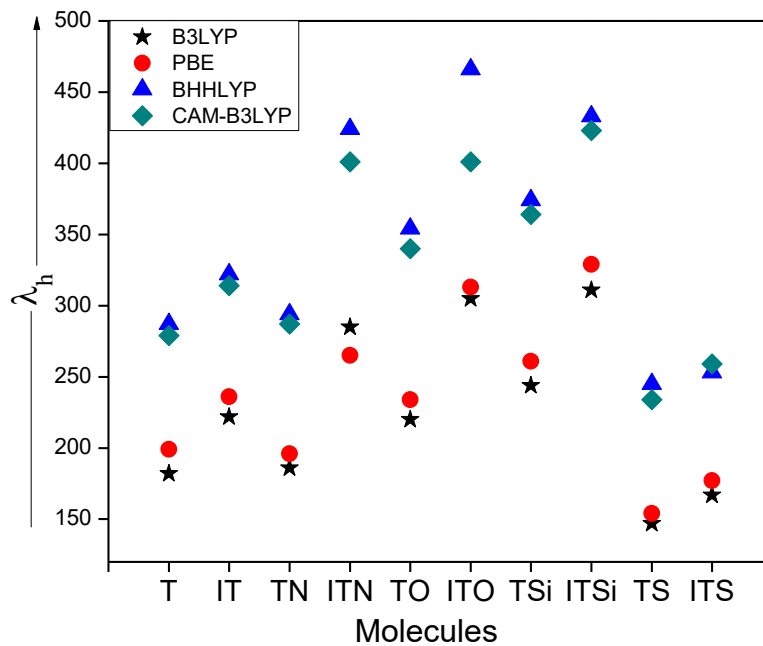


Figure 4B.10: Hole reorganization energies for all the molecules with B3LYP, BHandHLYP, PBE0 and CAM-B3LYP functionals

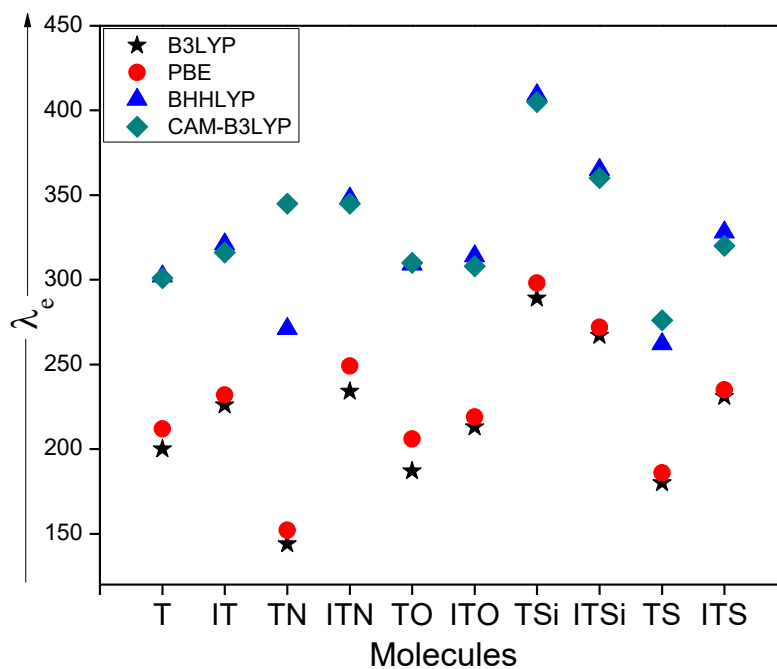


Figure 4B.11: Electron reorganization energies for all the molecules with B3LYP, BHandHLYP, PBE0 and CAM-B3LYP functionals

#### 4B.4. Conclusion

Here in this chapter a theoretical study of a series of symmetrical and asymmetrical truxene analogues has been carried out by means of DFT and TDDFT calculations. The absorption maxima of asymmetrical isomers are always 50-70 nm red-shifted than their corresponding symmetrical isomers. Among all studied molecules, calculated absorption maxima are highest for **ITS** and **ITN**. It is also found that when we disturb the symmetry of molecule, destabilization of HOMO and stabilization of LUMO take place which results in a decrease in HOMO-LUMO gap in asymmetrical isomers. Ionization potentials for asymmetrical isomers are always smaller than their corresponding symmetrical isomers suggesting that it is easy to create a hole in asymmetrical molecules. Higher electron affinity for ITSi, suggests it is easier to inject electrons from cathode to ETL. The smaller hole and electron reorganization energies as compared to standard molecules give better charge transport rate in the studied molecules. Moreover, the difference between the hole and electron reorganization energies are smaller ( $\sim 40\text{meV}$ ) and hence studied molecule can be used as an ambipolar charge transporting materials.

---

**References**

1. J. Huang, J.H. Su, H. Tian, *J. Mat. Chem.* **2012**, 22, 10977.
2. Y. L. Liu, J. K. Feng, A. M. Ren, *J. Phys. Org. Chem.* **2007**, 20, 600.
3. Y. Lin, Y. Li, X. Zhan, *Chem. Rev.* **2012**, 41, 4245.
4. Y. A. Duan, Y. Geng, H. B. Li, J. L. Jin, Y. Wu, Z. M. Su, *J. Comp. Chem.* **2013**, 34, 1611.
5. X. Zong, M. Liang, C. Fan, K. Tang, G. Li, Z. Sun, S. Xue, *J. Phys. Chem. C* **2012**, 116, 11241.
6. M. Reig, J. Puigdollers, D. Velasco, *J. Mater. Chem. C* **2015**, 3, 506.
7. S. R. Forrest, *Nature* **2004**, 428, 911.
8. M. M. Torrent, C. Rovira, *Chem. Rev.* **2011**, 111, 4833.
9. J. S. Yang, H. H. Huang, J. H. Ho, *J. Phys. Chem. B*, **2008**, 112, 8871.
10. J. S. Yang, H. H. Huang, Y. H. Liu, S. M. Reng, *Org. Lett.* **2009**, 11, 4942.
11. H. H. Huang, Ch. Prabhakar, K. C. Tang, P. T. Chou, G. J. Huang, J. S. Yang, *J. Am. Chem. Soc.* **2011**, 133, 8028.
12. F. Goubard, F. Dumur, *RSC Adv.* **2015**, 5, 3521.
13. J. S. Yang, Y. R. Lee, J. L. Yan, M. C. Lu, *Org. Lett.* **2006**, 8, 5813.
14. J. S. Yang, H. H. Huang, S. H. Lin, *J. Org. Chem.* **2009**, 74, 3974.
15. R. Sharma, D. Volyniuk, C. Popli, O. Bezikonnyi, J. V. Grazulevicius, R. Mishra, *J. Phys. Chem. C* **2018**, 122, 15614.
16. R. Sharma, R. Maragani, R. Mishra, *New J. Chem.* **2018**, 42, 882.
17. B. Kaur, D. Moghe, A. Dey, D. Kabra, J. Jacob, *J. Lumin.* **2018**, 196, 511.
18. K. H. Lin, A. Prlj, C. Corminboeuf, *J. Phys. Chem. C* **2017**, 121, 21729.
19. F. S. Kipping, *J. Chem. Soc. Trans.* **1894**, 65, 269.
20. K. F. Lang, M. Zander, E. A. Theiling, *Chem. Ber.* **1960**, 93, 321.
21. K. Hartke, A. S. Pindur, *Liebigs Ann. Chem.* **1984**, 12, 552.
22. J. Bergman, B. Egestad, *Chemica Scripta*, **1986**, 26, 287.
23. Y. N. Oded, I. Agranat, *Tetrahedron Lett.* **2014**, 55, 636.
24. J. Pei, J. L. Wang, X. Y. Cao, X. H. Zhou, W. B. Zhang, *J. Am. Chem. Soc.* **2003**, 125, 9944.
25. W. B. Zhang, W. H. Jin, X. H. Zhou, J. Pei, *Tetrahedron*, **2007**, 63, 2907.

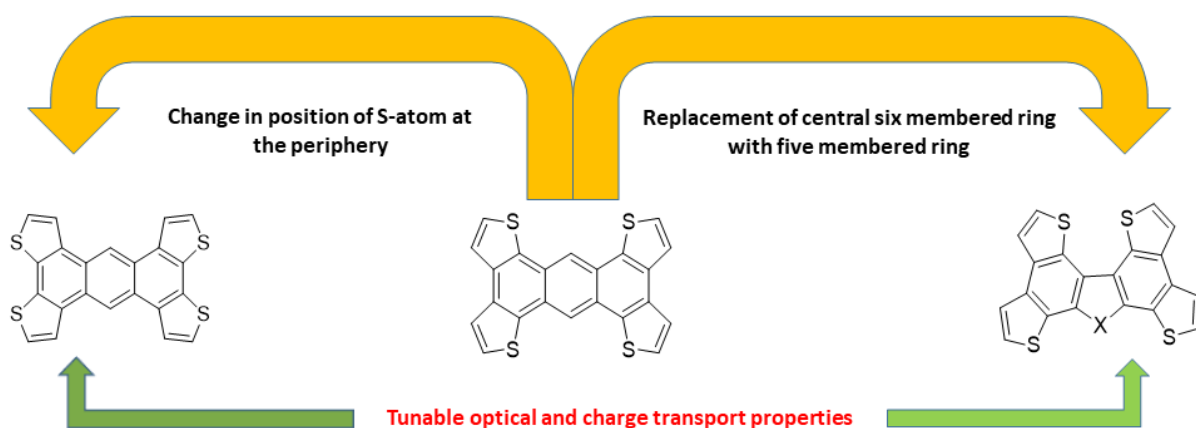
- 
26. X. Y. Cao, H. Zi, W. Zhang, H. Lu, J. Pie, *J. Org. Chem.* **2005**, 70, 3645.
  27. T. A. Liu, Ch. Prabhakar, J. Y. Yu, C. Chen, H. H. Huang, J. S. Yang, *Macromolecules*, **2012**, 45, 4529.
  28. V. Bocchi, G. Palla, *Tetrahedron*, **1986**, 42, 5019.
  29. M. Gordon, R. Andrew, *J. Chem. Soc. Faraday Trans.* **1994**, 90, 1121.
  30. N. Toworakajohnkun, M. Sukwattanasinitt, P. Rashatasakhon, *Tetrahedron Lett.* **2017**, 58, 4149.
  31. S. W. Shelton, T. L. Chen, D. E. Barclay, B. Ma, *Appl. Mater. Interfaces*, **2012**, 4, 2534.
  32. R. R. Reghu, D. Volyniuk, N. Kostiv, K. Norvaisa, *Dyes Pigm.* **2016**, 125, 159.
  33. C. Ruiz, E. M. G. Frustos, D. A. S. Filho, J. T. L. Navarrete, M. C. R. Delgado, B. G. Lor, *J. Phys. Chem. C* **2014**, 118, 5470.
  34. X. Du, M. S. Yuan, F. Xu, H. Wang, Q. Wang, W. Wang, D. E. Wang, J. Wang, *Spectrochimica Acta A* **2016**, 164, 33.
  35. P. Dai, H. Dong, M. Liang, H. Cheng, Z. Sun, S. Xue, *ACS Sustainable Chem. Eng.* **2017**, 5, 97.
  36. R. A. Valentine, A. Whyte, K. Awaga, N. Robertson, *Tetrahedron Lett.* **2012**, 53, 657.
  37. C. Coia, C. Ruiz, A. L. Alvarez, S. A. Garcia, E. M. G. Frutos, B. G. Lor, A. D. Andres, *Organic Electron.* **2012**, 13, 2138.
  38. Z. Yang, B. Xu, J. He, L. Xue, Q. Guo, W. Tian, *Organic Electron.* **2009**, 10, 954.
  39. H. Zhou, X. Zhao, T. Hung, R. Lu, H. Zhang, X. Qi, P. Xue, X. Liu, X. Zhang, *Org. Biomol. Chem.* **2011**, 9, 1600.
  40. M. S. Yuan, Z. Q. Liu, Q. Fang, *J. Org. Chem.* **2007**, 72, 7915.
  41. J. Bergman, N. Eklund, *Tetrahedron* **1980**, 36, 1445.
  42. T. Ogaki, E. Ohta, Y. Oda, H. Sato, Y. Matsui, M. Kumeda, H. Ikeda, *Asian J. Org. Chem.* **2017**, 6, 290.
  43. M. J. Frisch, Gaussian 16, Revision E.01; Gaussian, Inc.: Wallingford CT, **2016**.
  44. M. S. Yuan, Q. Fang, Z. Q. Liu, J. P. Guo, H. Y. Chen, W. T. Yu, G. Xue D. S. Liu, *J. Org. Chem.* **2006**, 71, 7858.
  45. M. Zander, W. H. Franke, *Chem. Ber.* **1968**, 101, 212.
  46. L. Wang, Q. Fang, Q. Lu, S. J. Zhang, Y. Y. Jin Z. Q. Liu, *Org. Lett.* **2015**, 17, 4164.
-



- 
47. L. Greci, G. Tommasi, R. Petrucci, G. Marrosu, A. Trazza, P. Sgarabotto, L. Right and A. Alberti, *J. Chem. Soc. Perkin Trans.* **2000**, 2, 2337.
  48. A. Thomas, R. K. Chitumalla, A. L. Puyad, K. V. Mohan, *Comput. Theor. Chem.* **2016**, 1089, 59.
  49. M. Malagoli, J. L. Bredas, *Chem. Phys. Lett.* **2000**, 327, 13.
  50. B. C. Lin, C. P. Cheng, Z. Q. You, C. P. Hsu, *J. Am. Chem. Soc.* **2005**, 127, 66.
  51. A. Irfan, R. Cui, J. Zhang, *J. Mol. Struc. Theochem.* **2010**, 956, 61.

# Chapter 5A

*Impact of replacement of central benzene ring in Anthracene by Heterocyclic ring on Electronic excitations and Reorganization energies in Anthratetrathiophene (ATT)*



*Results of this chapter published in J. Chin. Chem. Soc. 2018, 65, 918*





### 5A.1. Introduction

Recent developments in organic semiconductor materials has attracted much attention due to their numerous applications in the field of Organic Solar Cells[1-2], Organic Photovoltaic Cells (OPVs) [3-4], Organic light emitting diode (OLEDs) [5-6], Organic field effect transistors (OFETs) [7-9], etc. Further, due to their low cost, light weight, manufacturability and possibility of producing flexible and large area devices made these organic semiconductor materials to be the best alternative for inorganic semiconductors materials [10-11]. Organic semiconductor materials with  $\pi$ -conjugated star shaped oligomers has been designed and synthesized to tune desirable optical and electronic properties [12-14]. The studies on materials with  $\pi$ -conjugated oligomers and polycyclic aromatic hydrocarbons shows that, acene based molecules are with good optical and efficient charge transport properties, and these are suitable for optoelectronic applications [15-16]. But these molecules are having some drawbacks like low solubility and poor air stability owing to their high lying highest occupied molecular orbital level and smaller highest occupied molecular orbital (HOMO) lowest unoccupied molecular orbital (LUMO) gap (HOMO-LUMO gap) [17-19]. Takimiya and coworkers introduce a heteroaromatic-benzene system to these acenes and shown that fairly improved air stability with high field effect mobilities [20-21.] Neckers et.al. successfully synthesized sulphur containing stable unsubstituted heptacene with a high degree of charge carrier mobility when assemble with organic transistors [22]. In context to this, fused thiophenes are well known due to their increased stability as compared to linearly linked structure together with more efficient conjugation [8,23].

Thiophene based oligomers are suitable for organic semiconductors due to various inter and intra molecular interactions such as Van der Waals interactions, weak H-bonding and  $\pi$ - $\pi$  stacking are existing which are essential to achieve high charge carrier mobility. S...S (sulphur-sulphur) interactions originating in thiophene ring could strongly affect the solid-state packing and play an important role in achieving high carrier mobilities [24-28]. Liu et al. synthesized substituted Anthratetrathiophene (ATT) molecule (**1a** in scheme 5A.1), with the help of Negishi-coupling between 1,4-dibromo-2,5-diiodobenzene and 5-alkyl-2-thienylzinc chloride, followed by oxidative cyclization by  $\text{FeCl}_3$  [29]. They showed that, presence of a thiophene ring at the periphery of anthracene increases stability of the molecule and also favor  $\pi$ - $\pi$  interactions in a facile manner. It is also reported that, these molecules have a tendency to self-

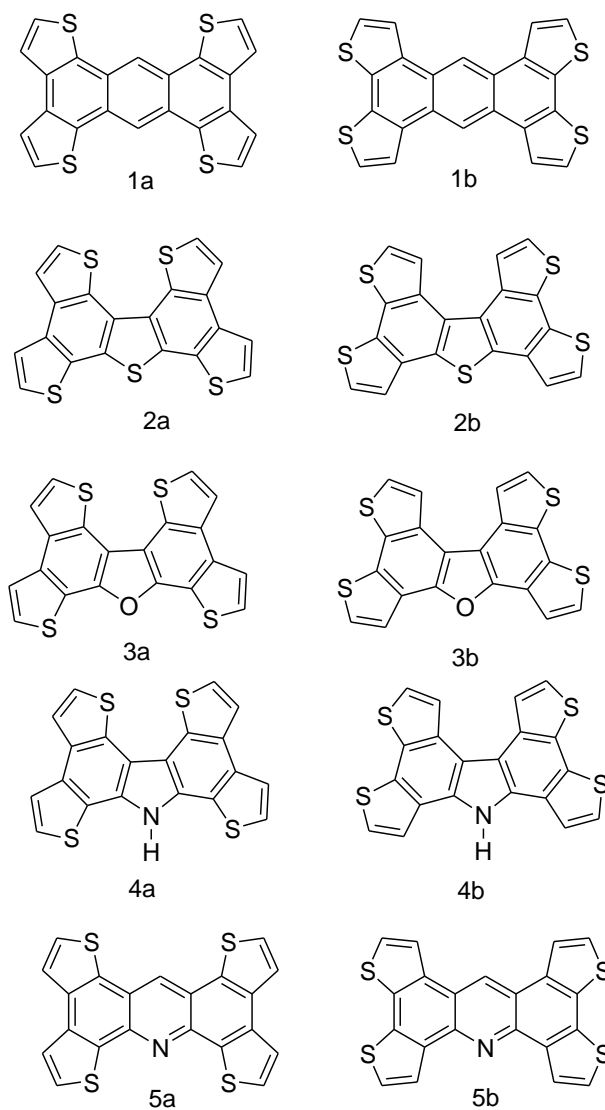
associate through  $\pi$ - $\pi$  stacking with high hole mobility ( $0.012\text{cm}^2\text{V}^{-1}\text{s}^{-1}$ ) and air stability [29]. In continuation to the work reported by Liu et al., Perepichka and coworkers synthesized another geometrical isomer of anthratetrathiophene (ATT) (molecule **1b** which is similar to **1a**, shown in scheme 5A.1); differ only in position of sulphur atom [16]. Molecule **1b** shows higher thermodynamic stability and S...S interactions than **1a**. Zang et al. reported a new seven-membered fused system dibenzothienotetrathiophene **2a** (scheme 5A.1), which exhibit high thermal and photo stability, strong solid state fluorescence makes them better molecule for application in optoelectronics [30]. Molecule **2a** is different from **1a** (**1b**) only by central ring system, in later case there is anthracene as central core while in the former central benzene ring of anthracene is replaced by thiophene ring. Further Y-A Duan et al. reported the theoretical studies on the hole transport properties of tetrathioenoarenes and shown that, chemical modifications like changing the position of hetero atom, introducing different substituents and  $\pi$ -conjugated cores are powerful molecular designing tools to optimize their optical and electrochemical properties [31]. By changing the position of sulphur atom in chemical structure, lead to significant change in optical and electrochemical properties of the molecule [31]. From these reports and also motivated by the fact that only slightly modification in organic molecule would lead to difference in optical and electrochemical properties. Here in this work we report Anthratetrathiophene (ATT) as basic skeleton and studied the effect of change of the central benzene ring of anthracene with different heterocyclic rings (five and six membered) and position of sulphur atom, on optical and hole/ electron transport properties. Molecule **1a** and **1b** are with anthracene as central moiety and thiophenes are substituted at the periphery of the benzene ring. To know the effect of heterocyclic ring on optical and hole/ electron transport properties, we considered molecules **2a** (**2b**), **3a** (**3b**), **4a** (**4b**) and **5a** (**5b**) along with molecule **1a** (**1b**). In which, the central benzene ring of anthracene (in **1a** and **1b**) is replaced by thiophene (**2**), furan (**3**), pyrrole (**4**) and pyridine (**5**) (scheme 5A.1).

## 5A.2. Computational Methodology

The ground state optimization of all the molecules has been performed using density functional theory (DFT) and time dependent DFT method with B3LYP functional. These optimized structures are without imaginary frequencies and hence are characterized as minima on the potential energy surface. With optimized ground state geometry, absorption spectra of all the

molecules are calculated using TD-DFT method. All the DFT calculations are performed with 6-311+ G (d, p) basis set by using the Gaussian 16 abinitio software (Frisch et al.) [32].

The calculation of hole ( $\lambda_h$ ) and electron ( $\lambda_e$ ) reorganization energies are done by using *equation 1.14* and *1.15* respectively (in chapter 1). Also the calculation of charge injection parameters i.e ionization potential (IP) and electron affinity (EA) are done by using formulae shown in *equations 1.17* and *1.18* respectively. Further hole and electron extraction potentials i.e. HEP and EEP are calculated by formulae shown in *equations 1.19* and *1.20* respectively.



Scheme 5A.1. Structure of ATT- based molecules consider for study

---

### 5A.3. Results and Discussions

#### 5A.3.1. Optical properties

The experimentally reported absorption maxima for compound **1a** (with the substituted hexyl group at thiophene ring) is 431 nm with very low intensity but the intense peak was reported at 336 nm [29]. A similar result was also reported by Perepichka, for compound **1a** and **1b** with the maxima absorption band at 418 nm and 379 nm respectively [16]. When we compare the absorption energies of the molecules **1a** and **1b**, later one is showing around 40 nm blue shifted absorption due to change in the position of sulphur atom at the periphery of the benzene ring. Experimentally determined electronic excitations for molecule **2a** were reported at 364, 357 and 314 nm. **2a** is showing around 50 nm blue shifted absorption than **1a** due to the replacement of central benzene ring (**1a**) of anthracene with thiophene (**2a**).

Further, to have a better understanding of absorption spectra in these molecules, the lowest electronic excitations of all the molecules have been calculated using TD-DFT methodology at B3LYP/6-311+ G (d, p) level. The calculated lowest three electronic excitations, oscillator strength and corresponding major orbital transitions are summarized in table 5A.1. All the calculations are performed in gas phase and solvent phase (hexane, tetrahydrofuran, dichloromethane and chloroform). Since recent studies on the optoelectronic properties of thieno[3,4-]pyrazine analogues benzosiloles show that, effect of solvent medium on absorption maxima is within 10 nm and also the orbital transitions corresponding to dominant absorption bands are similar in all medium. [33-34] A similar trend is observed with TDDFT calculations, showing there is hardly any effect of solvent on absorption energies, so our further discussion is based on gas phase calculations only (calculated absorption energies in various solvents are shown in table 5A.2)

From TDDFT calculations, the lowest electronic excitation for molecule **1a** is at 414 nm with low oscillator strength (0.004, shown in table 5A.1). The major transition for this excitation is from HOMO to LUMO. A second excitation is at 400 nm with 0.07 oscillator strength having transition from HOMO-1 to LUMO. Third excitation was also observed as intense peak at 328 nm which arises due to HOMO to LUMO+1 transition (shown in figure 5A.1). For molecule **1b**, calculated absorption energies are at 400 nm and 355 nm with oscillator strength 0.107 and 0.129 respectively. Absorption at 400 nm is due to excitation from HOMO to LUMO and 355



nm is due to HOMO-1 to LUMO. Similarly, calculated absorption energies for molecule **2a** are at 364, 357 and 314 nm. Absorption maxima at 364 nm excitation is due to transition between HOMO to LUMO, other weaker transitions 357 and 314 nm are arising from HOMO-1 to LUMO and HOMO-2 to LUMO respectively (shown in figure 5A.1). A blue shift (~50 nm) was observed in molecule **2a** when compared with **1a**; due to changes in the central benzene ring of anthracene (central benzene ring of anthracene was replaced by thiophene in **1a**). These calculated absorption energies for **1a**, **1b** and **2a** are in good agreement with the experimental values. Further, we extended this study for other molecules **3a-5a** and **2b-5b**. When we change the position of sulphur atom (at the periphery, **2b**) in **2a**, shows 14 nm blue shifted absorption (i. e., molecule **2b**) and its two excitation energies are almost degenerate and are showing absorption peaks at 352 and 350 nm, the major transitions are from HOMO-1 to LUMO and HOMO to LUMO respectively (lowest three electronic excitation with their molecular orbital pictures for molecule **1b** and **2b** are shown in figure 5A.2). In case of molecules **3a** and **3b**, the central benzene ring of anthracene (in molecule **1**) is replaced by five membered furan ring. These two molecules are shown approximately same absorption maxima at ~354 nm and the major transitions are from HOMO to LUMO (shown in figure 5A.3). A similar trend was observed for **4a** and **4b** (shown in figure 5A.4, in these molecules central benzene ring of molecule **1** is replaced by pyrrole ring). The lowest electronic excitations for these two isomers are also degenerate and showing absorption at 358 nm. Thus there is no effect of change in position of sulphur atom (at periphery) on absorption maxima in case of molecule **3a** & **3b** and **4a** & **4b**. In case of **5a** and **5b**, when a central benzene ring of anthracene in ATT is replaced by six membered pyridine ring, the absorption maxima has almost same as that of molecule **1a** but it is with intense absorption peak. The absorption maxima for molecule **5a** and **5b** are at 419 nm and 408 nm respectively shown in table 5A.1. Isomer **5b** show 10 nm blue shifted absorption compared to **5a** due to change in position of sulphur atom at the periphery. In both the isomers major transitions take place from HOMO to LUMO levels. Beside this **5a** and **5b** both are also showing absorption bands at 413 nm and 363 nm respectively due to transitions from HOMO-1 to LUMO with considerable oscillator strength (lowest three electronic excitations with molecular orbital pictures of **5a** and **5b** are shown in figure 5A.5). It is clear from the table 5A.1, by changing central benzene ring of anthracene in ATT with 5-membered heterocyclic ring shows blue shifted absorption (approx. 40nm) while

with 6-membered ring shows not much effect on absorption properties. Normalized absorption spectra for isomer 'a' and 'b' of all molecules are shown in figure 5A.6 and 5A.7 respectively.

Table 5A.1: Computed lowest three electronic excitations ( $\lambda_{\max}$  in nm), experimental absorption ( $\lambda_{\max}^{\text{Exp}}$  in nm), Oscillator strength ( $f$ ), Major Transitions (MT) and % weight (%  $C_i$ ) at TD-B3LYP/6-311+G (d, p) method.

Molecules	$\lambda_{\max}^{\text{Exp}}$	$\lambda_{\max}$	$f$	MT	% $C_i$
1a	431 <sup>a</sup> , 418 <sup>b</sup>	414	0.004	H→L	96
		400	0.070	H-1→L	76
	336 <sup>a</sup>	328	1.202	H→L+1	75
1b	379 <sup>b</sup>	400	0.107	H→L	97
		355	0.129	H-1→L	74
		311	0.005	H→L+3	77
2a	377 <sup>c</sup> , 356 <sup>c</sup> , 305 <sup>c</sup>	364	0.346	H→L	96
		357	0.031	H-1→L	81
		314	0.005	H-2→L	69
2b		352	0.033	H-1→L	80
		350	0.234	H→L	94
		321	0.030	H-1→L+1	43
3a		354	0.420	H→L	96
		337	0.003	H-1→L	65
		308	0.004	H→L+2	61
3b		353	0.338	H→L	96
		338	0.021	H-1→L	61
		314	0.233	H→L+1	59
4a		358	0.352	H→L	94
		355	0.016	H-1→L	82
		306	0.292	H→L+1	79
4b		359	0.261	H→L	95
		358	0.046	H-1→L	84
		326	0.144	H→L+1	81
5a		419	0.006	H→L	96
		413	0.209	H-1→L	88
		318	0.001	H-3→L	69
5b		408	0.090	H→L	97
		363	0.233	H-1→L	84
		361	0.056	H-2→L	92

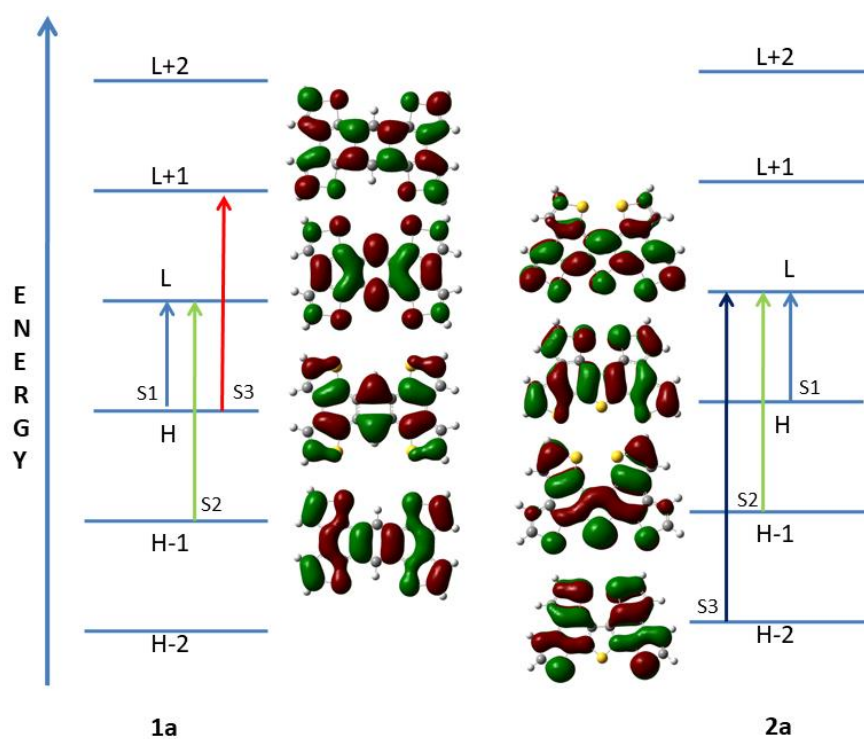
<sup>a</sup> *Org. Lett.* **2007**, 9, 4187

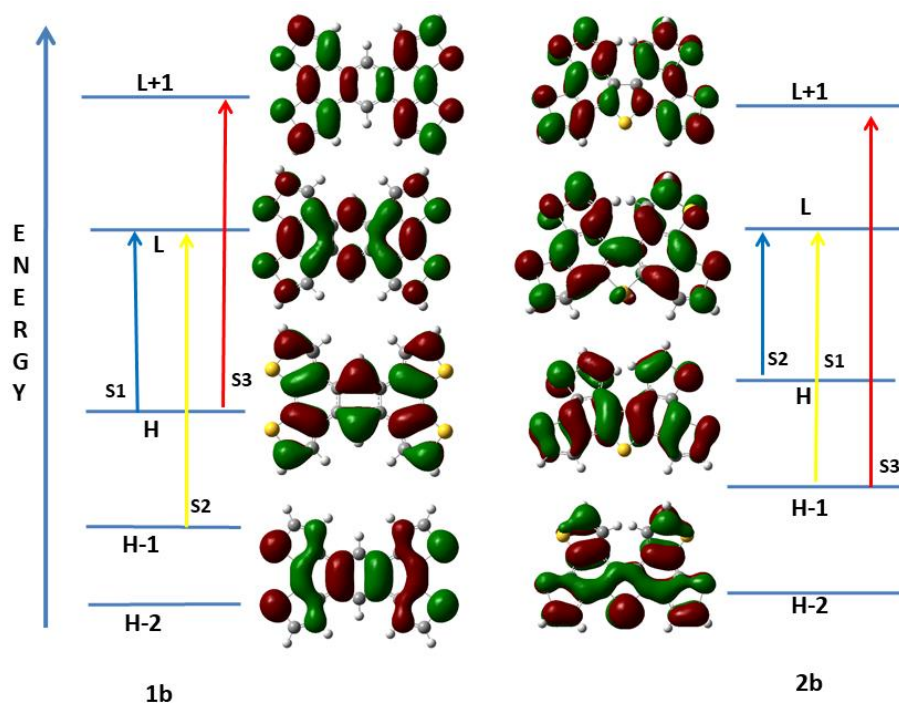
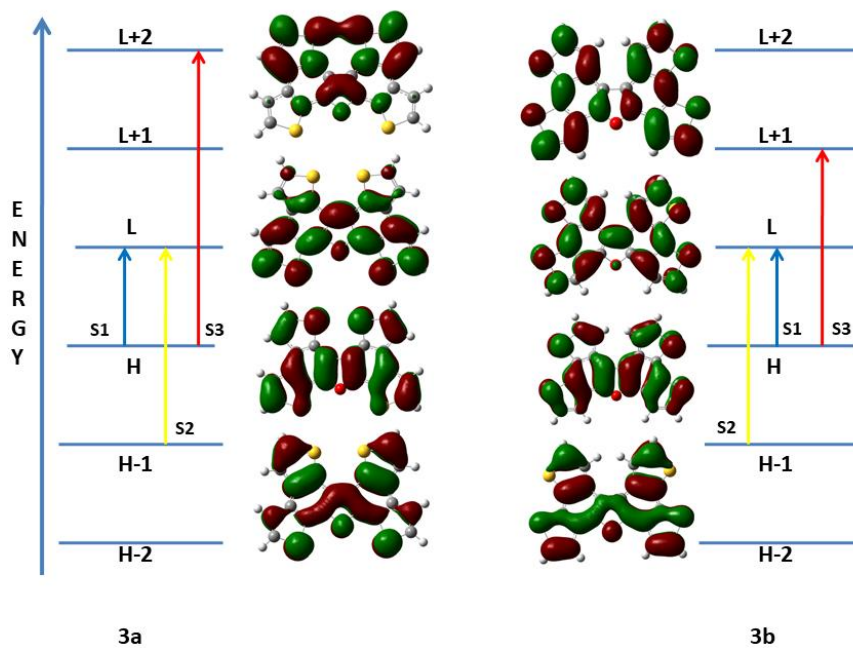
<sup>b</sup> *Chem. Mater.* **2008**, 20, 2484

<sup>c</sup> *Tetrahedron Lett.* **2012**, 68, 1192

Table 5A.2. Absorption maxima ( $\lambda_{\max}$  in nm) in different solvents calculated at TD-B3LYP-PCM/6-311+ G (d, p) method

Molecule	Gas phase	Hexane	THF	DCM	Chloroform
1a	414	417	417	417	417
1b	400	404	404	404	405
2a	364	369	370	370	370
2b	352	353	352	352	353
3a	354	361	361	362	362
3b	353	356	355	356	356
4a	358	362	361	361	362
4b	359	369	371	371	370
5a	419	421	422	422	422
5b	408	412	413	413	413

Figure 5A.1: Electronic transitions with their molecular orbitals for molecule **1a** and **2a**

Figure 5A.2: Electronic transitions with their molecular orbitals for molecule **1b** and **2b**Figure 5A.3: Electronic transitions with their molecular orbitals for molecule **3a** and **3b**

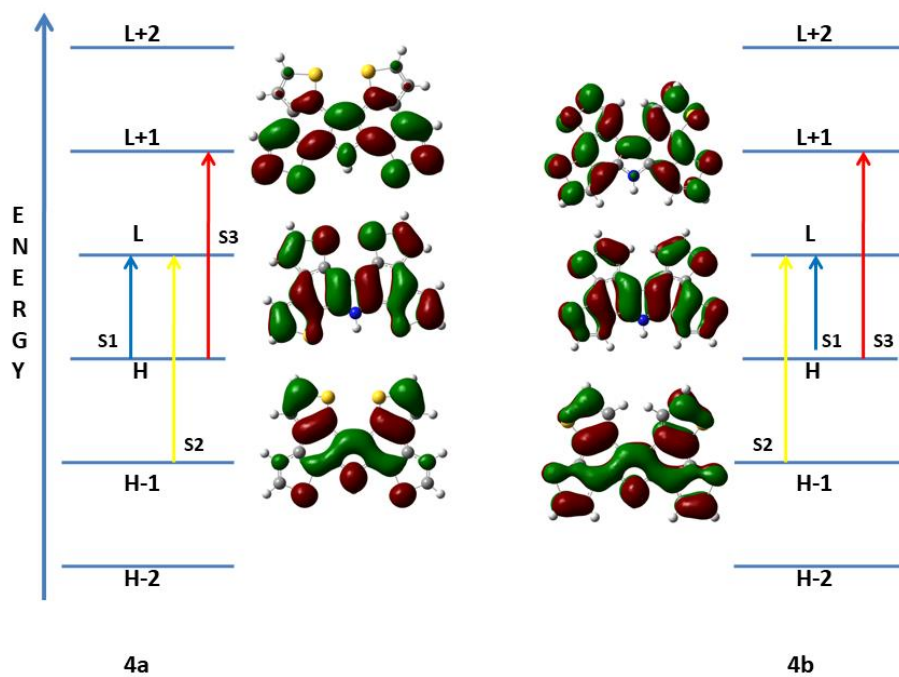


Figure 5A.4: Electronic transitions with their molecular orbitals for molecule **4a** and **4b**

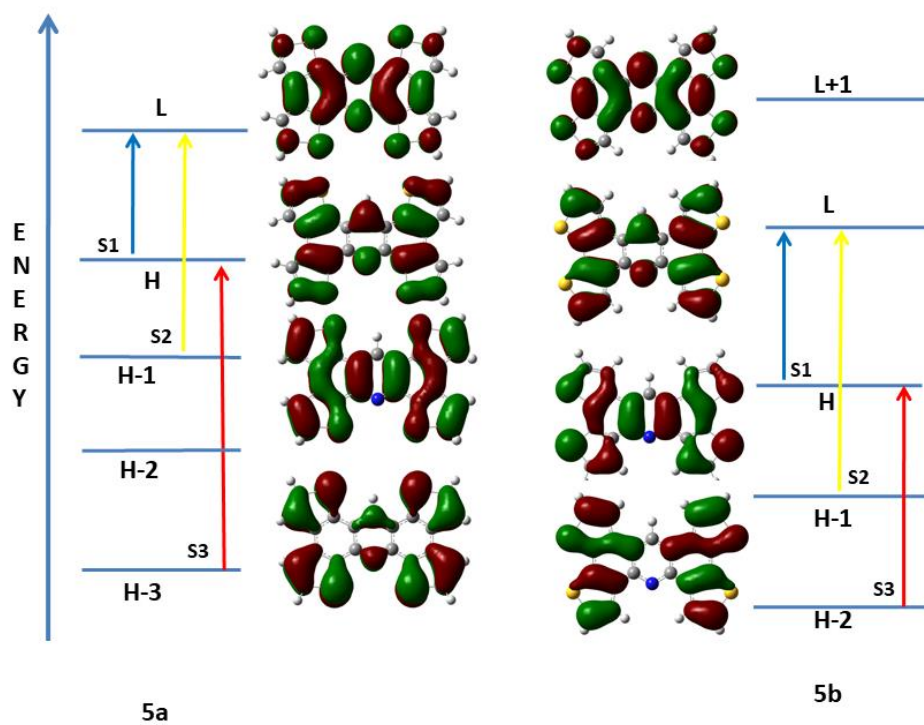


Figure 5A.5: Electronic transitions with their molecular orbitals for molecule **5a** and **5b**

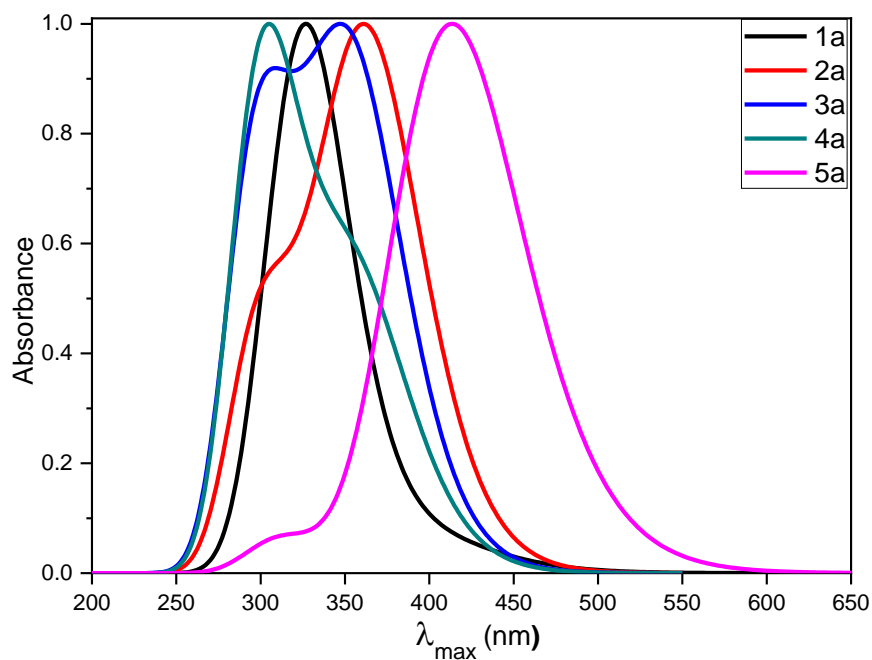


Figure 5A.6: Normalized Absorption spectra of isomer 'a' (1a-5a).

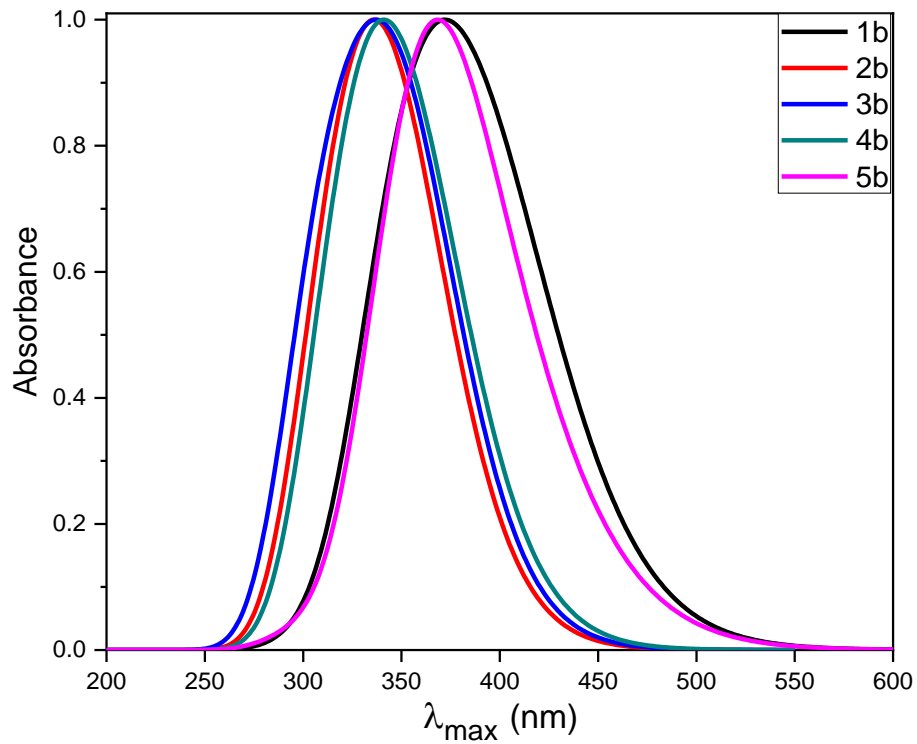


Figure 5A.7: Normalized Absorption spectra of isomer 'b' (1b-5b).

### 5A.3.2. Frontier Molecular Orbitals (FMOs)

The HOMO and LUMO energies of molecule **1a** is -5.60 eV and -2.16 eV respectively, and corresponding HOMO-LUMO gap is 3.44 eV (table 5A.3). On changing central benzene ring with thiophene ring, i.e. molecule **2a**, there is no change in HOMO level (-5.62 eV) but LUMO was (-1.83 eV) destabilized by 0.25 eV as compared to **1a**. Similar is the case for molecule **3a** and **4a**, in these molecules (**3a** and **4a**) LUMO energies are destabilized around 0.40 eV. While, in the case of **5a**, both HOMO and LUMO levels get stabilized around 0.25eV (HOMO and LUMO energies are -5.86 eV and -2.40 eV respectively) (shown in figure 5A.8). When we change the position of sulphur atom at the periphery, (i.e. isomer 'b') HOMO energies of **2b**, **3b** and **4b** (in these, central benzene ring of anthracene in ATT is replaced by five-membered heterocycles) are getting stabilized by ~0.15 eV to their corresponding isomers **a**(shown in figure 5A.9). While in case of **1b** and **5b** (central ring of ATT is with six membered ring) HOMO energies are destabilized by 0.10 eV as compared to their **a**-isomers. In case of **b**-isomers, there is small increase in HOMO-LUMO gap was observed when compared with their corresponding **a**-isomers. HOMO, LUMO and HOMO-LUMO gap energies are tabulated in table 5A.3.

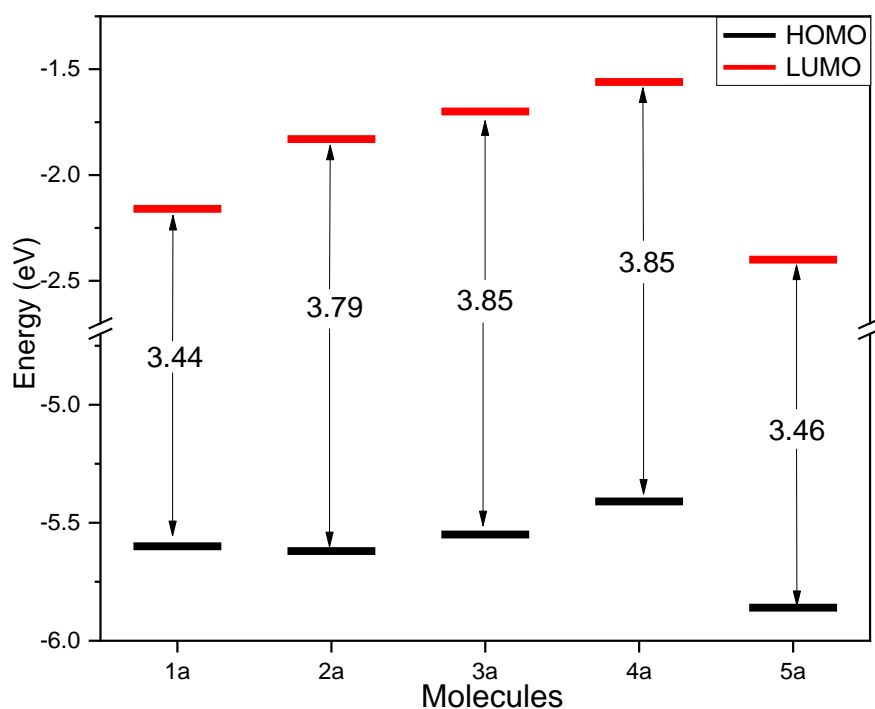


Figure 5A.8: HOMO, LUMO energy levels and HOMO-LUMO energy gap for 'a' isomers

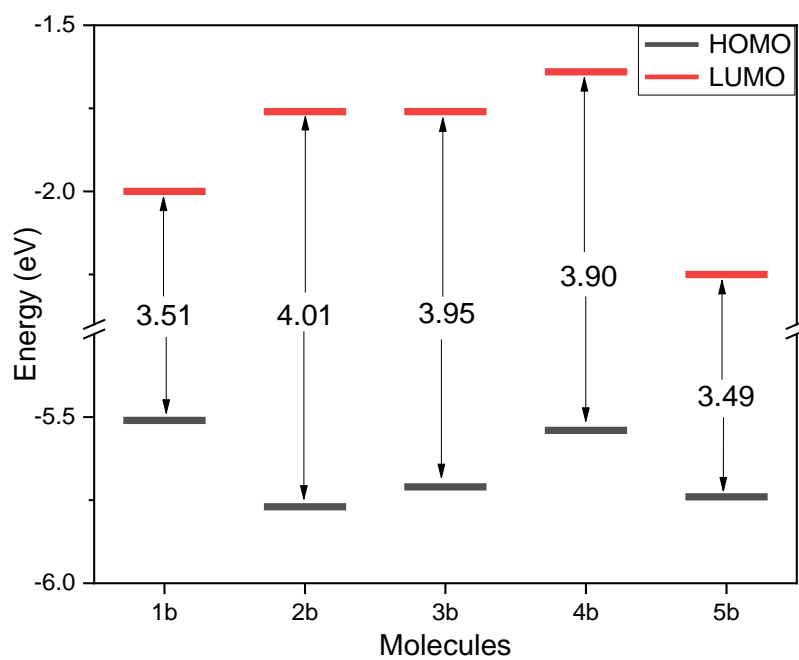


Figure 5A.9: HOMO, LUMO energy levels and HOMO-LUMO energy gap for 'b' isomers

Table 5A.3. Calculated energies of HOMO, LUMO and HOMO-LUMO gap (in eV) for all the molecules.

Molecule	HOMO	LUMO	H-L gap
1a	-5.60	-2.16	3.44
1b	-5.51	-2.00	3.51
2a	-5.62	-1.83	3.79
2b	-5.77	-1.76	4.01
3a	-5.55	-1.70	3.85
3b	-5.71	-1.76	3.95
4a	-5.41	-1.56	3.85
4b	-5.54	-1.64	3.90
5a	-5.86	-2.40	3.46
5b	-5.74	-2.25	3.49



### 5A.3.3. Ionization Potential (IP), Electron Affinity (EA), HEP and EEP

For better performances of optoelectronic devices, there should be efficient injecting of hole and electron into an organic molecule. Molecular ionization potential (IP) and Electron affinity (EA) are important factors for charge injection. IP is defined as the energy needed by the system when an electron is removed, IP must be low enough for an efficient hole injection into HOMO of the molecule. Electron affinity (EA) is defined as the energy releases when an electron is added to the system. EA must be enough high to allow an efficient electron injection into LUMO of the molecule. Thus we calculated IP, EA, HEP (hole extraction potential) and EEP (electron extraction potential) according to the above given formulae for all the molecules and are tabulated in table 5A.4. As seen from the table 5A.4, molecule **4a (4b)** has lowest ionization potentials 6.67 eV (6.80 eV) and 6.59 eV (6.67 eV) for vertical and adiabatic excitations respectively, resulting it is easy to create holes in these molecules compare to others. Along with observed ionization potentials for molecule **4a (4b)**, it also shows minimum hole extraction potentials (HEP) 6.50 eV (6.61 eV) among all studied molecules. This indicates, injection of the hole is easier in case molecules **4a (4b)**. Electron affinity (EA) is highest for **5a (5b)** molecule and its vertical and adiabatic values are 1.17 eV (1.02 eV) and 1.25 eV (1.12 eV) respectively, suggesting that there is an efficient electron injection in the HOMO level of this molecule as compared to others. Further the energy required to extract electron (EEP) for molecule **5a (5b)** is 1.32 eV and 1.21 eV respectively (table 5A.4). Among all studied molecules, EEP is maximum for molecule **5a (5b)** and next highest EEP is for molecule **1a (1b)**, shown in table **5A.4**. From these results one can predict that by changing the central ring of anthracene in ATT molecule or by changing position of sulphur atom in thiophene at the periphery of ATT molecule, a significant change in the electron accepting, donating and transporting properties.

Table 5A.4: Calculated Ionization Potentials (IP in eV), Electron Affinities (EA in eV), Hole Extraction potentials (HEP in eV), Electron Extraction potentials (EEP in eV) and reorganization energies ( $\lambda_h$  and  $\lambda_e$  in meV) at B3LYP/6311+ G (d, p) level of theory.

Molecule	IP <sub>v</sub>	IP <sub>a</sub>	EA <sub>v</sub>	EA <sub>a</sub>	HEP	EEP	$\lambda_h$	$\lambda_e$
1a	6.83	6.77	0.94	1.01	6.70	1.08	124	134
1b	6.73	6.66	0.80	0.89	6.60	0.98	132	175
2a	6.87	6.77	0.61	0.73	6.65	0.84	217	238
2b	7.09	6.92	0.56	0.65	6.81	0.74	279	177
3a	6.82	6.72	0.45	0.57	6.63	0.69	183	234
3b	6.99	6.89	0.56	0.64	6.79	0.72	197	164
4a	6.67	6.59	0.33	0.44	6.50	0.57	173	239
4b	6.80	6.71	0.44	0.52	6.61	0.60	197	159
5a	7.09	7.02	1.17	1.25	6.95	1.32	134	149
5b	6.96	7.34	1.02	1.12	7.28	1.21	318	181

#### 5A.3.4. Reorganization energy ( $\lambda$ )

For efficient charge transfer in a molecule, the reorganization energy must be small. The calculated reorganization energies for all the molecules are summarized in table 5A.4. The reorganization energies calculated for hole  $\lambda_h$  for all molecules (except **5b**) are smaller than that of N,N'-diphenyl- N,N'-bis(3-methylphenyl)-(1,1'-biphenyl)-4,4'-diamine (TPD) which is typical hole transport material  $\lambda_h=290$  meV [35]. Thus the hole transfer rates for all the studied molecule are higher than that of TPD. Also the reorganization energies calculated for electron  $\lambda_e$  for all the molecules are smaller than tris(8-hydroxyquinolino)aluminum(III) (Alq3) which is considered as typical electron transport material  $\lambda_e= 276$  meV [36-37]. Within two isomers (**a** and **b**), in all the cases 'a' isomer is having lower  $\lambda_h$  value than corresponding  $\lambda_e$  values, suggesting carrier mobility of the hole is larger than that of electron in these molecules (table **5A.4**). The graphical representation of hole and electron reorganization energies for 'a' isomers are shown in figure 5A.10. While the reverse is true for **b**-isomers (except **1b**),

molecules **2b**, **3b**, **4b** and **5b** are having  $\lambda_e$  values are smaller than those of  $\lambda_h$  value, suggesting carrier mobility of electron is larger than that of hole in these molecules. The graphical representation of hole and electron reorganization energies for 'b' isomers are shown in figure 5A.11. Hence, due to smaller reorganization energies, these can be used as electron transport materials in OLEDs. In addition to this, difference between  $\lambda_h$  and  $\lambda_e$  in most of the molecules are in the range of 15-50 meV, implying these isomers has better equilibrium properties of hole and electron transport properties and may be useful candidates as ambipolar charge transport materials.

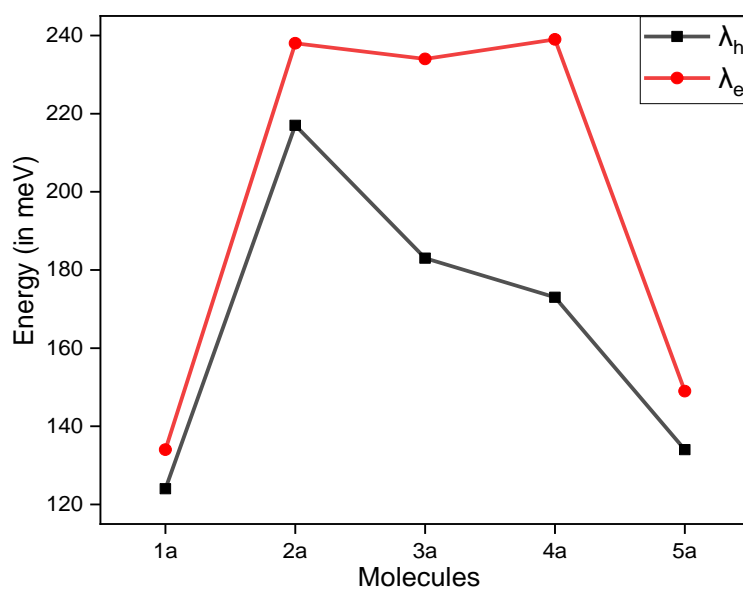


Figure 5A.10: Graphical representations of hole and electron reorganization energies of 'a' isomers

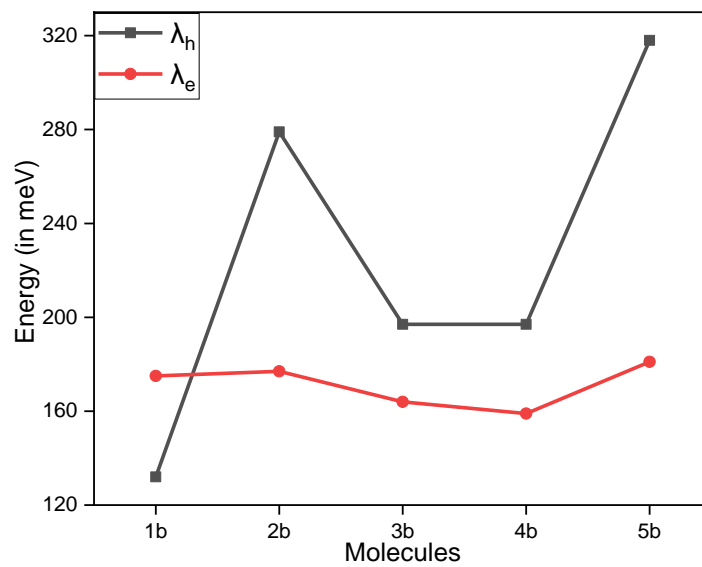


Figure 5A.11: Graphical representations of hole and electron reorganization energies of ‘b’ isomers

---

#### 5A.4. Conclusion

In this chapter we have performed DFT and TDDFT calculations on ATT based molecules. All the molecules have been optimized at B3LYP/6-311+G (d, p) level of theories and the calculated absorption energies are in good agreement with the experimental results. With change in the position of sulphur atom and by introducing a different heterocyclic ring system in place of the central benzene ring of anthracene in ATT molecule shows variation in optical properties and reorganization energies. As we replace the central benzene ring of anthracene in ATT, with different 5-membered heterocycles, there is almost 50 nm blue shift was observed in each case while with 6-membered heterocycles no considerable effect was observed. These ATT molecules can be used as electron transport material in OLEDs due to smaller reorganization energies. It is also shown that, there is an improvement in charge transfer properties in these molecules with slight modification in ATT (the change in the central benzene ring of anthracene with different heterocycles). By changing the position of sulphur atom (at the periphery), increases the HOMO-LUMO gap. Further, hole reorganization energies of all the 'a' isomers (sulphur facing inward) are smaller than corresponding 'b' isomer (sulphur exposing outside) suggesting these are better for hole transport materials. This study will be helpful for future design and preparation of high-performance charge transport materials.

---

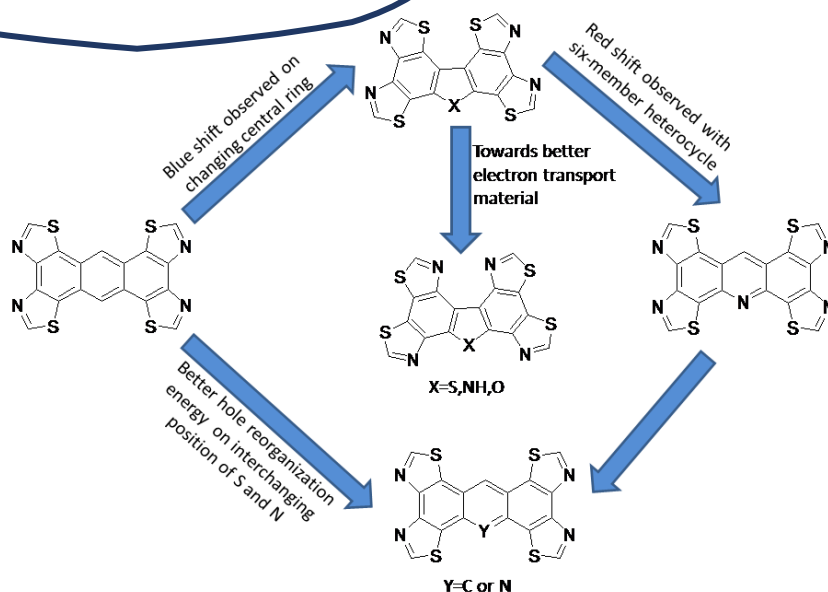
**References**

1. F. He, W. Wang, W. Chen, S. B. Darling, J. Strzalka, Y. Liu, L. Yu, *J. Am. Chem. Soc.* **2011**, 133 3284.
2. A. Irfan, A.G. Al-Sehemi, S. Muhammad, *Synt. Met.* **2014**, 190, 27.
3. Y. Lin, Y. Li, X. Zhan, *Chem. Rev.* **2012**, 41, 4245.
4. Y. A. Duan, Y. Geng, H. B. Li, J. L. Jin, Y. Wu, Z. M Su, *J. Comp. Chem.* **2013**, 34, 1611.
5. J. Huang, J-H. Su, H. Tian, *J. Mat. Chem.* **2012**, 22, 10977.
6. Y-L. Liu, J-K. Feng, A-M. Ren, *J. Phys. Org. Chem.* **2007**, 20, 600.
7. H. Meng, F. Sun, M. B. Goldfinger, G. D. Jaycox, Z. Li, W. J. Marshall, G. S. Blackman, *J. Am. Chem. Soc.* **2005**, 127, 2406.
8. K. Takimiya, H. Ebata, K. Sakamoto, T. Izawa, T. Otsubo, Y. Kunugi, *J. Am. Chem. Soc.* **2006**, 128, 12604.
9. T. Yamamoto, K. Takimiya, *J. Am. Chem. Soc.* **2007**, 129, 2224.
10. S. R. Forrest, *Nature* **2004**, 428, 911.
11. M. M. Torrent, C. Rovira, *Chem. Rev.* **2011**, 111, 4833.
12. J. S. Yang, H. H. Huang, J. H. Ho, *J. Phys. Chem. B*, **2008**, 112, 8871.
13. J. S. Yang, H. H. Huang, Y. H. Liu, S. M. Reng, *Org. Lett.* **2009**, 11,4942.
14. H. H. Huang, Ch. Prabhakar, K. C. Tang, P. T. Chou, G. J. Huang, J. S. Yang, *J. Am. Chem. Soc.* **2011**, 133, 8028.
15. J. E. Anthony, *Chem. Rev.* **2006**, 106, 5028.
16. J. L. Brusso, O. D. Hirst, A. Dadvand, S. Ganeshan, F. Cicoira, C. M. Robertson, R. T. Oakley, F. Rosei, D. F. Perepichka, *Chem. Mater.* **2008**, 20, 2484.
17. M. M. Payne, S. R. Parkin, J. E. Anthony, *J. Am. Chem. Soc.* **2005**, 127, 8026.
18. R. Mondal, R. M. Adhikari, B. K. Shah, D. C. Neckers, *Org. Lett.* **2007**, 9, 2505.
19. B. Purushothaman, S. R. Parkin, J. E. Anthony, *Org. Lett.* **2010**, 12, 2060.
20. K. Niimi, S. Shinamura, I. Osaka, E. Miyazaki, K. Takimiya, *J. Am. Chem. Soc.* **2011**, 133, 8732.
21. K. Takimiya, T. Yamamoto, H. Ebata, T. Izawa, *Sci. Technol. Adv. Mater.* **2007**, 8, 273.
22. P. K. De, D. C. Neckers, *Org. Lett.* **2012**, 14, 74.

- 
23. K. Xiao, Y. Lui, T. Qi, F. Wang, J. Gao, W. Qiu, Y. Ma, G. Cui, S. Chen, X. Zhan, G. Yu, J. Qin, W. Hu, D. Zhu, *J. Am. Chem. Soc.* **2005**, 127, 13281.
  24. T. Lei, J. Pei, *J. Mater. Chem.* **2012**, 22, 785.
  25. X. D. Tang, Y. Liao, H. Geng, Z-G. Shuai, *J. Mater. Chem.* **2012**, 22, 18181.
  26. T. Vehoff, B. Baumeier, A. Troisi, D. Andrienko, *J. Am. Chem. Soc.* **2010**, 132, 11702.
  27. X. Yang, L. Wang, C. Wang, W. Long, Z. Shuai, *Chem. Mater.* **2008**, 20, 3205.
  28. M. X. Zhang, G. J. Zhao, *J. Phys. Chem. C.* **2012**, 116, 19197.
  29. W. J. Liu, Y. Zhou, Y. Ma, Y. Cao, J. Wang, J. Pei, *Org. Lett.* **2007**, 9, 4187.
  30. J. Wang, H. Xu, B. Li, X. P. Cao, H. L. Zhang, *Tetrahedron Lett.* **2012**, 68, 1192.
  31. Y. A. Duan, H. B. Li, Y. Geng, Y. Wu, G. Y. Wang, Z. M. Su, *Org. Electron.* **2014**, 15, 602.
  32. M. J. Frisch, Gaussian 16, Revision E.01; Gaussian, Inc.: Wallingford CT, **2016**.
  33. G. Saranya, P. Kolandaivel, K. Senthilkumar, *Mol. Phys.* **2013**, 111, 3036.
  34. R.V. Solomon, A. P. Bella, S. A. Vedha, P. Venuvanalingam, *Phys. Chem. Chem. Phys.* **2012**, 14, 14229.
  35. N. E. Gruhn, D. A. da Silva Filho, T. G. Bill, M. Malagoli, V. Coropceanu, A. Kahn, J. L. Bredas, *J. Am. Chem. Soc.* **2002**, 124, 7918.
  36. B. C. Lin, C. P. Cheng, Z. Q. You, C. P. Hsu, *J. Am. Chem. Soc.* **2005**, 127, 66.
  37. A. Irfan, R. Cui, J. Zhang, *J. Mol. Struct. Theochem*, **2010**, 956,61.

# Chapter 5B

*Impact of replacement of central benzene ring in Anthracene by Heterocyclic ring on Electronic excitations and Reorganization energies in Anthratetrathiazole (ATTz)*



*Results of this chapter published in J. Sulfur Chem. 2019, 40, 361*







---

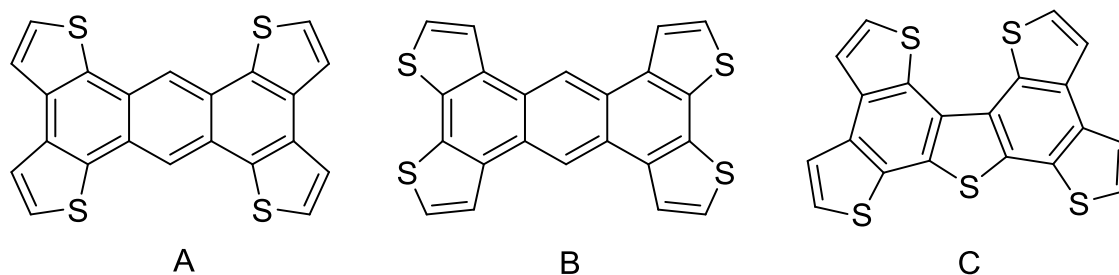
---

### 5B.1. Introduction

In the past two decades, researchers have found innumerable applications of organic compounds in the field of materials chemistry. These organic compounds are utilized in many semiconducting devices such as organic solar cells [1-2], organic field effect transistors (OFETs) [3-5], organic light emitting diodes (OLEDs) [6-7], organic photovoltaic cells (OPVs) [8-9], etc. The main advantage of organic materials is the economy and ease of manufacture making them a desirable replacement for inorganic semiconductor materials [10-11]. It has been shown that organic semiconductors containing  $\pi$ -conjugated oligomers or polycyclic aromatic hydrocarbons can be designed and manufactured to tune required optical and electronic properties [12-14]. Fused conjugated oligomers, in particular, have been found to be fascinating organic materials that have been used in a variety of semiconducting materials. These include linear acenes and oligothiophenes, which are the two a large number of studied classes of organic semiconducting materials [15-16]. To a large extent, charge carrier mobility depends upon conjugation in a molecule; the greater the conjugation implies a higher charge carrier mobility in the molecule. The hole mobility ( $\mu_h$ ) of tetracene and pentacene (0.12 and  $3.0 \text{ cm}^2\text{V}^{-1}\text{s}^{-1}$  respectively) are one of the best examples reported in the literature [17]. In the case of anthracene, no such recognizable hole mobility has been observed.

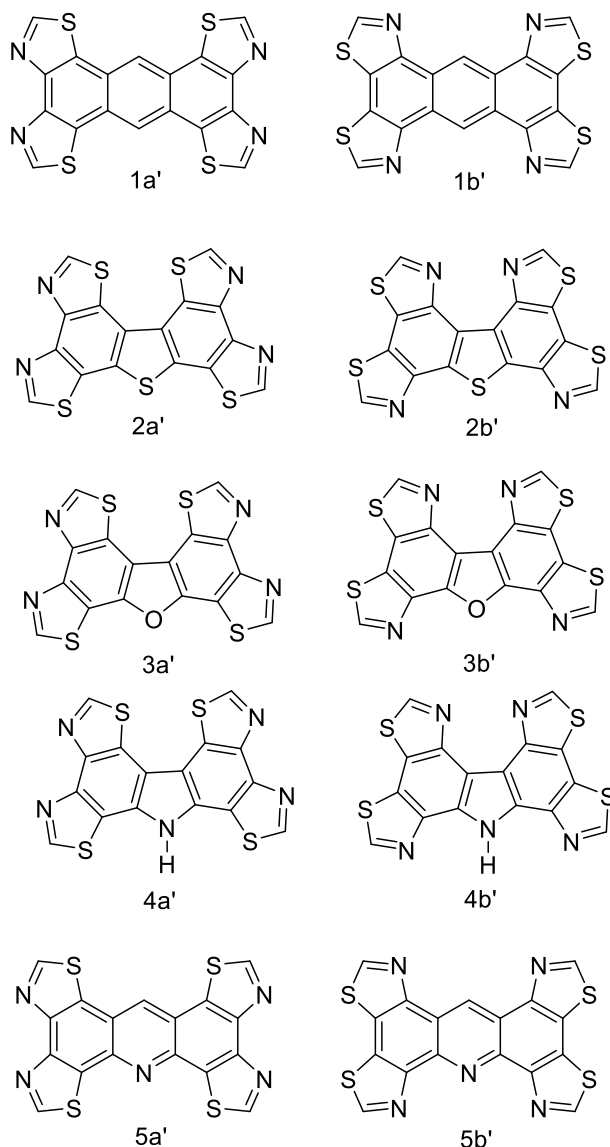
Currently, pentacene is considered as the best active *p*-type materials with high hole mobility [15]. Also, in fused thiophene oligomers there is more effective conjugation and higher stability compared to linearly linked acenes [18]. Further, the increase in conjugation in thienothiophenes results in the decrease in the stability of molecules because of significantly raised highest occupied molecular orbital (HOMO) in these molecules [18]. Due to several molecular interactions (inter or intra), such as Van der Waal interactions, hydrogen bonding and  $\pi$ - $\pi$  stacking makes the oligomer is suitable for an organic semiconductor. Further, presence of sulphur-sulphur (S...S) interactions strongly affect the solid state packing of species concerned and plays a vital role in attaining high carrier mobility and also determines the transport network [19-23]. In order to make anthracene molecule suitable for organic materials, anthratetrathiophene (ATT) molecule has been synthesized by Liu et.al. The reaction performed encompassed with the Negishi-coupling followed by oxidative cyclization (structure **A** in scheme 5B.1) [24]. Four thiophene rings present at the perimeter of three fused

benzene rings (anthracene) gave stability to the molecule and efficient  $\pi$ - $\pi$  interactions. Further, molecule **A** has an affinity to self-associate through  $\pi$ - $\pi$  stacking which in turn gives stability and high hole mobility ( $0.012\text{cm}^2\text{V}^{-1}\text{s}^{-1}$ ) to the molecule. Later, Perepichka group [16] identified and synthesized one more isomer of ATT, differing only in the place of the sulphur atom at the outside edge. In the former case, the sulphur atom is facing inward whereas the latter synthesized by Perepichka group, the sulphur atom is facing outward (structure **B** in scheme 5B.1) [16]. They reported that on altering the position of sulphur atom at the perimeter leads to prominent transformation in electrochemical as well as optical properties of the molecule. The resulting isomer **B** showed an improved thermal stability and better S...S interactions concerning corresponding **A** isomer. Further, Zhang et al. [25] synthesized dibenzothienotetrathiophene (structure **C** in scheme 5B.1), a novel seven-ring-fused system which differs from isomer **A** (or **B**) only by their central structure (the central six-membered anthracene ring of isomer **A** substituted with five-membered thiophene ring as shown in molecule **C**). Also, molecule **C** displays remarkable thermal and photo-stability and shows strong fluorescence in solid-state which makes it applicable in optoelectronics [25]. Taking all these factors into account and also considering the effect of slight alterations in the structure of the organic molecule, a noteworthy enhancement in the electrochemical and optical properties was observed. In chapter 5A.1, we studied the effect of altering the place of sulphur atom on the outside edge of anthracene and substituting heterocyclic rings in the position of central benzene. The results obtained showed that by altering the place of S-atom at the perimeter of anthracene there is a change in charge transport properties. Now, we wish to extend our study further to analyze the effect of other heteroatoms (S and N) on charge transport and optical properties of ATT.



Scheme 5B.1: Structures of Anthratetrathiophene (ATT) molecules (**A** & **B**) and dibenzothienotetrathiophene (**C**)

Here in this chapter, we have considered ten anthratetrathiazole (ATTz) molecules (scheme 5B.2) based on alterations in the position of S and N at the periphery and with substitutions in middle benzene of anthracene with various five or six-membered heterocyclic rings. As depicted in scheme 5B.2, the central moiety in compounds **1a'** and **1b'** is anthracene, and thiazole rings fused with the benzene ring. For other molecules, out of three fused benzene rings the central benzene ring is substituted by thiophene in **2a'**(**2b'**), furan in **3a'**(**3b'**), pyrrole in **4a'**(**4b'**) and pyridine **5a'**(**5b'**).



Scheme 5B.2: Structure of ATTz- based molecules consider for study

---

---

## 5B.2. Methodology

Geometry optimizations of ATTz-based molecules are performed by utilizing density functional theory (DFT) with B3LYP functional. The optimized structures of each molecule are without imaginary frequencies and hence were situated at the lowest position of the potential energy surface. Further, the electronic excitations for the molecules **1a'-5a'** and their isomers **1b'-5b'** were calculated by using TD-DFT method with B3LYP functional. The DFT and TD-DFT calculations were executed using 6-311+ G (d, p) basis set in Gaussian 09W program (Frisch et al.) [26]. We also considered the effect of solvent on all the molecules by using IEFPCM method using the same calculative methods [27].

The calculation of hole ( $\lambda_h$ ) and electron ( $\lambda_e$ ) reorganization energies for molecules **1a'-5a'** and their geometrical isomers i.e. **1b'-5b'** are evaluated using *equation 1.14* and *1.15* respectively (in chapter 1). Also the calculation of charge injection parameters i.e. ionization potential (IP) and electron affinity (EA) are done by using formulae shown in *equations 1.17* and *1.18* respectively. Further hole and electron extraction potentials i.e. HEP and EEP are calculated by formulae shown in *equations 1.19* and *1.20* respectively.

## 5B.3. Results and Discussions

### 5B.3.1. Electronic Excitations

The experimental excitation energies for compound A and B (scheme 5B.1) were observed at 418 nm and 379 nm respectively [16]. There is an almost 40 nm blue shift on changing the place of sulphur atom at the perimeter of benzene. Also, reported absorption maxima for molecule C (scheme 5B.1) are at 364, 357 and 314 nm [25]. For further analysis in these molecules (**A**, **B** and **C**), the lowest electronic excitations computed with various functional [28-30] (B3LYP, CAM-B3LYP, WB97XD, PBE0, M06, and BHandHLYP) and 6-311+G (d, p) basis set derived from B3LYP/6-311+G (d, p) optimized geometries. B3LYP is a hybrid global gradient approximate (GGA) functional with fixed 25% Hartree-Fock (HF) exchange [31-32]. The range separated functional, CAM-B3LYP is with 19% HF exchange and 81% Becke exchange interaction at short range while 65% HF and 35% Becke at the long range [33]. However, there is 100% HF exchange at long range and 19% HF exchange at short range

in WB97XD [34]. PBE0 functional uses 25% exact exchange and 75% DFT exchange [35]. M06 is a hybrid meta GGA functional having 27% HF exchange [36]. BHandHLYP comprises 50% HF exchange derives from Becke half and half exchange with LYP functional [37]. The absorption energies calculated using various functional tabulated in table 5B.1. Three functionals namely B3LYP, M06, and PBE0 exhibited approximately similar  $\lambda_{\max}$  and are comparable with the experimentally obtained absorption energies. Electronic excitations for compounds **A**, **B**, and **C** are also calculated in different solvents (hexane, tetrahydrofuran, chloroform, dichloromethane, methanol, and dimethylsulfoxide) to show that there is no effect of solvents on absorption maxima (shown in table 5B.2). Also, lowest three electronic excitations for molecules A, B and C calculated at B3LYP/6-311+G (d, p) level of theory are tabulated in table 5B.3 Further our discussion for electronic excitations is based on calculations at TD-B3LYP/6-311+G (d, p) level.

Table 5B.1: Calculated absorption energies ( $\lambda_{\max}$  in nm) and oscillator strength ( $f$ ) with different functional for molecules A, B and C.

Molecule (expt. $\lambda_{\max}$ )	B3LYP		CAM-B3LYP		WB97XD		PBE		M06		BHHLYP	
	$\lambda_{\max}$	$f$	$\lambda_{\max}$	$f$	$\lambda_{\max}$	$f$	$\lambda_{\max}$	$f$	$\lambda_{\max}$	$f$	$\lambda_{\max}$	$f$
A (418) <sup>a</sup>	414	0.004	363	0.003	355	0.003	400	0.004	409	0.003	368	0.002
B (379) <sup>b</sup>	400	0.107	351	0.176	344	0.188	386	0.118	395	0.115	356	0.176
C (377) <sup>c</sup>	364	0.346	327	0.377	321	0.375	352	0.363	362	0.322	327	0.379

<sup>a</sup> *Org. Lett.* **2007**, 9, 4187

<sup>b</sup> *Chem. Mater.* **2008**, 20, 2484

<sup>c</sup> *Tetrahedron Lett.* **2012**, 68, 1192

Table 5B.2: Calculated absorption energies ( $\lambda_{\max}$  in nm) in gas phase and different solvents at TD-B3LYP/6311 + G (d, p) method in gas phase.

Molecule	Gas Phase	Hexane	THF	Chloroform	DCM	Methanol	DMSO
A	414	417	417	417	417	417	417
B	400	404	404	405	404	404	405
C	364	369	370	370	370	369	370

Table 5B.3: Calculated Absorption energies ( $\lambda_{\max}$  in nm), Oscillator strength ( $f$ ), Configurations and % weight (%  $C_i$ ) at TD-B3LYP/6-311+G (d, p) method for molecules A, B and C.

Molecule	$\lambda_{\max}^{\text{Experimental}}$	$\lambda_{\max}$	$f$	Configuration	% $C_i$
A	418 <sup>a</sup> ,	414	0.004	H→L	96
		400	0.070	H-1→L	76
	336 <sup>b</sup>	328	1.202	H→L+1	75
B	379 <sup>b</sup>	400	0.107	H→L	97
		355	0.129	H-1→L	74
		311	0.005	H→L+3	77
C	377 <sup>c</sup> , 356 <sup>c</sup> ,	364	0.346	H→L	96
		357	0.031	H-1→L	81
	305 <sup>c</sup>	314	0.005	H-2→L	69

<sup>a</sup> *Org. Lett.* **2007**, 9, 4187

<sup>b</sup> *Chem. Mater.* **2008**, 20, 2484

<sup>c</sup> *Tetrahedron Lett.* **2012**, 68, 1192

The premeditated absorption results obtained at TD-B3LYP/6-311+G (d, p) level demonstrated in table 5B.3. The outcome of these studies points out that, on altering the central ring of anthracene in ATT (molecule **A**) with thiophene (molecule **C**), a blue-shift of 50 nm is observed. Since TD-B3LYP/6-311+G (d, p) level calculations reproduced considerable results for compounds **A**, **B**, and **C**, we further calculated absorption energies for all the other compounds (scheme 5B.2) which are tabulated in table 5B.4 (for **a'** isomers) and table 5B.5 (for **b'** isomers). From TD-DFT calculations, **1a'** is showing absorption at 415 nm with smaller oscillator strength (0.011). This absorption is due to HOMO→LUMO transition. The intense band was observed at 319 nm which is due to HOMO→LUMO+1 transition. On altering the position of sulphur and nitrogen atom at the outside edge in molecule **1a'** (i. e., molecule **1b'**), 10 nm blue shift was observed. The lowest three absorption peaks for molecule **1b'** are at 405 nm, 347 nm and 304 nm due to HOMO→LUMO, HOMO-1→LUMO, and HOMO→LUMO+3 respectively. Molecule **2a'** differs from **1a'** only in the middle ring structure, but the absorption maximum of **2a'** is 50 nm blue-shifted as compared to absorption of **1a'**. Calculated absorption energies of **2a'** are at 351 nm, 343 nm and 308 nm which arises due to transitions between HOMO-1→LUMO, HOMO→LUMO, and HOMO-1→LUMO+1 respectively. In figure 5B.1 major lowest three electronic excitations with molecular orbital pictures for molecule **1a'** and



**2a'**. On interchanging the position of S-atom and N-atom in molecule **2a'**, (i.e., molecule **2b'**) it shows absorption at 356 nm and 343 nm. Major transitions associated with these absorption energies are HOMO→LUMO and HOMO-1→LUMO. In figure 5B.2 major lowest three electronic excitations with molecular orbital pictures for molecule **1b'** and **2b'** are shown.

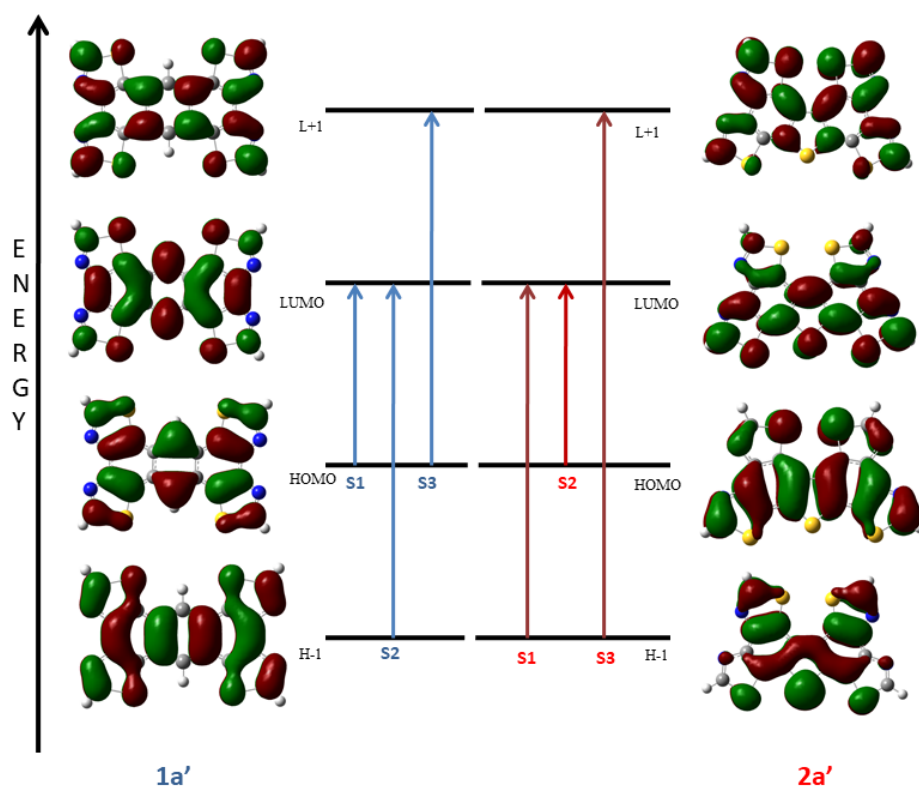


Figure 5B.1: Major electronic excitations with molecular orbital pictures of **1a'** and **2a'**.

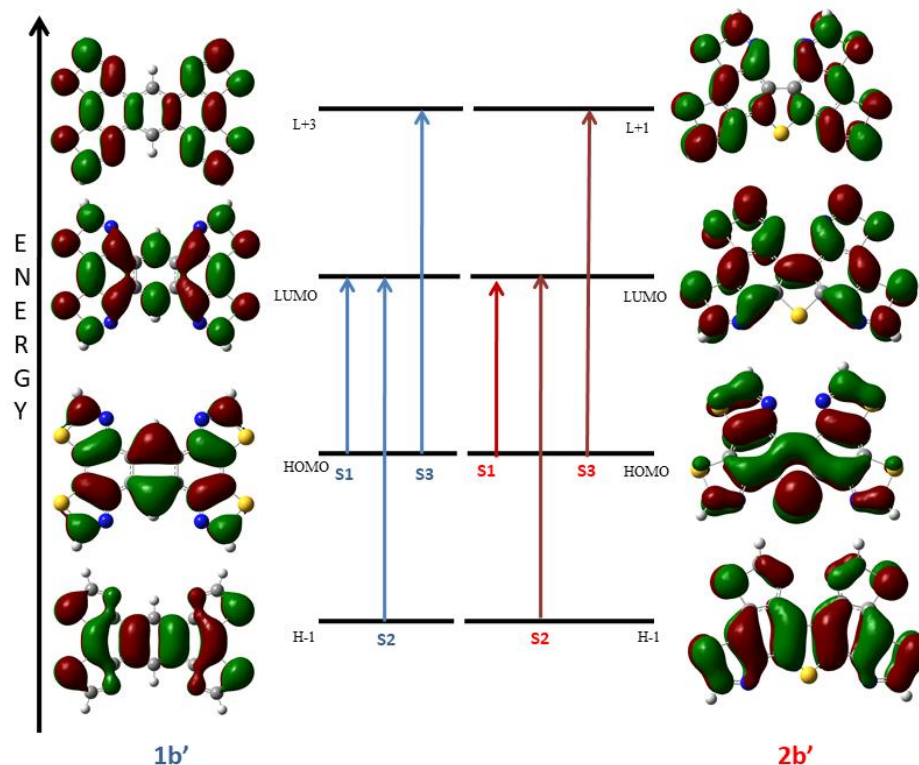


Figure 5B.2: Major electronic excitations with molecular orbital pictures of **1b'** and **2b'**.

Further blue shift of approximately 80 nm was observed when the middle benzene of anthracene replaced by furan (molecule **3a'** and **3b'**). In compound **3a'**, when sulphur atoms at the periphery are protruding inwards, the absorption maxima is observed at 335 nm while in case of **3b'** where sulphur atoms protruding outwards, molecule show 10 nm red shift and its absorption is at 346 nm (major excitations with molecular orbital pictures for **3a'** and **3b'** are shown in figure 5B.3). Similar to the molecule **3a'** and **3b'**; **4a'** is showing absorption at 351 nm while its isomer **4b'** is showing absorption at 362 nm (major excitations with molecular orbital pictures for **4a'** and **4b'** are shown in figure 5B.4). For the molecule **5a'** and **5b'**, middle benzene of anthracene is replaced by heterocyclic ring pyridine which results in the same absorption as that of molecule **1a'**. For molecule **5a'** the absorption maximum was observed at 420 nm, and major excitations are from HOMO  $\rightarrow$  LUMO. When the position of S and N was interchanged at the periphery (i.e., molecule **5b'**), there is almost 30 nm blue shift, and its absorption maximum is at 385 nm wherein the major transition is from HOMO  $\rightarrow$  LUMO (major excitations with molecular orbital pictures for **5a'** and **3b'** are shown in figure 5B.5).

Thus, it is evident as of table 5B.4 and 5B.5 that by varying the middle benzene of fused tetrathiazoles with the five-membered heterocyclic ring, blue shifted absorption (approx ~50 nm) occurs while with the six-membered ring the absorption properties remain unaffected. The interchanging of the position of S and N at periphery shows 10-15 nm blue/red shifted absorption. Premeditated absorption energies for isomer '1a'-5a' and '1b'-5b' shown in figure 5B.6 and 5B.7 respectively. The lowest electronic excitations for the compounds 1a'-5a' and their isomers 1b'-5b' also calculated by using various functionals, and the results are depicted in table 5B.6.

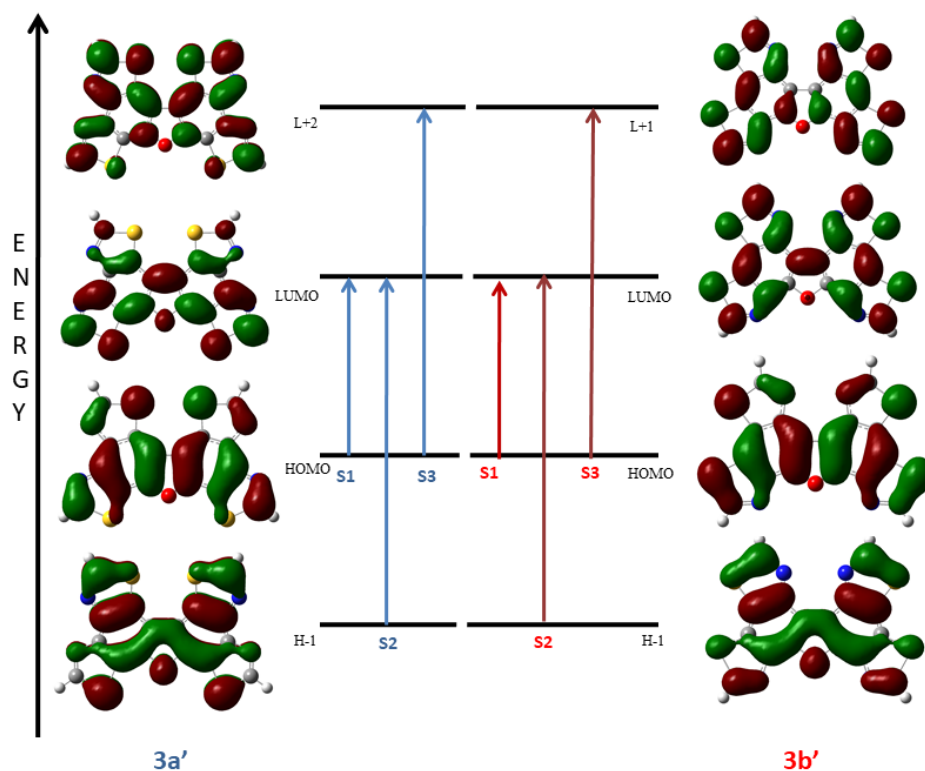


Figure 5B.3: Major electronic excitations with molecular orbital pictures of 3a' and 3b'

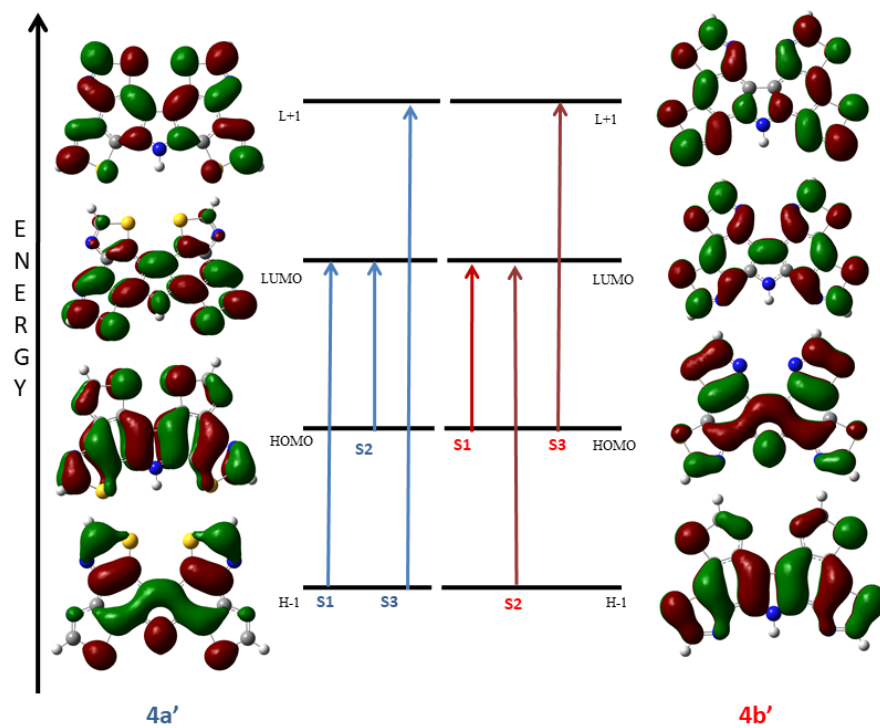
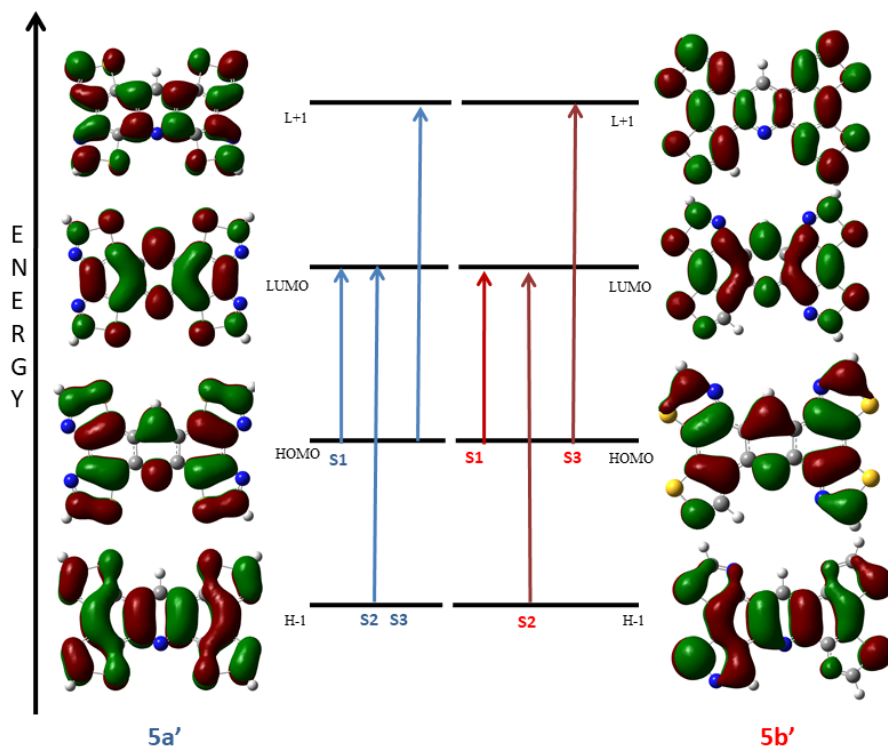
Figure 5B.4: Major electronic excitations with molecular orbital pictures of **4a'** and **4b'**Figure 5B.5: Major electronic excitations with molecular orbital pictures of **5a'** and **5b'**

Table 5B.4: Calculated Absorption energies ( $\lambda_{\max}$  in nm), Oscillator strength ( $f$ ), Configurations and % weight (%  $C_i$ ) at TD-B3LYP/6-311+G (d, p) method for molecules 1a' to 5a'

Molecule	State	$\lambda_{\max}$	$f$	configuration	% $C_i$
1a'	S1	415	0.011	H→L	97
	S2	380	0.001	H-1→L	51
				H→L+1	47
S3	319	1.290	H→L+1	51	
2a'	S1	351	0.041	H-1→L	85
	S2	343	0.336	H→L	94
	S3	308	0.021	H-1→L+1	51
H→L+2				32	
3a'	S1	335	0.417	H→L	95
	S2	330	0.007	H-1→L	70
	S3	301	0.004	H-2→L	40
H→L+2				53	
4a'	S1	351	0.024	H-1→L	84
	S2	340	0.300	H→L	89
	S3	303	0.363	H-1→L+1	73
5a'	S1	420	0.012	H→L	97
	S2	383	0.085	H-1→L	74
	S3	316	1.152	H→L+1	73

Table 5B.5: Calculated Absorption energies ( $\lambda_{\max}$  in nm), Oscillator strength ( $f$ ), Configurations and % weight (%  $C_i$ ) at TD-B3LYP/6-311+G (d, p) method for molecules 1b' to 5b'

Molecule	State	$\lambda_{\max}$	$f$	configuration	% $C_i$
1b'	S1	405	0.093	H→L	98
	S2	347	0.061	H-1→L	69
	S3	304	0.014	H→L+3	93
2b'	S1	356	0.036	H→L	89
	S2	343	0.165	H-1→L	91
	S3	328	0.123	H→L+1	88
3b'	S1	346	0.284	H→L	96
	S2	335	0.007	H-1→L	54
				H→L+1	42
S3	312	0.184	H-1→L	42	
			H→L+1	53	
4b'	S1	362	0.045	H→L	88
	S2	353	0.194	H-1→L	93
	S3	333	0.178	H→L+1	93
	S1	385	0.078	H→L	96

5b'	S2	356	0.271	H-1→L	85
	S3	323	0.001	H-2→L	50
				H→L+1	47

Table 5B.6: Computed absorption ( $\lambda_{\max}$  in nm) and Oscillator strength ( $f$ ), with different functionals at TD-B3LYP/6-311+G (d, p) optimized geometries.

Molecule	BHHLYP		M06		PBE0		CAM-B3LYP		WB97XD	
	$\lambda_{\max}$	$f$	$\lambda_{\max}$	$f$	$\lambda_{\max}$	$f$	$\lambda_{\max}$	$f$	$\lambda_{\max}$	$f$
1a'	367	0.013	410	0.010	401	0.012	362	0.014	355	0.015
1b'	357	0.154	398	0.103	390	0.103	352	0.153	345	0.162
2a'	309	0.374	345	0.040	339	0.044	311	0.051	308	0.051
2b'	304	0.065	349	0.043	342	0.041	311	0.049	307	0.049
3a'	303	0.462	334	0.400	325	0.439	303	0.446	299	0.438
3b'	301	0.391	340	0.291	333	0.317	304	0.404	299	0.413
4a'	307	0.365	342	0.021	339	0.026	309	0.029	306	1.029
4b'	311	0.082	352	0.047	348	0.050	316	0.062	312	0.062
5a'	366	0.013	412	0.011	405	0.013	362	0.014	355	0.015
5b'	341	0.133	378	0.084	372	0.086	338	0.131	332	0.139

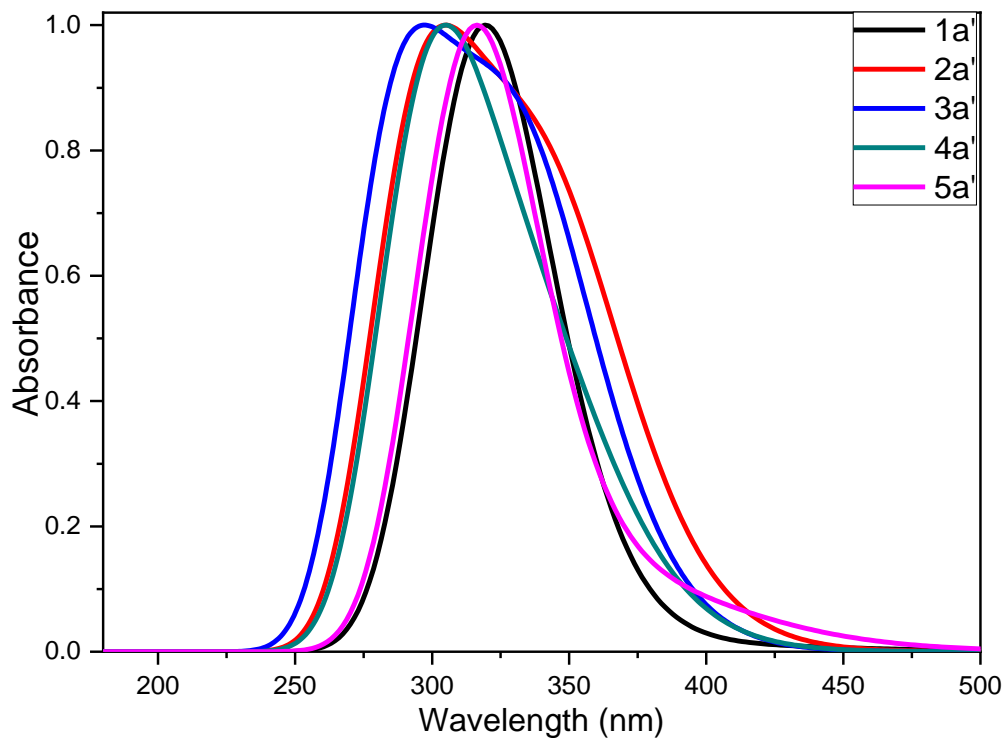


Figure 5B.6: Normalized absorption spectra of 'a' series isomers

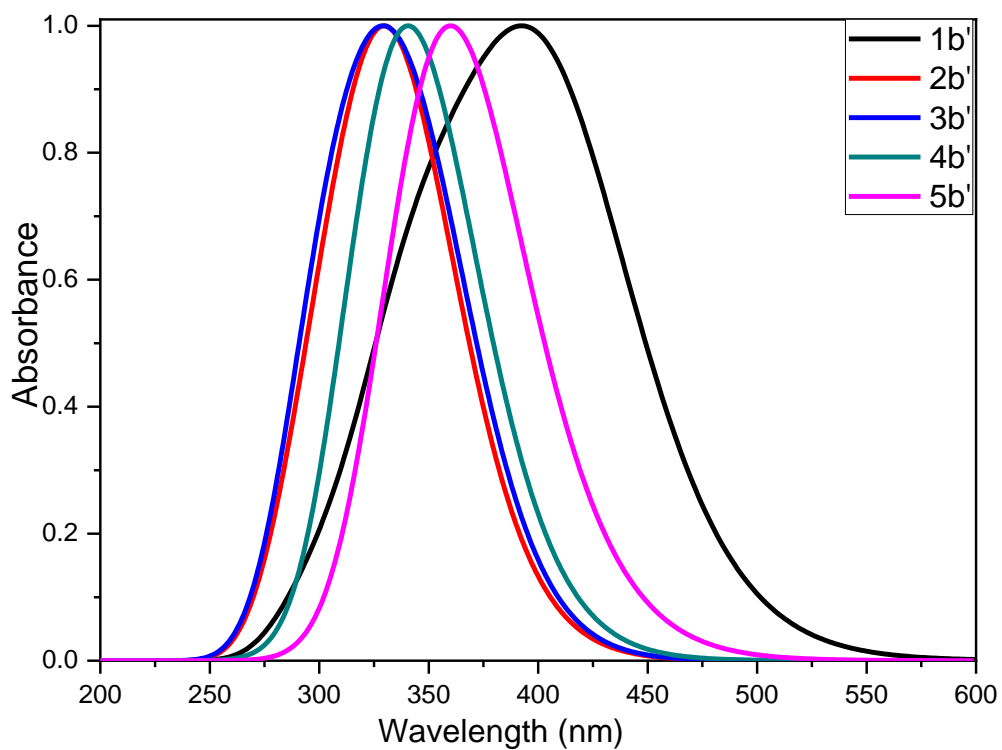


Figure 5B.7: Normalized absorption spectra of 'b' series isomers

---

### 5B.3.2. Frontier Molecular Orbitals (FMOs)

The HOMO and LUMO energies of molecule **1a'** are -6.08 eV and -2.65 eV respectively, resulting in a HOMO-LUMO gap of 3.43 eV (table **5B.7**). On varying the central benzene of fused tetrathiazoles with different five-membered heterocyclic rings, there is a stabilization of HOMO and destabilization of LUMO levels and the results obtained showed that there is an enhancement in the HOMO-LUMO gap (shown in figure 5B.8). In case of **2a'**, where the central ring is thiophene, HOMO level stabilized by 0.26 eV (-6.34 eV), and LUMO level gets destabilized by 0.31 eV (-2.34 eV) as compared to molecule **1a'** which increases the HOMO-LUMO gap (4.00 eV). Similarly, in case of **3a'** and **4a'**, HOMO levels are at -6.29 eV and -6.13 eV and LUMO levels are at -2.23 eV and -2.11 eV respectively, and their resultant HOMO-LUMO gap is 4.06 eV and 4.04 eV respectively. Molecule **5a'**, where the central ring is a six-membered heterocycle (pyridine) there is stabilization of HOMO and LUMO levels, and its resulting HOMO-LUMO gap is 3.44 eV. The isomers i.e. **b'** series molecules are also following a similar trend; molecule **1b'** and **5b'** show smaller HOMO-LUMO gap as compared to other molecules (shown in figure 5B.9). This decrease in the HOMO-LUMO gap in case of **1a'** and **5a'** are due to the six-membered central ring while in other molecules **2a'**, **3a'** and **4a'** the central six-membered ring is replaced by a five-membered heterocyclic ring which results in an increment of HOMO-LUMO gap. On moving from **a'** isomer (S inward and N outward facing) to **b'** isomer (N inward and S outward facing), i.e., change in position of heteroatom (S and N), leads to destabilization of both HOMO and LUMO levels.



Table 5B.7: HOMO, LUMO energy and H-L gap(in eV)

Molecule	HOMO	LUMO	H-L gap
1a'	-6.08	-2.65	3.43
1b'	-5.76	-2.29	3.47
2a'	-6.34	-2.34	4.00
2b'	-6.09	-2.07	4.02
3a'	-6.29	-2.23	4.06
3b'	-6.15	-2.11	4.04
4a'	-6.13	-2.09	4.04
4b'	-5.91	-1.97	3.94
5a'	-6.35	-2.91	3.44
5b'	-6.32	-2.67	3.65

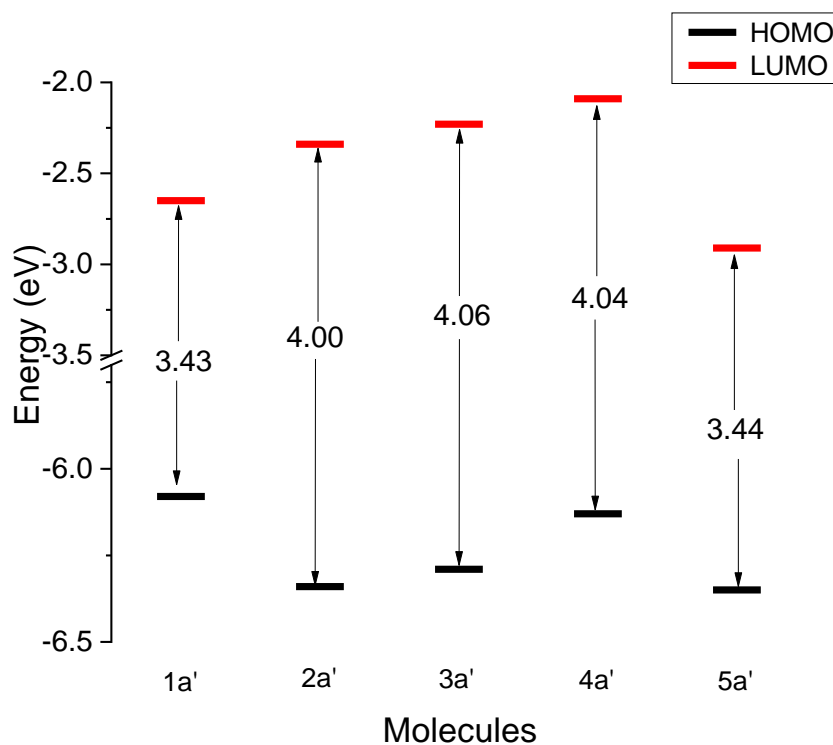


Figure 5B.8: Energy levels of Frontier molecular orbitals and their energy gap for 'a' series isomers

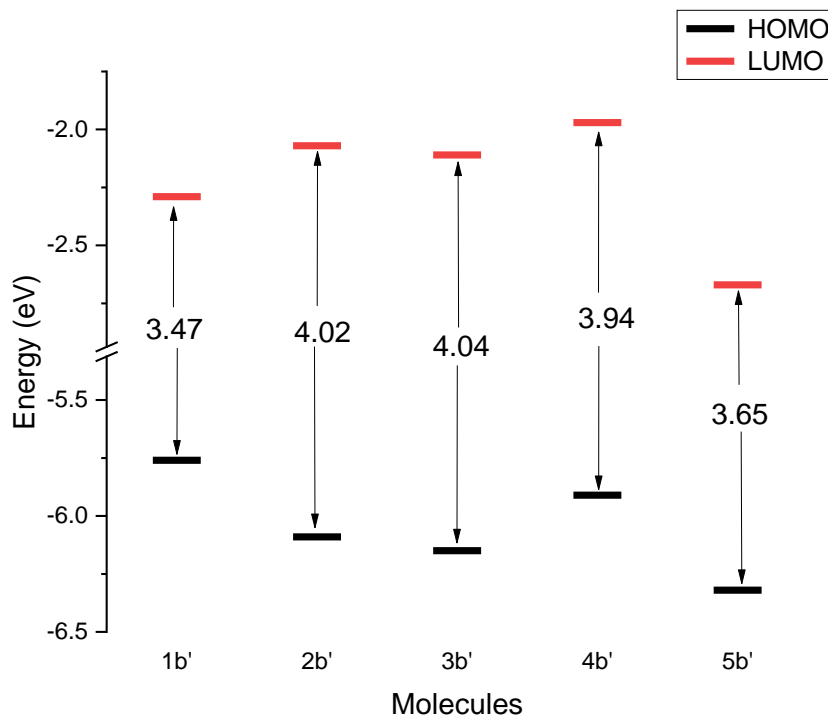


Figure 5B.9: Energy levels of Frontier molecular orbitals and their energy gap 'b' series isomers

### 5B.3.3. Ionization Potentials (IP), Electron Affinities (EA), HEP and EEP

For the efficient working of a device in optoelectronics, injection of hole and electron into an organic molecule must be easier. Molecular IP and EA are specific factors which play an essential role in charge injection properties. IP is the energy required by means of the structure once an electron is detached and it has to be small so that it is easy to inject hole into the HOMO of the molecule. On the other hand, EA is described as the energy released when an electron added to the structure. High EA value will permit an efficient electron inclusion into LUMO level of the molecule. Thus, we have calculated IP, EA, HEP and EEP as stated in the above-given formulas for all the compounds which tabulated in Table 5B.8. Among **a'** isomers vertical and adiabatic ionization potentials for molecule **1a'** are 7.34 eV and 7.27 eV respectively and is the lowest of all the **a'** isomers. In case of isomers of **b'**, **1b'** shows lowest vertical and adiabatic ionization potentials of 7.02eV and 6.95eV respectively. From Table 5B.8, the result suggests that **1a'** and **1b'** has the best ability to create a hole among other **a'** isomers and **b'** isomers respectively. In figure 5B.10 and figure 5B.11, graphical representation of adiabatic IP and EA and vertical IP and EA of all the molecules are shown respectively. It

is clear from figure 5B.10 and figure 5B.11, **b'** molecules are showing smaller IP(adiabatic and vertical) than corresponding **a'** isomers suggesting it is easy to inject hole in **b'** molecule compare to their corresponding isomers. While higher EA (adiabatic and vertical) of **a'** molecule suggest it is easy to inject electron into the LUMO of molecule compared to **b'** molecule. Among all the molecules, **1a'** (within **a'** isomers) and **1b'** (within **b'** isomers) are showing smallest HEP values of 7.20 eV and 6.89 eV respectively suggesting it is easy to inject hole in these molecules as match up to others (figure 5B.12). EA is maximum for **5a'** (**5b'**) and their vertical and adiabatic values are 1.65 eV (1.43 eV) and 1.72 eV (1.51 eV) correspondingly, suggesting that there is an efficient injection of electrons in the HOMO level of these compounds as compared to others. The energy required to extract electron (EEP) for molecule **5a'** (**5b'**) is 1.80 eV (1.60 eV) correspondingly (table 5B.8 and figure 5B.12).

Table 5B.8: Calculated Ionization Potentials ( $IP_v$  and  $IP_a$  in eV), Electron Affinities ( $EA_v$  and  $EA_a$  in eV), Extraction potentials (HEP and EEP in eV) and reorganization energies ( $\lambda_h$  and  $\lambda_e$  in meV) at B3LYP/6311+ G (d, p) level of theory for all the molecules.

Molecule	$IP_v$	$IP_a$	$EA_v$	$EA_a$	HEP	EEP	$\lambda_h$	$\lambda_e$
1a'	7.34	7.27	1.40	1.47	7.20	1.54	138	137
1b'	7.02	6.95	1.08	1.16	6.89	1.24	131	161
2a'	7.73	7.52	1.08	1.20	7.41	1.31	326	225
2b'	7.41	7.34	0.85	0.93	7.26	1.01	142	161
3a'	7.61	7.49	0.96	1.07	7.38	1.18	230	224
3b'	7.46	7.35	0.88	0.96	7.24	1.04	221	157
4a'	7.50	7.33	0.82	0.93	7.22	1.05	283	231
4b'	7.25	7.14	0.75	0.83	7.03	0.90	220	154
5a'	7.61	7.54	1.65	1.72	7.46	1.80	149	156
5b'	7.58	7.51	1.43	1.51	7.43	1.60	143	175

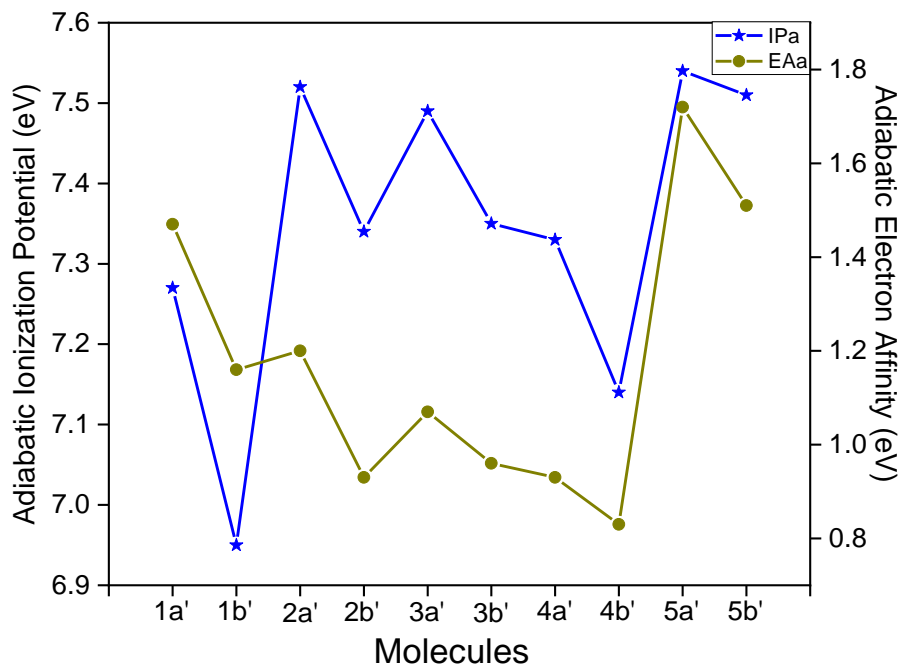


Figure 5B.10: Adiabatic Ionization Potential ( $IP_a$ ) and Electron Affinity ( $EA_a$ ) for  $a'$  and  $b'$  series molecules obtained at B3LYP/6-311 + G (d, p) level.

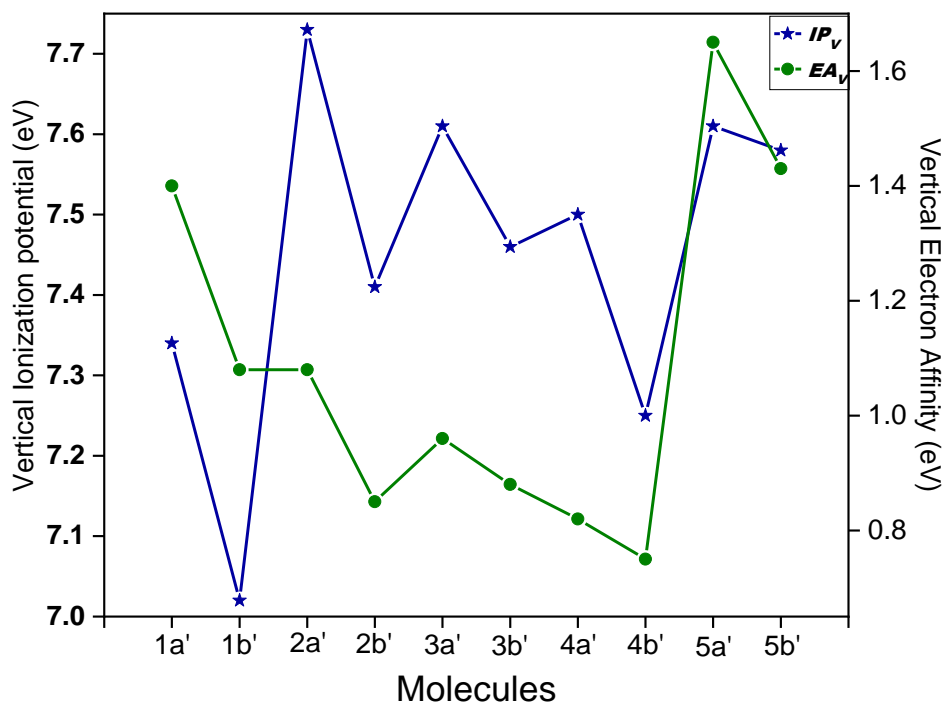


Figure 5B.11: Vertical Ionization Potential ( $IP_v$ ) and Electron Affinity ( $EA_v$ ) for  $a'$  and  $b'$  series molecules obtained at B3LYP/6-311 + G (d, p) level.

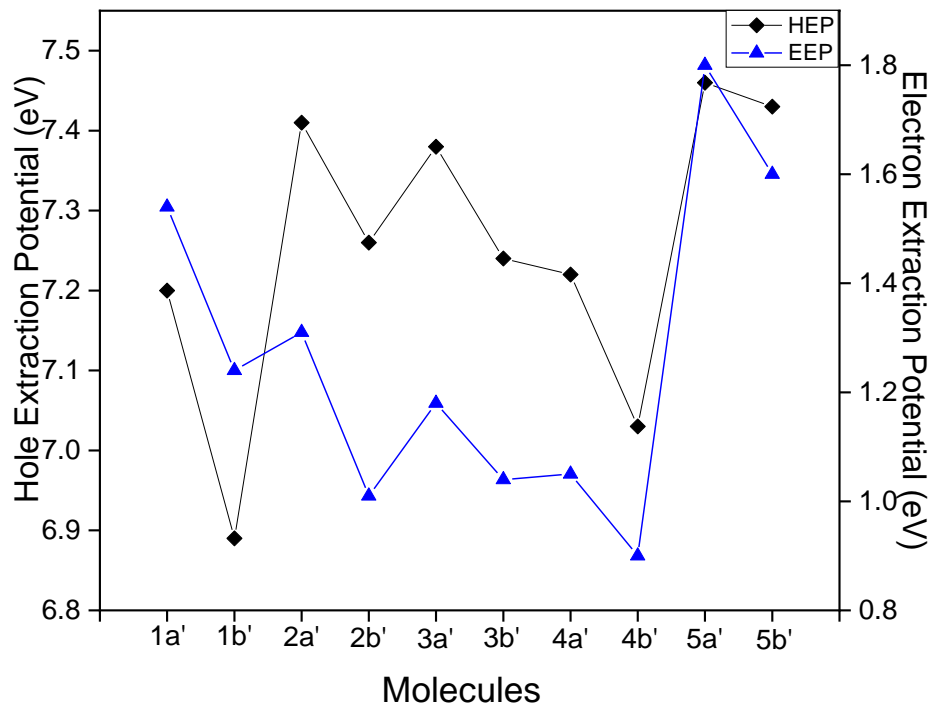


Figure 5B.12: Hole extraction potential (HEP) and Electron extraction potentials (EEP) for **a'** and **b'** series molecules obtained at B3LYP/6-311 + G (d, p) level.

#### 5B.3.4. Reorganization energies ( $\lambda$ )

For high charge transfer rate in a molecule, the  $\lambda$  must be low. In table 5B.8, we summarized  $\lambda$  for all the molecules based on B3LYP method (also calculated reorganization energies are represent in figure 5B.13). The calculated hole reorganization energies ( $\lambda_h$ ) for **1a'-5a'** and their isomers (except **2a'**) are lower than that of N,N'-diphenyl- N,N'-bis(3-methylphenyl)-(1,1'-biphenyl)-4,4'-diamine (TPD) which is a specific hole transport material having  $\lambda_h=290$  meV [38]. Thus, hole transfer rate in designed thiazole fused molecules in this work is higher than TPD. Also, the calculated electron reorganization energies ( $\lambda_e$ ) for **1a'-5a'** are lower than tris(8-hydroxyquinolato)aluminum(III) (Alq3) which is measured as standard electron transport material  $\lambda_e= 276$ meV [39-40]. Within these two set of isomers, **b'** isomers are having always smaller  $\lambda_h$  values than their corresponding **a'** isomers, which results in **b'** isomers are better for hole transport material than **a'** isomers.

On the other hand,  $\lambda_e$  values for molecule **1a'** and **5a'** are smaller than their corresponding **b'** isomers while in others molecule **b'** isomers i.e. **2b'**, **3b'** and **4b'** having smaller  $\lambda_e$  value. This decrease in  $\lambda_e$  values in case of **2b'**, **3b'** and **4b'** are due to alterations in the position of sulphur and nitrogen at the periphery of the molecule. Moreover, the difference of  $\lambda_h$  and  $\lambda_e$  for the majority of the molecules are in between 15-50 meV, indicating that the studied molecules are having superior equilibrium properties of hole and electron transport and may serve as new candidates for ambipolar charge transport materials.

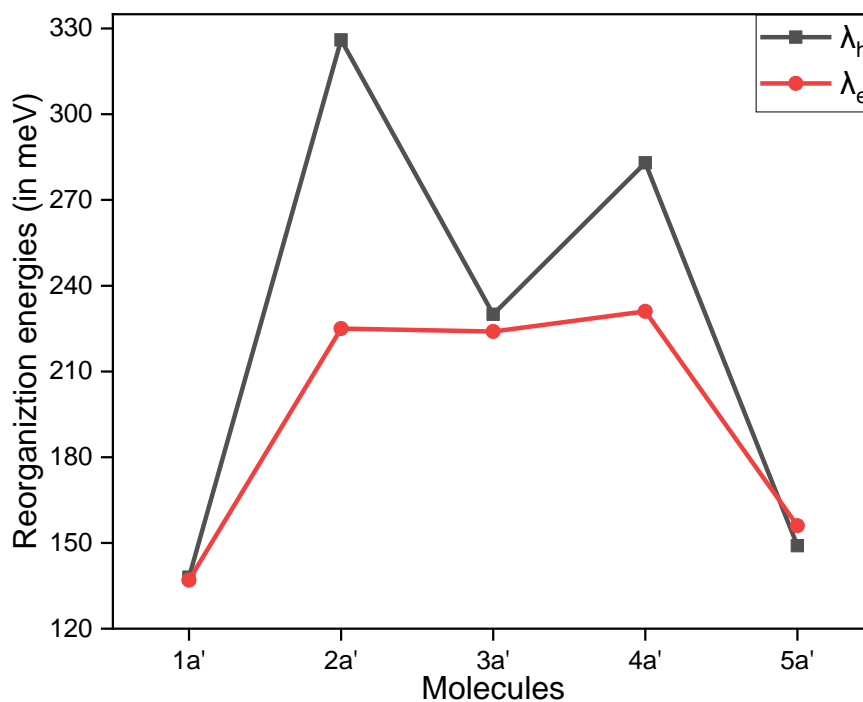


Figure 5B.13: Variation of Hole Reorganization Energy( $\lambda_h$  in meV) with with B3LYP functional

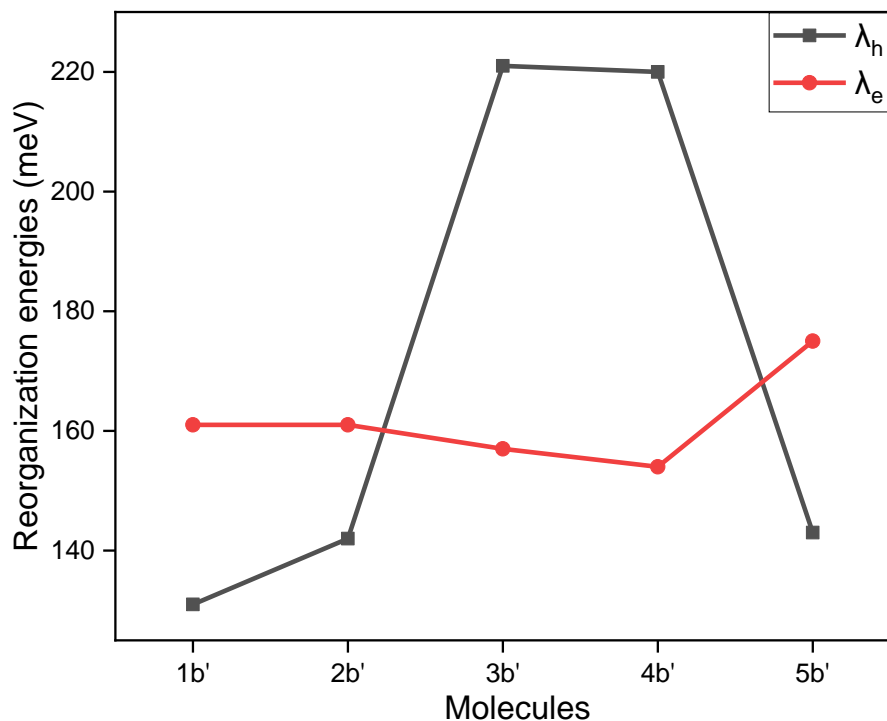


Figure 5B.14: Calculated Electron Reorganization Energy ( $\lambda_e$  in meV) with B3LYP functional

In order to see the effect of functional on reorganization energies calculations are performed with PBE0 and M06 functionals. The calculated  $\lambda_h$  for molecule **1a'** with B3LYP, PBE0 and M06 are 138meV, 140meV and 147meV respectively, showing functional are giving same  $\lambda_h$  value. Similar is the case for  $\lambda_e$  value for **1b'** are 161meV, 165meV and 172meV with B3LYP, PBE0 and M06 functional respectively. Same trend is observed for the other molecules and are calculated hole and electron reorganization with different functional are tabulated in table 5B.9. Also in figure 5B.15 and 5B.16 calculated hole and electron reorganization energies respectively with PBE0 and M06 functionals are represented.

Table 5B.9: Calculated hole ( $\lambda_h$ ) and electron ( $\lambda_e$ ) reorganization energies of all the molecules with different functionals

Molecules	B3LYP		PBE0		M06	
	$\lambda_h$	$\lambda_e$	$\lambda_h$	$\lambda_e$	$\lambda_h$	$\lambda_e$
1a'	138	137	140	145	147	152
1b'	131	161	136	165	138	172
2a'	326	225	348	230	365	234
2b'	142	161	144	165	148	170
3a'	230	224	242	230	249	234
3b'	221	157	228	160	240	166
4a'	283	231	315	230	351	236
4b'	220	154	227	156	231	163
5a'	149	156	151	166	159	171
5b'	143	175	147	181	153	188



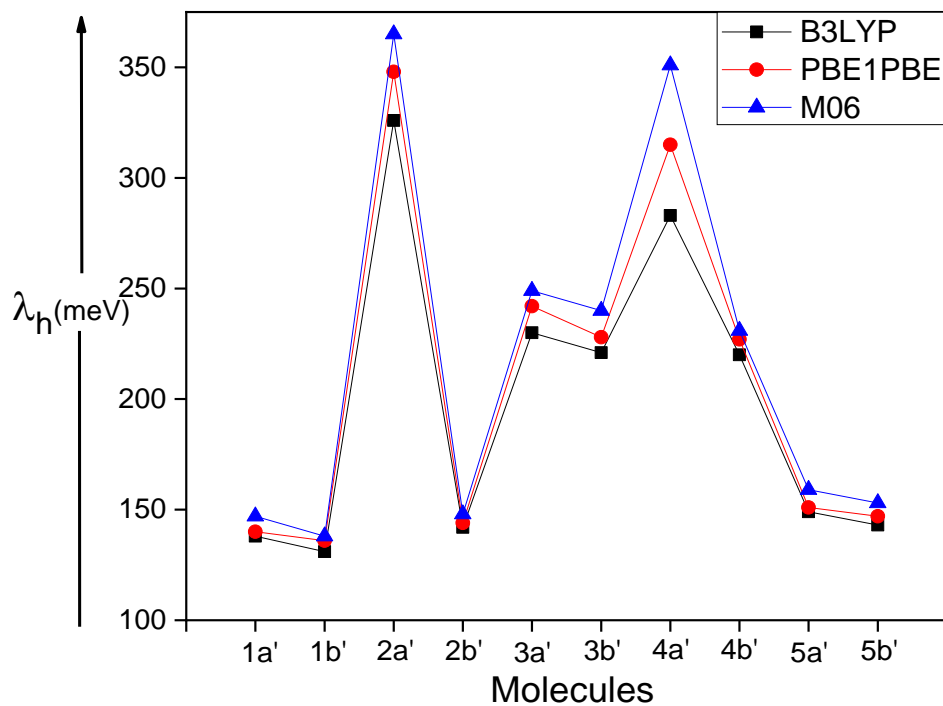


Figure 5B.15: Variation of Hole Reorganization Energy ( $\lambda_h$  in meV) with B3LYP, PBE0 and M06 functionals.

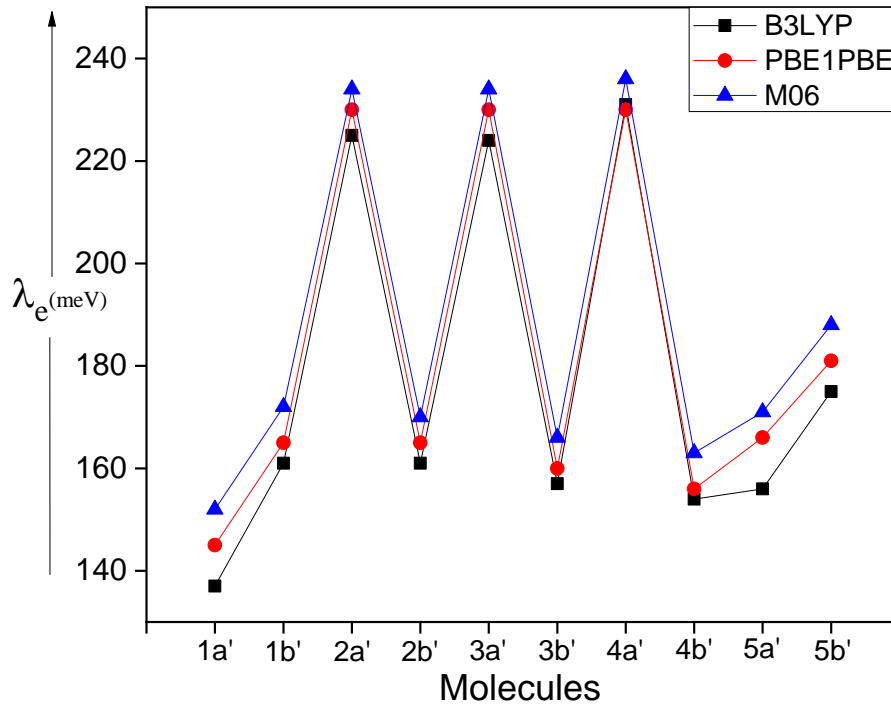


Figure 5B.16: Variation of Electron Reorganization Energy ( $\lambda_e$  in meV) with B3LYP, PBE0 and M06 functionals

---

#### 5B.4. Conclusion

In this chapter, we performed DFT and TD-DFT studies on ten novel molecules and analyzed their optoelectronic properties and reorganization energies. From the analysis, it is evident that on altering the central benzene of fused tetrathiazole by means of different 5-membered heterocycles, approximately 50 nm blue shift was noticed in all modified molecules while with 6-membered heterocycles there is no significant effect on absorption energies. Smaller HOMO-LUMO gap also observed when the central ring is six-membered rather than five-membered. The small HOMO-LUMO gap is due to the low degree of aromaticity in 5-membered heterocycles than benzene central ring system. The  $\lambda_h$  of all the **b'** isomers (sulphur facing outward position) are lower than corresponding **a'** isomer (sulphur facing inward position) suggesting molecules of **b'** isomers are better for hole transport materials than analogous **a'** isomers. Compounds, **1a'** & **5a'** and their isomers (**1b'** and **5b'**) have lowest hole and electron reorganization energies due to the central six-member ring (benzene or pyridine) of anthracene. All the compounds have smaller  $\lambda_h$  value than TPD suggesting that these molecules under study are better hole transport materials. Further,  $\lambda_e$  values showed that studied molecules are also better electron transport material than standard Alq3. All these computational studies on fused terathiazolearene based compounds offer a theoretical background with rational molecular design and the synthesis of new active materials for high-performance charge transport materials are warranted.

---

**Reference**

1. F. He, W. Wang, W. Chen, S. B. Darling, J. Strzalka, Y. Liu, L. Yu, *J. Am. Chem. Soc.* **2011**, 13, 3284.
  2. A. Irfan, A. G. Al-Sehemi, S. Muhammad, *Synth. Met.* **2014**, 190, 27.
  3. H. Meng, F. Sun, M. B. Goldfinger, G. D. Jaycox, Z. Li, W. J. Marshall, G. S. Blackman, *J. Am. Chem. Soc.* **2005**, 127, 2406.
  4. K. Takimiya, H. Ebata, K. Sakamoto, T. Izawa, T. Otsubo, Y. Kunugi, *J. Am. Chem. Soc.* **2006**, 128, 12604.
  5. T. Yamamoto, K. Takimiya, *J. Am. Chem. Soc.* **2007**, 129, 2224.
  6. J. Huang, J. H. Su, H. Tian, *J. Mat. Chem.* **2012**, 22, 10977.
  7. Y. L. Liu, J. K. Feng, A. M. Ren, *J. Phys. Org. Chem.* **2007**, 20, 600.
  8. Y. Lin, Y. Li, X. Zhan, *Chem. Rev.* **2012**, 41, 4245.
  9. Y. A. Duan, Y. Geng, H. B. Li, J. L. Jin, Y. Wu, Z. M. Su, *J. Comp. Chem.* **2013**, 34, 1611.
  10. S. R. Forrest, *Nature.* **2004**, 428, 911.
  11. M. M. Torrent, C. Rovira, *Chem. Rev.* **2011**, 111, 4833.
  12. J. S. Yang, H. H. Huang, J. H. Ho, *J. Phys. Chem. B.* **2008**, 112, 8871.
  13. J. S. Yang, H. H. Huang, Y. H. Liu, S. M. Reng, *Org. Lett.* **2009**, 11, 4942.
  14. H. H. Huang, C. Prabhakar, K. C. Tang, P. T. Chou, G. J. Huang, J. S. Yang, *J. Am. Chem. Soc.* **2011**, 133, 8028.
  15. J. E. Anthony, *Chem. Rev.* **2006**, 106, 5028.
  16. J. L. Brusso, O. D. Hirst, A. Dadvand, S. Ganeshan, F. Cicoira, C. M. Robertson, R. T. Oakley, F. Rosei, D. F. Perepichka, *Chem. Mater.* **2008**, 20, 2484.
  17. D. J. Gundlach, J. A. Nichols, L. Zhou, T. N. Jackson, *Appl. Phys. Lett.* 2002, 80, 2925.
  18. B. Lee, M. S. Yavuz, G. A. Sotzing, *Macromolecules*, **2006**, 39, 3118.
  19. T. Lei, J. Pei, *J. Mater. Chem.* **2012**, 22, 785.
  20. X. D. Tang, Y. Liao, H. Geng, Z. G. Shuai, *J. Mater. Chem.* **2012**, 22, 18181.
  21. T. Vehoff, B. Baumeier, A. Troisi, D. Andrienko, *J. Am. Chem. Soc.* **2010**, 132, 11702.
  22. X. Yang, L. Wang, C. Wang, W. Long, Z. Shuai, *Chem. Mater.* **2008**, 20, 3205.
  23. M. X. Zhang, G. J. Zhao, *J. Phys. Chem. C* **2012**, 116, 19197.
  24. W. J. Liu, Y. Zhou, Y. Ma, Y. Cao, J. Wang, J. Pei, *Org. Lett.* **2007**, 9, 4187.
  25. J. Wang, H. Xu, B. Li, X. P. Cao, H. L. Zhang, *Tetrahedron Lett.* **2012**, 68, 1192.
-

- 
26. M. J. Frisch, Gaussian 16, Revision E.01; Gaussian, Inc.: Wallingford CT, **2016**.
  27. J. Tomasi, B. Mennucci, R. Cammi, *Chem. Rev.* **2005**, 105, 2999.
  28. S. Muhammad, S. Kumar, J. Koh, M. Saravanabhavan, K. Ayub, M. Chaudhary, *Mol. Simul.* **2018**, 44, 1191.
  29. S. Muhammad, G. A. Al-Sehemi, A. Irfan, H. Algarni, Y. Qiu, H. Xu, Z. Su, J. Iqbal, *J. Mol. Graph.* **2018**, 81, 25.
  30. S. Muhammad, A. R. Chaudhary, G. A. Al-Sehemi. *Optik* **2017**, 147,439.
  31. A. D. Becke. *Phys. Rev. A*, **1988**, 38, 3098.
  32. C. Lee, W. Yang, R. G. Parr, *Phys. Rev. B*, **1988**, 37, 785.
  33. T. Yanai, D. P. Tew, N. C. Handy, *Chem. Phys. Lett.* **2004**, 393, 51.
  34. J. D. Chai, M. H. Gordon, *J. Chem. Phys.* **2008**, 128, 084106.
  35. C. Adamo, V. Barone, *J. Chem. Phys.* **1999**, 110, 6158.
  36. Y. Zhao, D. G. Truhlar, *Theor. Chem. Acc.* **2008**, 120,215
  37. A. D. Becke, *J. Chem. Phys.* **1993**, 98, 1372.
  38. N. E. Gruhn, D. A. d S. Filho, T. G. Bill, M. Malagoli, V. Coropceanu, A. Kahn, J. L. Bredas. *J. Am. Chem. Soc.* **2002**, 124,7918.
  39. B. C. Lin, C. P. Cheng, Z. Q. You, C. P. Hsu. *J. Am. Chem. Soc.* **2005**, 127,66.
  40. A. Irfan, R. Cui, J. Zhang. *J. Mol. Struc. Theochem.* **2010**, 956, 61.





---

---

## List of Publications

### Publications from Thesis

1. Enhanced charge transport properties in heteroatomic (NH, O, Se) analogs of benzotrithiophene isomers: a DFT insight. **A. Tripathi**, Ch. Prabhakar. *Mol. Sim.*, **2020**, 46(7), 548-556.
2. Optical and charge transport properties of Chalcogens (O, S and Se) based acene molecules. **A. Tripathi**, Ch. Prabhakar. *J. Mol. Struct.*, **2020**, 1203, 127397(1-8).
3. A DFT study on optical, electronic and charge transport properties of star-shaped benzo[1,2-b:3,4-b',5,6-b''] trithiophene oligomers. **A. Tripathi**, Oleg K, Khidmet S, Ch. Prabhakar. *J. Phys. Org. Chem.*, **2020**, 33(3), e4037. (*Cover Article*).
4. Optoelectronic and charge transport properties of truxene, isotruxene and its heteroatomic (N, O, Si and S) analogs: A DFT Study. **A. Tripathi**, Ch. Prabhakar. *J. Phys. Org. Chem.*, **2019**, 32(6), e3944.
5. Optoelectronic properties of benzotrithiophene isomers: A density functional theory study. **A. Tripathi**, Ch. Prabhakar. *J. Chin. Chem. Soc.*, **2019**, 66(8), 891-898.
6. Impact of heteroatom (S and N) positions and change in central ring of anthracene with heterocyclic ring on charge transport and optical properties in anthratetrathiazole (ATTz). **A. Tripathi**, Ch. Prabhakar. *J. Sulfur. Chem.*, **2019**, 40, 361-376.
7. Impact of replacement of central benzene ring in anthracene by heterocyclic ring on electronic excitations and reorganization energies in anthratetrathiophene molecules. **A. Tripathi**, Ch. Prabhakar. *J. Chin. Chem. Soc.*, **2018**, 65(8), 918-924.

---

---

## Publications from Project and Collaboration work

1. Influence of internal acceptor and thiophene based  $\pi$ -spacer in D-A- $\pi$ -A systems on photophysical and charge transport properties for efficient DSSCs: A DFT insight. **A. Tripathi**, A. Ganjoo, Ch. Prabhakar. *Sol. Energy*, **2020**, 209, 194-205.
2. Structural assessment and identification of 11 $\beta$ -hydroxysteroid dehydrogenase type 1 inhibitors, A. Ganjoo, **A. Tripathi**, Ch. Prabhakar. *J. Biomol. Struct. Dyn.*, **2019** 1-10.
3. A Coumarin-Benzothiazole Derivative as a FRET-Based Chemosensor of Adenosine 5'-Triphosphate, Moustafa T. Gabr, Mostafa M. H. Ibrahim, **A. Tripathi**, Ch. Prabhakar. *Chemosensors*, **2019**, 7(3), 34.
4. Linear and femtosecond nonlinear optical properties of soluble pyrrolo [1, 2-a] quinoxalines. C. Biswas, K. N. Krishnakanth, J. J. Lade, A. C. Chasker, **A. Tripathi**, Ch. Prabhakar, V. R. Soma, S. S. K. Ravi. *Chem. Phys. Lett.* **2019**, 730, 638-642.
5. Corrosion of  $\alpha$ -Brass in Solutions Containing Chloride Ions and 3-Mercaptoalkyl-5-amino-1H-1, 2, 4-triazoles. O. Kozaderov, K. Shikhaliev, Ch. Prabhakar, **A. Tripathi**, D. Shevtsov, A. Kruzhilin, E. Komarova, A. Potapov, I. Zartsyn, Y. Kuznetsov. *Appl. Sci.*, **2019**, 9 (14), 2821.
6. Eco-friendly synthesis, crystal structures, photophysical properties and DFT studies of new N-arylthiazole-5-carboxamides. J. Miryala, **A. Tripathi**, Ch. Prabhakar, D. Sarma, S. Pola, B. Satyanarayana. *J. Mol. Struct.*, **2019**, 1184, 193-199.
7. Linear, non-linear optical properties and reorganization energies of D- $\pi$ -A star-shaped triazine derivatives: A DFT study. V. M. Vidya, **A. Tripathi**, Ch. Prabhakar. *J. Mol. Struct.*, **2019**, 1176, 855-864.
8. A comparative computational study of CN and CC bonding visible to NIR absorbing croconines. **A. Tripathi**, Ch. Prabhakar. *J. Mol. Struct.*, **2018**, 1155, 561-567.
9. Visible to NIR absorbing C-N and C-C bonding squaraines: A computational study. **A. Tripathi**, P. Dhanda, Ch. Prabhakar. *J. Phys. Org. Chem.*, **2018**, 31(2), e3758.



10. Mono-, di-and tri-substituted S-triazine as anti cancer agents: A comparative molecular docking study. A. Joshi, **A. Tripathi**, Ch. Prabhakar. *Indian J. Chem. Sec B.*, **2018**, 57B, 816-822.
11. Dicyanomethylene substituted oxocarbon dianions: A comparative computational study. Promila, **A. Tripathi**, Ch. Prabhakar. *Indian J. Chem. Sec A.*, **2018**, 57A, 1121-1127.
12. Visible absorbing croconium dyes with intramolecular hydrogen bonding: A combined experimental and computational study. Ch. Prabhakar, P. Dhanda, **A. Tripathi**, K. Bhanuprakash, and V. Jayathirtharao. *J. Mol. Struct.*, **2018**, 1146, 684-691.
13. Visible absorbing symmetrical squaraine and croconine dye derivatives: A comparative computational study. **A. Tripathi**, P. Dhanda and Ch. Prabhakar. *J. Phys. Org. Chem.*, **2018**, 30(10), e3673. (*Cover Article*).

---

---

## Conferences and workshop attended

1. Poster presentation on topic “*A DFT study of Optoelectronic and Charge Transport properties on Truxene, Isotruxene and their heteroatom (N, O, Si, S) analogs*” by **A. Tripathi** and Ch. Prabhakar. In 7th National Conference on “*Nanoscience and Instrument Technology (NCNIT)*” during 9<sup>th</sup>-10<sup>th</sup> March 2019 organized by Department of Physics, NIT Kurukshetra, India.
2. Poster presentation on the topic “*Impact of replacement of central benzene ring in Anthracene by Heterocyclic ring on electronic excitations and reorganization energies*” by **A. Tripathi** and Ch. Prabhakar. In an international conference on “*Multifunctional Materials Analytical Techniques and Diverse Applications (MMAD18)*” during 20<sup>th</sup> January 2018 organized by Department of Chemistry NIT Kurukshetra, India.
3. Oral presentation on topic “*A DFT study on Electronic excitations and Charge transfer properties in benzotrithiophenes (BTTs)*” by **A. Tripathi** and Ch. Prabhakar. In an “*International Conference on Advances in Analytical Sciences (ICAAS)*” during 15<sup>th</sup>-17<sup>th</sup> March 2018, organized by CSIR-Indian Institute of Petroleum Dehradun, India.
4. Attended five-day GIAN course on “*Electrochemical Energy Conversion and Storage*” from 26<sup>th</sup> -30<sup>th</sup> November 2018 organized by Department of Chemistry, NIT Kurukshetra, India.
5. Attended five-day GIAN course on “*Vibrational Spectroscopy and Molecular Vibrations*” organized by Department of Chemistry, NIT Kurukshetra, India.
6. Attended five-day workshop on “*Molecules & Materials Technology: Interface with R&D and Industries (MMT-2017)*” organized by Department of Chemistry, NIT Kurukshetra, Kurukshetra held on 21<sup>st</sup> -26<sup>th</sup> March 2017.